Construction and Exhumation of the Sierra Nevada Range: an investigation of geochronology, thermochronology and trace element mineral chemistry

By

John P. Lee

Submitted to the graduate degree program in Geology and the Graduate Faculty of the University of Kansas in partial fulfillment of the requirements for the degree of Doctor of Philosophy.

Chair, Dr. J. Douglas Walker

Co-Chairperson, Dr. Daniel F. Stockli

Dr. Michael H. Taylor

Dr. Andreas Möller

Dr. David Braaten

Date Defended: December 5, 2018

The Dissertation Committee for John P. Lee
certifies that this is the approved version of the following dissertation:

Construction and Exhumation of the Sierra Nevada Range: an investigation of geochronology, thermochronology and trace element mineral chemistry

Chair, Dr. J. Douglas Walker

Co-Chairperson, Dr. Daniel F. Stockli

Date approved: December 5, 2018

ABSTRACT

This dissertation describes the development of the Sierra Nevada range from its construction as a magmatic arc to its current configuration as a significant tectonic block or microplate in the western North American Cordillera. The Sierra Nevada range is a large coherent physiographic and tectonic block built upon a Mesozoic age batholith that is one of the most well studied extinct continental arc systems in the world. Models of batholith construction, magmatic evolution and subduction mechanics have all been refined as a result of the geologic relationships observed in the Sierra Nevada. However, several important questions related to processes of continental arc systems are still unresolved. Specifically, the complex interplay between orogenesis and erosion in the Sierra Nevada is debated, as is the 'longevity' of the range created during Mesozoic and early Cenozoic subduction. The cause and source of voluminous magmas emplaced during magmatic flare-up events (e.g. late-Cretaceous flare-up of the Sierra Nevada) is not yet resolved. It is speculated that crustal thickening results in anatexis of the lower crust, but robust validation of this model in the chemistry of flare-up magmas is needed. This dissertation applies multiple geochronologic, thermochronometric and geochemical techniques to examine these questions. In Chapter 1, we investigate the timing and magnitude of erosion in the central Sierra Nevada range. Interpretation of the data presented here supports previous investigations in the southern and northern Sierra Nevada, which posit high rates of erosion in the late Cretaceous and early Cenozoic. The data presented in Chapter 1 also indicates that the paleotopography of the late Cretaceous range was of significant topographic relief and that the distribution of major paleotopographic features (e.g. river canyons, major interfleuve divides) in the late

Cretaceous were similar to those of the modern range. Chapter 2 investigates the cooling trends observed in batholithic rocks from temperatures of 800°C <T<60°C. We interpret these results to indicate a characteristic pattern of post-emplacement cooling that reflects two dominating mechanisms: (1) post-emplacement conductive equilibration of temperatures followed by (2) cooling as a result of exhumation. Chapter 3 investigates the long-term fractionation of magmas during the late-Cretaceous flare-up event by analyzing trace element concentrations in magmatic zircons. We find evidence for increasingly fractionated melts throughout the flare-up event; an observation that supports models of anatexis as a result of crustal thickening. We also find that the late-Cretaceous flare-up may have started earlier in the northern portions of the range and migrated south over a period of 10-15 Ma, thus indicating a temporal and spatial progression not yet recognized.

ACKNOWLEDGEMENTS

This work was funded by a variety of organizations and institutions, all of which were essential to the results produced here. I am grateful to the National Science Foundation, the Swiss National Science Foundation, the University of Lausanne, the United States Geological Survey and the University of Kansas.

I am also grateful for the many people that helped make this study happen. Specifically, I extend a great thank you to Chris Hager and Eugene Szymanski for the many rock-laden miles of wilderness that I drug them through. The widespread and remote sample locations represented in this study are a testament to your hard work and determination. I also extend a special thanks to Roman Kislitsyn. Without your assistance, guidance and technical expertise, the data that is central to this study would have been lacking.

This research project was the brainchild of Michael Cosca. Thank you for providing me with the ideas, tools and facilities to move forward with this research as well as being my guide in a strange new country. You facilitated memories for a lifetime. Additionally, this research would not have come to fruition without the efforts and funding of Daniel Stockli. You supported the transition of my studies and I will always be grateful for your efforts and support through that process. I would also like to thank Doug Walker. When the fire was dim, you stoked the flames. You were an invaluable mentor, motivator and guide through the final stages of this process. Your extraordinary efforts in the final months were transformational and will always be deeply appreciated.

Finally, I would like to thank my loving wife, Chrissy. Despite the all-consuming demands of new businesses and new family, you not only supported and motivated me; you carried the extra weight of my circumvented responsibilities. Honestly and truly, this study would not be a realization without you. I will always be in awe and admiration of you.

TABLE OF CONTENTS

LIST OF FIGURES

LIST OF TABLES

CHAPTER 1

Low-Temperature Thermochronology of the Sierra Nevada and Evidence for Early Uplift and Unroofing

Abstract

This study presents a new thermochronologic data collected to better understand the late Cretaceous to early Cenozoic patterns of exhumation in the Sierra Nevada Range. Apatite and zircon (U-Th)/He dating of a widely dispersed set of 46 bedrock samples taken across the elevation range of the Sierra Nevada provides insight into the spatial and temporal variations in erosion throughout the area. The new data are combined with a rich, preexisting dataset of (U-Th)/He data from the region. Histograms of the combined dataset show a pulse of cooling and exhumation at 70-60 Ma. Age distributions throughout the central and northern range appear to be independent of major modern topographic features. Additionally, erosion rates calculated using the difference between the apatite and zircon ages imply a systematic increase in exhumation rates throughout the Cretaceous, peaking at over 1 km/my at 60 Ma. Each of these observations provides additional evidence for late Cretaceous exhumation of the Mesozoic batholith that may reflect regional uplift of the range.

Introduction

The history of uplift of the Sierra Nevada Range (SNR) to its current elevation remains controversial subject (Henry, 2009, Putirka and Busby, 2011; Jones and Saleeby, 2013). This comes in part from the fact that estimates of absolute paleo-elevation are difficult to make and the link between uplift and surface elevation can be complicated (Molnar; 1990; Reiners, 2007). Models and supporting evidence for late Cenozoic uplift of the Sierra Nevada Range come from 4 main sources of data: (1) paleodrainage reconstructions and range tilt calculations (Huber, 1981, Huber, 1990; Unruh, 1991; Wakabayashi and Sawyer, 2001; Wakabayashi, 2013; Martel et al., 2014), (2) modern surface movements as indicated by Global Positioning System (GPS) and remote sensing techniques (Hammond et al., 2012; Hammond et al., 2016), (3) isostatic-driven uplift due to thermal and gravitational instabilities in the lower crust (Zandt et al., 2004; Jones et al. 2014; Jones and Saleeby, 2013; Chapman et al., 2017) and (4) fluvial incision as indicated by cosmogenic studies of cave sediments (Stock et al., 2004; Stock et al., 2005). In contrast, other datasets indicate that uplift of the Sierra Nevada Range occurred largely in the late Cretaceous and/or early Cenozoic and include: (1) paleoelevation/relief estimates as indicated by stable isotopes (Poage and Chamberlain, 2002; Mulch et al., 2006; Crowley et al., 2008; Henry, 2009; Cassel et al., 2009; Molnar, 2010), (2) cooling data from low-temperature thermochonologic studies (House et al., 1997; House et al., 2001; Cecil et al., 2006; Blythe and Longinotti, 2013), and (3) sedimentologic studies of early Cenozoic fluvial and volcanic deposits (Yeend, 1974; Creely and Force, 2007; Henry, 2008; Cassel et al., 2009). Other syntheses of data have suggested that the uplift

history of the SNR is both spatially and temporally variable (Small and Anderson, 1995; Wernicke et al., 1996; McPhillips and Brandon, 2012; Blythe and Longinotti, 2013).

In this paper, we present new results and a regional synthesis for the erosional history of the SNR using (U-Th)/He thermonchronology on zircon (ZHe) and apatite (AHe) for samples from the area between Lake Tahoe and the Merced River (Fig. 1.1). These results provide a valuable link between the previous (U-Th)/He work on the southern (House et al., 2001) and northern Sierra Nevada (Cecil et al.; 2006). Our results are combined with these existing datasets to yield a more complete history of exhumation from the Sierran crest to the western foothills. Although not a direct measure of the paleoelevation of the range, it is both an important recorder or exhumation and can give information about paleotopographic features such as deep incision in river systems.

Background

The Sierra Nevada Range is an iconic example of a subduction related batholith. The plutonic rocks of the Sierra Nevada orogen formed within a continental arc environment starting at about 220 Ma and ending at roughly 85 Ma (Chen and Moore, 1982; Barth et al., 2018). It now sits at an elevation of 3 to 4 km at its crest. Geological and geophysical data suggest that roughly 20-25 km of the 30km thick crust is granitic (Ague and Brimhall, 1988; Wernicke, 1996; Ducea, 2001), indicating that the restitic root material has been removed (Manley et al., 2000; Farmer et al., 2002).

Delamination of the eclogitic root has implications for the uplift and erosion histories, and some research suggests uplift of the Sierra Nevada range after ca. 8 Ma as inferred from volcanic activity containing mantel xenoliths with geochemical signals

indicating delamination of the crustal root (Ducea, 2001; Saleeby and Foster, 2004, Putirka and Busby, 2007; Jones and Saleeby, 2013). Independent studies of the late Cenozoic uplift of the Sierra Nevada suggest 1.0 to 2.5 km of rock uplift in the last 10 Ma along the crest of the entire Sierra Nevada, perhaps due to a combination of slab detachment coupled with movement of the normal fault system on its east boundary. These studies are largely based on stream incision rates (e.g. Wakabayashi and Sawyer, 2001) and westward tilting of volcanic and geomorphic surfaces (Clark et al., 2001). Other studies support the idea of late uplift of the Sierra Nevada range from high post-10Ma erosion rates calculated through cosmogenic dating of cave sediments (Stock et al., 2004).

In contrast, several studies attribute the uplift of the Sierra Nevada Range late Cretaceous time (Yeend, 1974; House et al., 1997; House et al., 2001; Poage and Chamberlain, 2002; Mulch et al., 2006; Cecil et al., 2006, Creely and Force, 2007; Crowley et al., 2008; Henry, 2009, Cassel et al., 2009; Cassel et al., 2009; Henry, 2008; Cecil et al., 2010; Molnar, 2010) with subsequent uplift and slow erosion throughout the Cenozoic. Studies of (U-Th)/He dates in the southern SNR have suggested early Cenozoic creation of high relief (~2km) followed by slow erosion and relief decreases (e.g. House et al., 1997; House et al., 2001). More recent thermochronologic studies in the northern Sierra Nevada exhibit similar age patterns and signify early exhumation of the granitic batholith (Cecil et al., 2006). In addition to the thermochonologic studies, stable isotope data from east and west of the range argue for the existence of an orographic barrier coincident with the modern SNR in early Cenozoic time (e.g. Cassel et al., 2009; Henry, 2009). Finally, the occurrence of Eocene deposits along the western

margin of the range indicate a very high-energy fluvial system existed that drained a topographic high to the east (Unruh, 1991). This, in turn, indicates the existence of high relief early in the Cenozoic.

This study attempts to better delineate to the cooling history and exhumation recorded in rocks of the SNR by filling the data gap that exists between the southern and northern AHe datasets. We also integrate zircon (U-Th)/He analysis and data into the study to provide better constraints on the uplift and erosion history of the Sierra Nevada Range. Below, we describe the methods including sample collection, (U-Th)/He procedures and data collection, and uncertainties. This is followed by a discussion of the significance of the results for interpreting the region.

Methods

In this study we report 74 new AHe and ZHe results from 46 samples collected between the Merced River and Lake Tahoe from the crest to the western foothills of the Sierra Nevada range (Fig. 1.1). We first describe sample collection strategy and processing, then the (U-Th)/He methods along with their uncertainties as the basis for T and cooling T/t interpretations.

Sample Collection and Mineral Separation

We collected all samples from bedrock exposures of Mesozoic plutonic rocks. In total, 150 samples were collected of which 46 selected and analyzed (Table 1.1). As shown in Figure 1.1, transects were collected from the Merced, Tuolumne, American, and Mokelumne river drainages. Additional transects were collected from the interfluve

areas between the rivers. Each transect started at the westernmost extent of the plutonic rock outcrop and extended eastward to as close to the Sierra crest as access allowed.

Mineral separation was performed at the University of Kansas. Samples were crushed, milled and sorted by density on a water table. The resulting heavies were processed by using heavy liquids. The denser fractions were then further processed using a Frantz magnetic separator and methylene iodide to isolate apatite and zircon fractions.

(U-Th)/He Technique

(U-Th)/He analysis was performed on both apatite and zircon separates at the University of Kansas. Mineral separates were inspected under a stereomicroscope to identify representative, euhedral, and inclusion free grains. The grain's dimensions were measured using the stereomicroscope and microscope imaging software. Single selected grains were loaded into platinum foil and heated with a Nd:YAG laser to a temperature of 1050°C for apatite and 1200°C for zircon. Reheats were performed to test for re-extracts of helium and the presence of inclusions. The helium content was calculated by means of isotope dilution and measured on a quadrapole, gas-source mass spectrometer. Grains were then spiked and digested in acid and analyzed for uranium, thorium, and samarium concentrations by ICPMS (inductively coupled plasma mass spectrometer).

The (U-Th)/He dating technique is based on the decay of ^{235}U, ^{238}U, ^{232}Th, and ^{147}Sm by alpha (^{4}He nucleus) emission (Farley, 2002). At temperatures above ~80°C, ^{4}He is completely expelled from apatite and is almost totally retained below ~40°C (termed the Partial Retention Zone or PRZ; Stockli et al., 2000). In zircon, the PRZ corresponds to temperatures between 150°C and 190°C (Reiners, 2005). Dates are initially determined using just the concentrations of parent (^{235}U, ^{238}U, ^{232}Th, and ^{147}Sm) and daughter (^{4}He)

isotopes. A complicating factor is that the decay energy of the parents, up to ~8 MeV, is associated with α-recoil of the parent nucleus and energetic emission of the α particle with high kinetic energy (Farley et al., 1996). This causes the α particles to travel significant distances before coming to rest, leading to potential α loss during decay. Resulting (U-Th)/He dates must be corrected for daughter loss by this ejection effect. To estimate lost daughter, a correction (FT correction described in Farley et al., 1996) is made using a statistical approach taking into account mineral density and crystal geometry.

Propagated analytical uncertainties for individual analysis are generally 3-4% at 2σ, when uncertainty in the FT correction is considered. These uncertainties do not seem to account for scatter in most sample dates, and the accepted practice in (U-Th)/He dating is to apply a percentage error to individual analyses based on the reproducibility of laboratory standards: 6% for apatite and 8% for zircon (Farley et al., 2000; Reiners and Farley, 2005). We then compute the mean date of a sample by simply taking the average of the individual grain dates. We apply an overall uncertainty of 6% or 8% to the mean date. Although we could compute the standard error of the sample dates with multiple analyses, e.g. using $\sigma/\sqrt{n}$, we choose to be somewhat more conservative, because we are still not considering systematic errors in the correction parameter or elemental and damage zoning in grains. Other approaches to computing ages and errors accounting for over dispersion are described in Vermeesch (2008).

Results

The (U-Th)/He mean sample ages are shown in Figure 1.2; summary results are given in Table 1.1 and individual grain analyses are reported in the supplementary tables. Dates from individual samples were generally reproducible within the uncertainty analysis described above. Of the 176 individual AHe analyses, a total of eight were excluded because of their dates. Four analyses yielded an age at or near 0 Ma indicating that the grain was lost in analysis, and another four analysis yielded ages far greater than the other grains in the sample and probably reflecting the presence of U-Th rich inclusions not identified during grain selection. Of the 106 individual zircon analyses, only 3 analyses were excluded due to dates far outlying the main sample population. The general agreement of dates of samples within close spatial proximity and the overall reproducibility between grains from single samples indicates that the calculated ages probably reflect cooling ages through the respective PRZs. We also find that age/grain size (date vs. FT) relationships show no significant trend (see supplemental data; SP1.1), consistent with grains undergoing a relatively simple, monotonic cooling history. Because of this, we use the mean sample ages rather than single grain ages in our interpretations.

It has been well documented in previous studies (e.g Schuster et al., 2006, Flowers et al., 2007, Lee et al., 2013) that samples residing in the PRZ for extended periods of time commonly show a positive correlation between individual grain ages and effective uranium concentration (eU), which represents the alpha radiation dose that a mineral grain would receive. The data presented here were inspected to identify a

possible correlation. However, Figure 1.3 shows no significant correlation between date and eU, probably indicating that the rocks cooled relatively rapidly through the PRZ.

Figure 1.2A illustrates how AHe ages have a trend towards older ages to the north and west and younger ages to the east and south. The oldest AHe ages come from the westernmost samples of the Mokelumne river drainage with a sample dated at 103.0 ± 6.2 Ma and having a corresponding oldest ZHe age at 95.9 ± 7.7 Ma. The youngest ages come from the upper reaches of the Tuolumne and Merced drainages with one AHe as young as 37.7 ± 2.3 Ma. As discussed in subsequent sections, a regional younging trend is observed in the AHe dataset so that the youngest cooling ages are generally observed along the Sierra Crest (Fig. 1.2). ZHe data also display a trend towards younger ages in the east and older ages in the west (Fig. 1.2B). However, the spatial extent of the sample set is significantly smaller than that of the AHe and, therefore, allows less robust information on regional age trends.

An important exception to the regional age trend is the AHe dates from the Emigrant Wilderness. Nearby Miocene volcanics of the Mehrten Formation overlie the granitic basement nonconformably and AHe ages were partially or fully reset. Here, AHe ages are observed as young as 6.3 ± 0.4 Ma and are thought to provide a maximum age for the eruption event as discussed later.

Discussion

Late Mesozoic Cooling Rates

The AHe ages recorded in the SNR span almost 70 Ma. The earliest cooling ages are latest Early Cretaceous (Albian, 103 Ma, SN0802) while the youngest are 31.6 Ma in

the Southern Sierra (i.e. MH97-K9, House et al., 1997; we exclude samples reset by overlying Miocene volcanics in this discussion). Despite the large range in cooling ages, a reproducible and characteristic age distribution occurs in the north, central, and southern regions of the SNR. Figure 1.4 illustrates the distribution of AHe and ZHe ages available from multiple studies. The AHe and ZHe ages appear normally distributed excluding the reset samples. The peak of this distribution occurs between 55 and 65 Ma in the AHe ages and at 65-75 Ma in the ZHe ages. Most AHe cooling ages younger than 60 Ma are from the southern portion of the range.

Because the closure temperatures of in AHe and ZHe systems differ by approximately 90°C, an average erosion rate can be calculated using the time between the systems with following formula:

$$C = \Delta T_C / \Delta A$$

where C is the cooling rate, ΔT_C is the difference in closure temperatures between zircon and apatite (90 °C using 150 °C for zircon and 60 °C for apatite; Reiners, 2005), and ΔA is the difference in AHe and ZHe ages for a given sample. Figure 1.5 shows the results of this calculation, and indicates that erosion rates increased in a systematic fashion from 3-4 °C/My at 95 Ma to over 20 °C/My at 65 Ma. In some samples, AHe and ZHe ages are within error of one another yielding a calculated cooling rate is markedly higher (over 40°C/Ma). All samples that produced both AHe and ZHe ages are included in this plot, and samples from the north SNR (i.e. Cecil et al., 2006) and central SNR (this study) are differentiated by symbol shape. It is apparent that the systematic increase in cooling rates into the late Cretaceous is shared by both the northern and central SNR. As of yet, no

ZHe data exists for the southernmost SNR so this correlation cannot be extended farther south than the Merced drainage.

Early Paleomorphology of the Sierra Nevada Range

We examined dates from all the datasets for the SNR for any correlation between modern topography and AHe ages to assess any paleomorphologic signal for the late Cretaceous to early Cenozoic. As discussed by House and others (1997, 2001), the presence of a direct correlation between He ages and modern high-relief topography would indicate that samples cooled in an environment of regionally horizontal isotherms, reflecting a lack of paleotopography. Because topographic relief in the SNR approaches 2km, it is likely that samples from drainages would have been in their PRZs prior to latest uplift. For that reason, drainage samples should show a consistent signal of younger cooling ages whereas interfluve areas will not. This would be the correlation of young ages with lower elevations and older elevations with higher elevations. Conversely, if the elevations do not correlate with the age, then all samples were at a similar exposure level/depth at the older time of cooling meaning that paleo-isotherms were similar to current landscape features. This would be most consistent with a paleotopography pattern and relief that is like the modern picture of the SNR. Quantification and identification of such a correlation is problematically sensitive to parameters such as paleo-geothermal gradients, regional heat-flow patterns, paleo-lapse rate, and others (Reiners, 2007 and references therein). We think that because our samples are widely distributed and our analysis is along a specific corridor, that any signal in the dates should be recorded regardless of the other parameters.

The topographic/age profile plot shown in Figure 1.6 illustrates mostly a lack of correlation of modern topography with age. A linear fit of ages vs. distance along section is shown, and with only a few notable exceptions, dates fall within 20Ma of the fit. Figure 1.7 shows samples plotted based on whether they are regional and interfluve in scope or from drainage bottoms. Mean ages derived using this distinction are the same within error. We discuss both ways of viewing the data below.

In Figure 1.6 there are 3 locations that show significant deviations from the best-fit line. These are a sample from Kern River Canyon, one from Kings Canyon, and three samples from the Toulemne River Canyon that exhibit ages greater than 20Ma off the linear fit. All these areas have been interpreted have complex incision histories. Both the Kings Canyon and Kern River Canyon are considered to have undergone recent and significant incision (House et al., 1997; House et al.; 2001; Clark et al., 2005; Wakabayashi, 2013 and references therein; Cecil et al., 2014; Krugh and Foreshee, 2018**).** Both areas exhibit distinctive 'inner canyons' and contain fluvial systems that do not appear to be in erosional equilibrium, thus supporting the idea that these canyon systems have a multi-stage incision history. The more recent event was large enough to be reflected in the AHe data by erosion into the PRZ of these samples. The other area is the Toulemne River drainage in Yosemite National Park (labeled TR, Figure 1.6). We suggest that these ages support a previous suggestion that the canyon of the upper Tuolumne River is a younger feature than the geomorphically distinct lower reaches. Unruh (1990) argued that the distribution of volcanic rocks of the Merhten Formation provides evidence that the canyon of the upper Tuolumne River was damned by the widespread Late Miocene volcanic rocks. As a result, the Tuolumne River was diverted

away from the paleochannel and to its present path leading to relatively recent incision of the modern Tuolumne Canyon. In this scenario, the absence of the modern Tuolumne River Canyon would mean that samples 08SNTD01 and 08SNTD04 would have resided approximately 1.5 km or more beneath the surface and possibly in the He PRZ (depending on paleo-geothermal gradients), thus leading to their anomalously young ages. This observation appears to be the first thermochronologic evidence for the recent incision of the upper Tuolumne River canyon, but data supporting this hypothesis would certainly benefit from more thermochronometric data.

Assuming that the 5 samples that deviate from the trend of Figure 1.6 by more than 20Ma are in areas of complex incision history, there is not a correlation of dates with modern elevation; rather, ages are uniform with distance along cross section (with a small trend of younging to the south). Indeed, there is also no tendency for any correlation of scatter to lower ages as drainages are approached. For this reason, we consider this pattern to be most consistent with late Cretaceous and early Cenozoic paleotopography being generally similar to that at present.

An age/elevation plot of all available AHe data for the SNR (excluding thermally reset samples) is shown in Figure 1.7 and further supports this interpretation. Samples here are categorized into either regional interfluve samples or as drainage bottom samples; dissimilar symbols in Figure 1.7 differentiate the age/elevation points based upon this categorization. Using reasoning similar to that outlined above, in a cooling scenario where isotherms are horizontal (e.g. low-topography), samples of relatively high elevation (i.e., interfluve samples) would cool sooner and be older than those from lower elevations (i.e., drainage bottom samples). Conversely, in scenarios where isotherms are

deflected downward beneath topographic lows, samples in drainage bottoms cool nearer to or at the time as higher elevation samples from the surrounding interfluves (see Lee et al., 2013 for more). In this latter case, there should be little difference between drainage and interfluve sample ages, on average. Figure 1.7 illustrates that the mean age difference for drainage and interfluve samples is only 2.9Ma when all samples are considered. Five samples included in this plot yield relatively young ages and are thought to be influenced by late Cenozoic incision of up to 2km of the SNR as discussed in the preceding paragraphs. If these drainage bottom samples are disregarded from the mean ages, then the mean age difference between drainage and interfluve samples shrinks to 0.8Ma, well within the scatter for both area types. This observation indicates that samples in modern topographic lows were cooling, on average, at the same time as samples from the topographically higher drainage divides. This, in turn, supports a scenario in which the drainage samples cooled under paleotopographic lows that were in roughly the same location as modern topographic drainages, and thus arguing for significant paleotopography in the late Cretaceous and early Cenozoic.

Relief Peak Formation Age Constraints

Six samples collected from the Emigrant Wilderness indicate that they were at least partially reset from overlying volcanic rocks of the Relief Peak Formation. These six samples, shown in Figure 1.8 lie adjacent to the volcanic rocks and show ages significantly younger than the cooling ages of other samples from the same batholithic unit: the Topaz Lake granodiorite. We suggest that the youngest of the reset ages offers a maximum age of the overlying volcanic eruptive event. The Relief Peak Formation is part of the regionally extensive Mehrten Formation and was first described by Curtis

(1954). The Mehrten Formation provides an important time marker to help resolve the topographic nature of the Sierra Nevada range at the time of eruption and also provides important constraints of fluvial incision rates (refs in Wakabayashi and Sawyer, 2001). However, the age of the Mehrten formation is not well understood. Dalrymple (1964) presented K/Ar whole rock data for the Relief Peak formation with an age of 9.5 Ma. Additional whole rock K/Ar ages of the Relief Peak formation were published by Morton et al. (1977) and report ages of 19.2 ± 0.8 and 20.0 ± 0.8. Busby et al.'s (2008) more recent study of Sierra Nevadan volcanic rocks reported $^{40}Ar/^{39}Ar$ ages of the Relief Peak formation that are between 10.17 ± 0.18 to 10.35 ± 0.25. These variable results are at odds with a maximum age of 6.3 ± 0.4 Ma as inferred from the reset apatite (U-Th)/He ages presented here. We suggest that the age of the Relief Peak formation still remains unresolved and demands further attention as many of the late Cenozoic erosion rate calculations depend heavily on the age of these late Cenozoic volcanic rocks.

Tectonic Framework

The highest cooling rates in this study correlate temporally with the onset of the Laramide Orogeny in Maastrichtian time (66-75Ma, e.g. Dickenson et al., 1998; Decelles, 2004; Jones et al., 2011). This observation, in addition of the apparent presence of paleotopography of the SNR during the late-Cretaceous and early Cenozoic, augments other lines of geologic evidence supporting the existence of a significantly uplifted and eroded SNR by the early Cenozoic. These additional lines of evidence include Eocene-aged river gravels in the foothills of the SNR have long been used as an argument for early uplift and unroofing (Yeend, 1974; Creely and Force, 2007; Cassel et al., 2009; Henry, 2008; Cecil et al., 2010, Cassel et al., 2012), and various studies addressing stable

isotopic signatures (e.g. Paoge and Chaimberlain, 2002; Horton et al., 2004; Mulch et al., 2006; Crowley et al., 2008; Cassel et al., 2009).

Figure 1.9 compiles some of the major tectonic events associated with the SNR. In it, apparent magmatic flux rates within the Sierra Nevada batholith and convergence rates of the North American and Farallon Plates are shown. Erosion rates from this study, as shown in Figure 1.9, are calculated from the cooling trend identified in Figure 1.4 and assumes a geothermal gradient between 20°C/km and 60°C/km. As noted earlier, the calculated erosion rate rapidly increases through the late Cretaceous and into the early Cenozoic. However, the presence of Cretaceous AHe ages at the surface indicate that the high erosion rates of the late Cretaceous/Early Cenozoic inevitably slowed, as data from the AHe vertical transects of Clark et al., 2005 indicate. These data indicate relatively slow erosion rates of portions the Sierra Nevada Batholith from the early Eocene to the late Miocene.

Conclusions

The data presented in this study sheds light on the nature of the Sierra Nevada with regard to topography and erosion rates in the Cretaceous and early Cenozoic. We augment previous thermochronologic studies with new data from the central part of the SNR and offer a synthesis of all available (U-Th)/He data. AHe ages older than 103 Ma indicate that western portions of the range have undergone relatively little erosion (<3km assuming a geothermal gradient of 20°C/km) since the Albian. However, in the central and eastern portions of the range, cooling rates systematically increased from about 2-4°C/my at 95Ma to rates as high as 40°C/my between 55 and 65 Ma. Although

quantification of the scale of paleotopographic relief is not possible by the techniques undertaken in this study, indications from the data presented here are that the range possessed paleotopographic features that are spatially equivalent to today and that the scale of those features was large enough to deflect isotherms in the AHe partial retention zone. Following rapid exhumation of the batholith before 50 Ma, erosion rates quickly subside by more than an order of magnitude and remain relatively low until the late Miocene to Pliocene, when numerous other studies document late and rapid incision of fluvial valleys and terraces (e.g. Wakabayashi and Sawyer, 2001; Wakabayashi, 2013; Stock et al., 2004; Dalrymple, 1963). It is our assertion that these overall observations are not contradictory. While more recent structural and flexural processes appear to have resulted in renewed uplift and subsequent localized erosion of the Sierra Nevada Range, the data presented here indicate that the late Mesozoic/early Cenozoic SNR was significantly uplifted, probably leaving it topographically high, rugged and eroded to within a just a few kilometers of its present surface.

References Cited

Ague, J.J., and Brimhall, G.H., 1988, Magmatic arc asymmetry and distribution of anomalous plutonic belts in the batholiths of California: Effects of assimilation, crustal thick- ness, and depth of crystallization: Geological Society of America Bulletin, v. 100, p. 912–927.

Blythe, A.E., Longinotti, N., 2013, Exhumation of the southern Sierra Nevada–eastern Tehachapi Mountains constrained by low-temperature thermochronology: Implications for the initiation of the Garlock fault: Lithosphere, v. 5, no. 3, p. 321–327. doi: https://doi-org.www2.lib.ku.edu/10.1130/L252.1

Busby, C.J., DeOreo, S.B., Skilling, I., Gans, P.B., and Hagan, J.C., 2008, Carson Pass–Kirkwood paleocanyon system: Paleogeography of the ancestral Cascades arc and implications for landscape evolution of the Sierra Nevada (California): Geological Society of America Bulletin, v. 120, p. 274-299.

Cassel, E.J., Graham, S.A., and Chamberlain, C.P., 2009, Cenozoic tectonic and topographic evolution of the northern Sierra Nevada, California, through stable isotope paleoaltimetry in volcanic glass: Geology, v. 37, p. 547 - 550.

Cecil M.R., Ducea M.N., Reiners P.W., Chase C.G., 2006, Cenozoic exhumation of the northern Sierra Nevada, California, from (U-Th)/He thermochronology: Geological Society of America Bulletin, v. 118, p. 1481– 148

Chapman, A.D, Wood, D.J., Saleeby, J.B., Saleeby, Z., 2017, Late Cretaceous to early Neogene tectonic development of the southern Sierra Nevada region, California: Field Excursions in Southern California: Field Guides to the 2016 GSA Cordilleran Section Meeting.

Chen, J.H. and Moore, J.G., 1982, Uranium-lead isotopic ages from the Sierra Nevada Batholith, California: Journal of Geophysical Research, v. 87, p.4761-4784.

Christensen, M.N., 1966, Late Cenozoic crustal movements of the Sierra Nevada of California: Geological Society of America Bulletin, v.77, p163-182.

Clark, M.K., Maheo, G., Saleeby, J., and Farley, K.A., 2005, The non-equilibrium landscape of the southern Sierra Nevada, California: GSA Today, v. 15, no. 9, p. 4–10, doi: 10.1130/1052-5173(2005)015[4:TNLOTS]2.0.CO;2.

Clark, M.K., Maheo, G., Saleeby, J., and Farley, K.A., 2001, The non-equilibrium landscape of the southern Sierra Nevada, California: GSA Today, v.15, p. 4-10.Clark et al., 2001

Creely S., Force E.R., 2007, Type region of the Ione Formation (Eocene), central California: Stratigraphy, paleogeography, and relation to Auriferous Gravels: U.S. Geological Survey Open-File Report 2006–1378, 65 p

Curtis, G. H., 1954, Mode and Origin of the Pyroclastic Debris in the Mehrten Formation of the Sierra Nevada: Univeristy of California Science Bulletin. v. 29. p. 453-502.

Dalrymple, G.B., 1964, Cenozoic Chronology of the Sierra Nevada, California: University of California Publishing, 41p

Dalrymple, G.B., 1963, Potassium-argon dates of some Cenozoic volcanic rocks of the Sierra Nevada: Geological Society of America Bulletin, v. 74 p. 379-390

DeCelles P.G., 2004, Late Jurassic to Eocene evolution of the Cordilleran thrust belt and foreland basin system, western U.S.A.: American Journal of Science, v. 304, p. 105–168

Dickinson, W.R., 2004, Evolution of the North American Cordillera: Annual Review of Earth and Planetary Sciences, v. 32, p. 13-45

Dubrovine, P.V., and Tarduno, J.A., 2008, A revised kinematic model for the relative motion between Pacific oceanic plates and North America since the Late Cretaceous: Journal of Geophysical Research, v. 113, p. 1-20

Ducea, M.N, 2001, The California Arc; thick granitic batholiths, eclogitic residues, lithospheric-scale thrusting, and magmatic flare-ups: GSA Today, v.11, p. 4-10

England, P., and Molnar, P., 1990, Surface uplift, uplift of rocks, and exhumation of rocks: Geology, v. 18, no. 12, p. 1173–1177

Farmer, L.G., Glazner, A.F., and Manley, C.R., 2002, Did lithospheric delamination trigger late Cenozoic potassic volcanism in the southern Sierra Nevada, California?: Geological Society of America Bulletin, v.114, p.754 - 768.

Farley, K.A., 2002, (U-Th)/He Dating: Techniques, Calibrations, and Applications: Reviews in Mineralogy and Geochemistry, v. 47, no. 1, p. 819–844. doi: https://doi-org.www2.lib.ku.edu/10.2138/rmg.2002.47.18

Farley, K,A., 2000, Helium diffusion from apatite: General behavior as illustrated by durango fluorapatite: Journal of Geophysical Research, v. 105, p. 2903–2914.

Farley, K.A., Wolf, R.A., and Silver, L.T., 1996, The effects of long alpha-stopping distances on (U-Th)/He ages: Geochimica Cosmochimica Acta, v. 60, p. 4223–4229.

Flowers, R.M., Shuster, D.L., Wernicke, B.P., Farley, K.A., 2007, Radiation damage control on apatite (U-Th)/He dates from the Grand Canyon region, Colorado Plateau:Geology, v. 35. no. 5, p. 447–450

Hammond, W.C., Blewitt, G., Kreemer, C., 2016, GPS imaging of vertical land motion in California and Nevada; implications for Sierra Nevada uplift: Journal of Geophysical Research: Solid Earth, v. 121, no. 10, p. 7681-7703

Hammond, W.C., Blewitt, G., Li, C., Plag, H.P., and Kreemer, C., 2012, Contemporary uplift of the Sierra Nevada, western United States, from GPS and InSAR measurements: Geology, v. 40, p. 667–670, doi:10.1130 /G32968.1.

Henry, C.D., 2009, Uplift of the Sierra Nevada, California: Geology, v.37, p. 575 - 576.

Henry, C.D., 2008, Ash-flow tuffs and paleovalleys in north- eastern Nevada: Implications for Eocene paleogeog- raphy and extension in the Sevier hinterland, northern Great Basin: Geosphere, v. 4, p. 1–35, doi: 10.1130 /GES00122.1.

Horton, T.W., Sjostrom, D.J., Abruzzese, M.J., Poage, M.A., Waldbauer, J.R., Hren, M., Wooden, J., and Chamberlain, C.P., 2004, Spatial and temporal variation of Cenozoic surface elevation in the Great Basin and Sierra Nevada: American Journal of Science, v. 304 p. 862-888

House, M.A., Wernicke,, B.P., and Farley, K.A., 2001, Paleo-geomorphology of the Sierra Nevada, California, from (U-Th)/He ages in apatite: American Journal of Science, v. 301, p. 77-102

House, M.A., Wernicke, B.P., Farley, K.A., and Dumitru, T.A., 1997, Cenozoic thermal evolution of the central Sierra Nevada, California, from (U-Th)/He thermochronometry: Earth and Planetary Science Letters, v. 151, p.167-179.

Huber, N.K., 1990, The late Cenozoic evolution of the Tuolumne River, central Sierra Nevada, California: Geological Society of America Bulletin, v. 102, p. 102–115, doi:10.1130/0016-7606(1990)102<0102:TLCEOT>2.3 .CO;2.

Jones, C.H., Reeg, H., Zandt, G., Gilbert, H., Owens, T.J., Stachnik, J., 2014, P-wave tomography of potential convective downwellings and their source regions, Sierra Nevada, California: Geosphere, v. 10, no. 3, p. 505-533

Jones, C.H., Saleeby, J.B., 2013, Introduction: Geodynamics and Consequences of Lithospheric Removal in the Sierra Nevada, California: Geosphere, v. 9, no. 2, p. 188–190. doi: https://doi-org.www2.lib.ku.edu/10.1130/GES00907.1

Jones, C.H., Farmer, G.L., Sageman, B., Zhong, S., 2011, Hydrodynamic mechanism for the Laramide orogeny. Geosphere, v. 7, no. 1, p. 183–201. doi: https://doi-org.www2.lib.ku.edu/10.1130/GES00575.1

Lee, J.P., Stockli, D.F., Kelley, S.A., Pederson, J.L., Karlstrom, K.E., Ehlers, T.A., 2013, New thermochronometric constraints on the Tertiary landscape evolution of the central and eastern Grand Canyon, Arizona: Geosphere, v. 9, p. 216-228.

Martel, S.J., Stock, G.M., Ito, G., 2014, Mechanics of relative and absolute displacements across normal faults, and implications for uplift and subsidence along the eastern escarpment of the Sierra Nevada, California: Geosphere, v. 10, no. 2, p. 243–263. doi: https://doi-org.www2.lib.ku.edu/10.1130/GES00968.1

McPhillips, D., and Brandon, M.T., 2012, Topographic evolution of the Sierra Nevada measured directly by inversion of low-temperature thermochronology: American Journal of Science, v. 312, p. 90–116, doi:10.2475 /02.2012.02.

Molnar, P., 2010, Deuterium and oxygen isotopes, paleoelevations of the Sierra Nevada, and Cenozoic climate: Geological Society of America Bulletin, v. 122, p. 1106–1115, doi:10.1130/B30001.1.

Morton, J.L., Silberman, M.L., Bonham, H.F., Garside, L.J., and Noble, D.C., 1977, K-Ar ages of volcanic rocks, plutonic rocks, and ore deposits in Nevada and eastern California—Determinations run under the USGS-NBMG cooperative program: Isochron/West, v. 20 p. 19-29

Mulch A., Graham S.A., Chamberlain C.P., 2006, Hydrogen isotopes in Eocene river gravels and paleoelevation of the Sierra Nevada: Science, v. 313, p. 87–89

Poage, M.A., and Chamberlain, C.P., 2002, Stable isotopic evidence for a pre-middle Miocene rain shallow in the western Basin and Range; implications for the paleotopography of the Sierra Nevada: Tectonics, v. 21, p. 1034

Reiners, P.W., 2007, Thermochronologic Approaches to Paleotopography: Reviews in Mineralogy and Geochemistry, v. 66, no. 1, p. 243–267. doi: https://doi-org.www2.lib.ku.edu/10.2138/rmg.2007.66.10

Reiners, P.W., 2005, Zircon (U-Th)/He Thermochronometry: Reviews in Mineralogy and Geochemistry, 2005, v. 58, p. 151-179

Reiners, P.W., Ehlers, T.A., 2005, Low-temperature thermochronology; techniques, interpretations, and applications: Reviews in Mineralogy and Geochemistry, v. 58, p. 622

Putirka, K., and Busby, C.J., 2007, The tectonic significance of high-K_2O volcanism in the Sierra Nevada, California: Geology, v. 35, p. 923–926, doi:10.1130/G23914A.1.

Saleeby, J. and Foster, Z., 2004, Topographic response to mantle lithosphere removal in the southern Sierra Nevada region, California: Geology, v. 32, p. 245 - 248.

Shuster, D.L., Flowers, R.M., Farley, K.A., 2006, The influence of natural radiation damage on helium diffusion kinetics in apatite: Earth and Planetary Science Letters, v. 249, no. 3, p. 148-161

Small, E.E., and Anderson, R.S., 1995, Geomorphically driven late Cenozoic rock uplift in the Sierra Nevada, California: Science, v. 270, p. 277–281, doi:10.1126 /science.270.5234.277.

Stock, G.M., Anderson, R.S., and Finkel, R.C., 2005, Rates of erosion and topographic evolution of the Sierra Nevada, California, inferred from cosmogenic ^{26}Al and ^{10}Be concentrations: Earth Surface Processes and Landforms, v. 30, p. 985–1006, doi:10.1002/esp .1258.

Stock, G.M., Anderson, R.S., and Finkel, R.C., 2004, Pace of landscape evolution in the Sierra Nevada, California, revealed by cosmogenic dating of cave sediments: Geology, v. 32, p. 193 - 196.

Stockli, D.F., Farley, K.A., and Dumitru, T.A., 2000, Calibration of the apatite (U-Th)/He thermochronometer on an exhumed fault block, White Mountains, California: Geology, v. 28, p. 983–986.

Unruh, J.R., 1991, The uplift of the Sierra Nevada and implications for late Cenozoic epeirogeny in the western Cordillera: GSA Bulletin, v. 103, no. 11, p. 1395, 1404.

Vermeesch, P., 2008, Three new ways to calculate average (U-Th)/He ages: Chemical Geology, v. 249, p. 339-347, doi:10.1016/j.chemgeo.2008.01.027.

Wakabayashi, J., 2013, Paleochannels, stream incision, erosion, topographic evolution, and alternative explanations of paleoaltimetry, Sierra Nevada, California. Geosphere, v. 9, no. 2, p. 191–215. doi: https://doi-org.www2.lib.ku.edu/10.1130/GES00814.1

Wakabayashi, J. and Sawyer, T.L., 2001, Stream incision, tectonics, uplift, and evolution of topography of the Sierra Nevada, California: Journal of Geology, v.109 p.539-562.

Wernicke, B.P., and 18 others, 1996, Origin of high mountains in the continents: The southern Sierra Nevada: Science, v. 271, p. 190–193, doi:10.1126/science.271.5246.190.

Yeend, W.H., 1974, Gold Bearing Gravel of the Ancestral Yuba River, California: U.S. Geological Survey Professional Paper. n. 72.

Zandt, G., Gilbert, H., Owens, T.J., Ducea, M., Saleeby J.B., Jones, C.H., 2004, Active foundering of a continental arc root beneath the southern Sierra Nevada in California: Nature, v. 431, p. 41-46

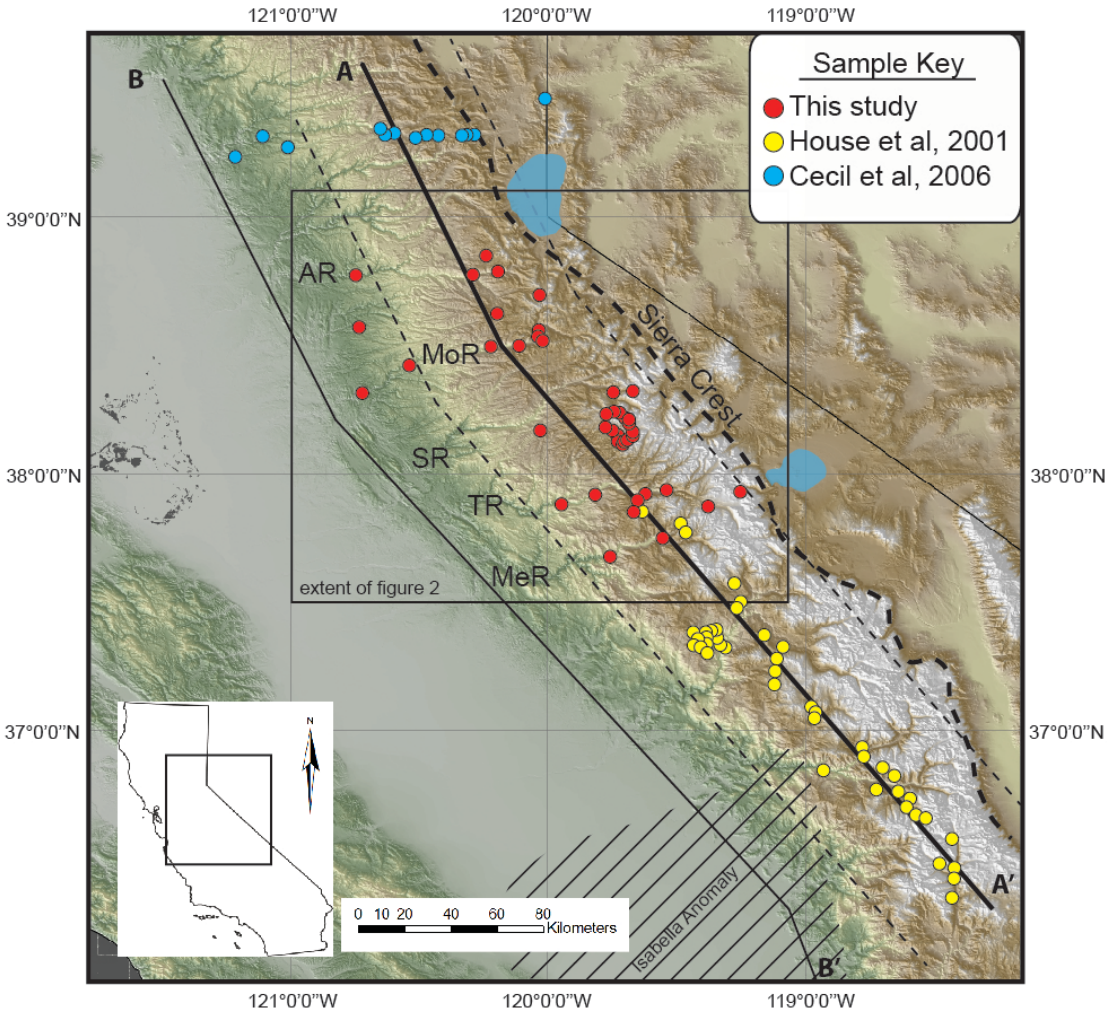
121°0'0"W
120°0'0"W
119°0'0"W
39°0'0"N
38°0'0"N
37°0'0"N
B
A
Sample Key
This study
House et al, 2001
Cecil et al, 2006
AR
MoR
SR
TR
MeR
Sierra Crest
extent of figure 2
Isabella Anomaly
A'
B'
0 10 20 40 60 80
Kilometers
N

Figure 1.1

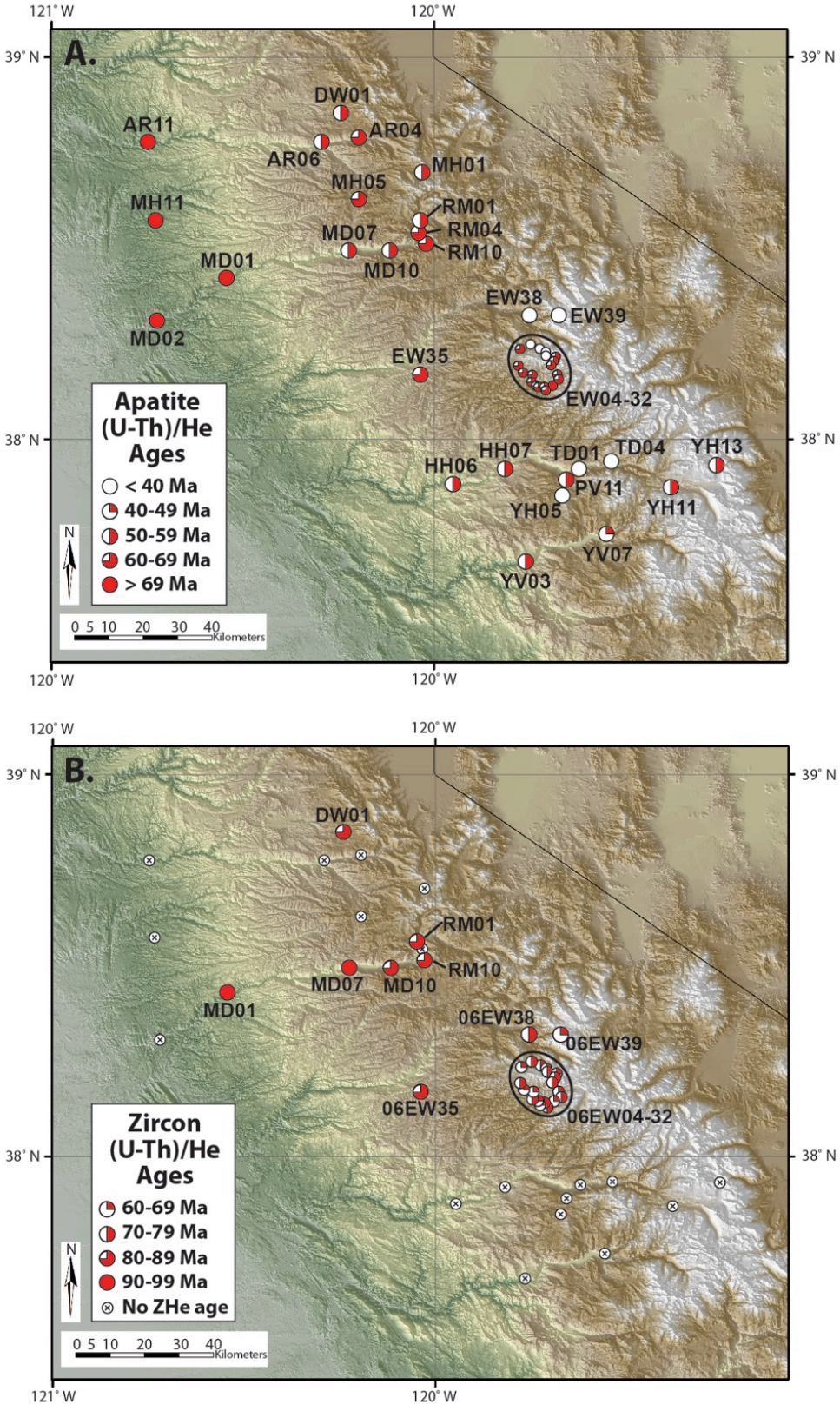
A.
121° W
120° W
39° N
38° N
DW01
AR11
AR04
AR06
MH01
MH05
MH11
RM01
RM04
MD07
RM10
MD01
MD10
EW38
EW39
MD02
EW35
EW04-32
Apatite (U-Th)/He Ages
< 40 Ma
40-49 Ma
50-59 Ma
60-69 Ma
> 69 Ma
HH07
TD01
TD04
YH13
HH06
PV11
YH05
YH11
YV07
YV03
N
0 5 10 20 30 40 Kilometers
B.
06EW38
06EW39
06EW35
06EW04-32
Zircon (U-Th)/He Ages
60-69 Ma
70-79 Ma
80-89 Ma
90-99 Ma
No ZHe age

Figure 1.2

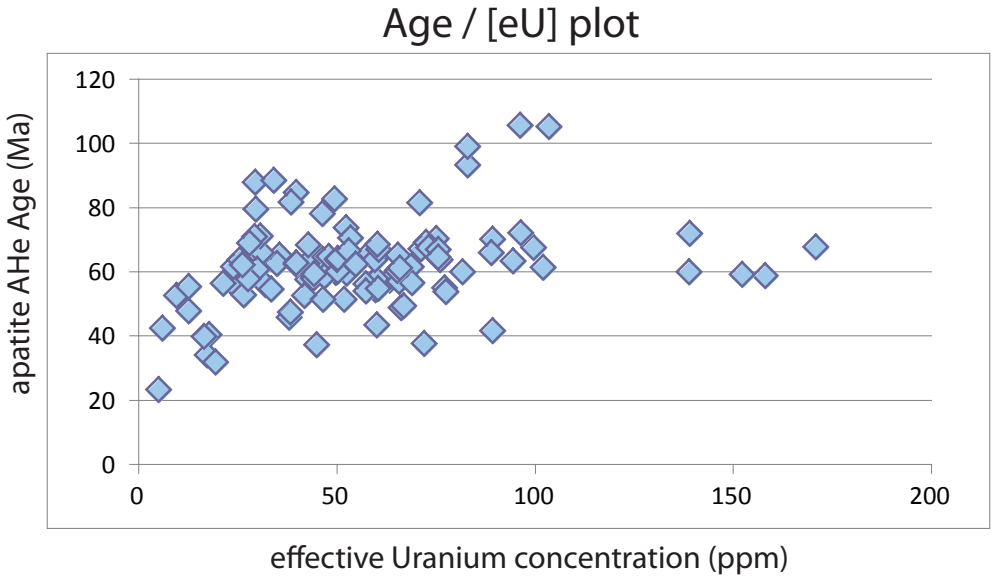
Age / [eU] plot
apatite AHe Age (Ma)
120
100
80
60
40
20
0
0
50
100
150
200
effective Uranium concentration (ppm)

Figure 1.3

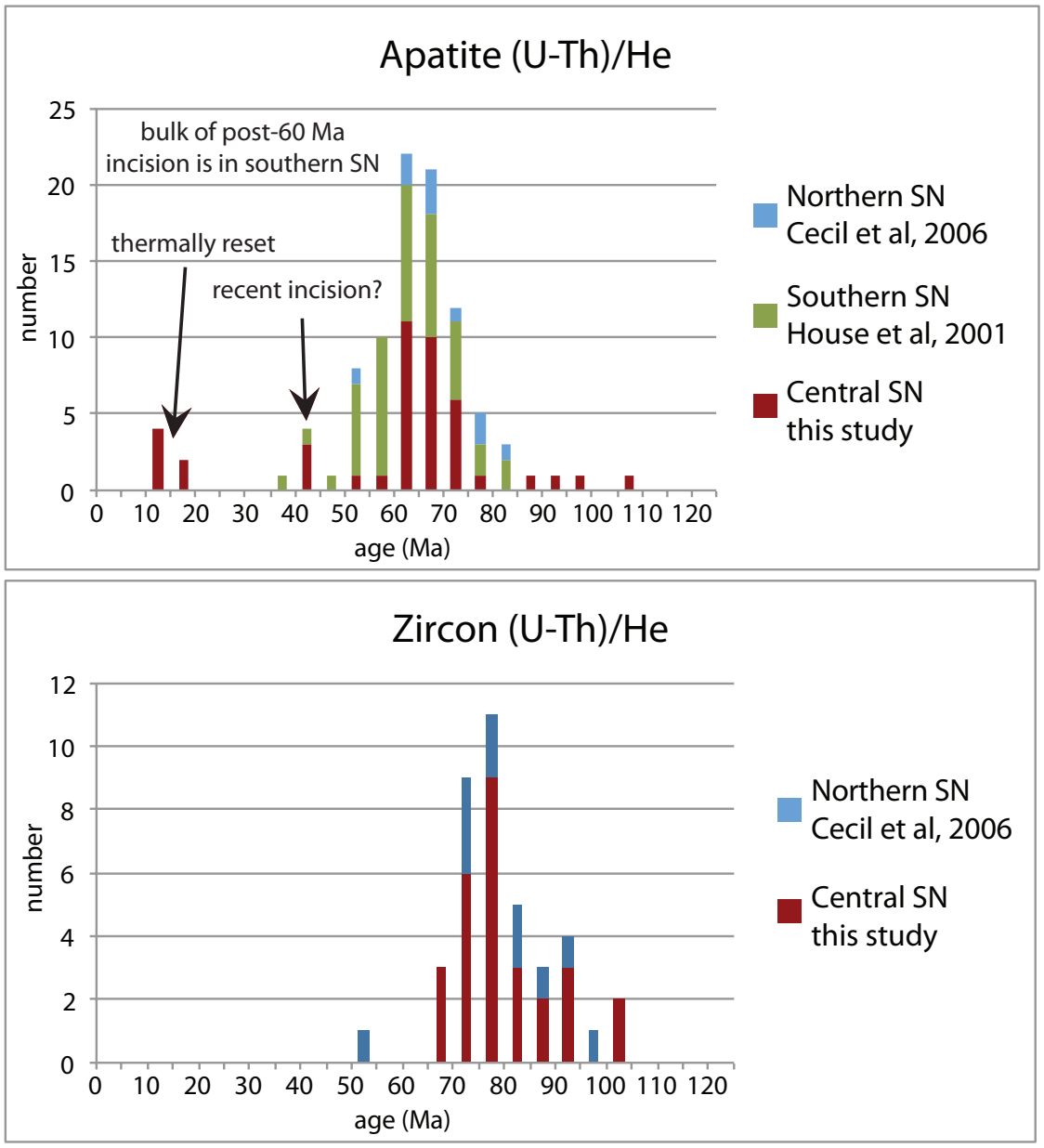
Apatite (U-Th)/He
bulk of post-60 Ma
incision is in southern SN
thermally reset
recent incision?
number
age (Ma)
Northern SN
Cecil et al, 2006
Southern SN
House et al, 2001
Central SN
this study
Zircon (U-Th)/He
number
age (Ma)
Northern SN
Cecil et al, 2006
Central SN
this study

Figure 1.4

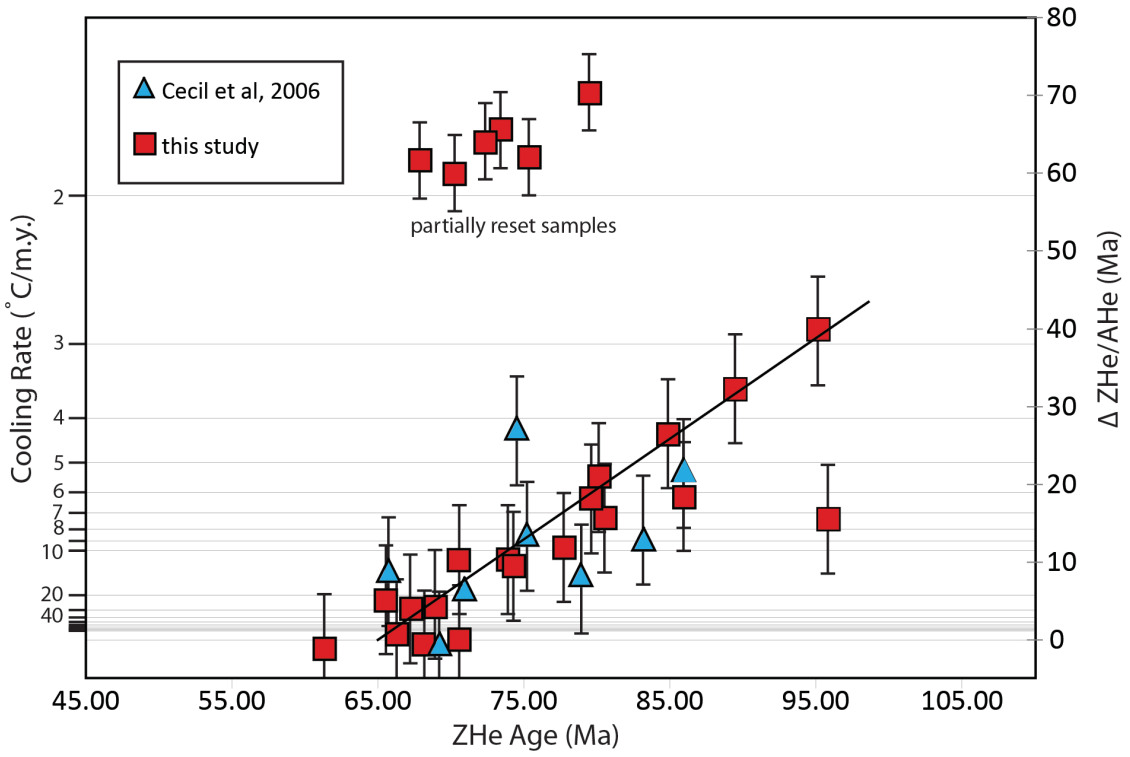
Cecil et al, 2006
this study
partially reset samples
Cooling Rate (˚C/m.y.)
2
3
4
5
6
7
8
10
20
40
45.00
55.00
65.00
75.00
85.00
95.00
105.00
ZHe Age (Ma)
80
70
60
50
40
30
20
10
0
Δ ZHe/AHe (Ma)

Figure 1.5

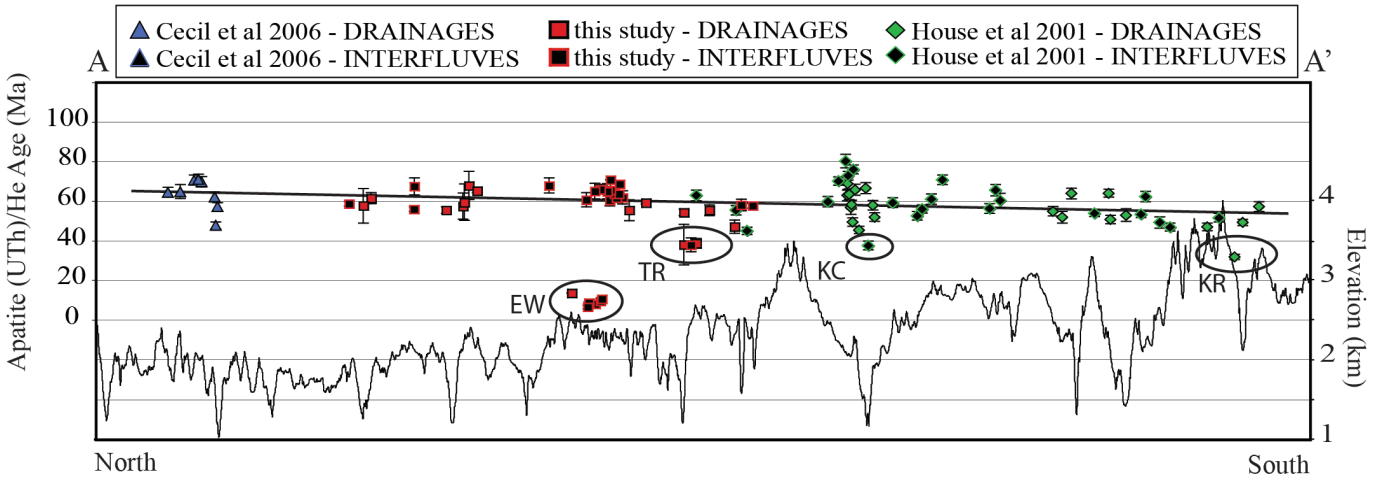
Cecil et al 2006 - DRAINAGES
Cecil et al 2006 - INTERFLUVES
this study - DRAINAGES
this study - INTERFLUVES
House et al 2001 - DRAINAGES
House et al 2001 - INTERFLUVES
A
A'
Apatite (UTh)/He Age (Ma)
100
80
60
40
20
0
4
3
2
1
Elevation (km)
EW
TR
KC
KR
North
South

Figure 1.6

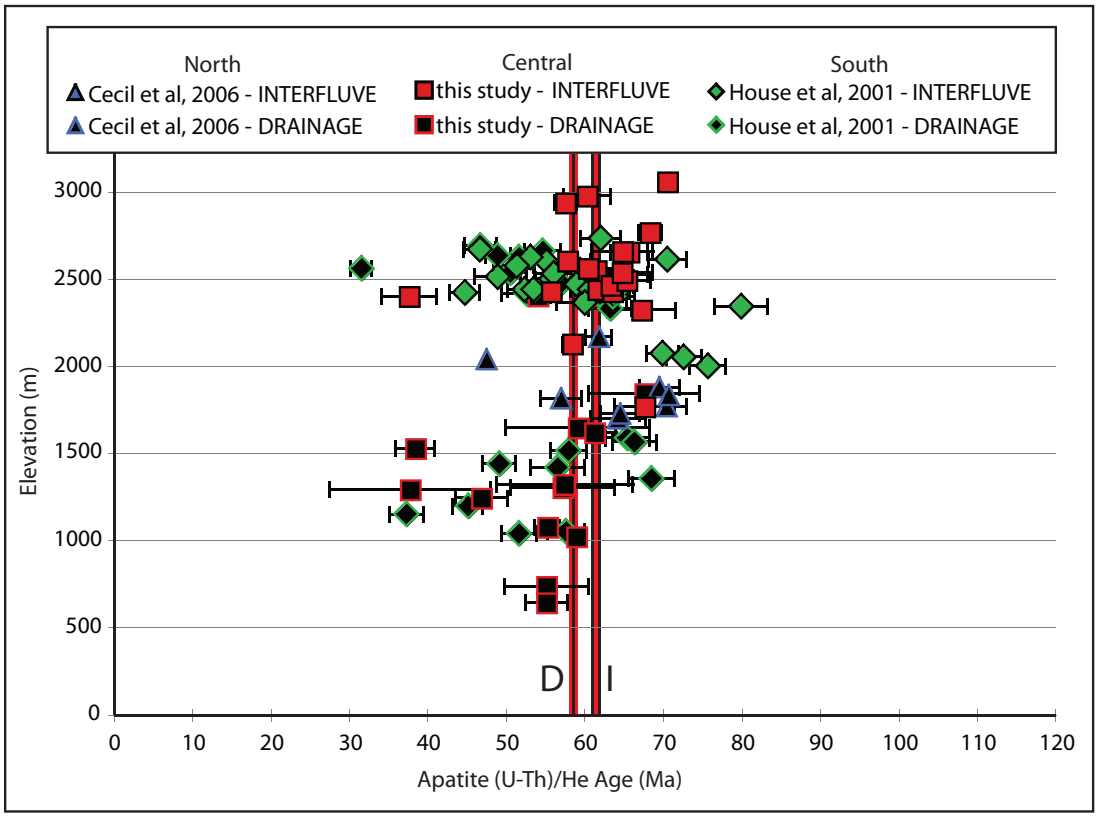
North
Cecil et al, 2006 - INTERFLUVE
Cecil et al, 2006 - DRAINAGE
Central
this study - INTERFLUVE
this study - DRAINAGE
South
House et al, 2001 - INTERFLUVE
House et al, 2001 - DRAINAGE
Elevation (m)
3000
2500
2000
1500
1000
500
0
D
I
0
10
20
30
40
50
60
70
80
90
100
110
120
Apatite (U-Th)/He Age (Ma)

Figure 1.7

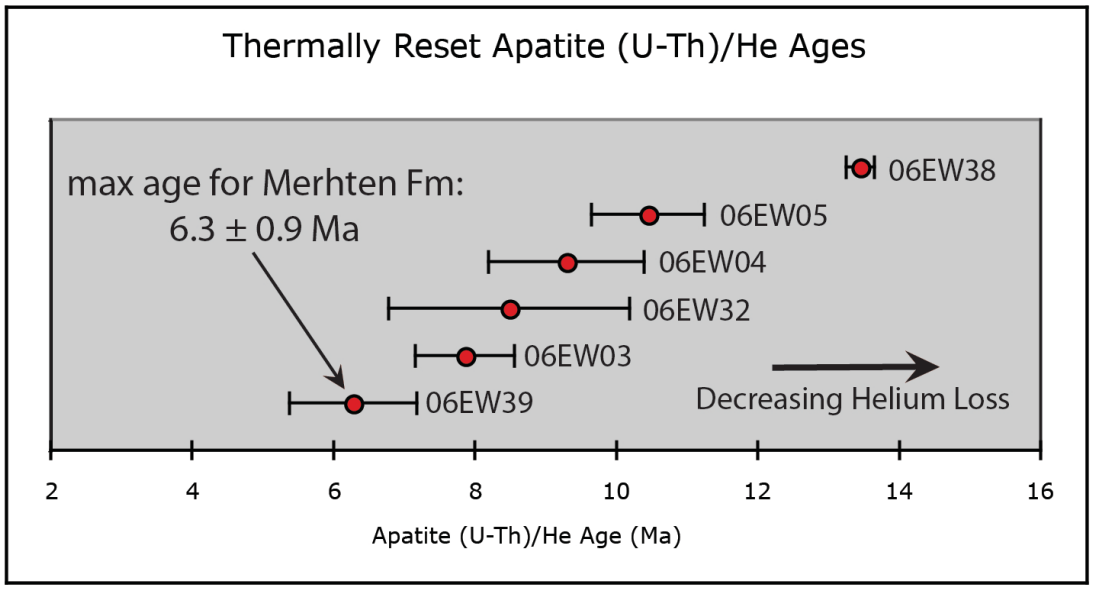
Thermally Reset Apatite (U-Th)/He Ages
max age for Merhten Fm:
6.3 ± 0.9 Ma
06EW38
06EW05
06EW04
06EW32
06EW03
06EW39
Decreasing Helium Loss
2
4
6
8
10
12
14
16
Apatite (U-Th)/He Age (Ma)

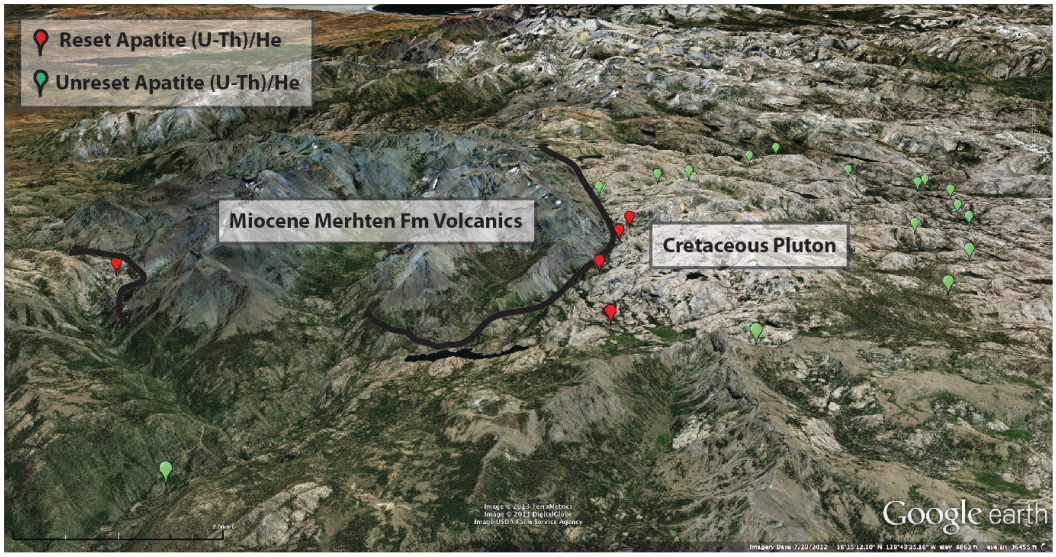
Reset Apatite (U-Th)/He
Unreset Apatite (U-Th)/He
Miocene Merhten Fm Volcanics
Cretaceous Pluton
Google earth

Figure 1.8

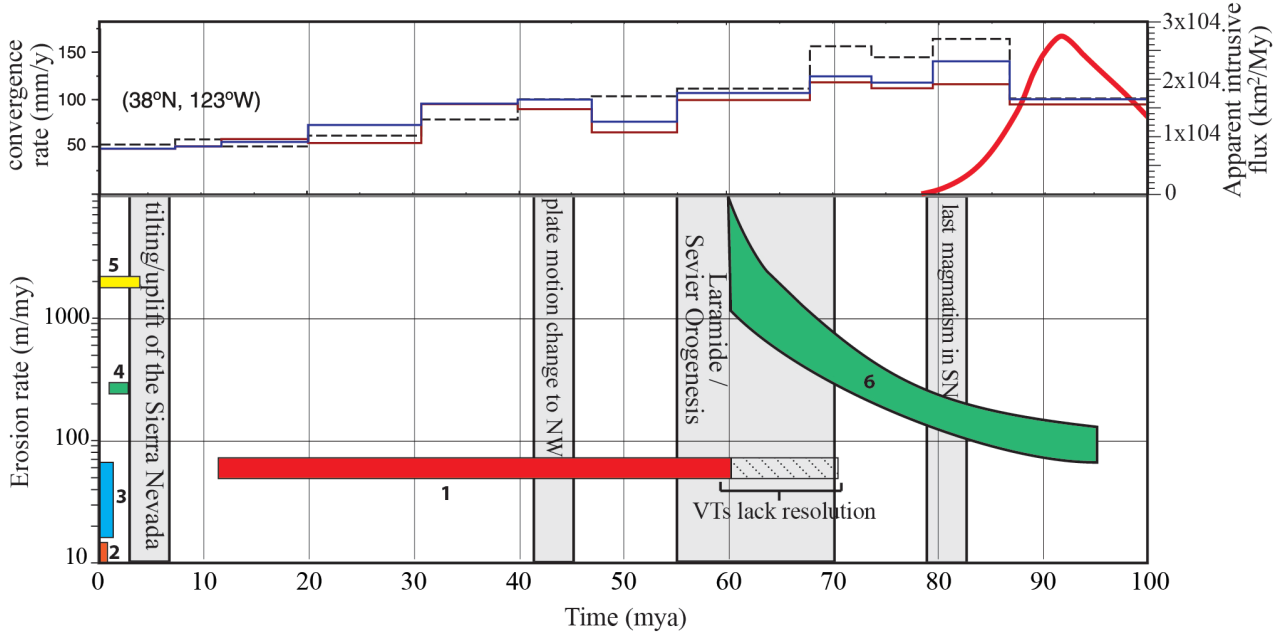
convergence rate (mm/y)
150
100
50
(38°N, 123°W)
3x104
2x104
1x104
0
Apparent intrusive flux (km²/My)
Erosion rate (m/my)
1000
100
10
5
4
3
2
1
6
tilting/uplift of the Sierra Nevada
plate motion change to NW
Laramide / Sevier Orogenesis
last magmatism in SN
VTs lack resolution
0
10
20
30
40
50
60
70
80
90
100
Time (mya)

Figure 1.9

Table 1.1 Mean apatite and zircon (U-Th)/He ages

Sample Information				Apatite (U-Th)/He Information						Zircon (U-Th)/He Information				
Sample Group	**Sample Identification**	**LATITUDE (°N)**	**LONGITUDE (°W)**	**elevation (m)**	**eU (ppm)**	**FT**	**number of analysis**	**Age (Ma)**	**2σ (Ma)**	**eU (ppm)**	**FT**	**number of analysis**	**Age (Ma)**	**2σ (Ma)**
Tuolumne Drainage	SN08HH06	37.8793	119.9486	733	59.6	0.67	3	55.2	3.3	-	-	-	-	-
Tuolumne Drainage	SN08HH07	37.9224	119.8153	1020	150	0.68	3	59.0	3.5	-	-	-	-	-
Tuolumne Drainage	SN08TD01	37.9216	119.6202	1288	21.6	0.65	5	37.8	2.3	-	-	-	-	-
Tuolumne Drainage	SN08TD04	37.9395	119.5364	1525	69	0.62	3	38.5	2.3	-	-	-	-	-
Merced Drainage	SN08YV03	37.6791	119.7608	640	48	0.64	3	55.2	3.3	-	-	-	-	-
Merced Drainage	SN08YV07	37.7511	119.5508	1241	64.7	0.62	3	46.9	2.8	-	-	-	-	-
Tuolumne/Merced Interfleuve	SN08YH05	37.8509	119.6637	2400	17.5	0.61	3	37.7	2.3	-	-	-	-	-
Tuolumne/Merced Interfleuve	SN08YH11	37.8736	119.3769	2602	23.2	0.68	3	57.9	3.5	-	-	-	-	-
Tuolumne/Merced Interfleuve	SN08YH13	37.9293	119.2539	2935	57.7	0.60	3	57.6	3.5	-	-	-	-	-
Tuolumne/Merced Interfleuve	SN08PV11	37.8928	119.6531	2403	31	0.63	3	54.1	3.2	-	-	-	-	-
Mokelumne/American Interfleuve	SN08MH01	38.6992	120.0309	2426	70.9	0.59	3	55.8	3.3	-	-	-	-	-
Mokelumne/American Interfleuve	SN08MH05	38.6251	120.1969	2321	135	0.60	3	67.3	4.0	-	-	-	-	-
Mokelumne/American Interfleuve	SN08MH11	38.5711	120.7331	2032	83.4	0.65	1	90.3	5.4	-	-	-	-	-
Desolation Wilderness	SN08DW01	38.8509	120.2391	2125	45.7	0.61	3	58.5	3.5	494.0	0.84	3	84.9	6.8
Mokelumne Drainage	SN08MD01	38.4231	120.5409	703	55.9	0.60	3	80.4	4.8	468.0	0.79	2	95.9	7.7
Mokelumne Drainage	SN08MD02	38.3135	120.7207	204	94.5	0.57	3	103.0	6.2	-	-	-	-	
Mokelumne Drainage	SN08MD07	38.4939	120.2229	1074	61.6	0.66	3	55.3	3.3	512.0	0.84	3	95.2	7.6
Mokelumne Drainage	SN08MD10	38.4978	120.1130	1301	19.5	0.59	3	57.3	3.4	283.0	0.82	3	89.5	7.2
Mokelumne Drainage	SN08RM01	38.5589	120.0372	1643	71.2	0.50	3	59.2	3.6	780.0	0.80	3	80.2	6.4
Mokelumne Drainage	SN08RM04	38.5397	120.0352	1842	52.3	0.63	3	67.7	4.1	-	-	-	-	
Mokelumne Drainage	SN08RM10	38.5140	120.0225	2498	39.8	0.48	2	65.0	3.9	575.0	0.80	1	80.6	6.4
American River Drainage	SN08AR04	38.7875	120.1947	1618	45.5	0.61	3	61.3	3.7	-	-	-	-	
American River Drainage	SN08AR06	38.7736	120.2932	1320	32.9	0.65	3	57.5	3.5	-	-	-	-	
American River Drainage	SN08AR11	38.7761	120.7481	395	34.7	0.54	3	86.6	5.2	-	-	-	-	

Table 1.1 Mean apatite and zircon (U-Th)/He ages (continued)

Sample Information					Apatite (U-Th)/He Information					Zircon (U-Th)/He Information				
Sample Group	**Sample Identification**	**LATITUDE (°N)**	**LONGITUDE (°W)**	**elevation (m)**	**eU (ppm)**	**FT**	**number of analysis**	**Age (Ma)**	**2σ (Ma)**	**eU (ppm)**	**FT**	**number of analysis**	**Age (Ma)**	**2σ (Ma)**
Emigrant Wilderness	06EW - 03	38.2376	119.7230	2530	25.6	0.73	3	7.9	0.5	863.0	0.75	3	73.5	5.9
Emigrant Wilderness	06EW - 04	38.2256	119.7089	2591	26.2	0.75	3	9.3	0.6	819.0	0.71	2	79.5	6.4
Emigrant Wilderness	06EW - 05	38.2213	119.7057	2685	27.8	0.73	3	10.4	0.6	519.0	0.80	3	70.3	5.6
Emigrant Wilderness	06EW - 06	38.2168	119.6815	2774	-	-	-	-		939.9	0.78	3	64.9	5.2
Emigrant Wilderness	06EW - 08	38.2033	119.6867	2974	28.0	0.70	3	60.4	3.6	835.5	0.76	3	70.6	5.6
Emigrant Wilderness	06EW - 09	38.1968	119.6908	3056	30.1	0.73	3	70.6	4.2	704.6	0.78	2	70.6	5.6
Emigrant Wilderness	06EW - 11	38.1670	119.6748	2765	78.0	0.72	3	68.4	4.1	440.3	0.80	3	68.2	5.5
Emigrant Wilderness	06EW - 13	38.1550	119.6709	2807	-	-	-	-		503.5	0.77	3	71.2	5.7
Emigrant Wilderness	06EW - 15	38.1422	119.6887	2438	68.7	0.73	3	61.7	3.7	384.9	0.83	3	61.0	4.9
Emigrant Wilderness	06EW - 21	38.1383	119.7245	2548	48.2	0.71	3	61.5	3.7	684.1	0.71	3	79.6	6.4
Emigrant Wilderness	06EW - 22	38.1423	119.7314	2426	46.6	0.70	3	63.6	3.8	242.7	0.81	3	73.9	5.9
Emigrant Wilderness	06EW - 23	38.1300	119.7071	2396	-	-	-	-		836.3	0.80	2	64.8	5.2
Emigrant Wilderness	06EW - 24	38.1375	119.7118	2463	67.7	0.71	3	63.4	3.8	471.2	0.78	3	67.3	5.4
Emigrant Wilderness	06EW - 26	38.1498	119.7423	2491	50.4	0.71	3	65.4	3.9	470.6	0.77	1	77.6	6.2
Emigrant Wilderness	06EW - 27	38.1662	119.7409	2536	65.7	0.67	1	64.8	3.9	537.1	0.78	3	69.0	5.5
Emigrant Wilderness	06EW - 29	38.1748	119.7657	2655	75.3	0.70	3	65.7	3.9	494.7	0.81	3	66.4	5.3
Emigrant Wilderness	06EW - 30	38.1916	119.7766	2658	71.8	0.70	3	64.9	3.9	333.3	0.78	3	74.3	5.9
Emigrant Wilderness	06EW - 31	38.2333	119.7730	2560	33.8	0.72	3	60.5	3.6	606.3	0.81	3	65.6	5.2
Emigrant Wilderness	06EW - 32	38.2465	119.7453	2380	29.4	0.74	3	8.5	0.5	733.7	0.81	3	72.4	5.8
Emigrant Wilderness	06EW - 35	38.1719	120.0330	1765	90.8	0.70	3	67.7	4.1	96.3	0.80	3	86.0	6.9
Emigrant Wilderness	06EW - 38	38.3210	119.7496	1927	31.1	0.75	3	13.4	0.8	893.9	0.75	3	75.4	6.0
Emigrant Wilderness	06EW - 39	38.3194	119.6707	2586	22.5	0.76	3	6.3	0.4	711.5	0.79	3	67.9	5.4

FIGURE CAPTIONS

Figure 1.1. A relief map of the central Sierra Nevada showing sample locations, major drainages, and the cross section lines are referred to in the text. The drainages are as follows: AR is the American River, MoR is the Mokelumne River, SR is the Stanislaus River, TR is the Tuolumne River, MeR is the Merced River.

Figure 1.2. A relief map showing sample localities and (U-Th)/He ages. Both apatite and zircon (U-Th)/He ages are shown where available. The high sample density of the Emigrant Wilderness is shown as a grouping. Specific ages are not shown here for clarity. Refer to Tables 1 and 2 for corresponding data.

Figure 1.3. An apatite (U-Th)/He cooling age vs eU plot of data presented in this study. As noted in the text, the lack of a strong correlation between age and the effective uranium concentration (eU) indicates that samples cooled quickly through the partial retention zone (i.e 40°C – 80°C). For clarification, 6 samples (18 analyses) that underwent thermal resetting were excluded from this plot.

Figure 1.4. Histograms of apatite and zircon (U-Th)/He data from this study and others. Ages are divided into bins based upon 5 million year increments.

Figure 1.5. A plot of cooling rate vs time for all samples yielding both apatite and zircon (U-Th)/He ages. Cooling rate is derived from the difference between the zircon (U-

Th)/He age and the apatite (U-Th)/He age. The closure temperatures for each system are 150°C for zircon and 60°C for apatite (see Reiners, 2005).

Figure 1.6. A plot of apatite (U-Th)/He ages across a range-parallel topographic projection of the Sierra Nevada range. The axis used for the topographic projection is shown in Figure 1 as cross section line A-A'. Because a West-East age trend exists, samples collected further than 40 kilometers from the cross section line are excluded from this graph. The dashed lines parallel to cross section line A-A' indicates a distance of 40 km. As a result, 4 samples from this study and 4 samples from Cecil et al., 2006, are excluded. Black- or color-filled symbols indicate samples near drainages or regional interfluves. Ovals around data identify groups of data where AHe ages are observed that vary greater than 20Ma from the statistically derived linear fit shown. The equation for the linear fit is $y = -3.0x+65$, where y is the age and x is the distance along cross section line A-A'. TR identifies samples from the Tuolumne River Canyon. KR is Kern River Canyon; KC is Kings Canyon. EW identifies thermally reset samples from the Emigrant Wilderness.

Figure 1.7. An Age/Elevation plot of apatite (U-Th)/He data from the Sierra Nevada Range. The mean sample age for drainages and interfluves are indicated by the colored vertical lines labeled D and I, respectively. Sources of data are differentiated by symbol. Black- or color-filled symbols differentiate the proximity of samples to drainages or regional interfluves. Samples collected further than 40 kilometers from the cross section line A-A' (figure 1) are excluded from this graph. The dashed lines parallel to cross

section line A-A' indicates a distance of 40 km. Four samples from this study and 4 samples from Cecil et al., 2006, are excluded from this graph. Thermally reset samples from the Emigrant Wilderness are not included for clarity. The mean drainage age is 58.5Ma and the mean interfluve age is 61.4Ma (excluding thermally reset samples).

Figure 1.8. Thermally reset apatite (U-Th)/He age data from the Emigrant Wilderness. Increasingly reset ages are a result of thermal heating due to the late eruption and deposition of the relief Peak formation. Reset samples were all collected from Cretaceous granite.

Figure 1.9. A compilation of erosion rates through time as measured in several studies. Tectonic data, are compiled by DeCelles (2004) and includes convergence rates of the North American Plate and Farallon Plate as calculated at 38°N (compiled by Doubrovine and Tarduno, 2008), and the apparent intrusive flux rate (Ducea, 2001). Erosion rates are based on results from: (1) low-temperature thermochonology of vertical transects from Clark et al., 2005, (2) cosmogenic studies of abandoned cave sediments due to fluvial incision by Stock et al., 2004, (3) cosmogenic dating of upland granites by Riebe et al., 2005, (4) fluvial incision and water table changes as indicated by cosmogenic dating by Stock et al., 2005, (5) Fluvial incision rates of the Kern River by Dalrymple (1963) and Ross (1986), and (6) this study. The vertical height of the erosion rate boxes approximates the uncertainty associated with the data as calculated in the respective studies.

Chapter 1 - Supplemental figures and tables.

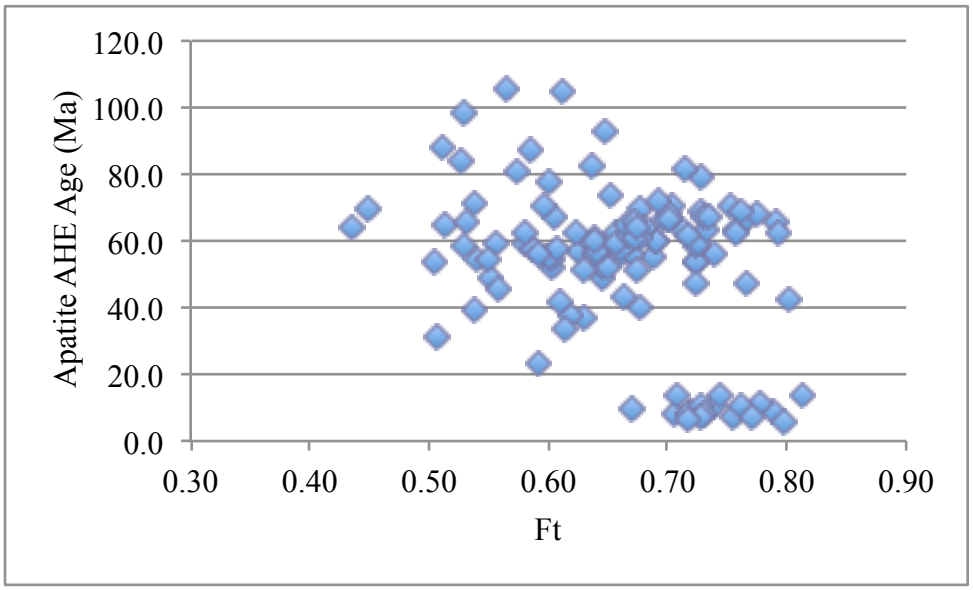

Supplemental Figure SP1.1. Apatite (U-Th)/He age data plotted against Ft. A plot of all apatite (U-Th)/He analyses against the Ft corrective factor shows that no correlation exists between the two datasets.

Supplemental Table SP1.2. Apatite (U-Th)/He data

Individual analyses consisted of multiple grain aliquots; typically 3 apatite grains each. Age error for individual analyses is 6%. Relatively young ages can occur if apatite grain loss occurs during packaging or preparation. As such, analyses with anomalously young ages are disregarded and are noted below by strikethrough text. Relatively old ages can be observed when non-apatite inclusions are present. In such a scenario, helium is diffused and analyzed but U, Th and Sm are often undigested and, therefore, absent in the measurement. Accordingly, anomalously old ages are also disregarded and noted via strikethrough text.

Sample	Age [Ma]	± [Ma]	U [ppm]	Th [ppm]	Sm [ppm]	Th/U	He [nmo/g]	mass [mg]	eU	Ft	stddev
SN08DW01-1	59.5	1.0	35.8	60.2	94.4	1.7	10.77	6.7	50.0	0.66	
SN08DW01-2	57.1	0.9	32.0	46.5	76.5	1.5	8.40	5.2	42.9	0.62	
SN08DW01-3	58.8	1.0	32.1	51.1	77.5	1.6	7.91	2.8	44.1	0.56	
SN08DW01	***58.5***	***0.9***	***33.3***	***52.6***	***82.8***	***82.8***	***1.58***	***9.0***	**45.7**	***0.61***	***1.2***
SN08MD07-1	54.0	0.5	44.7	65.4	60.3	1.5	12.79	12.5	60.1	0.72	
SN08MD07-2	57.1	0.6	44.5	81.2	77.0	1.8	12.83	6.7	63.6	0.65	
SN08MD07-3	55.0	0.5	46.0	65.0	60.9	1.4	10.98	5.6	61.2	0.60	
SN08MD07	***55.3***	***0.6***	***45.1***	***70.5***	***66.1***	***66.1***	***1.57***	***12.2***	**61.6**	***0.66***	***1.6***
SN08TD04-1	36.8	0.3	37.3	33.5	40.7	0.9	5.70	5.3	45.2	0.63	
SN08TD04-2	37.4	0.4	56.5	67.1	75.0	1.2	9.08	5.5	72.2	0.62	
SN08TD04-3	41.3	0.3	72.3	73.4	63.7	1.0	12.27	4.4	89.6	0.61	
SN08TD04	***38.5***	***0.3***	***55.4***	***58.0***	***59.8***	***59.8***	***1.03***	***9.0***	**69.0**	***0.62***	***2.5***
SN08PV11-1	55.6	0.9	24.9	31.4	60.6	1.3	6.79	9.3	32.3	0.69	
SN08PV11-2	52.4	1.1	21.3	23.4	60.4	1.1	4.66	4.9	26.8	0.60	
SN08PV11-3	54.3	0.9	27.9	25.0	57.1	0.9	6.07	3.9	33.8	0.60	
SN08PV11	***54.1***	***0.9***	***24.7***	***26.6***	***59.4***	***59.4***	***1.08***	***5.8***	**31.0**	***0.63***	***1.6***
SN08YH05-1	40.1	1.7	10.8	31.1	95.1	2.9	2.77	9.1	18.1	0.68	
SN08YH05-2	33.7	1.0	11.7	25.1	62.6	2.1	2.03	4.5	17.6	0.61	
SN08YH05-3	39.4	1.6	10.7	26.0	74.1	2.4	2.00	2.6	16.8	0.54	
SN08YH05	***37.7***	***1.4***	***11.1***	***27.4***	***77.3***	***77.3***	***2.48***	***2.3***	**17.5**	***0.61***	***3.5***
SN08YV07-1	48.5	0.3	45.3	90.3	35.7	2.0	11.30	6.2	66.5	0.64	
~~SN08YV07-2~~	~~27.6~~	~~0.2~~	~~70.0~~	~~85.5~~	~~40.9~~	~~1.2~~	~~7.75~~	~~3.6~~	90.1	~~0.57~~	
SN08YV07-3	49.0	0.3	44.8	95.5	21.2	2.1	9.85	3.1	67.2	0.55	
SN08YV07-4	43.1	2.6	45.6	63.1	26.9	1.4	9.36	6.8	60.4	0.66	
~~SN08YV07-5~~	~~235.8~~	~~14.1~~	~~60.8~~	~~93.5~~	~~22.7~~	~~1.5~~	~~60.44~~	~~3.7~~	82.8	~~0.57~~	
SN08YV07	***46.9***	***1.1***	***45.2***	***83.0***	***27.9***	***1.8***	***10.2***	***5.4***	**64.7**	***0.62***	***3.3***
SN08MD01-1	81.1	0.9	48.5	96.8	87.1	2.0	18.17	3.6	71.2	0.57	
SN08MD01-2	77.8	1.1	32.4	60.5	73.3	1.9	11.96	4.0	46.6	0.60	
SN08MD01-3	82.3	1.0	34.3	65.8	64.7	1.9	14.28	5.2	49.8	0.64	
SN08MD01	***80.4***	***1.0***	***38.4***	***74.4***	***75.0***	***75.0***	***1.93***	***14.8***	**55.9**	***0.60***	***2.4***
SN08MD10-1	52.2	3.1	6.6	13.7	54.8	2.1	1.88	5.8	9.8	0.65	
SN08MD10-2	55.0	3.3	6.8	25.9	60.9	3.8	2.40	4.0	12.9	0.60	
SN08MD10-3	64.8	3.9	21.8	60.1	112.9	2.8	6.62	2.8	35.9	0.51	
SN08MD10	***57.3***	***3.4***	***11.7***	***33.2***	***76.2***	***2.9***	***3.6***	***4.2***	**19.5**	***0.59***	***6.6***
SN08YH13-1	56.4	0.3	40.2	84.8	20.2	2.1	11.76	6.1	60.1	0.64	
SN08YH13-2	59.2	0.3	34.6	77.2	11.7	2.2	9.84	3.7	52.7	0.58	
SN08YH13-3	57.3	0.3	39.9	86.4	13.2	2.2	10.98	3.8	60.2	0.59	
SN08YH13	***57.6***	***0.3***	***38.2***	***82.8***	***15.0***	***15.0***	***2.17***	***10.9***	**57.7**	***0.60***	***1.4***
SN08YV03-1	55.9	0.7	45.2	52.6	80.6	1.2	11.62	6.9	57.6	0.66	
SN08YV03-2	52.2	0.6	33.0	38.8	55.6	1.2	7.83	5.9	42.1	0.65	
SN08YV03-3	57.6	0.7	33.9	44.3	59.9	1.3	8.48	4.1	44.3	0.61	
SN08YV03	***55.2***	***0.7***	***37.4***	***45.2***	***65.4***	***65.4***	***1.22***	***9.3***	**48.0**	***0.64***	***2.7***

Sample	Age [Ma]	± [Ma]	U [ppm]	Th [ppm]	Sm [ppm]	Th/U	He [nmo/g]	mass [mg]	eU	Ft	stddev
SN08TD01-1	22.9	1.3	3.6	7.2	9.8	2.0	0.39	2.7	5.3	0.59	
SN08TD01-2	45.5	0.5	28.2	42.7	31.0	1.5	5.29	2.7	38.2	0.56	
SN08TD01-3	31.6	0.8	15.0	19.7	29.4	1.3	1.72	1.9	19.6	0.51	
SN08TD01-5	47.0	2.8	29.3	39.7	18.6	1.4	7.55	12.7	38.6	0.77	
SN08TD01-4	42.1	2.5	4.9	6.0	3.4	1.2	1.16	21.5	6.3	0.80	
SN08TD01	***37.8***	***1.6***	***16.2***	***23.1***	***18.4***	***1.5***	***3.2***	***8.3***	**21.6**	***0.65***	***10.3***
SN08YH11-1	56.4	0.5	14.6	38.5	21.2	2.6	5.39	15.8	23.7	0.74	
SN08YH11-2	56.0	0.5	14.6	29.9	19.1	2.1	4.43	8.0	21.6	0.67	
SN08YH11-3	61.2	0.5	14.9	39.5	18.6	2.7	5.16	7.1	24.2	0.64	
SN08YH11	***57.9***	***0.5***	***14.7***	***36.0***	***19.6***	***19.6***	***2.45***	***5.0***	**23.2**	***0.68***	***2.9***
SN08HH06-1	53.5	0.3	44.9	54.1	12.4	1.2	12.09	8.1	57.6	0.72	
SN08HH06-2	61.1	0.3	53.3	67.3	12.9	1.3	15.29	6.8	69.1	0.67	
SN08HH06-3	50.9	0.3	42.1	42.9	12.5	1.0	9.06	4.7	52.2	0.63	
SN08HH06	***55.2***	***0.3***	***46.7***	***54.7***	***12.6***	***12.6***	***1.16***	***12.1***	**59.6**	***0.67***	***5.3***
SN08HH07-1	58.5	0.3	120.2	162.2	54.8	1.3	36.41	8.5	158.4	0.72	
SN08HH07-2	59.6	0.3	105.5	143.2	52.4	1.4	30.08	7.2	139.1	0.67	
SN08HH07-3	58.9	0.3	117.7	148.1	49.9	1.3	31.05	7.5	152.5	0.64	
SN08HH07	***59.0***	***0.3***	***114.5***	***151.2***	***52.4***	***52.4***	***1.32***	***32.5***	**150.0**	***0.68***	***0.6***
SN08MH01-1	56.7	3.4	51.0	64.1	59.1	1.3	13.09	5.2	66.0	0.64	
SN08MH01-2	54.5	3.3	59.9	75.2	46.3	1.3	12.40	3.2	77.5	0.54	
SN08MH01-3	56.3	3.4	51.8	74.5	54.1	1.4	12.57	3.8	69.3	0.59	
SN08MH01	***55.8***	***3.3***	***54.2***	***71.3***	***53.2***	***1.3***	***12.7***	***4.1***	**70.9**	***0.59***	***1.1***
SN08MH05-1	62.9	3.8	77.4	73.9	47.3	1.0	21.53	5.9	94.8	0.66	
SN08MH05-2	67.4	4.0	134.6	155.4	71.9	1.2	37.86	3.8	171.1	0.60	
SN08MH05-3	71.6	4.3	112.1	115.5	68.6	1.0	29.12	3.1	139.3	0.54	
SN08MH05	***67.3***	***4.0***	***108.0***	***115.0***	***62.6***	***1.0***	***29.5***	***4.3***	**135.0**	***0.60***	***4.3***
SN08MH11-1	93.0	5.6	68.7	62.2	32.8	0.9	27.26	5.5	83.4	0.65	
~~SN08MH11-2~~	~~0.0~~	~~0.0~~	~~73.3~~	~~68.4~~	~~30.4~~	~~0.9~~	~~0.00~~	~~3.9~~	89.3	~~0.57~~	
~~SN08MH11-3~~	~~98.3~~	~~5.9~~	~~67.2~~	~~52.8~~	~~29.5~~	~~0.8~~	~~23.55~~	~~3.6~~	79.6	~~0.56~~	
SN08MH11	***93.0***	***5.6***	***68.7***	***62.2***	***32.8***	***0.9***	***27.3***	***5.5***	**83.4**	***0.65***	***-***
SN08AR04-1	63.6	3.8	30.9	66.6	79.5	2.2	10.95	8.3	46.6	0.67	
SN08AR04-2	62.2	3.7	29.1	58.5	77.4	2.0	9.11	5.5	42.8	0.62	
SN08AR04-3	58.3	3.5	32.3	62.8	94.6	1.9	7.99	2.5	47.1	0.53	
SN08AR04	***61.3***	***3.7***	***30.8***	***62.7***	***83.8***	***2.0***	***9.3***	***5.4***	**45.5**	***0.61***	***2.8***
SN08AR06-1	62.2	1.1	25.6	40.9	66.2	1.6	7.89	4.6	35.2	0.66	
SN08AR06-2	62.8	0.8	35.4	64.1	64.8	1.8	10.07	3.8	50.5	0.58	
SN08AR06-3	47.5	2.8	9.3	15.5	15.5	1.7	2.43	11.4	12.9	0.72	
SN08AR06	***57.5***	***1.6***	***23.4***	***40.2***	***48.8***	***1.7***	***6.8***	***6.6***	**32.9**	***0.65***	***8.7***
SN08AR11-1	87.5	5.3	23.6	25.7	45.1	1.1	8.33	2.6	29.6	0.59	
SN08AR11-2	84.2	5.1	33.3	28.6	47.6	0.9	9.73	2.0	40.0	0.53	
SN08AR11-3	88.1	5.3	29.5	20.7	38.0	0.7	8.46	1.7	34.3	0.51	
SN08AR11	***86.6***	***5.2***	***28.8***	***25.0***	***43.6***	***0.9***	***8.8***	***2.1***	**34.7**	***0.54***	***2.1***
SN08RM01-1	54.4	3.3	49.5	47.3	23.6	1.0	9.80	2.1	60.6	0.55	
SN08RM01-2	53.4	3.2	64.0	58.6	14.6	0.9	11.35	1.5	77.8	0.50	
SN08RM01-3	69.9	4.2	62.0	56.6	30.4	0.9	12.79	1.4	75.3	0.45	
SN08RM01	***59.2***	***3.6***	***58.5***	***54.2***	***22.9***	***0.9***	***11.3***	***1.7***	**71.2**	***0.50***	***9.2***

Sample	Age [Ma]	± [Ma]	U [ppm]	Th [ppm]	Sm [ppm]	Th/U	He [nmo/g]	mass [mg]	eU	Ft	stddev
~~SN08RM10-1~~	~~9.5~~	~~0.6~~	~~143.2~~	~~192.2~~	~~50.0~~	~~1.3~~	~~5.89~~	~~4.0~~	188.3	~~0.61~~	
SN08RM10-2	65.6	3.9	23.2	34.5	72.6	1.5	6.03	2.5	31.3	0.53	
SN08RM10-3	64.3	3.9	33.5	63.1	97.8	1.9	7.45	1.3	48.3	0.44	
SN08RM10	***65.0***	***3.9***	***28.4***	***48.8***	***85.2***	***1.7***	***6.7***	***1.9***	**39.8**	***0.48***	***0.9***
SN08RM04-1	73.3	4.4	38.5	59.9	67.4	1.6	13.76	6.6	52.6	0.65	
SN08RM04-2	59.8	3.6	37.7	54.9	61.6	1.5	10.56	6.1	50.6	0.64	
SN08RM04-3	70.1	4.2	39.6	60.2	55.8	1.5	12.25	5.0	53.8	0.60	
SN08RM04	***67.7***	***4.1***	***38.6***	***58.3***	***61.6***	***1.5***	***12.2***	***5.9***	**52.3**	***0.63***	***7.1***
SN08MD02-1	104.9	6.3	81.7	94.1	39.6	1.2	36.24	4.3	103.8	0.61	
SN08MD02-2	105.3	6.3	78.1	78.5	37.3	1.0	31.16	2.7	96.5	0.56	
SN08MD02-3	98.8	5.9	65.5	75.5	34.0	1.2	23.66	2.2	83.3	0.53	
SN08MD02	***103.0***	***6.2***	***75.1***	***82.7***	***37.0***	***1.1***	***30.4***	***3.1***	**94.5**	***0.57***	***3.7***
06EW03-1	7.1	0.4	16.0	33.5	11.1	2.1	0.70	21.4	23.8	0.76	
06EW03-2	7.9	0.5	16.4	34.9	9.8	2.1	0.75	16.1	24.6	0.71	
06EW03-3	8.5	0.5	18.6	41.5	12.3	2.2	0.94	17.4	28.4	0.72	
06EW03	***7.9***	***0.5***	***17.0***	***36.6***	***11.1***	***11.1***	***2.15***	***0.8***	**25.6**	***0.73***	***0.7***
06EW04-1	9.2	0.1	17.1	38.5	14.7	2.3	1.03	31.8	26.1	0.79	9.30
06EW04-2	10.5	0.1	18.8	41.0	12.4	2.2	1.19	21.0	28.4	0.74	
06EW04-3	8.2	0.0	16.1	34.4	9.4	2.1	0.77	14.5	24.2	0.72	
06EW04	***9.3***	***0.1***	***17.3***	***37.9***	***12.2***	***12.2***	***2.19***	***1.0***	**26.2**	***0.75***	***1.1***
06EW05-1	11.4	0.7	19.5	40.9	13.8	2.1	1.40	21.1	29.1	0.78	
06EW05-2	10.1	0.6	18.6	36.0	13.2	1.9	1.08	15.0	27.0	0.73	
06EW05-3	9.8	0.6	18.2	38.5	10.6	2.1	0.97	12.7	27.3	0.67	
06EW05	***10.4***	***0.6***	***18.8***	***38.5***	***12.5***	***12.5***	***2.05***	***1.2***	**27.8**	***0.73***	***0.8***
06EW08-1	63.5	3.8	17.4	36.3	10.9	2.1	6.77	22.7	25.9	0.76	
06EW08-2	60.3	3.6	19.9	44.0	12.8	2.2	6.85	12.1	30.2	0.69	
06EW08-3	57.5	3.4	18.5	40.4	12.9	2.2	5.78	10.7	28.0	0.66	
06EW08	***60.4***	***3.6***	***18.6***	***40.3***	***12.2***	***12.2***	***2.17***	***6.5***	**28.0**	***0.70***	***3.0***
06EW09-1	70.7	1.6	20.5	44.5	12.8	2.2	8.95	20.6	30.9	0.75	
06EW09-2	79.1	1.4	20.1	41.8	12.5	2.1	9.37	17.0	29.9	0.73	
06EW09-3	70.5	1.1	19.9	40.9	9.8	2.1	7.96	16.7	29.5	0.70	
06EW09	***73.4***	***1.4***	***20.2***	***42.4***	***11.7***	***11.7***	***2.10***	***8.8***	**30.1**	***0.73***	***4.9***
06EW11-1	66.8	3.2	59.8	50.0	23.3	0.8	19.90	21.5	71.6	0.77	
06EW11-2	68.7	2.3	59.6	56.5	28.1	0.9	19.76	13.5	72.8	0.73	
06EW11-3	69.8	1.8	75.5	59.5	25.5	0.8	22.96	10.2	89.5	0.68	
06EW11	***68.4***	***2.4***	***65.0***	***55.3***	***25.6***	***25.6***	***0.86***	***20.9***	**78.0**	***0.72***	***1.5***
06EW15-1	65.7	3.9	51.0	32.3	26.3	0.6	16.49	21.7	58.5	0.79	
06EW15-2	59.5	3.6	68.2	58.7	36.3	0.9	19.21	14.2	82.0	0.72	
06EW15-3	60.0	3.6	53.2	52.7	32.6	1.0	14.77	9.7	65.6	0.69	
06EW15	***61.7***	***3.7***	***57.5***	***47.9***	***31.7***	***31.7***	***0.83***	***16.8***	**68.7**	***0.73***	***3.4***
06EW21-1	62.1	3.7	32.5	32.2	9.5	1.0	10.72	9.7	40.1	0.79	
06EW21-2	63.4	3.8	43.9	68.2	38.1	1.6	14.04	9.1	59.9	0.68	
06EW21-3	59.0	3.5	31.2	57.1	24.2	1.8	9.39	7.3	44.6	0.66	
06EW21	***61.5***	***3.7***	***35.9***	***52.5***	***23.9***	***23.9***	***1.46***	***11.4***	**48.2**	***0.71***	***2.3***

Sample	Age [Ma]	± [Ma]	U [ppm]	Th [ppm]	Sm [ppm]	Th/U	He [nmo/g]	mass [mg]	eU	Ft	stddev
06EW22-1	63.4	1.4	35.3	64.4	14.6	1.8	12.36	14.3	50.4	0.71	
06EW22-2	81.2	1.4	28.1	45.4	10.3	1.6	12.25	11.9	38.8	0.71	
06EW22-3	63.9	1.1	36.0	61.9	13.5	1.7	11.94	12.3	50.5	0.68	
06EW22	***69.5***	***1.3***	***33.1***	***57.2***	***12.8***	***12.8***	***1.72***	***12.2***	**46.6**	***0.70***	***10.2***
06EW24-1	62.4	3.7	32.4	32.7	7.1	1.0	10.26	12.2	40.1	0.76	
06EW24-2	66.7	4.0	43.7	72.6	15.9	1.7	15.42	11.2	60.8	0.70	
06EW24-3	61.1	3.7	75.5	114.1	31.3	1.5	22.93	7.4	102.3	0.68	
06EW24	***63.4***	***3.8***	***50.5***	***73.1***	***18.1***	***18.1***	***1.39***	***16.2***	**67.7**	***0.71***	***2.9***
06EW26-1	68.0	1.7	31.9	47.2	10.3	1.5	12.32	18.4	43.0	0.78	
06EW26-2	66.2	1.2	38.7	61.9	12.5	1.6	13.32	10.8	53.2	0.70	
06EW26-3	62.0	0.8	41.6	57.3	8.6	1.4	12.36	7.9	55.1	0.67	
06EW26	***65.4***	***1.2***	***37.4***	***55.5***	***10.5***	***10.5***	***1.49***	***12.7***	**50.4**	***0.71***	***3.1***
~~06EW27-1~~	~~470.1~~	~~28.2~~	~~4.6~~	~~8.0~~	~~14.7~~	~~1.7~~	~~12.53~~	~~15.4~~	6.4	~~0.73~~	
~~06EW27-2~~	~~208.3~~	~~12.5~~	~~45.6~~	~~63.4~~	~~18.4~~	~~1.4~~	~~49.19~~	~~8.9~~	60.5	~~0.71~~	
06EW27-3	64.8	3.9	50.7	63.8	12.4	1.3	15.36	9.6	65.7	0.67	
06EW27	***64.8***	***3.9***	***50.7***	***63.8***	***12.4***	***1.3***	***15.4***	***9.6***	**65.7**	***0.67***	***-***
06EW29-1	63.4	3.8	60.6	66.9	18.1	1.1	19.24	15.0	76.3	0.73	
06EW29-2	68.2	4.1	46.5	59.5	17.7	1.3	15.71	11.6	60.5	0.70	
06EW29-3	65.5	3.9	68.6	87.7	26.5	1.3	21.28	10.8	89.2	0.67	
06EW29	***65.7***	***3.9***	***58.6***	***71.4***	***20.8***	***20.8***	***1.22***	***18.7***	**75.3**	***0.70***	***2.4***
06EW30-1	67.1	4.0	53.5	84.7	16.4	1.6	19.54	16.0	73.4	0.73	
06EW30-2	66.6	4.0	54.4	91.2	19.1	1.7	19.25	12.4	75.8	0.70	
06EW30-3	60.8	3.7	48.6	75.0	29.6	1.5	14.74	11.4	66.2	0.67	
06EW30	***64.9***	***3.9***	***52.2***	***83.6***	***21.7***	***21.7***	***1.60***	***17.8***	**71.8**	***0.70***	***3.5***
06EW31-1	68.6	4.1	18.5	41.0	16.3	2.2	8.03	23.5	28.2	0.76	
06EW31-2	61.8	3.7	17.6	37.7	13.5	2.1	6.39	15.0	26.5	0.72	
06EW31-3	51.1	3.1	35.3	49.1	16.4	1.4	8.74	11.6	46.8	0.67	
06EW31	***60.5***	***3.6***	***23.8***	***42.6***	***15.4***	***15.4***	***1.91***	***7.7***	**33.8**	***0.72***	***8.9***
~~06EW32-1~~	~~0.0~~	~~0.0~~	~~22.7~~	~~45.8~~	~~15.5~~	~~2.0~~	~~0.00~~	~~35.2~~	33.5	~~0.78~~	
06EW32-2	10.4	0.6	21.6	45.1	15.1	2.1	1.39	22.5	32.2	0.76	
06EW32-3	7.9	0.5	22.6	45.4	12.4	2.0	1.03	15.9	33.2	0.73	
06EW32-4	7.2	0.4	15.2	32.0	8.3	2.1	0.64	15.9	22.7	0.73	
06EW32	***8.5***	***0.5***	***19.8***	***40.9***	***11.9***	***11.9***	***2.07***	***1.0***	**29.4**	***0.74***	***1.7***
06EW35-1	67.3	4.0	67.6	137.7	58.0	2.0	26.90	10.3	99.9	0.73	
06EW35-2	71.8	4.3	64.4	137.6	55.3	2.1	26.21	12.6	96.7	0.69	
06EW35-3	64.1	3.8	51.8	102.4	35.8	2.0	17.84	10.5	75.8	0.67	
06EW35	***67.7***	***4.1***	***61.2***	***125.9***	***49.7***	***49.7***	***2.05***	***23.6***	**90.8**	***0.70***	***3.8***
06EW38-1	13.5	0.8	17.5	39.6	10.3	2.3	1.60	42.3	26.8	0.81	
06EW38-2	13.6	0.8	24.8	53.8	10.5	2.2	2.05	23.4	37.4	0.74	
06EW38-3	13.3	0.8	19.6	40.6	7.6	2.1	1.48	19.4	29.2	0.71	
06EW38	***13.4***	***0.8***	***20.6***	***44.7***	***9.5***	***9.5***	***2.17***	***1.7***	**31.1**	***0.75***	***0.2***
06EW39-1	7.2	0.4	20.0	45.9	8.4	2.3	0.92	19.8	30.8	0.77	
06EW39-2	6.4	0.4	18.5	44.3	8.7	2.4	0.72	14.1	29.0	0.72	
06EW39-3	5.3	0.3	5.0	11.4	2.1	2.3	0.18	32.4	7.7	0.80	
06EW39	***6.3***	***0.4***	***14.5***	***33.9***	***6.4***	***2.3***	***0.6***	***22.1***	**22.5**	***0.76***	***0.9***

Supplemental Table SP1.3. Zircon (U-Th)/He data

Individual analyses consisted of multiple grain aliquots; typically 1 zircon grain each. Age error for individual analyses is 8%. Samples that fail to completely degas after three laser heat steps are considered suspect and disregarded. Such analyses are indicated by strikethrough text below.

Sample	Age [Ma]	± [Ma]	U [ppm]	Th [ppm]	Th/U	He [nmo/g]	mass [mg]	eU	Ft	stddev
zSN08DW01-1	84.2	6.73	392.9	137.4	0.35	165.9	23.16	425.22	0.85	
zSN08DW01-2	88.9	7.11	382.9	123.7	0.32	164.7	13.78	412.00	0.83	
zSN08DW01-3	81.6	6.53	591.6	235.1	0.40	235.9	14.07	646.88	0.82	
ZSN08DW01	***84.9***	***6.8***	***455.8***	***165.4***	***0.4***	***188.8***	***17.0***	**494.70**	***0.84***	***3.7***
~~zSN08MD01-1~~	~~53.7~~	~~4.29~~	~~951.6~~	~~232.9~~	~~0.24~~	~~232.0~~	~~8.90~~	1006.32	~~0.79~~	
zSN08MD01-2	95.8	7.66	718.5	154.0	0.21	300.6	6.32	754.72	0.77	
zSN08MD01-3	96.0	7.68	171.8	42.7	0.25	76.6	9.29	181.83	0.81	
ZSN08MD01	***95.9***	***7.7***	***445.2***	***98.4***	***0.2***	***188.6***	***7.8***	**468.28**	***0.79***	***0.2***
zSN08MD07-1	101.7	8.14	205.1	51.3	0.25	102.3	26.81	217.20	0.85	
zSN08MD07-2	90.5	7.24	616.2	136.2	0.22	265.3	15.60	648.24	0.83	
zSN08MD07-3	93.5	7.48	627.5	180.7	0.29	280.0	14.27	670.00	0.82	
ZSN08MD07	***95.2***	***7.6***	***483.0***	***122.7***	***0.3***	***215.8***	***18.9***	**511.81**	***0.84***	***5.8***
zSN08MD10-1	78.7	6.30	46.5	36.3	0.78	19.0	10.87	55.08	0.81	
zSN08MD10-2	102.7	8.21	326.5	161.5	0.49	159.4	8.72	364.48	0.78	
zSN08MD10-3	87.1	6.97	396.1	147.2	0.37	173.4	23.03	430.75	0.85	
ZSN08MD10	***89.5***	***7.2***	***256.4***	***115.0***	***0.5***	***117.3***	***14.2***	**283.43**	***0.82***	***12.1***
zSN08RM01-1	84.2	6.74	708.0	312.3	0.44	286.2	9.20	781.42	0.80	
zSN08RM01-2	83.6	6.69	611.2	186.1	0.30	240.8	11.31	654.89	0.81	
zSN08RM01-3	72.7	5.82	832.6	304.7	0.37	284.0	9.31	904.22	0.80	
ZSN08RM01	***80.2***	***6.4***	***717.3***	***267.7***	***0.4***	***270.32***	***9.9***	**780.18**	***0.80***	***6.5***
zSN08RM10-3	80.6	6.45	518.7	238.9	0.46	202.1	12.43	574.85	0.80	
ZSN08RM10	***80.6***	***6.5***	***518.7***	***238.9***	***0.5***	***202.1***	***12.4***	**574.85**	***0.80***	***-***
Z06EW03-1	77.0	6.2	684.3	241.7	0.4	243.69	10.1	741.08	0.79	
Z06EW03-2	69.8	5.6	947.7	284.8	0.3	276.90	3.6	1014.58	0.72	
Z06EW03-3	73.5	5.9	771.5	263.1	0.3	243.58	4.3	833.30	0.73	
Z06EW03	***73.5***	***5.9***	***801.1***	***263.2***	***0.3***	***254.72***	***6.0***	**862.99**	***0.75***	***3.6***
Z06EW04-2	75.1	6.0	748.8	278.1	0.4	237.12	3.6	814.14	0.72	
Z06EW04-3	84.0	6.7	739.5	359.4	0.5	265.78	3.0	823.91	0.71	
Z06EW04	***79.5***	***6.4***	***744.1***	***318.8***	***0.4***	***251.45***	***3.3***	**819.02**	***0.71***	***6.3***
Z06EW05-1	76.2	6.1	524.6	184.5	0.4	184.84	10.2	567.98	0.79	
Z06EW05-2	77.5	6.2	511.1	175.7	0.3	187.30	13.9	552.35	0.81	
Z06EW05-3	57.1	4.6	404.5	137.5	0.3	107.25	10.0	436.79	0.80	
Z06EW05	***70.3***	***5.6***	***480.0***	***165.9***	***0.3***	***159.80***	***11.4***	**519.04**	***0.80***	***11.5***
Z06EW06-1	58.9	4.7	1197.3	309.3	0.3	311.30	5.4	1270.00	0.77	
Z06EW06-2	71.3	5.7	718.5	230.0	0.3	232.55	6.9	772.51	0.78	
Z06EW06-3	64.4	5.2	725.5	219.7	0.3	213.87	6.7	777.18	0.79	
Z06EW06	***64.9***	***5.2***	***880.4***	***253.0***	***0.3***	***252.57***	***6.3***	**939.90**	***0.78***	***6.2***
Z06EW08-1	55.9	4.5	863.3	289.9	0.3	217.33	6.0	931.48	0.77	
Z06EW08-2	75.4	6.0	662.5	302.1	0.5	230.51	5.9	733.48	0.77	
Z06EW08-3	80.4	6.4	767.5	314.4	0.4	268.51	3.7	841.43	0.73	
Z06EW08	***70.6***	***5.6***	***764.5***	***302.2***	***0.4***	***238.78***	***5.2***	**835.47**	***0.76***	***13.0***

Sample	Age [Ma]	± [Ma]	U [ppm]	Th [ppm]	Th/U	He [nmo/g]	mass [mg]	eU	Ft	stddev
Z06EW09-1	68.9	5.5	525.9	235.5	0.4	171.59	9.9	581.22	0.79	
Z06EW09-2	72.2	5.8	743.3	360.6	0.5	249.05	6.7	828.02	0.77	
~~Z06EW09-3~~	~~63.3~~	~~5.1~~	~~1059.9~~	~~615.2~~	~~0.6~~	~~322.89~~	~~7.3~~	1204.44	~~0.78~~	
Z06EW09	***70.6***	***5.6***	***634.6***	***298.0***	***0.5***	***210.3***	***8.3***	**704.62**	***0.78***	***2.4***
Z06EW11-1	62.8	5.0	387.0	68.2	0.2	110.97	9.4	403.08	0.81	
Z06EW11-2	74.2	5.9	264.3	81.7	0.3	91.11	8.8	283.50	0.80	
Z06EW11-3	67.5	5.4	594.5	169.5	0.3	180.36	6.5	634.37	0.78	
Z06EW11	***68.2***	***5.5***	***415.3***	***106.5***	***0.3***	***127.48***	***8.2***	**440.32**	***0.80***	***5.7***
Z06EW13-1	64.1	5.1	675.9	194.9	0.3	185.45	4.7	721.67	0.74	
Z06EW13-2	72.3	5.8	382.3	125.1	0.3	128.65	9.0	411.71	0.80	
Z06EW13-3	77.0	6.2	338.9	162.9	0.5	121.62	6.4	377.13	0.77	
Z06EW13	***71.2***	***5.7***	***465.7***	***160.9***	***0.4***	***145.24***	***6.7***	**503.50**	***0.77***	***6.5***
Z06EW15-1	57.0	4.6	418.0	82.5	0.2	111.60	14.7	437.42	0.83	
Z06EW15-2	65.0	5.2	312.6	84.1	0.3	98.08	17.8	332.42	0.84	
Z06EW15	***61.0***	***4.9***	***365.3***	***83.3***	***0.2***	***104.84***	***16.2***	**384.92**	***0.83***	***5.7***
Z06EW21-1	89.6	7.2	454.8	171.9	0.4	171.63	3.6	495.21	0.71	
Z06EW21-2	71.2	5.7	861.0	288.8	0.3	251.57	2.7	928.89	0.70	
Z06EW21-3	78.1	6.2	584.6	185.1	0.3	185.64	4.0	628.13	0.70	
Z06EW21	***79.6***	***6.4***	***633.5***	***215.2***	***0.3***	***202.95***	***3.4***	**684.07**	***0.71***	***9.3***
Z06EW22-1	80.0	6.4	241.9	123.4	0.5	91.60	7.4	270.92	0.78	
Z06EW22-2	74.0	5.9	130.1	70.0	0.5	46.87	8.2	146.53	0.80	
Z06EW22-3	67.8	5.4	289.4	90.0	0.3	96.22	19.9	310.51	0.84	
Z06EW22	***73.9***	***5.9***	***220.5***	***94.5***	***0.5***	***78.23***	***11.8***	**242.65**	***0.81***	***6.1***
Z06EW23-1	62.4	5.0	891.6	373.8	0.4	252.82	6.4	979.49	0.76	
Z06EW23-2	67.3	5.4	652.3	173.6	0.3	209.07	17.8	693.05	0.83	
Z06EW23	***64.8***	***5.2***	***771.9***	***273.7***	***0.3***	***230.94***	***12.1***	**836.27**	***0.80***	***3.5***
Z06EW24-1	75.6	6.0	275.7	108.2	0.4	96.53	7.1	301.16	0.78	
Z06EW24-2	58.7	4.7	514.2	226.0	0.4	144.68	11.3	567.34	0.80	
Z06EW24-3	67.8	5.4	489.3	237.4	0.5	153.63	6.2	545.11	0.77	
Z06EW24	***67.3***	***5.4***	***426.4***	***190.5***	***0.4***	***131.61***	***8.2***	**471.20**	***0.78***	***8.5***
Z06EW26-1	77.6	6.2	435.8	148.3	0.3	152.32	6.0	470.64	0.77	
~~Z06EW26-2~~	~~96.5~~	~~7.7~~	~~447.6~~	~~408.6~~	~~0.9~~	~~218.67~~	~~6.1~~	~~543.61~~	~~0.77~~	
Z06EW26	***87.0***	***7.0***	***441.7***	***278.5***	***0.6***	***185.50***	***6.0***	**507.12**	***0.77***	***13.3***
Z06EW27-1	79.6	6.4	389.1	205.2	0.5	150.06	9.2	437.32	0.80	
Z06EW27-2	72.3	5.8	548.7	267.0	0.5	186.37	7.0	611.41	0.78	
Z06EW27-3	55.0	4.4	485.6	327.3	0.7	128.80	7.9	562.48	0.77	
Z06EW27	***69.0***	***5.5***	***474.4***	***266.5***	***0.6***	***155.08***	***8.0***	**537.07**	***0.78***	***12.7***
Z06EW29-1	69.8	5.6	353.5	110.8	0.3	115.90	10.1	379.56	0.81	
Z06EW29-2	64.0	5.1	416.9	134.6	0.3	127.80	15.0	448.56	0.82	
Z06EW29-3	65.2	5.2	618.0	161.2	0.3	187.53	10.3	655.88	0.81	
Z06EW29	***66.4***	***5.3***	***462.8***	***135.5***	***0.3***	***143.74***	***11.8***	**494.67**	***0.81***	***3.0***

Sample	Age [Ma]	± [Ma]	U [ppm]	Th [ppm]	Th/U	He [nmo/g]	mass [mg]	eU	Ft	stddev
Z06EW30-1	78.9	6.3	323.0	126.7	0.4	120.37	9.5	352.81	0.80	
Z06EW30-2*	33.4	2.7	622.6	257.1	0.4	99.30	10.4	683.03	0.81	
Z06EW30-3	69.8	5.6	293.0	88.9	0.3	89.96	6.4	313.88	0.76	
Z06EW30	***74.3***	***5.9***	***308.0***	***107.8***	***0.3***	***105.17***	***8.0***	**333.34**	***0.78***	***6.5***
Z06EW31-1	63.8	5.1	320.4	122.1	0.4	101.74	29.4	349.08	0.84	
Z06EW31-2	66.8	5.3	559.0	232.9	0.4	177.95	11.2	613.70	0.80	
Z06EW31-3	66.0	5.3	809.1	200.6	0.2	240.48	9.5	856.20	0.79	
Z06EW31	***65.6***	***5.2***	***562.8***	***185.2***	***0.3***	***173.39***	***16.7***	**606.32**	***0.81***	***1.5***
Z06EW32-1	74.5	6.0	531.3	235.4	0.4	195.42	14.0	586.59	0.83	
Z06EW32-2	71.6	5.7	693.0	331.3	0.5	239.25	10.0	770.88	0.80	
Z06EW32-3	71.1	5.7	777.2	282.1	0.4	256.50	8.3	843.52	0.79	
Z06EW32	***72.4***	***5.8***	***667.2***	***282.9***	***0.4***	***230.39***	***10.8***	**733.66**	***0.81***	***1.8***
Z06EW35-1	84.7	6.8	70.4	43.5	0.6	29.56	13.4	80.57	0.80	
Z06EW35-2	83.7	6.7	90.3	51.8	0.6	38.26	20.2	102.42	0.82	
Z06EW35-3	89.7	7.2	93.2	54.3	0.6	39.80	10.4	105.92	0.77	
Z06EW35	***86.0***	***6.9***	***84.6***	***49.8***	***0.6***	***35.87***	***14.7***	**96.31**	***0.80***	***3.2***
Z06EW38-1	69.8	5.6	1132.5	300.9	0.3	338.29	4.1	1203.17	0.74	
Z06EW38-2	79.4	6.3	808.3	270.6	0.3	279.52	3.8	871.91	0.75	
Z06EW38-3	77.0	6.2	563.1	184.8	0.3	191.58	5.0	606.50	0.76	
Z06EW38	***75.4***	***6.0***	***834.6***	***252.1***	***0.3***	***269.80***	***4.3***	**893.86**	***0.75***	***5.0***
Z06EW39-1	76.6	6.1	456.6	176.1	0.4	160.51	8.5	497.93	0.78	
Z06EW39-2	62.3	5.0	648.5	236.2	0.4	193.89	13.6	704.05	0.82	
Z06EW39-3	64.9	5.2	853.5	335.9	0.4	256.37	7.2	932.44	0.78	
Z06EW39	***67.9***	***5.4***	***652.9***	***249.4***	***0.4***	***203.59***	***9.8***	**711.47**	***0.79***	***7.6***

THIS PAGE INTENTIONALLY LEFT BLANK

CHAPTER 2

Emplacement to Exhumation: Cooling trends in magmatic rocks of the Sierra Nevada Range, California.

Abstract

This study investigates cooling histories of batholithic rock of the central Sierra Nevada. We present new biotite and hornblende $^{40}Ar/^{39}Ar$ and zircon U-Pb age data to understand the emplacement and higher temperature history of the samples and combine this with apatite and zircon (U-Th)/He ages to provide thermochronometric data ranging from ~800°C (closure of zircon U/Pb) to ~70°C (closure of apatite (U-Th)/He) from singular rock samples. New thermochronometric data are presented for 29 samples, of which 25 samples yielded 4 or more thermochronometric ages and are utilized to generate time/Temperature graphs which are validated by thermal modeling of 4 selected samples by the software package HeFTy. This dataset provides the largest and most concentrated wide-temperature thermochronometric analysis of the central Sierra Nevada batholithic rocks. The rocks studied span early Jurassic to the early Cenozoic time, but the majority are Cretaceous in age. We identify a ubiquitous 2-stage cooling pattern, reproducible in most cooling histories, that is divided by a distinct change in cooling rates observed between the closure of biotite Ar/Ar (~325°C) and zircon (U-Th)/He (~170°C). The initial cooling stage yields a mean rate of 58°C/Ma from about ~800°C to ~325°C over a typical span of 8.2Ma. The second stage appears to be much slower with cooling rate averaging 6.8°C/Ma from ~325°C to ~70°C over a span of 37.5Ma. The first cooling episode follows emplacement whereas the second stage is late Cretaceous to

early Tertiary age in all rocks. We attribute this pattern of cooling in two distinct phases to: (1) post-emplacement conductive cooling of the magmatic rocks followed by (2) cooling dominated by erosional unroofing. The results also indicate that late cooling remain relatively low through the early Cenozoic and increase towards the late Cenozoic. Such an increase in cooling rates correlate with the late Cretaceous magmatic flare-up and is a possible result of increased erosion from crustal thickening from magmatic input and/or uplift and subsequent erosion due to the post-flare-up loss of restitic root material.

Introduction

There has been debate over the timing and mechanics of uplift of the Sierra Nevada Range (SNR) to its current elevation for well over a century (references below). The earliest studies of the SNR disagreed on the driving forces between incision and valley formation. J.D. Whitney (1880, 1882) postulated that uplift was driven by climate-controlled mechanisms such as glaciation while J. LeConte (1880, 1886) argued for a regional tilting and uplift of the SNR, thus leading to regional erosion of the SNR. Subsequent studies largely supported and advanced the hypothesis of regional tilting and uplift (Lindgren, 1911; Matthes, 1930; Christensen, 1966; Huber, 1981). As the early models of SNR uplift developed, a secondary debate emerged: What lower crustal or mantle process was associated with uplift? Progressive uplift of an isostatically supported SNR would require progressive thickening of a relatively buoyant crust as proposed by Lawson (1936). Lawson (1936) proposed lower crustal thrusting to produce progressive crustal thickening and support for the uplift of the SNR. Contemporaneously with Lawson's proposal, early observations were outlined regarding the significant dextral-component extensional corridor known as the Walker Lane (Gianella and Callaghan, 1934; Locke et al., 1940) that could play a role in the more recent tilting and (relative?) uplift of the SNR. Early geophysical observations renewed debate on the uplift timing of the SNR. Some argued for the presence of a thick crust of greater than 60km (Oliver et al. 1961; Eaton, 1963; 1966; Bateman and Eaton, 1967), whose makeup was largely Mesozoic in age (Bateman and Wahrhaftig, 1966) while others proposed that the uplifted nature of the SNR was supported by dynamic forces within a hot and buoyant upper mantle (Carder et al., 1970; Carder, 1973; Crough and Thompson, 1977; and Mavko and Thompson, 1983; Jones 1987). More recent studies of geophysical data would ultimately demonstrate that the crust of the SNR is less than 40km in thickness and not thick enough to support the uplifted SNR by static Airy isostacy (Jones et al., 1994; Fliender and Ruppert, 1996; Fliendner et al., 1996; Jones and Phinney, 1998) indicating

that some mantle-driven source of buoyancy was probable. Studies of xenoliths contained within late Cenozoic volcanics demonstrated a fundamental shift in geochemistry between 8 and 3.5Ma that likely signaled the loss of dense crustal residuum (Ducea and Saleeby, 1996; 1998). Furthermore, modern geophysical conditions indicated an incompatibility with the lower crustal conditions indicated by xenoliths between 8 and 12 Ma in age (Manley et al., 2000; Farmer et al., 2002), thus indicating the recent removal of a crustal root. The subsequent increase in buoyancy would explain the high-standing condition of the SNR observed today (Wernicke et al., 1996). Further studies of incision rates indicate that an increase in erosion rates correspond in space and time with the post-10Ma uplift of the SNR as a result of the loss of a crustal residuum (Wakabayashi and Sawyer, 2001; Stock et al., 2004). Hence it seems that the high elevation of the SNR is a relatively recent phenomenon.

At the same time, there is a growing body of evidence for much earlier uplift and significant erosion of the SNR that would have to correspond to creation of at least moderate elevation and significant topographic relief of the range. Cooling data observed in (U-Th)/He indicate a much earlier phase of uplift of the SNR. House et al. (1998; 2001) present a strong argument for regional and rapid erosion of the SNR in the late Cretaceous. Additional thermochronometric studies are consistent with these findings (Cecil et al., 2006; Cassel et al., 2009; this study, Chapter 1). Investigations of stable isotope patterns have largely yielded supporting results, indicating that the SNR was an uplifted topographic barrier to the continental interior throughout the early Cenozoic (Poage and Chamerlain, 2002; Mulch et al., 2006; Crowley et al., 2008; Henry, 2009; Cassel et al., 2009; Molnar, 2010). Paleobotanical studies also show high elevation ecosystems in the early Cenozoic (Wolfe et al., 1997; 1998) as do the deposition of gold-bearing, high-energy fluvial deposits that occur in the western slopes of the SNR (Garside et al., 2005, Cassel et al., 2012).

The seemingly incompatible patterns of early vs. late uplift have been the source of much debate in that the dynamic and recent processes that are posited to support the range today are at odds with a thickened, buoyant crustal section uplifting the SNR in the late Cretaceous and early Cenozoic. However, recent studies have started to detail thermochronometric and geomorphologic evidence for multiple uplift episodes of the SNR (Small and Anderson, 1995; Wernicke et al., 1996; Clark et al., 2005; McPhillips and Brandon, 2012; Blythe and Longinotti, 2013). Furthermore, DeCelles and coworkers (Decelles et al., 2009, Decelles et al., 2015, Decelles and Grahm, 2015) have proposed a cyclical process in Cordilleran systems that explains the observation of magmatic flare-up events and has implications for the loss of lower crustal roots. They further speculate that such a system may lead to cyclical uplift of Cordilleran systems on the time period of roughly 20Ma. Such a mechanism could help explain the existence of robust datasets that indicate uplift of the SNR in the late Cretaceous and in the late Cenozoic. This study documents cooling dates and rates for part of the SNR from the time of pluton emplacement to recent. These cooling trends, in turn, help evaluate the uplift history of the range and the viability of cyclical uplift models.

Rock samples utilized in this study were collected as part of a regional sample-set from surface bedrock localities covering the extent of the central Sierra Nevada (Figure 2.1). Samples were collected from a variety of geographic features, including the base of major trunk stream canyons, drainage divides, interfluve divides, and a host of locations in between. Samples were collected at elevations ranging from 204 meters to 3056 meters. New data presented here includes $^{40}Ar/^{39}Ar$ analysis of biotite and hornblende, and U/Pb analysis of zircon via the SHRIMP method. Results also incorporate the data obtained from apatite and zircon (U-Th)/He analysis which are presented in Chapter 1 of this study.

Methods and Results

Analytical Techniques

The (U/Th)/He data utilized in this study was presented in Chapter 1 of this study, and detailed description of the analysis methodology is presented there. Most of the samples presented in Chapter 1 were also analyzed for biotite and amphibole $^{40}Ar/^{39}Ar$ ages and zircon U/Pb ages. Table 2.1 includes the new age data for these samples.

We produced $^{40}Ar/^{39}Ar$ ages by step heating on a subset of 30 samples listed in Table 2.1. When available, we obtained age spectra for both biotite and hornblende. Mineral separates were produced by crushing hand samples with a jaw crusher, pulverizing with a disk mill, followed by density separation using a Diamond brand water shaking table. The denser fractions were then isolated under a stereomicroscope and biotite and hornblende were hand picked for analysis. We selected only grains we considered to be unaltered and visibly representative of the population. Typical grain sizes ranged from 0.2 - 2 mm in diameter. Samples were irradiated in the central thimble position of the USGS TRIGA reactor (Dalrymple et al., 1981) while being rotated at 1rpm. Isotopic production ratios were determined from co-irradiation of zero-aged K-glass and salts of KCl and CaF_2. Cadmium shielding was used during irradiation and prevented the production of measurable $(^{40}Ar/^{39}Ar)_K$. Sanidine crystals of the Fish Canyon Tuff were also co-irradiated to determine neutron flux, using assumed age of 28.201 ± 0.046. Ma (Kuiper et al., 2008). Samples, standards and isotopic production monitors were loaded into numbered positions of a stainless steel planchette with an externally pumped ZnSe window and then pumped to ultrahigh vacuum conditions in a fully automated extraction system designed, built and operated at the USGS Argon Geochronology Laboratory in Denver, CO. Grains were incrementally heated using a 50watt CO_2 laser. Gas was collected in an ultrahigh vacuum extraction line and purified using a cold trap and hot SAES GP50 getters. The purified gas was then analyzed on either a MAP 215-50 mass spectrometer or a Thermo/Fischer Argus mass spectrometer.

On the MAP 215-50, isotopic ratios were determined via peak-jumping using an electron multiplier in analog mode. Data were acquired during 10 measurement cycles. Signals were fit with linear and/or polynomial regressions to determine time-zero intercepts. On the Thermo/Fischer Argus, isotopic ratios were acquired via multicollection on 4 farday collectors (^{40}Ar, ^{39}Ar, ^{38}Ar, ^{37}Ar) and one electron multiplier (^{36}Ar). All data were corrected for mass discrimination, blanks, radioactive decay and interfering nucleogenic reactions. Data reduction and age determination was done using the Masspec computer program written by A. Deino of the Berkley Geochronology Center. ^{40}Ar/^{39}Ar plateau ages are preferred over integrated ages, when available. Plateau ages are calculated if samples yield three or more consecutive heating steps that release >50% of the total ^{39}Ar and that have statistically indistinguishable ^{40}Ar/^{39}Ar ages. In this case, a weighted mean age was calculated. Otherwise, the integrated age is reported as the preferred age. All ^{40}Ar/^{39}Ar ages are reported in Table 2.1. Analytical data, standard reporting and correction corrective factors are reported in supplemental data.

The processed rock samples were also further separated using bromoform, methylene iodide and a Frantz Magnetic separator to yield pure zircon separates. For selected samples, the zircon separates were then inspected under a high power polarizing stereomicroscope in order to select grains that were morphologically intact, relatively free of inclusions, and of appropriate size (i.e. >75μm in diameter when possible). Grains were individually selected, applied to double-sided tape and mounted in epoxy along with R33 as a standard (Black et al., 2004). Grains were then ground to half-thickness using 2500-grit sandpaper and polished using 6μm and 1μm diamond suspension polish. All mounts were then imaged using reflected and transmitted light using a petrographic microscope and integrated digital camera. Using a scanning electron microscope, zircon mounts were imaged by cathodoluminescence (CL) to determine zoning and growth patterns within individual zircon grains. The zircon mounts were analyzed by sensitive

high-resolution ion microprobe-reverse geometry (SHRIMP-RG) at the USGS/Stanford Micro Analysis Center in Stanford, California. Using the reflected light and CL imagery as a guide, spot locations were selected to avoid grain overgrowths and areas of problematic zonation in grain cores. Shallow pits (typically 1 μm) of about 25 μm diameter, were excavated using a primary oxygen beam into the gold-coated, polished grain interiors. Positively charged ions extracted during sputtering were accelerated into the reverse geometry mass spectrometer for measurement by electron multipliers at relevant positions. Squid2 (Ludwig, 2009) was used to reduce the raw data into isotopic ratios for the calculation of U/Pb ages. Ages were standardized against the R33 zircon standard (Black et al., 2004). Age data is reported in Table 2.1; isotopic data are available in supplemental data.

Analytical Results

Table 2.1 gives the $^{40}Ar/^{39}Ar$ age interpretations and Figure 2.2 contains the release spectra. Supplemental data includes isotopic data tables and correction coefficients. In all, 29 samples were analyzed for biotite $^{40}Ar/^{39}Ar$ ages and those ages ranged from 157.5 ±1 to 80.3 ± 0.3 Ma. Of the 29 samples analyzed, 20 yielded naturally occurring plateaus. All but three of these samples contained amphibole, and one additional sample contained amphibole and not biotite. In all, we obtained 27 amphibole $^{40}Ar/^{39}Ar$ ages that ranged from 162.6 ± 1.2 to 84.0 ± 0.3 Ma. Generally, amphibole age data yield larger errors than biotite due to the higher Ca content (interfering radiogenic ^{36}Ar) and lower radiogenic ^{40}Ar content. Of the 27 samples analyzed, 15 provided plateaus.

As a first-order observation, $^{40}Ar/^{39}Ar$ release spectra support the interpretation of a simple, monotonic cooling history for most samples because most samples yielded relatively flat release spectra with overlapping age steps as grains are progressively degassed. In all but one sample, amphibole $^{40}Ar/^{39}Ar$ ages are as old or older, within error, as the corresponding biotite $^{40}Ar/^{39}Ar$ age as would be expected in scenarios with

simple cooling histories. The one exception, SN08EW39, yielded a biotite $^{40}Ar/^{39}Ar$ age of 85.3 ± 0.3 and an amphibole $^{40}Ar/^{39}Ar$ age of 84.0 ± 0.3. Neither the biotite nor amphibole data yielded an age plateau. Because several other samples yielded biotite ages near or within error of corresponding amphibole ages, we speculate that the ages are valid in the context of this study, but may have some unaccounted for small uncertainties as evidenced by the SN08EW39 sample.

We also present 20 new zircon U/Pb ages. Table 2.1 outlines the age data, which ranges from 166.9 ± 3.1 Ma to 88.3 ± 1.5 Ma. Supplemental data contains isotopic data and analytical results. In all samples, observed zircon U/Pb ages were older than corresponding amphibole $^{40}Ar/^{39}Ar$ ages; the mean difference between the two age sets is 3.1 Ma. Figure 2.3 shows the grain layout and analysis locations for 2 selected samples (SN08MD07 and SN08AR11). Zircon grains were mounted in epoxy and imaged using transmitted light and CL. The diameter of analysis locations was about 25um and was selected to avoid inclusion and complex zoning. Overgrowths, when observed, were also avoided. Typically, the grain cores were avoided to help eliminate complication of post-emplacement ages through the analysis of possibly inherited grain cores or antecrysts.

Cooling Patterns

We consider two possible approaches, (1) thermal modeling and (2) generation of cooling paths by plotting age vs. closure temperature (T_C) to establish cooling histories of the samples. It has been demonstrated that closure temperature is a function of many parameters such as grain size (i.e. diffusion domain size), cooling rate, mineral chemistry and more (McDougall and Harrison, 1999; Reiners, 2005). For this reason, the generation of cooling paths by plotting age vs. closure temperature could be problematic due to the variability in closure temperature. We address whether this variability in closure temperature invalidates the use of simple time/closure temperature paths by comparing those results to models produced by the software package HeFTy (Ketchum, 2005), which take the variable nature of T_C into account. HeFTY uses an inverse

approach that utilizes Monte-Carlo simulation to generate random thermal histories within a set of user-defined constraints. Each generated thermal history is then compared with the observed thermochronologic data. Thermal histories that produce thermochonologic ages within error of the observed error are considered acceptable. Hefty does not provide direct input for $^{40}Ar/^{39}Ar$ ages or for U/Pb ages but utilizing the built-in options allows creation of a custom model with user-defined diffusion coefficients. We did this to incorporate biotite and amphibole $^{40}Ar/^{39}Ar$ data. U/Pb ages are assumed to reflect the timing of crystallization and emplacement, and are used as a high-temperature starting point for the modeling. Of the 45 samples considered in this study, 5 samples yielded each of the 5 different thermochronometric analyses, and four of these were selected for modeling. The sample that yielded 5 analysis but was not modeled was due to the fact that that sample experienced thermal resetting of the apatite (U-Th)/He system from overlying volcanics (as discussed in Chapter 1). The selected samples for modeling also yielded age distributions that would indicate a variety of cooling rates and, and as a result, would provide a robust test for the validity of our simpler age vs. closure temperature cooling paths.

For the cooling histories based upon age vs. T_C, we used established closure temperatures for the dating systems of 70±10°C for apatite (U-Th)/He (Reiners, 2005), 170±15°C for zircon (U-Th)/He (Reiners, 2005), 325±50°C for biotite Ar/Ar (McDougall and Harrison, 1999), 500±50°C for hornblende Ar/Ar (McDougall and Harrison, 1999), and 800±50°C for zircon U/Pb. Figure 2.4 overlays the age vs. T_C plots with results of the thermal modeling. The modeled thermal histories are uniformly in close agreement with the age vs. T_C plots. We interpret this to mean that the effect of variable cooling rates and grain size on T_C are, at best, of secondary importance and that the simpler approach of generating age vs. T_C plots is a reasonable way of interpreting cooling histories. As a result, we generate cooling diagrams and cooling rates based upon the

observed ages and assigned T_C for all samples presented in this study. We suspect that this relatively simplistic approach works because of the simple, monotonic cooling history of the samples analyzed here; samples that undergo more complicated thermal histories, or those experiencing protracted time near closure temperatures, may require the more nuanced approach of thermal modeling to produce accurate thermal history reconstructions.

Upon inspection of the cooling diagrams (age vs. T_C plots), it became apparent that many samples shared similar cooling histories. To better characterize the regional cooling trend, samples were grouped together based on geographical proximity and likeness of cooling histories. Those 7 regions are shown in Figure 2.5. Age vs. T_C cooling paths are depicted in Figure 2.6 and arranged based on the groups shown in Figure 2.5. Due to the similarity of cooling paths for each of the regions, a composite cooling path is constructed and is indicated by the grey swath in Figure 2.6. To simplify the presentation of regional cooling trends, the composite cooling paths are assembled in Figure 2.7. Also shown in Figure 2.7 are the mean cooling rates between each of the thermochronometric analysis techniques used here.

Discussion

Cooling Rates

Deciphering the dominant mechanisms of cooling for magmatic systems can be difficult and complicated. The crystallization of a magmatic body followed by its conductive cooling and erosional and/or structural unroofing control the thermochronometric systems that record the progress of emplacement to exposure. However, cooling that is related to unroofing can be difficult to extricate from conductive cooling. The dataset presented here presents an opportunity to separate the magnitude and timing of conductive cooling and cooling related to unroofing. Because there are no large-scale structures present in the SNR (Jones, 1987, Jennings et al., 2010) that can

account for significant structural unroofing (e.g., as in Stockli et al., 2003, Walker et al., 2014, Gorynski et al., 2014, 2015, Bidgoli et al., 2015a, 2015b), any unroofing must related to erosion.

Nadin and Saleeby (2008) produced and compiled multiple sources of Al-in-hbl data (Picket and Saleeby, 1993; Dixon, 1995; Ague, 1997; Nadin and Saleeby, 2008) into a dataset for the central and southern SNR. Although no barometric data were collected in this study, the density of existing barometric data allows for the extrapolation of emplacement pressure values. Figure 2.5 shows a color-contoured map based upon existing barometric data for the region of the central SNR as well as locations of the samples presented in this study. Emplacement pressures vary between ~2 and 4 kbar for the samples utilized here but a majority of the samples concentrated in areas that correspond to emplacement pressures between 2.5 and 3.0 kbar. Using a depth/pressure gradient between 3.5 and 4 kbar/km, is can be assumed that a majority of the samples in this study were emplaced at depth between ~9 and 12 km (consistent with many models for arc pluton emplacement, e.g., Richards, 2011, Ducea et al., 2015). A steady-state geothermal gradient between 20° and 25°C/km (e.g., gradient appropriate following emplacement and initial cooling) would then correspond to temperatures between 175 and 300°C and, thus, somewhere between the closure temperatures of argon in biotite and helium in zircon.

Analysis of the data presented allow for the calculation of average cooling rates between the closure temperatures of each of the 5 thermochronometers utilized here using the following equation:

$$\dot{C}(°C/my) = \frac{n(T_{C1}(°C) - T_{C2}(°C))}{\sum_1^n (A_1(my) - A_2(my))}$$

Where $\dot{C}$ is the mean cooling rate, T_C is closure temperature, A is cooling age, 1 refers to the higher temperature technique and 2 refers to the lower temperature technique (e.g. 1=zircon U/Pb, 2=hornblende Ar/Ar, or 1= hornblende Ar/Ar, 2=biotite Ar/Ar; etc).

The results are illustrated in Figure 2.7 and are as follows: (1) The mean cooling rate between zircon U/Pb and hornblende Ar/Ar is 67.6°C/Ma, (2) the mean cooling rate between hornblende Ar/Ar and biotite Ar/Ar is 46.0°C/Ma, (3) the mean cooling rate between biotite Ar/Ar and zircon (U-Th)/He is 9.6°C/Ma, and (4) the mean cooling rate between zircon (U-Th)/He and apatite (U-Th)/He is 7.8°C/Ma. Samples SN08EW-03, -04, -05 -32, -38, and -39 were excluded from the mean cooling rate calculations between zircon (U-Th)/He and apatite (U-Th)/He because of sample reheating and partial degassing from overlying volcanics well after the samples were initially cooled below the apatite (U-Th)/He closure temperature (for more, see Chapter 1). Although little information has been published on post-emplacement cooling rates in plutonic rocks, the rates observed in this study agree with those observed in a few studies of cooling rates in arc environments. For example, Sawada and Itaya (1993) reported a cooling rate of 80-40°C/Ma of late Cretaceous granite near Lake Biwa, Japan and Yuhara and Kagami (1996) estimate a cooling rate of 19°C/Ma for the Inutagiri granite from the Ina district, Japan.

Conductive Cooling vs. Erosion-Controlled Cooling

Inspection of the cooling paths in Figures 2.6 and 2.7 shows that all regional trends exhibit a two-stage cooling path: an earlier period corresponding to initial cooling from higher temperatures (800-325°C) at higher cooling rates (57°C/Ma), and a second period corresponding to lower temperatures (325-70°C) and slower cooling rates (9°C/Ma). Again, thermal modeling shown Figure 2.4 indicates to us that this break is justified in the data, and not simply a result of how we have plotted cooling trends or an artifact of simple cooling equation presented above. We posit the different cooling rates represent a change from mostly conductive, post-emplacement cooling to that of cooling dominated by erosional unroofing. As noted above, it is speculated that the depths of

emplacement, as indicated by Al-in-hbl barometry, places the samples at depths between 9 km and 12 km and temperatures of 175 and 300°C. This temperature range is between that between the closure temperatures of biotite Ar/Ar and zircon (U-Th)/He and precisely where a vast majority of cooling paths in this study show an inflection point and change of cooling rate from 57°C/Ma (800-325°C) to 9°C/Ma (325-70°C). Additionally, we observe that the time periods of rapid cooling are similar even though the rocks span an age range of almost 80 Ma. The reproducibility of such a pattern seems to support the assumption that initial cooling is attributable to the thermal equilibration of emplaced magmatic bodies with relatively little variation in emplacement depth. The second, slower cooling we consider to be erosion related. Assuming a geothermal gradient between 20°C/km and 40°C/km, the latter corresponds to erosion rates between 0.4 and 0.2 km/Ma

If the inflection point present in a majority of the cooling paths is interpreted to represent the end of faster conductive cooling (following emplacement) and the start of slower erosional cooling, then a characteristic time span appears to indicate the time between emplacement and the end (of significant slowing) of conductive cooling. This time span can be obtained by calculating the mean difference between zircon U/Pb ages and biotite Ar/Ar age and whose result is 8.2 ± 5.3 Ma. Roughly 10 Ma appears to be the characteristic period of post-emplacement cooling in the Sierra Nevada from the late Jurassic to the late Cretaceous.

Changes in Erosion Controlled Cooling

Sample group A (SN08MH11 and SN08AR11) and samples SN08EW35 and SN08MD01 represent a grouping of the oldest samples collected and analyzed in this study U/Pb that also gave $^{40}Ar/^{39}Ar$ biotite ages. These older samples show cooling rates between the T_C biotite $^{40}Ar/^{39}Ar$ (~325°C) apatite (U-Th)/He (~70°C) averaging about 5°C/Ma. In contrast, when all 29 samples that yielded biotite $^{40}Ar/^{39}Ar$ and apatite (U-

Th)/He ages are considered, an average cooling rate between biotite Ar/Ar and apatite (U-Th)/He is 9°C/Ma. Hence the older samples have somewhat slower cooling rates. We interpret this pattern to represent slower erosion rates from the late Jurrasic (earliest biotite $^{40}Ar/^{39}Ar$ closures) until the late Cretaceous (apatite (U-Th)/He closure of multiple samples). Although the strength of this interpretation would certainly benefit from the generation of cooling patterns from additional samples, this interpretation has implications for models of cyclical processes in subduction systems as proposed by Decelles et al. (2009), and specifically in the North American Cordillera (Decelles and Grahm, 2015). In these models, magmatic high flux events are cyclical and followed by loss of a dense, restitic root, resulting in arc uplift because of subsequent increased buoyancy. According to this model, isostatic-driven uplift following the late Cretaceous high flux event and restitic root removal corresponds with the increase in cooling rates observed in the late Cretaceous observed in this study.

Conclusions

This study provides important insights into the thermal evolution of the Sierra Nevada batholith between pluton emplacement and near surface exposure. Previous research has outlined broad emplacement patterns associated with arc magmatism (Everden and Kistler, 1970; Chen and Moore, 1982; Bateman, 1988; Dickinson, 2004, 2008 and references within; Cecil et al., 2012), and more recent research has shown that exhumation of the batholith has both old and young constituent histories (Small and Anderson, 1995; Wernicke et al., 1996; Clark et al., 2005; McPhillips and Brandon, 2012; Blythe and Longinotti, 2013). However, the techniques applied in this study allows us to illuminate the post-emplacement thermal equalization patterns as well as the timing and rate of exhumation after emplacement. The data presented here show that the

batholithic rocks of the Sierra Nevada cooled to about <325°C in a relatively short period of time after emplacement (8.8 ± 5.3 Ma). The <325°C temperature is consistent with available paleobarometry estimations for pluton emplacement at 2-4 kbar. We interpret this to mean that the plutons probably cooled relatively quickly to an ambient geotherm of around 25°C/km at about 10 km depths.

The data also show that after reaching about 300<170°C, the rocks then cooled at a rate between 5°C/Ma and 9°C/Ma until the closure of the apatite (U-Th)/He system at about 70°C. Additional thermochronometric studies from the area have previously established that the SNR underwent periods of rapid cooling in the late Cretaceous and that the rocks that make up the surface of the SNR today were eroded to depths low enough to result in closure of the apatite (U-Th)/He system (Dumitru, 1990; House et al. 1997; Cecil et al., 2012; this dissertation, Chapter 1). However, estimating these depths in the early Cenozoic is inherently problematic due to the difficulty in establishing robust constraint of a paleogeothermal gradient (Dumitru, 1990; Dumitru et al., 1991). We can confidently speculate, however, that the initial thermal equilibration of magmatic rocks emplaced throughout the Cretaceous took place over a period typically less than 10 Ma and that unroofing of those batholithic rocks to the near surface took another 20-45 Ma. Furthermore, the more extensive study of zircon and apatite He-ages in Chapter 1 shows that all samples seem to experience increased cooling rates and therefore unroofing towards the end of the Cretaceous and correlate with proposed models for increased crustal buoyancy and thickening (Decelles, 2009; Decelles and Grahm, 2015; Ducea et al., 2015).

References Cited

Ague, J., 1997, Thermodynamic calculation of emplacement pressures for batholithic rocks, California: Implications for the aluminum-in-hornblende barometer: Geology, v. 25, p. 563–566, doi:10.1130/0091-7613(1997)025<0563:TCOEPF>2.3.CO;2.

Bateman, P. C., and Eaton, J. P., 1967, Sierra Nevada batholith: Science, v. 158, p. 1407–1417.

Bateman, P.C., 1988, Constitution and Genesis of the Central Sierra Nevada Batholith, California. U.S: Geological Survey Open File Reports: 88-382, 284p.

Bidgoli, T., Amir, E., Walker, J.D., Stockli, D.F., Andrew, J.E., and Caskey, J.S., 2015, Low-temperature thermochronology of the Black and Panamint mountains, Death Valley, CA: Implications for geodynamic controls on Cenozoic intraplate strain: Lithosphere, v. 7, no. 4, p. 473-480 doi: 10.1130/L406.1.

Bidgoli, T.S., Stockli, D.F., and Walker, J.D., 2015, Low-temperature thermochronologic constraints on the kinematic histories of the Castle Cliffs, Tule Springs, and Mormon Peak detachments, southeastern Nevada and southwestern Utah: Geosphere, v. 11, p. 850-867.

Black, L.P., Kamo, S.L., Allen, C.M., Davis, D.W., Aleinikoff, J.N., Valley, J.W., Mundil, R., Campbell, I.H., Korsch, R.J., Williams, I.S., and Foudoulis, C., 2004, Improved 206Pb/238U microprobe geochronology by the monitoring of a trace-element–related matrix effect; SHRIMP, ID-TIMS, ELA-ICP-MS and oxygen isotope documentation for a series of zircon standards: Chemical Geology, v. 205, no. 1–2, p. 115–140

Blythe, A.E., Longinotti, N., 2013, Exhumation of the southern Sierra Nevada–eastern Tehachapi Mountains constrained by low-temperature thermochronology: Implications for the initiation of the Garlock fault: Lithosphere. v. 5, no. 3, p. 321–327. doi: https://doi-org.www2.lib.ku.edu/10.1130/L252.1

Carder, D.S., Qamar, A., and McEvilly, T.V., 1970, Trans- California seismic profile—Pahute Mesa to San Francisco Bay: Bulletin of the Seismological Society of America, v. 60, p. 1829–1846.

Carder, D.S., 1973, Trans-California seismic profile, Death Valley to Monterey Bay: Bulletin of the Seismological Society of America, v. 63, p. 571–586.

Cassel, E.J., Graham, S.A., and Chamberlain, C.P., 2009, Cenozoic tectonic and topographic evolution of the northern Sierra Nevada, California, through stable isotope paleoaltimetry in volcanic glass: Geology, v. 37, p. 547–550, doi:10.1130/G25572A.1.

Cassel, E.J., Graham, S.A., Chamberlain, C.P., and Henry, C.D., 2012, Early Cenozoic topography, morphology, and tectonics of the northern Sierra Nevada and western

Basin and Range: Geosphere, v. 8, p. 229–249, doi:10.1130/GES00671.1.

Cecil M.R., Ducea M.N., Reiners P.W., Chase C.G., 2006, Cenozoic exhumation of the northern Sierra Nevada, California, from (U-Th)/He thermochronology: Geological Society of America Bulletin, v. 118, p. 1481– 148

Chen, J.H., Moore, J.G., 1982, Uranium-lead isotopic ages from the Sierra Nevada batholith, California: Journal of Geophysical Research. v. 87, no. B6, p. 4761–4784, doi:10.1029/JB087iB06p04761.

Christensen, M.N., 1966, Late Cenozoic crustal movements in the Sierra Nevada of California: Geological Society of America Bulletin, v. 77, p. 163–182, doi:10.1130/00167606(1966)77[163:LCCMIT]2.0.CO;2.

Clark, M.K., Maheo, G., Saleeby, J., and Farley, K.A., 2005, The non-equilibrium landscape of the southern Sierra Nevada, California: GSA Today, v. 15, no. 9, p. 4–10, doi:10.1130/10525173(2005)015[4:TNLOTS]2.0.CO;2.

Crough, S.T., and Thompson, G.A., 1977, Upper mantle origin of the Sierra Nevada uplift: Geology, v. 5, p. 396–399, doi:10.1130/0091-7613(1977)5<396:UMOOSN>2.0 .CO;2.

Crowley, B.E., Koch, P.L., and Davis, E.B., 2008, Stable isotope constraints on the elevation history of the Sierra Nevada Mountains, California: Geology, v. 120, p. 588–598.

Dalrymple, G.B., Alexander, E.C., Lanphere, M.A., and Kraker, G.P., 1981, Irradiation of Samples for 40Ar/39Ar Dating Using the Geological Survey TRIGA Reactor: U.S. Geological Survey Professional Paper 1176, 62 p

DeCelles, P.G., Ducea, M.N., Kapp, P., and Zandt, G., 2009, Cyclicity in Cordilleran orogenic systems: Nature Geoscience, v. 2, p. 251–257, doi:10.1038/ngeo469.

DeCelles, P.G., Zandt, G., Beck, S.L., Currie, C.A., Ducea, M.N., Kapp, P., Gehrels, G.E., Carrapa, B., Quade, J., and Schoenbohm, L.M., 2015, Cyclical orogenic processes in the Cenozoic central Andes. In P.G. DeCelles, M.N. Ducea, B. Carrapa, and P.A. Kapp, Eds., Geodynamics of a Cordilleran Orogenic System: The Central Andes of Argentina and Northern Chile. Geological Society of America Memoirs, v. 212, p. 459–490. doi:10.1130/2015.1212(22).

DeCelles, P.G., Graham, S.A., 2015, Cyclical processes in the North American Cordilleran orogenic system. *Geology*, v. 43, no. 6, p. 499–502. doi: https://doi.org/10.1130/G36482.1

Dickinson, W.R., 2004, Evolution of the North American Cordillera: Annual Review of Earth and Planetary Sciences, v. 32, p. 13–45, doi: 10.1146/annurev. earth.32.101802.120257.

Dickinson, W.R., 2008, Accretionary Mesozoic–Cenozoic expansion of the Cordilleran continental margin in California and adjacent Oregon: Geosphere, v. 4, p. 329–353, doi:10.1130/GES00105.1.

Dixon, E.T., 1995, An evaluation of hornblende barometry, Isabella to Tehachapi region, southern Sierra Nevada, California [M.S. thesis]: Ann Arbor, University of Michigan, 150 p.

Ducea, M.N., and Saleeby, J.B., 1996, Buoyancy sources for a large, unrooted mountain range, the Sierra Nevada, California: Evidence from xenolith thermobarometry: Journal of Geophysical Research, v. 101, p. 8229– 8244, doi:10.1029/95JB03452.

Ducea, M.N., and Saleeby, J.B., 1998, A case for delamination of the deep batholithic crust beneath the Sierra Nevada, California: International Geology Review, v. 40, p. 78–93, doi:10.1080/00206819809465199.

Ducea, M.N., Paterson, S.R., DeCelles, P.G., 2015, High-volume magmatic events in subduction systems: Elements , v. 11, no. 2, p. 99–104.

Dumitru, T.A., 1990, Subnormal Cenozoic geothermal gradients in the extinct Sierra Nevada magmatic arc: Consequences of Laramide and post-Laramide shallow-angle subduction: Journal of Geophysical Research , v. 95, no. B4, p. 4925–4941, doi:10.1029/JB095iB04p04925.

Dumitru T.A. Gans P.B. Foster D.A. Miller E.L., 1991, Refrigeration of the Western Cordilleran lithosphere during Laramide shallow-angle subduction: Geology , v. 19, p. 1145–1148, doi:10.1130/0091-7613(1991)019<1145:ROTWCL>2.3.CO;2.

Eaton, J.P., 1963, Crustal structure from San Francisco, California, to Eureka, Nevada, from seismic-refraction measurements: Journal of Geophysical Research, v. 68, p. 5789–5806, doi:10.1029/JZ068i020p05789.

Eaton, J.P., 1966, Crustal structure in northern and central California from seismic evidence, *in* Bailey, E.H., ed., Geology of Northern California: Bulletin of the California Division of Mines and Geology, v. 190, p. 419–426.

Evernden, J.F., and R.W. Kistler, 1970, Chronology and Emplacement of Mesozoic Batholithic complexes in California and Western Nevada. U.S. Geological Survey Professional Paper 623, 42p.

Farmer, G.L., Glazner, A.F., and Manley, C.R., 2002, Did lithospheric delamination trigger Late Cenozoic potassic volcanism in the southern Sierra Nevada, California?:

Geological Society of America Bulletin, v. 114, p. 754–768, doi:10.1130/0016-7606(2002)114<0754 :DLDTLC>2.0.CO;2.

Fliedner, M.M., Ruppert, S., and SSCD Working Group, 1996, Three-dimensional crustal structure of the southern Sierra Nevada from seismic fan profiles and gravity modeling: Geology, v. 24, p. 367–370, doi:10.1130/0091 - 7613(1996)024<0367:TDCSOT>2.3.CO;2.

Garside, L., Henry, C.D., Faulds, J.E., and Hinz, N.H., 2005, The upper reaches of the Sierra Nevada auriferous gold channels, California and Nevada, *in* Proceedings, Symposium 2005: Window to the World: Reno, Nevada, Geological Society of Nevada, p. 209–235.

Gianella, V.P., Callaghan, E., 1934. The earthquake of December 20, 1932, at Cedar Mountain, Nevada and its bearing on the genesis of Basin and Range structure. Journal of Geology, v. 47, p. 1–22.

Gorynski, K.E., Stockli, D.F., and Walker, J.D., 2013, Thermochronometrically constrained anatomy and evolution of a Miocene extensional accommodation zone and tilt domain boundary: the southern Wassuk Range, Nevada: Tectonics, v. 32, p. 516-539, doi: 10.1002/tect.20044.

Gorynski,K.E., Walker, J.D., and Stockli, D.F., 2014, Apatite (U-Th)/He thermochronometry as an innovative geothermal exploration tool: A case study from the southern Wassuk Range, Nevada: Journal of Volcanology and Geothermal Research, v. 270, p. 99-114.

Henry, C.D., 2009, Uplift of the Sierra Nevada, California: Geology, v. 37, p. 575 - 576.

House, M.A., Wernicke, B.P., and Farley, K.A., 1998, Dating topography of the Sierra Nevada, California, using apatite (U-Th)/He ages: Nature, v. 396, p. 66–69, doi: 10.1038/23926.

House, M.A., Wernicke, B.P., and Farley, K.A., 2001, Paleogeomorphology of the Sierra Nevada, California, from (U-Th)/He ages in apatite: American Journal of Science, v. 301, no. 2, p. 77–102, doi:10.2475/ajs.301.2.77.

Huber, N.K., 1981, Amount and timing of late Cenozoic uplift and tilt of the central Sierra Nevada, California— Evidence from the upper San Joaquin River basin: U.S. Geological Survey Professional Paper 1197, 28 p.

Jennings, C.W., Gutierrez, C., Bryant, W., Saucedo, G., Wills, C., Geologic Map of California: Department of Conservation, California Geologic Survey, GDM No. 2

Jones, C.H., 1987, Is extension in Death Valley accommodated by thinning of the mantle

lithosphere beneath the Sierra Nevada, California?: Tectonics, v. 6, p. 449–473, doi:10.1029/TC006i004p00449.

Jones, C.H., Kanamori, H., and Roecker, S.W., 1994, Missing roots and mantle "drips": Regional Pn and teleseismic arrival times in the southern Sierra Nevada and vicinity, California: Journal of Geophysical Research, v. 99, p. 4567–4601, doi:10.1029/93JB01232.

Jones, C.H., and Phinney, R.A., 1998, Seismic structure of the lithosphere from teleseismic converted arrivals observed at small arrays in the southern Sierra Nevada and vicinity, California: Journal of Geophysical Research, v. 103, p. 10,065–10,090, doi:10.1029 /97JB03540.

Ketcham RA, 2005, Forward and inverse modeling of low-temperature thermochronometry data: Reviews in Mineral Geochem, v. 58, p. 275-314

Kuiper, K.F., Deino, A., Hilgen, F.J., Krigjsman, W., Renne, P.R., Wijbrans, J.R., 2008, Synchronizing Rock Clocks of Earth History: Science, pg. 500-504

Lawson, A.C., 1936, The Sierra Nevada in the light of isostasy: Geological Society of America Bulletin, v. 47, p. 1691–1712.

Locke, A., Billingsley, P., Mayo, E.B., 1940, Sierra Nevada tectonic patterns. Geological Society of America Bulletin, v. 51, p. 513–540.

LeConte, J., 1880, The old river-beds of California: American Journal of Science, v. 19, p. 176–190.

LeConte, J., 1886, A post-Tertiary elevation of the Sierra Nevada shown by the river beds: American Journal of Science, v. 32, no. 189, p. 167–181.

Lindgren, W., 1911, The Tertiary gravels of the Sierra Nevada: U.S. Geological Survey Professional Paper 73, 226 p.

Ludwig, K.R., 2009, Squid 2, a User's Manual . Berkeley Geochronology Center, University of California, Berkeley, California (Spec. Publ. 2).

Manley, C.R., Glazner, A.F., and Farmer, G.L., 2000, Timing of volcanism in the Sierra Nevada of California: Evidence for Pliocene delamination of the batholithic root?: Geology, v. 28, p. 811–814, doi:10.1130/0091 - 7613(2000)28<811:TOVITS>2.0.CO;2.

Matthes, F.E., 1930, Geologic history of the Yosemite Val- ley: U.S. Geological Survey Professional Paper 160, 137 p.

Masaki Y., Hiroo K., 2006, Rb-Sr whole-rock and mineral isochron ages of the Otagiri granites from the Ina district, Ryoke belt, Southwest Japan Arc: Journal of

Minerology, v. 91, no. 7, p. 275-282, doi:/10.2465/ganko.91.275, https://www.jstage.jst.go.jp/article/ganko/91/7/91_7_275/_article/-char/en

Mavko, B.B., and Thompson, G.A., 1983, Crustal and upper mantle structure of the northern and central Sierra Nevada: Journal of Geophysical Research, v. 88, p. 5874–5892, doi:10.1029/JB088iB07p05874.

McDougall I, Harrison TM ,1999, Geochronology and Thermochronology by the 40Ar/39Ar Method, Second Edition. Oxford University Press, Oxford

McPhillips, D., and Brandon, M.T., 2012, Topographic evolution of the Sierra Nevada measured directly by inversion of low-temperature thermochronology: American Journal of Science, v. 312, p. 90–116, doi:10.2475 /02.2012.02.

Molnar, P., 2010, Deuterium and oxygen isotopes, paleoelevations of the Sierra Nevada, and Cenozoic climate: Geological Society of America Bulletin, v. 122, p. 1106–1115, doi:10.1130/B30001.1.

Mulch A., Graham S.A., Chamberlain C.P., 2006, Hydrogen isotopes in Eocene river gravels and paleoelevation of the Sierra Nevada: Science, v. 313, p. 87–89

Nadin, E.S., Saleeby, J.B., 2008, Disruption of regional primary structure of the Sierra Nevada batholith by the Kern Canyon fault system, California, in Wright, J.E., Shervais, J.W., eds., Ophiolites, arcs, and batholiths: A tribute to Cliff Hopson: Geological Society of America Special Paper 438 , p. 429–454, doi:10.1130/2008.2438(15).

Oliver, H.W., Pakiser, L.C., and Kane, M.F., 1961, Gravity anomalies in the central Sierra Nevada, Califor- nia: Journal of Geophysical Research, v. 66, no. 12, p. 4265–4271, doi:10.1029/JZ066i012p04265.

Pickett, D.A., Saleeby, J.B., 1993, Thermobarometric constraints on the depth of exposure and conditions of plutonism and metamorphism at deep levels of the Sierra Nevada batholith, Tehachapi Mountains, California: Journal of Geophysical Research, v. 98, no. B1, p. 609–629, doi:10.1029/92JB01889.

Poage, M.A., and Chamberlain, C.P., 2002, Stable isotopic evidence for a pre-middle Miocene rain shallow in the western Basin and Range; implications for the paleotopography of the Sierra Nevada: Tectonics, v. 21, p. 1034

Reiners, P.W., 2005, Zircon (U-Th)/He Thermochronometry: Reviews in Mineralogy and Geochemistry, 2005, v. 58, p. 151-179

Richards, J.P., 2011, Magmatic to hydrothermal metal fluxes in convergent and collided margin: Ore Geology Reviews, v. 40, p. 1-26

Small, E.E., and Anderson, R.S., 1995, Geomorphically driven late Cenozoic rock uplift in the Sierra Nevada, California: Science, v. 270, p. 277–281, doi:10.1126 /science.270.5234.277.

Stock, G.M., Anderson, R.S., and Finkel, R.C., 2004, Pace of landscape evolution in the Sierra Nevada, California, revealed by cosmogenic dating of cave sediments: Geology, v. 32, p. 193–196, doi:10.1130/G20197.1.

Stockli, D.F., Dumitru, T.A., McWilliams, M.O., and Farley, K.A., 2003, Cenozoic Tectonic Evolution of the White Mountains, California and Nevada. Geological Society of America Bulletin, v. 115, p. 788–816.

Walker, J.D., Bidgoli, T.S., Didericksen, B.D., Stockli, D.F, and Andrew, J.E., 2014, Middle Miocene to recent exhumation of the Slate Range, eastern California, and implications for the timing of extension and the transition to transtension: Geosphere, v. 10, no. 2, p. 276-291 doi:10.1130;GES00947.1.

Wakabayashi, J., and Sawyer, T.L., 2001, Stream incision, tectonics, uplift and evolution of topography of the Sierra Nevada, California: The Journal of Geology, v. 109, p. 539–562, doi:10.1086/321962.

Wakabayashi, J., 2013, Paleochannels, stream incision, erosion, topographic evolution, and alternative explanations of paleoaltimetry, Sierra Nevada, California: Geosphere, v. 9, doi:10.1130/GES00814.1.

Wernicke, B., Clayton, R., Ducea, M., Jones, C.H., Park, S., Ruppert, S., Saleeby, J., Snow, J.K., Squires, L., Fliedner, M., Jiracek, G., Keller, R., Klemperer, S., Luetgert, J., Malin, P., Miller, K., Mooney, W., Oliver, H., and Phinney, R., 1996, Origin of high mountains in the continents: The Southern Sierra Nevada: Science, v. 271, no. 5246, p.190-193.

Whitney, J.D., 1880, The auriferous gravels of the Sierra Nevada of California, Memoirs of the Museum of Comparative Zoölogy, v. 6: Cambridge, University Press and John Wilson & Son, 569 p.

Whitney, J.D., 1882, The climatic changes of later geological times, Memoirs of the Museum of Comparative Zoölogy, v. 7, part 2: Cambridge, University Press and John Wilson & Son, 394 p.

Wolfe, J.A., Schorn, H.E., Forest, C.E., and Molnar, P., 1997, Paleobotanical evidence for high altitudes in Nevada during the Miocene: Science, v. 276, p. 1672– 1675, doi:10.1126/science.276.5319.1672.

Wolfe, J.A., Forest, C.E., and Molnar, P., 1998, Paleobotanical evidence of Eocene and Oligocene paleoaltitudes in midlatitude western North America: Geological Society of America Bulletin, v. 110, p. 664–678, doi:10.1130 /0016-

7606(1998)110<0664:PEOEAO>2.3.CO;2.

Yoshihiro S., Tetsumaru I., 2008, K-Ar ages of Late Cretaceous granitic ring complex around southern Lake Biwa, Southwest Japan: Cooling history of a huge cauldron: The Journal of the Geological Society of Japan, v. 99, no. 12, p. 975-990. doi:10.5575/geosoc.99.975, https://www.jstage.jst.go.jp/article/geosoc1893/99/12/99_12_975/_article/-char/en

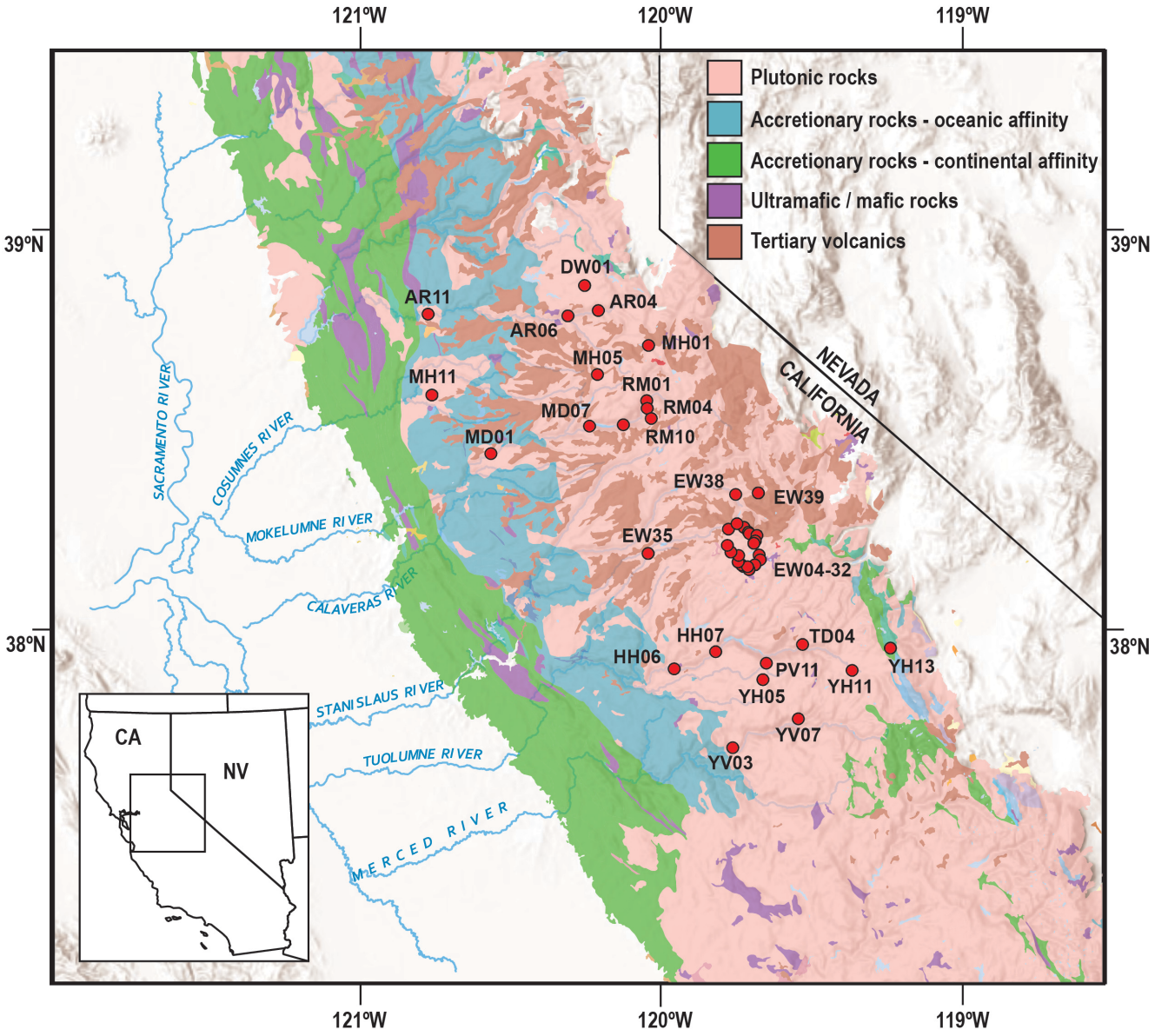
121°W
120°W
119°W
39°N
38°N
Plutonic rocks
Accretionary rocks - oceanic affinity
Accretionary rocks - continental affinity
Ultramafic / mafic rocks
Tertiary volcanics
DW01
AR11
AR04
AR06
MH01
MH05
MH11
RM01
RM04
MD07
RM10
MD01
EW38
EW39
EW35
EW04-32
HH07
TD04
HH06
PV11
YH13
YH11
YH05
YV07
YV03
NEVADA
CALIFORNIA
SACRAMENTO RIVER
COSUMNES RIVER
MOKELUMNE RIVER
CALAVERAS RIVER
STANISLAUS RIVER
TUOLUMNE RIVER
MERCED RIVER
CA
NV

Figure 2.1

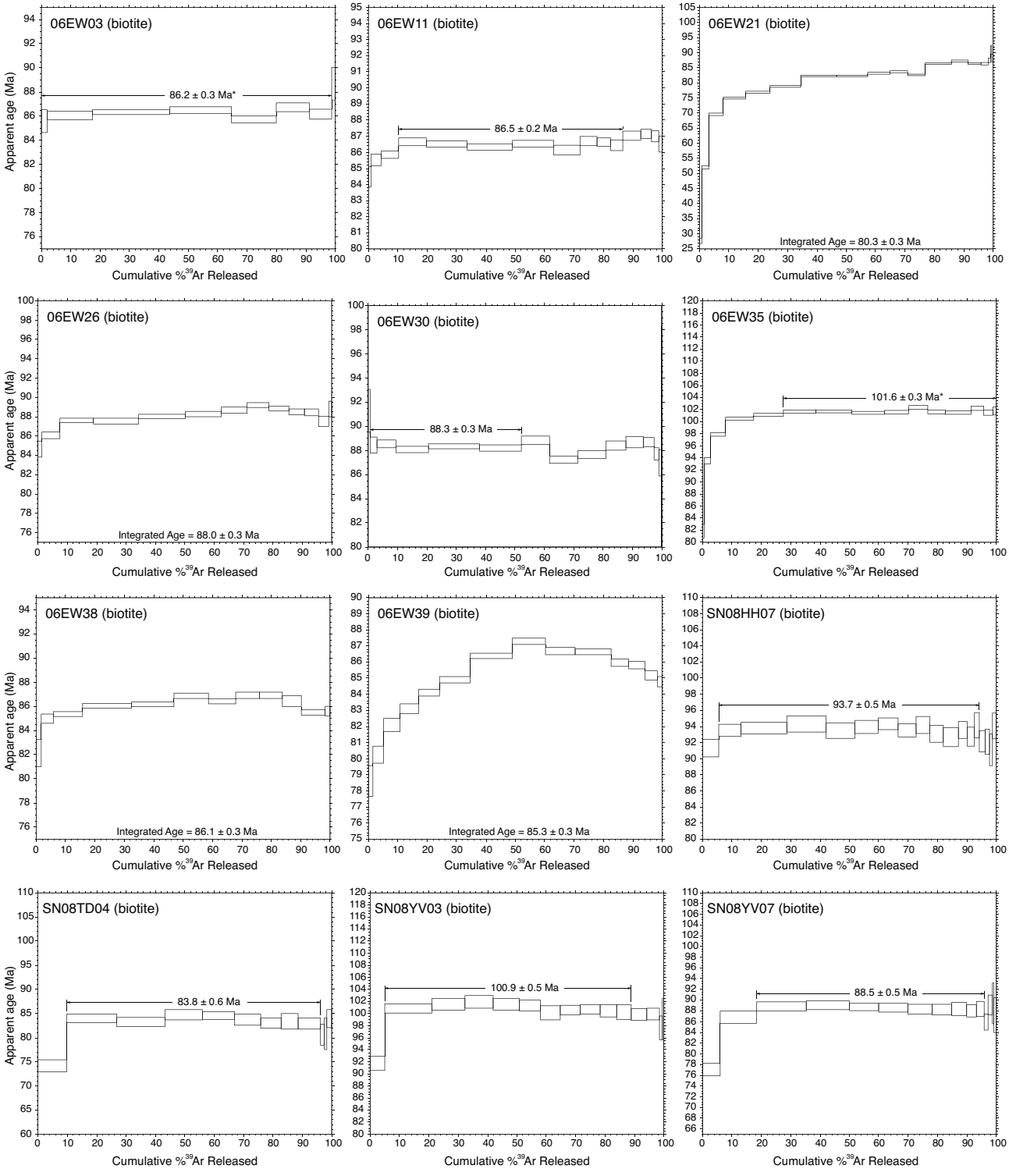
06EW03 (biotite)
86.2 ± 0.3 Ma*
06EW11 (biotite)
86.5 ± 0.2 Ma
06EW21 (biotite)
Integrated Age = 80.3 ± 0.3 Ma
06EW26 (biotite)
Integrated Age = 88.0 ± 0.3 Ma
06EW30 (biotite)
88.3 ± 0.3 Ma
06EW35 (biotite)
101.6 ± 0.3 Ma*
06EW38 (biotite)
Integrated Age = 86.1 ± 0.3 Ma
06EW39 (biotite)
Integrated Age = 85.3 ± 0.3 Ma
SN08HH07 (biotite)
93.7 ± 0.5 Ma
SN08TD04 (biotite)
83.8 ± 0.6 Ma
SN08YV03 (biotite)
100.9 ± 0.5 Ma
SN08YV07 (biotite)
88.5 ± 0.5 Ma
Apparent age (Ma)
Cumulative %39Ar Released

Figure 2.2

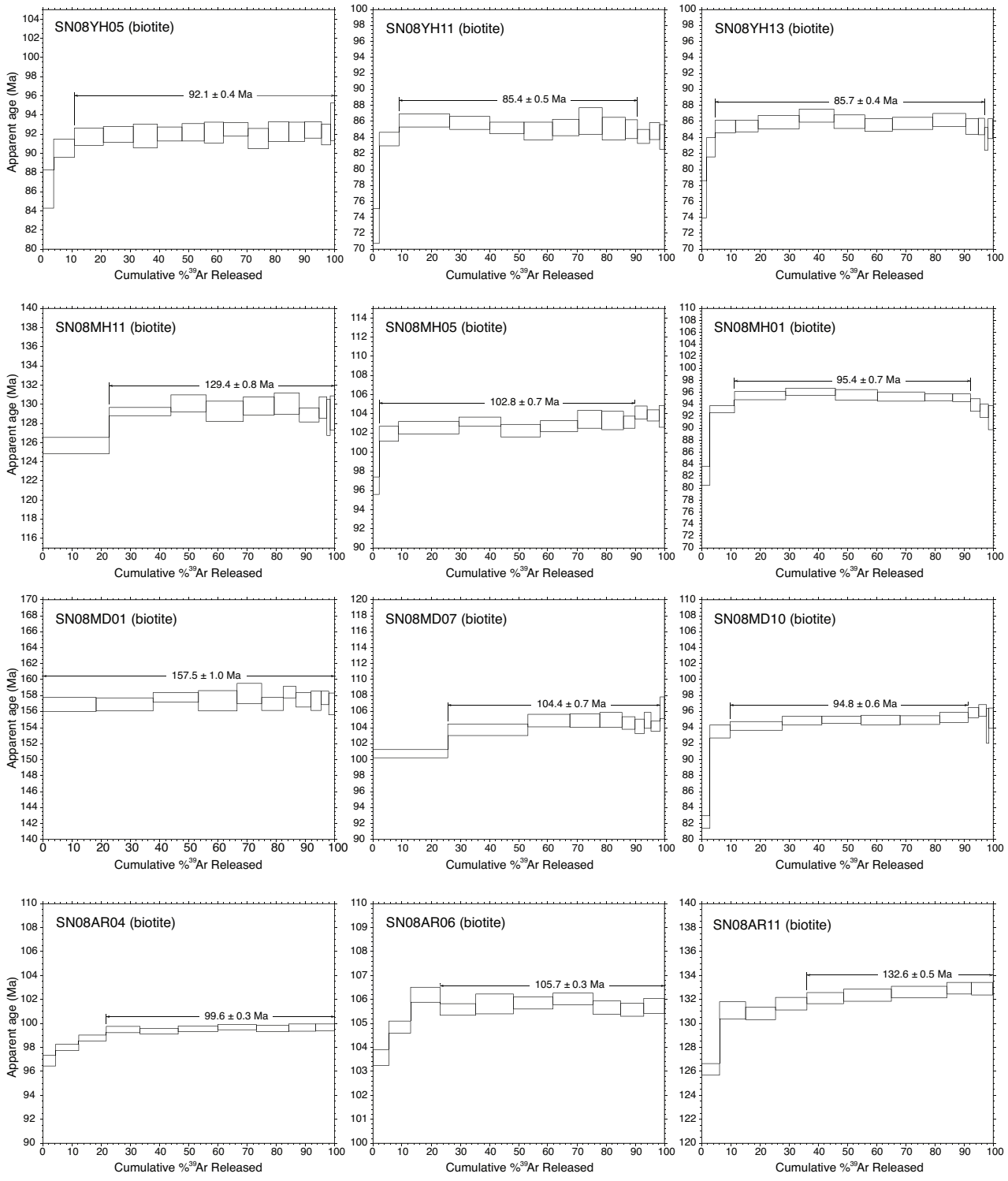

Figure 2.2 *(continued)*

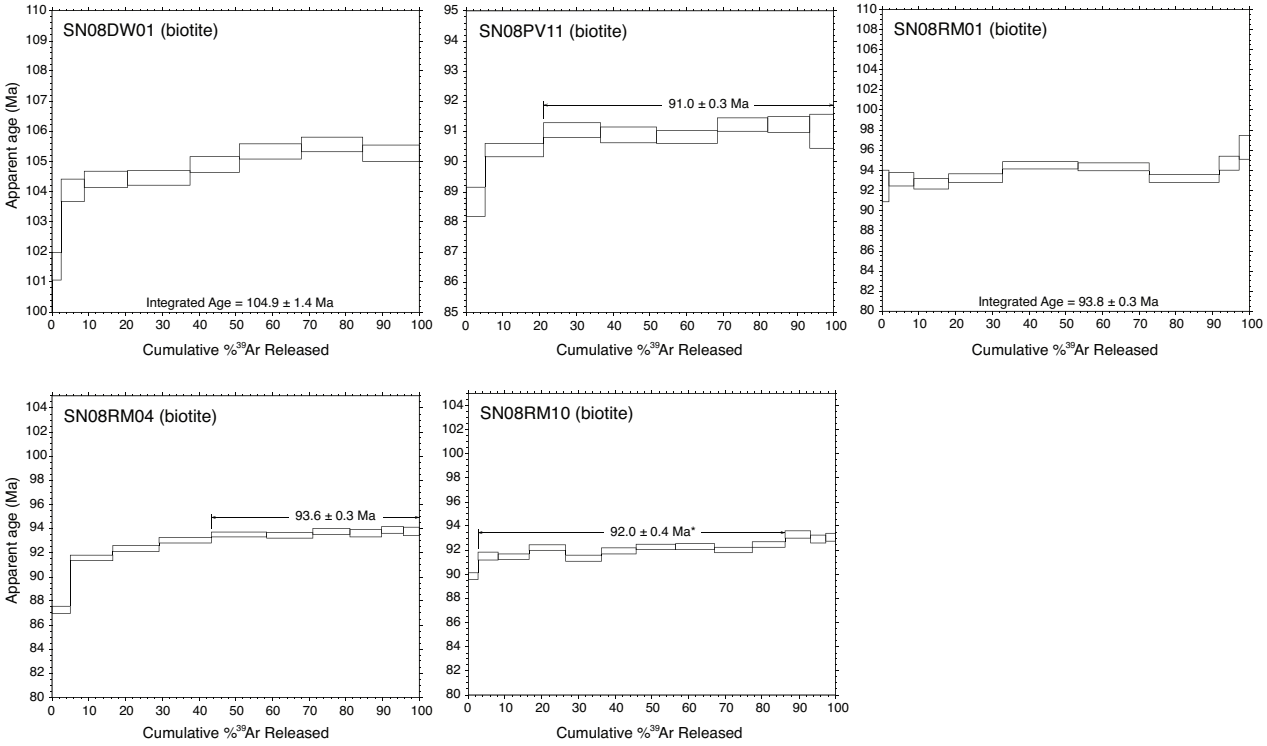

Figure 2.2 *(continued)*

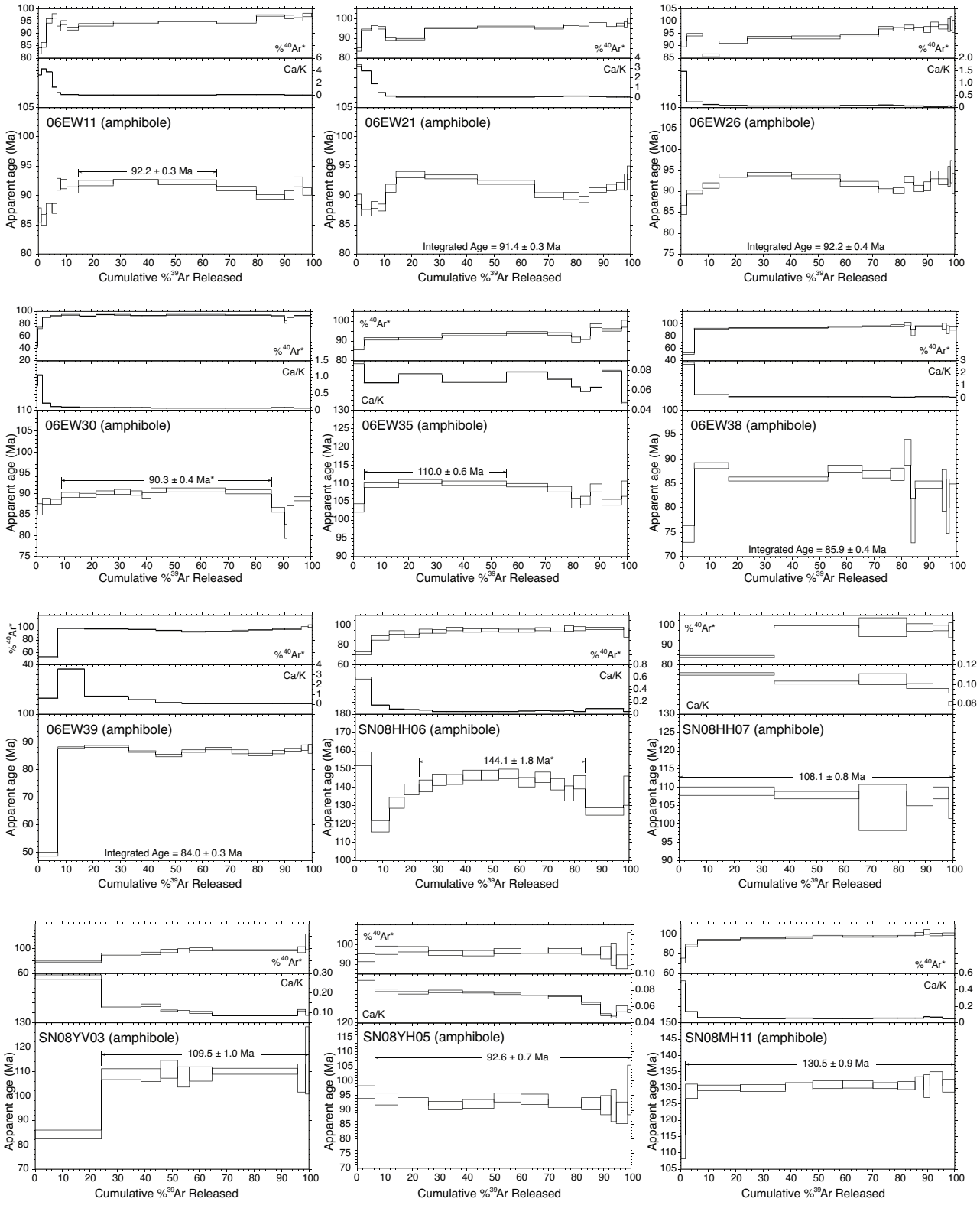

Figure 2.2 *(continued)*

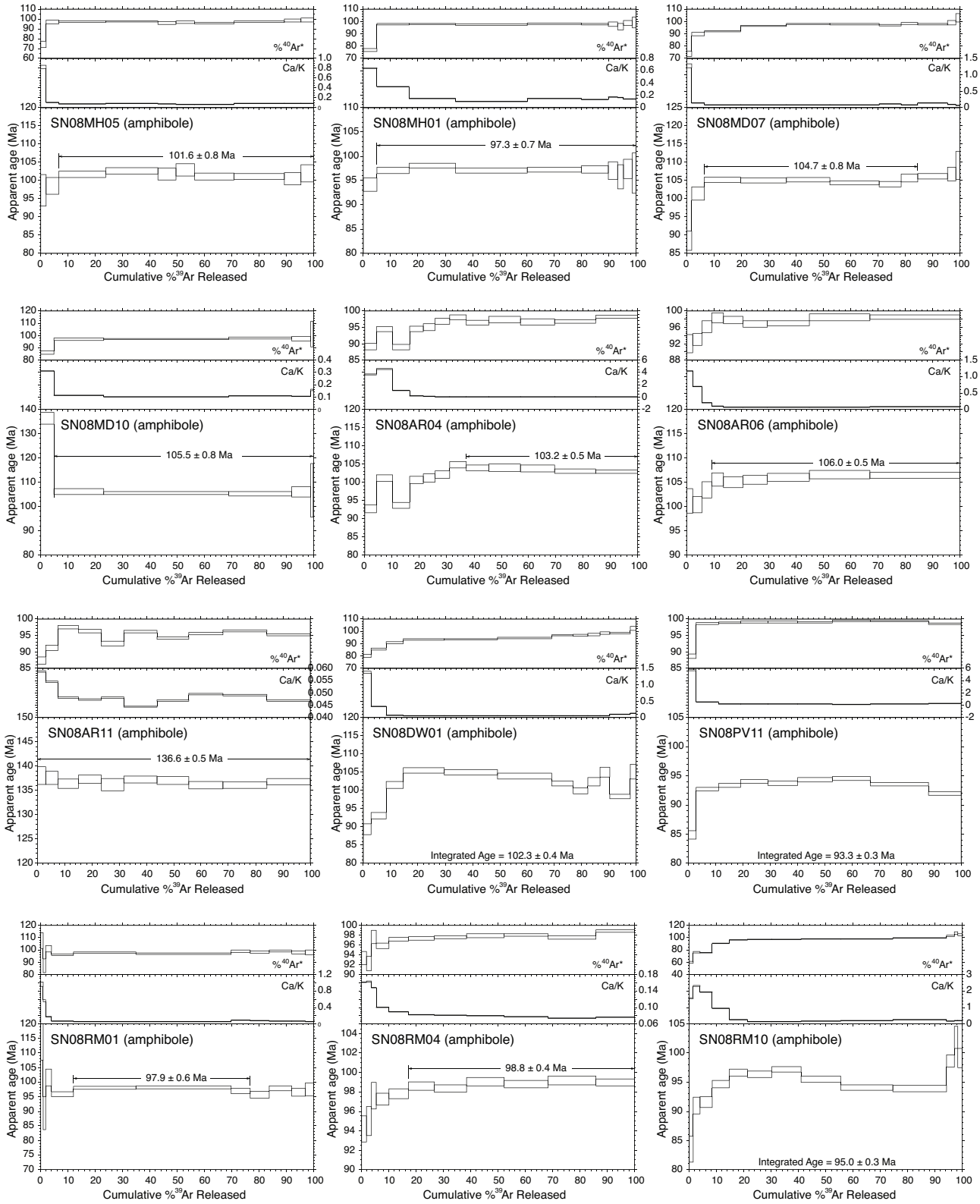

Figure 2.2 *(continued)*

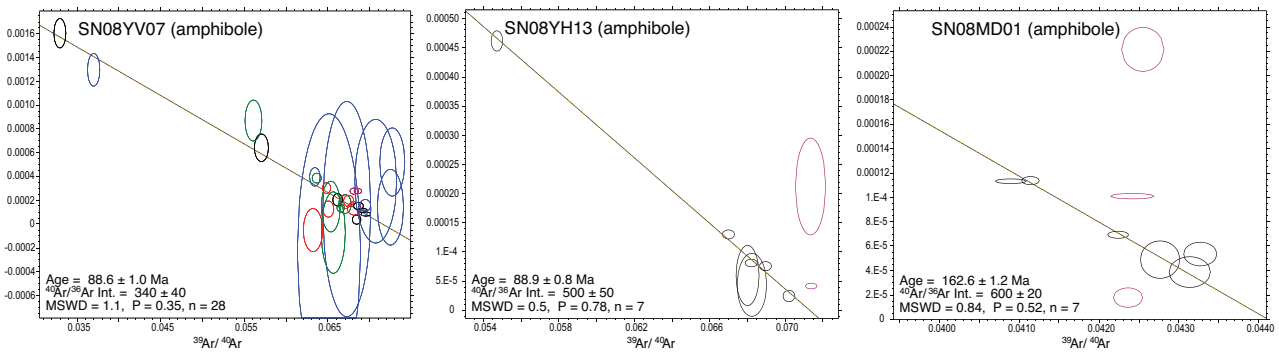

Figure 2.2 *(continued)*

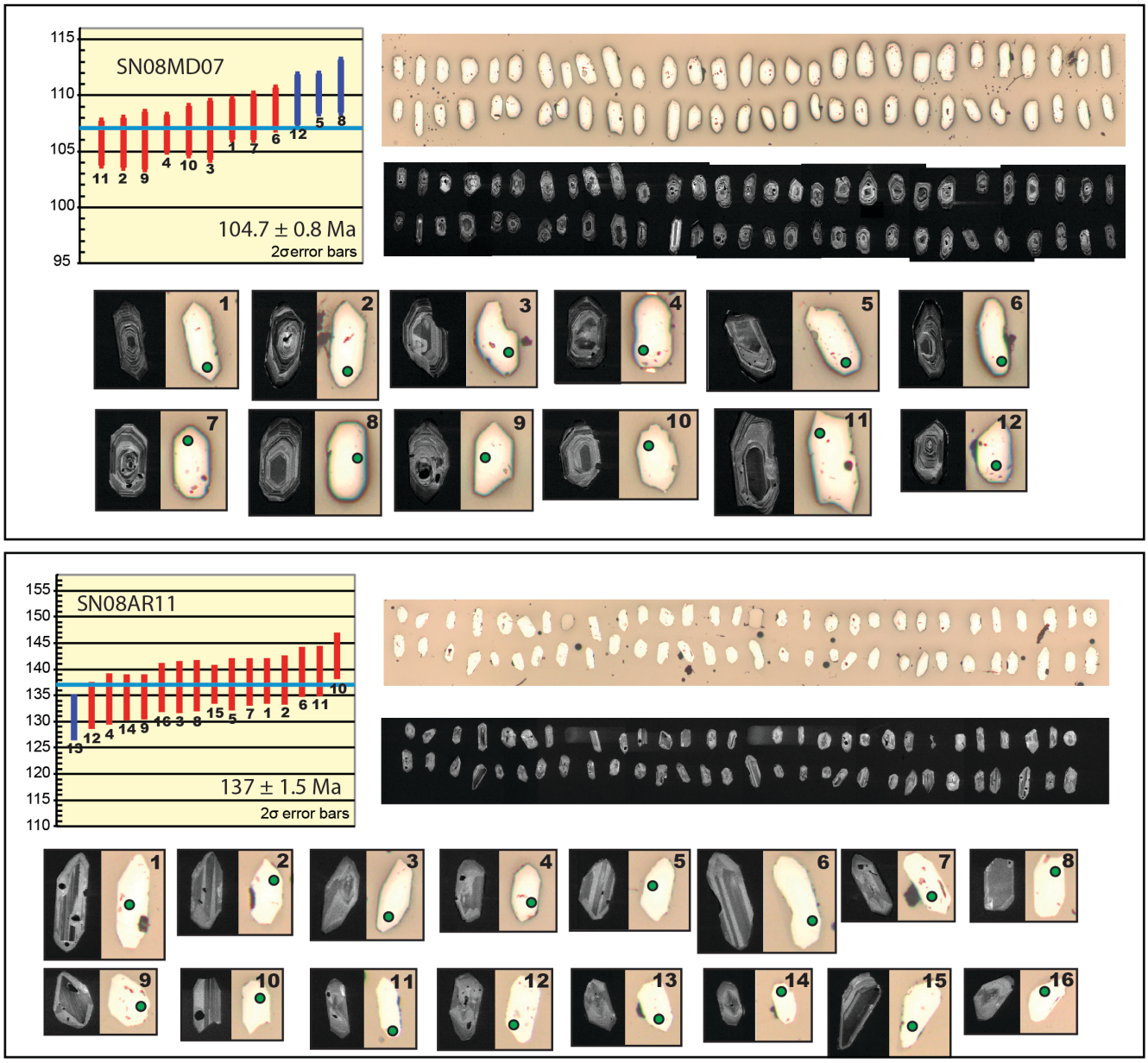
SN08MD07
104.7 ± 0.8 Ma
2σerror bars
SN08AR11
137 ± 1.5 Ma
2σ error bars

Figure 2.3

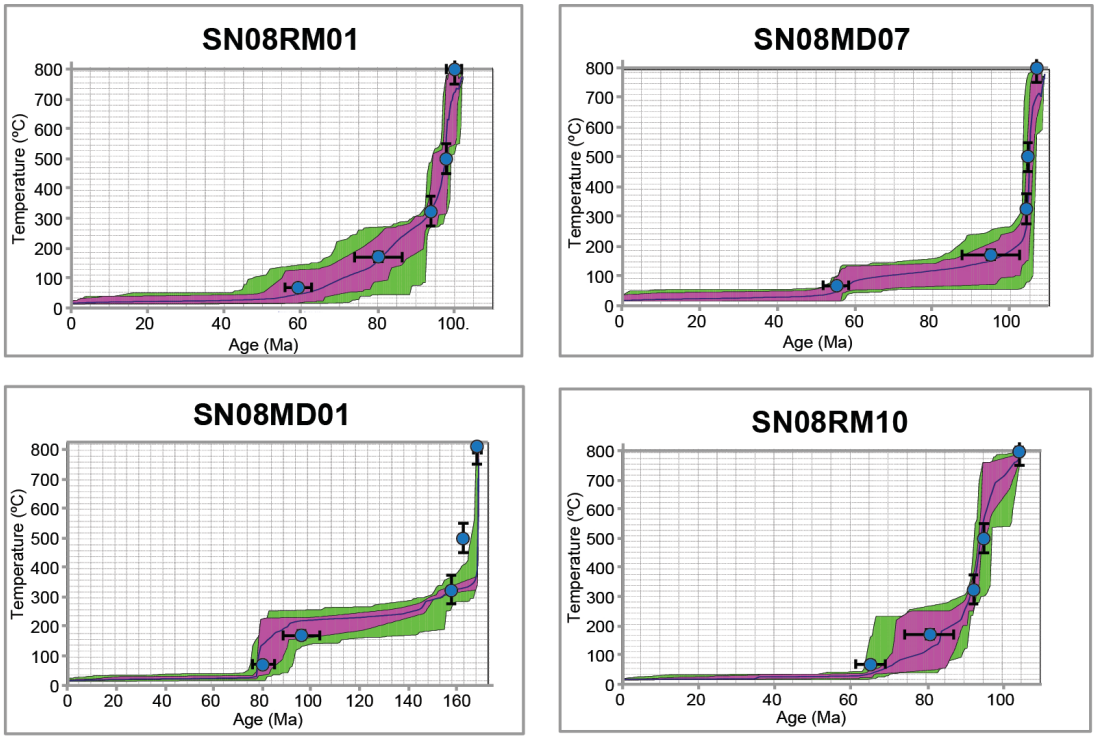
SN08RM01
SN08MD07
SN08MD01
SN08RM10
Temperature (ºC)
Age (Ma)

Figure 2.4

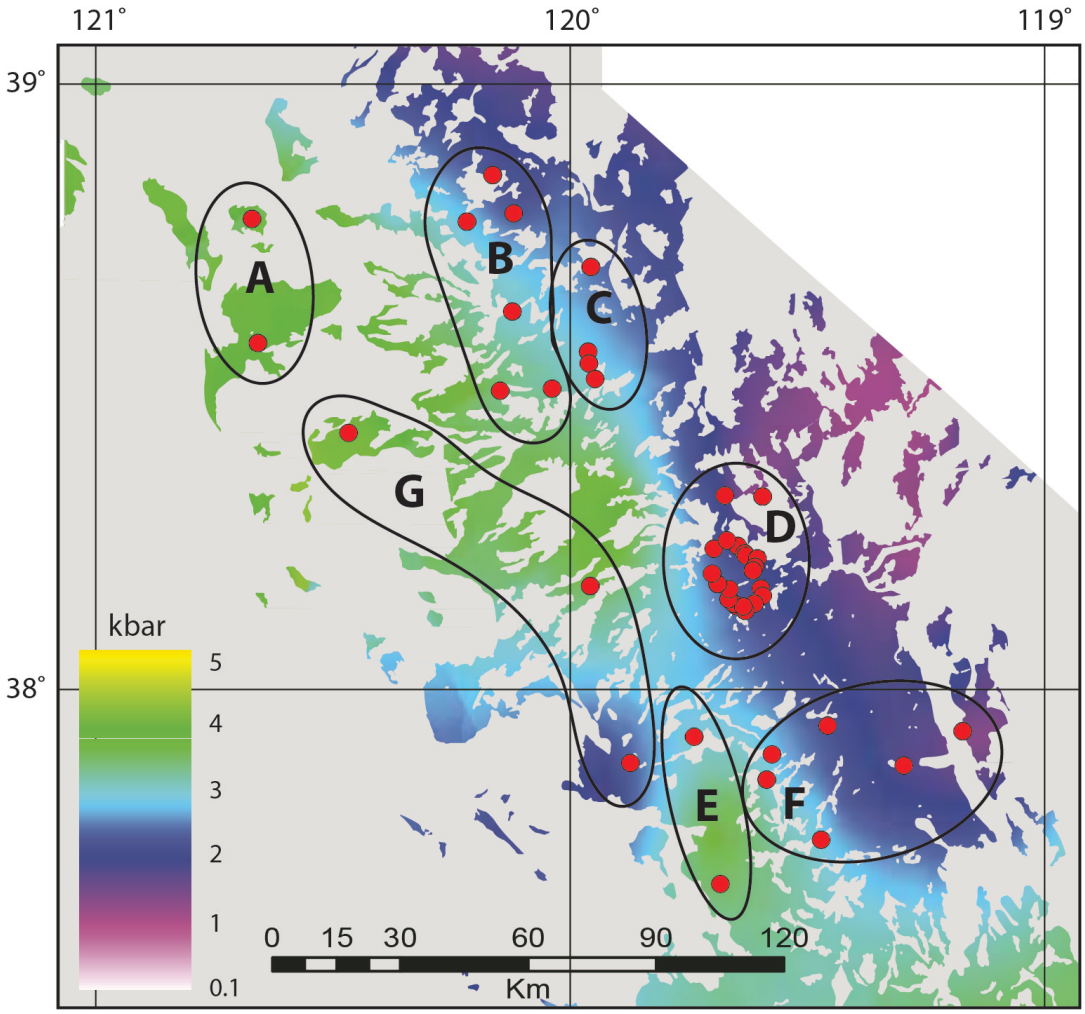

Figure 2.5

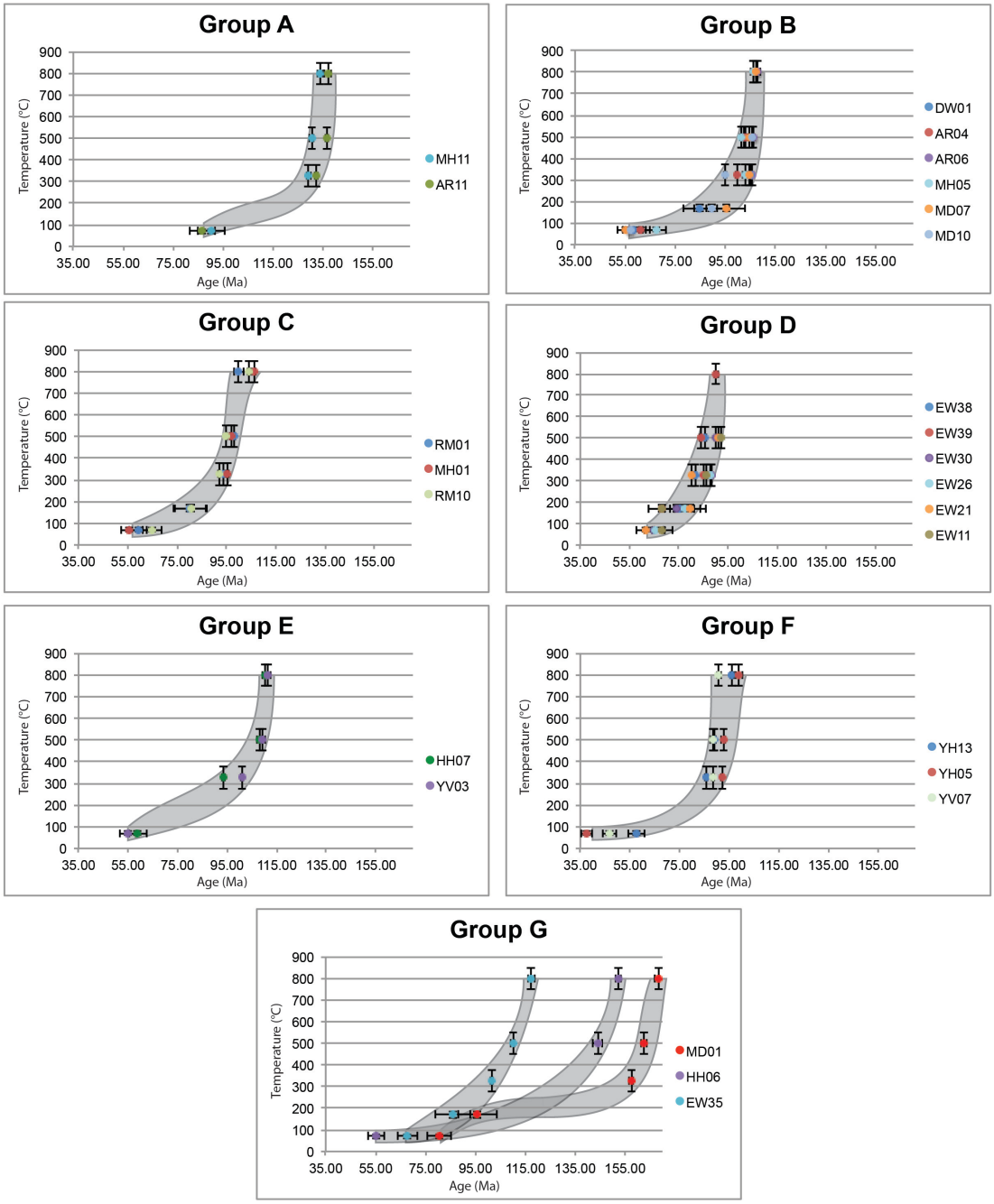
Group A
Temperature (°C)
900
800
700
600
500
400
300
200
100
0
35.00 55.00 75.00 95.00 115.00 135.00 155.00
Age (Ma)
MH11
AR11
Group B
Temperature (°C)
Age (Ma)
DW01
AR04
AR06
MH05
MD07
MD10
Group C
Temperature (°C)
Age (Ma)
RM01
MH01
RM10
Group D
Temperature (°C)
Age (Ma)
EW38
EW39
EW30
EW26
EW21
EW11
Group E
Temperature (°C)
Age (Ma)
HH07
YV03
Group F
Temperature (°C)
Age (Ma)
YH13
YH05
YV07
Group G
Temperature (°C)
Age (Ma)
MD01
HH06
EW35

Figure 2.6

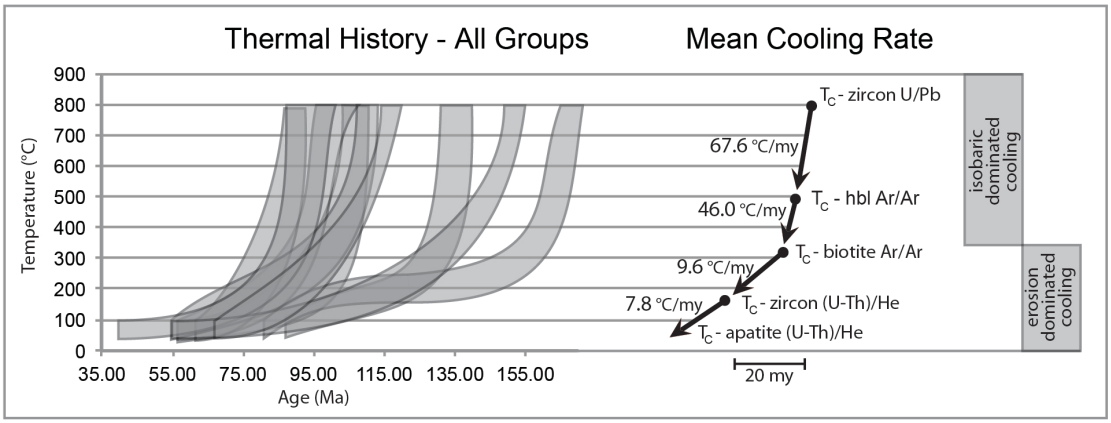
Thermal History - All Groups
Mean Cooling Rate
Temperature (°C)
900
800
700
600
500
400
300
200
100
0
35.00
55.00
75.00
95.00
115.00
135.00
155.00
Age (Ma)
T_C - zircon U/Pb
67.6 °C/my
T_C - hbl Ar/Ar
46.0 °C/my
T_C - biotite Ar/Ar
9.6 °C/my
7.8 °C/my
T_C - zircon (U-Th)/He
T_C - apatite (U-Th)/He
20 my
isobaric dominated cooling
erosion dominated cooling

Figure 2.7

Table 2.1. Mean age data

Sample Data				AGE DATA									
Sample Identification	**LATITUDE (°N)**	**LONGITUDE (°W)**	**elevation (m)**	**Apatite (U-Th)/He (± 1σ, Ma)**	**Zircon (U-Th)/He (± 1σ, Ma)**	**Ar/Ar Biotite (± 2σ, Ma)**	**Age Type***	**Ar/Ar Amphibole (± 2σ, Ma)**	**Age Type***	**U/Pb (± 2σ, Ma)**	**Age Type***	**num in group**	**num excluded**
SN08HH06	37.8793	119.9486	733	55.2 ± 5.3	-	-	-	144.1 ± 1.8	FP	152.4 ± 0.9	MG	8	0
SN08HH07	37.9224	119.8153	1020	59 ± 0.6	-	93.7 ± 0.5	NP	108.1 ± 0.8	NP	110.3 ± 1		11	1
SN08TD01	37.9216	119.6202	1288	37.8 ± 10.3	-	-	-	-	-	-	-	-	-
SN08TD04	37.9395	119.5364	1525	38.5 ± 2.5	-	83.8 ± 0.6	NP	-	-	104.2 ± 1.7	TZ	9	5
SN08YV03	37.6791	119.7608	640	55.2 ± 2.7	-	100.9 ± 0.5	NP	109.5 ± 1	NP	111.5 ± 1.2	MG	15	0
SN08YV07	37.7511	119.5508	1241	46.9 ± 3.3	-	88.5 ± 0.5	NP	88.6 ± 1	ISO	-	-	-	-
SN08YH05	37.8509	119.6637	2400	37.7 ± 3.5	-	92.1 ± 0.4	NP	92.6 ± 0.7	NP	99 ± 1.3	MG	11	1
SN08YH11	37.8736	119.3769	2602	57.9 ± 2.9	-	85.4 ± 0.5	NP	-	-	88.8 ± 0.8	TZ	8	3
SN08YH13	37.9293	119.2539	2935	57.6 ± 1.4	-	85.7 ± 0.4	NP	88.9 ± 0.8	ISO	96.3 ± 0.6	MG	14	2
SN08PV11	37.8928	119.6531	2403	54.1 ± 1.6	-	91 ± 0.3	NP	93.3 ± 0.3	IA	-	-	-	-
SN08MH01	38.6992	120.0309	2426	55.8 ± 1.1	-	95.4 ± 0.7	NP	97.3 ± 0.7	NP	106.2 ± 0.8	MG	8	4
SN08MH05	38.6251	120.1969	2321	67.3 ± 4.3	-	102.8 ± 0.7	NP	101.6 ± 0.8	NP	106 ± 1	MG	10	0
SN08MH11	38.5711	120.7331	2032	90.3 ± 5.6	-	129.4 ± 0.8	NP	130.5 ± 0.9	NP	133.9 ± 1	MG	20	0
SN08DW01	38.8509	120.2391	2125	58.5 ± 1.2	84.9 ± 3.7	104.9 ± 1.4	IA	102.3 ± 0.4	IA	90.8 ± 0.9	TZ	10	6
SN08MD01	38.4231	120.5409	703	80.4 ± 2.4	95.9 ± 0.2	157.5 ± 1	NP	162.6 ± 1.2	ISO	168.4 ± 1.6	TZ	9	6
SN08MD02	38.3135	120.7207	204	103 ± 3.7	-	-	-	-	-	-	-	-	-
SN08MD07	38.4939	120.2229	1074	55.3 ± 1.6	95.2 ± 7.6	104.4 ± 0.7	NP	104.7 ± 0.8	NP	107.1 ± 0.8	MG	9	3
SN08MD10	38.4978	120.1130	1301	57.3 ± 6.6	89.5 ± 7.2	94.8 ± 0.6	NP	105.5 ± 0.8	NP	-	-	-	-
SN08RM01	38.5589	120.0372	1643	59.2 ± 9.2	80.2 ± 6.5	93.8 ± 0.3	IA	97.9 ± 0.6	NP	100 ± 2.1	TZ	7	5
SN08RM04	38.5397	120.0352	1842	67.7 ± 7.1	-	93.6 ± 0.3	NP	98.8 ± 0.4	NP	-	-	-	-
SN08RM10	38.5140	120.0225	2498	65 ± 0.9	80.6 ± 4.8	92 ± 0.4	FP	95 ± 0.3	IA	104.2 ± 0.7	MG	11	3
SN08AR04	38.7875	120.1947	1618	61.3 ± 2.8	-	99.6 ± 0.3	NP	103.2 ± 0.5	NP	106.2 ± 1.2	MG	11	1
SN08AR06	38.7736	120.2932	1320	57.5 ± 8.7	-	105.7 ± 0.3	NP	106 ± 0.5	NP	107.9 ± 1.1	MG	15	1
SN08AR11	38.7761	120.7481	395	86.6 ± 2.1	-	132.6 ± 0.5	NP	136.6 ± 0.5	NP	137 ± 1.5	MG	15	1

Table 2.1. Mean age data (continued)

Sample Data				AGE DATA									
Sample Identification	**LATITUDE (°N)**	**LONGITUDE (°W)**	**elevation (m)**	**Apatite (U-Th)/He (± 1σ, Ma)**	**Zircon (U-Th)/He (± 1σ, Ma)**	**Ar/Ar Biotite (± 2σ, Ma)**	**Age Type***	**Ar/Ar Amphibole (± 2σ, Ma)**	**Age Type***	**U/Pb (± 2σ, Ma)**	**Age Type***	**num in group**	**num excluded**
06EW - 03	38.2376	119.7230	2530	7.9 ± 0.7	73.5 ± 3.6	86.2 ± 0.3	FP	-	-	-	-	-	-
06EW - 04	38.2256	119.7089	2591	9.3 ± 1.1	79.5 ± 6.3	-	-	-	-	-	-	-	-
06EW - 05	38.2213	119.7057	2685	10.4 ± 0.8	70.3 ± 11.5	-	-	-	-	-	-	-	-
06EW - 06	38.2168	119.6815	2774	-	64.9 ± 6.2	-	-	-	-	-	-	-	-
06EW - 08	38.2033	119.6867	2974	60.4 ± 3	70.6 ± 13	-	-	-	-	-	-	-	-
06EW - 09	38.1968	119.6908	3056	70.6 ± 0.1	70.6 ± 2.4	-	-	-	-	-	-	-	-
06EW - 11	38.1670	119.6748	2765	68.4 ± 1.5	68.2 ± 5.7	86.5 ± 0.2	NP	92.2 ± 0.3	NP	-	-	-	-
06EW - 13	38.1550	119.6709	2807	-	71.2 ± 6.5	-	-	-	-	-	-	-	-
06EW - 15	38.1422	119.6887	2438	61.7 ± 3.4	61 ± 5.7	-	-	-	-	-	-	-	-
06EW - 21	38.1383	119.7245	2548	61.5 ± 2.3	79.6 ± 9.3	80.3 ± 0.3	IA	91.4 ± 0.3	IA	-	-	-	-
06EW - 22	38.1423	119.7314	2426	63.6 ± 0.3	73.9 ± 6.1	-	-	-	-	-	-	-	-
06EW - 23	38.1300	119.7071	2396	-	64.8 ± 3.5	-	-	-	-	-	-	-	-
06EW - 24	38.1375	119.7118	2463	63.4 ± 2.9	67.3 ± 8.5	-	-	-	-	-	-	-	-
06EW - 26	38.1498	119.7423	2491	65.4 ± 3.1	77.6 ± -	88 ± 0.3	IA	92.2 ± 0.4	IA	-	-	-	-
06EW - 27	38.1662	119.7409	2536	64.8 ± 3.888	69 ± 12.7	-	-	-	-	-	-	-	-
06EW - 29	38.1748	119.7657	2655	65.7 ± 2.4	66.4 ± 3	-	-	-	-	-	-	-	-
06EW - 30	38.1916	119.7766	2658	64.9 ± 3.9	74.3 ± 6.5	88.3 ± 0.3	NP	90.3 ± 0.4	FP	-	-	-	-
06EW - 31	38.2333	119.7730	2560	60.5 ± 3.6	65.6 ± 1.5	-	-	-	-	-	-	-	-
06EW - 32	38.2465	119.7453	2380	8.5 ± 0.5	72.4 ± 1.8	-	-	-	-	-	-	-	-
06EW - 35	38.1719	120.0330	1765	67.7 ± 3.8	86 ± 3.2	101.6 ± 0.3	FP	110 ± 0.6	NP	117.4 ± 1.4	MG	9	1
06EW - 38	38.3210	119.7496	1927	13.4 ± 0.2	75.4 ± 5	81.6 ± 0.3	IA	85.9 ± 0.4	IA	-	-	-	-
06EW - 39	38.3194	119.6707	2586	6.3 ± 0.9	67.9 ± 7.6	85.3 ± 0.3	IA	84 ± 0.3	IA	90.3 ± 0.7	MG	7	1

Chapter 2 Figure Captions

Figure 2.1. Generalized geologic map of the central Sierra Nevada Range, showing sample locations for this study. Samples extend from the south fork of the American River drainage in the North to the Merced River drainage in the South. All samples were collected from surface exposure of plutonic rocks of the Sierra Nevada batholithic complex.

Figure 2.2. $^{40}Ar/^{39}Ar$ age spectra of samples from incremental heating experiments. Each age spectrum plots the cumulative % ^{39}Ar released per heating step versus the apparent age (Ma). When naturally occurring plateaus occur, they are the preferred age. Naturally occurring plateaus are defined by ≥3 contiguous heating steps comprising ≥50% of cumulative ^{39}Ar released with ages overlapping at the 2σ level of uncertainty. Integrated ages are used for samples that fail to give a plateau. Three amphibole step heating experiments yielded erratic age spectra. We suspect these results are due to alteration and/or incorporation of extraneous (i.e. non-atmospheric) argon. For these three samples, inverse isochron plots (generated in MassSpec) were utilized to establish ages and are included in figure 2.2. In all three samples, $^{40}Ar/^{36}Ar$ intercepts imply non-atmospheric ratios of non-radiogenic ^{40}Ar and ^{36}Ar were incorporated into the grains. Red error ellipses indicate heating steps that are omitted from calcualtions. All reported ages (steps, plateaus, and integrated) are shown with 2σ levels of uncertainty. Release spectra for amphibole analysis also include the Ca/K ratio and radiogenic ^{40}Ar yield.

Figure 2.3. Grain mounts, analyses locations and U-Pb age data for two selected samples. U/Pb age analysis, in this study, was done at the USGS/Stanford Super High Resolution Ion Microprobe 9 Reverse Geometry (SHRIMP-RG) laboratory in Palo Alto, CA. Zircon mounts were made for each sample and photographed using transmitted light and using cathedoluminescence to determine inclusion locations and abnormal zoning. The mounts are shown above, as are the individual analysis, which avoided grain cores and rim overgrowths. Age spectra are shown on the left and are shown with 2σ levels of uncertainty. Analyses excluded from the calculation of the mean sample age are shown in blue. Ages were determined using Squid2 (Ludwig, 2009).

Figure 2.4. Comparison of thermal models and cooling paths based on ages and closure temperatures. Individual $T_c t$ points are shown as blue circles with error bars. Green fields show thermal histories that result in modeled ages within 1σ error of observed ages and violet fields produce modeled ages within 2σ error of observed ages. See text for more details about the modeling and error analysis. The modeled thermal histories closely correlate with the plotted time/closure-temperature data-points..

Figure 2.5. A gradient map of geobarometry of Sierran plutons (from Nadin and Saleeby, 2008) of the central Sierra Nevada Range. Also shown are sample locations and sample groupings for rocks analyzed in this study. In an effort to simplify the large number of t/T paths generated by the data in this study, we identified regions whose samples shared geographic proximity and similar cooling ages. These samples were grouped as

illustrated in figure 2.5. The t/T plots of the data from each group produces similar t/T paths and a representative t/T envelope for that area is generated, as shown in figure 2.6.

Figure 2.6: Cooling histories of all samples yielding 4 or more thermochronometric analysis. Sample groups are illustrated in figure 2.5. Temperature data is based on: (1) U/Pb ages, (2) amphibole $^{40}Ar/^{39}Ar$ ages, (3) biotite $^{40}Ar/^{39}Ar$ ages, (4) zircon (U-Th)/He ages and (5) apatite (U-Th)/He data. Closure temperatures are: (1) 800 ± 50°C, (2) 500 ± 50°C, (3) 325 ± 50°C, (4) 170 ± 15°C and (5) 70 ± 10°C, respectively. Composite (grey) time/Temperature (t/T) envelopes are drawn to encompass the extent of most data and errors for each sample group and identify the possible t/T path representative of the sample group.

Figure 2.7: A summary of t/T paths based upon regions and average cooling rates. The composite t/T envelopes illustrated in figure 2.4 are compiled into a singular plot to show the variation in cooling histories between the different regions of this study. Also shown are the average cooling rates calculated using the age data and closure temperatures outlined in Figure 2.4. To produce the average cooling rates, all available geo- and thermochronologic data produced in this study is used. A transition from higher cooling rates to lower cooling rates is identified and discussed in the text. Distinct cooling regimes are also identified on this figure.

Chapter 2 - Supplemental tables.

Supplemental Table SP2.1. $^{40}Ar/^{39}Ar$ Isotopic Data

		Relative Isotopic Abundances										Derived Results									Inverse Isochron Data				
Lab ID#	Watts	^{40}Ar ±1σ		^{39}Ar ±1σ		^{38}Ar ±1σ		^{37}Ar ±1σ		^{36}Ar ±1σ		^{39}Ar Mol × 10^{-14}	^{39}Ar % of total	% $(^{36}Ar)_{Ca}$	Ca/K ±1σ		% $^{40}Ar^{*}$	Age (Ma) ±1σ		w/±J ±1σ	$^{36}Ar/^{40}Ar$ ±% 1σ		$^{39}Ar/^{40}Ar$ ±% 1σ		$^{36}Ar/^{39}Ar$ Er. Corr.
SN08HH06 - amphibole - irradiation:DT-2																									
119-02A	0.5	65.0095	0.2002	1.8581	0.0111	0.0290	0.0094	1.6355	0.0247	0.0633	0.0014	0.24	5.8	0.7	1.725	0.028	71.4	155.52	1.91	1.94	0.00097	2.43	0.02858	0.71	0.2539
119-02B	0.7	46.2711	0.2402	2.1335	0.0161	0.0300	0.0100	7.6807	0.1023	0.0224	0.0013	0.28	6.6	8.9	7.056	0.109	87.0	118.66	1.58	1.60	0.00044	6.19	0.04607	0.95	0.1098
119-02C	0.9	40.3331	0.1204	1.7823	0.0094	0.0213	0.0087	10.7019	0.0845	0.0129	0.0011	0.23	5.5	21.6	11.769	0.113	92.6	131.47	1.43	1.45	0.00025	11.29	0.04412	0.64	0.0559
119-02D	1.0	43.8393	0.1304	1.7626	0.0093	0.0262	0.0085	11.9667	0.0667	0.0193	0.0012	0.23	5.5	16.1	13.307	0.104	89.1	138.76	1.50	1.52	0.00037	7.23	0.04013	0.64	0.0872
119-02E	1.1	36.9616	0.1005	1.5421	0.0101	0.0249	0.0073	12.1210	0.0905	0.0110	0.0011	0.20	4.8	28.6	15.406	0.155	93.7	140.62	1.61	1.63	0.00021	13.49	0.04163	0.74	0.0436
119-02F	1.2	40.9502	0.1005	1.6655	0.0101	0.0240	0.0081	19.2454	0.1085	0.0139	0.0011	0.22	5.2	36.0	22.649	0.190	93.6	144.07	1.50	1.53	0.00022	11.87	0.04054	0.69	0.0499
119-02G	1.3	47.0253	0.1204	1.9605	0.0099	0.0311	0.0091	22.3813	0.1265	0.0122	0.0011	0.26	6.1	47.6	22.375	0.172	96.0	144.13	1.36	1.38	0.00014	17.90	0.04156	0.61	0.0347
119-02H	1.4	52.7848	0.2302	2.1349	0.0101	0.0355	0.0100	26.8264	0.1386	0.0164	0.0011	0.28	6.6	42.5	24.629	0.175	94.7	146.59	1.37	1.39	0.00018	11.75	0.04031	0.68	0.0601
119-02I	1.5	52.2091	0.1703	2.1123	0.0111	0.0366	0.0094	23.5668	0.2047	0.0153	0.0012	0.28	6.5	40.0	21.868	0.224	94.8	146.60	1.37	1.40	0.00018	12.70	0.04034	0.66	0.0506
119-02J	1.6	57.5307	0.1803	2.3009	0.0111	0.0569	0.0055	25.0797	0.0968	0.0178	0.0013	0.30	7.1	36.7	21.364	0.135	94.2	147.34	1.33	1.36	0.00020	11.14	0.03988	0.62	0.0581
119-02K	1.7	46.9786	0.1304	1.9400	0.0101	0.0291	0.0084	19.9136	0.1508	0.0145	0.0010	0.25	6.0	35.6	20.119	0.187	94.1	142.70	1.31	1.34	0.00020	11.11	0.04118	0.63	0.0562
119-02L	1.8	44.7820	0.1104	1.8432	0.0111	0.0272	0.0087	17.0222	0.2592	0.0109	0.0011	0.24	5.7	40.5	18.101	0.298	95.7	145.44	1.46	1.49	0.00015	17.24	0.04106	0.69	0.0344
119-02M	1.9	39.6064	0.1005	1.6616	0.0111	0.0289	0.0080	16.5939	0.1029	0.0111	0.0011	0.22	5.2	38.8	19.574	0.181	94.9	141.70	1.56	1.58	0.00017	15.86	0.04184	0.75	0.0365
119-02N	2.0	24.4159	0.0836	1.0826	0.0084	0.0126	0.0041	10.2043	0.1812	0.0055	0.0010	0.14	3.4	48.7	18.475	0.360	96.6	136.63	2.05	2.07	0.00011	36.43	0.04423	0.88	0.0160
119-02O	2.2	32.6669	0.1104	1.3823	0.0111	0.0211	0.0066	16.3993	0.1090	0.0083	0.0010	0.18	4.3	51.3	23.253	0.245	96.3	142.61	1.83	1.85	0.00012	25.37	0.04218	0.90	0.0227
119-02P	2.5	94.2797	0.4001	4.5048	0.0291	0.0819	0.0020	26.4328	0.3563	0.0182	0.0007	0.59	14.0	37.8	11.501	0.173	96.5	126.79	1.05	1.07	0.00012	6.29	0.04771	0.81	0.1047
119-02Q	3.0	14.1562	0.0422	0.5931	0.0089	0.0120	0.0030	7.3174	0.1272	0.0056	0.0011	0.08	1.8	33.9	24.180	0.559	92.3	138.11	3.93	3.94	0.00026	29.70	0.04176	1.56	0.0135
SN08HH07 - amphibole - irradiation:DT-2																									
121-01A	1.6	418.0815	0.5704	20.3999	0.0641	0.6436	0.0111	94.1784	0.4169	0.2479	0.0026	2.67	34.8	9.9	9.049	0.050	84.2	108.91	0.58	0.61	0.00053	1.42	0.04874	0.40	0.4455
121-01B	1.8	312.9336	0.6102	18.1294	0.0621	0.5658	0.0100	90.7280	0.5647	0.0345	0.0014	2.37	30.9	68.4	9.809	0.071	99.0	107.85	0.50	0.54	0.00003	13.40	0.05786	0.45	0.0477
121-01C	2.0	169.9205	2.8001	10.1680	0.2602	0.2956	0.0064	49.2745	0.3391	0.0193	0.0007	1.33	17.3	66.5	9.498	0.254	98.9	104.42	3.15	3.15	0.00004	11.58	0.05977	3.09	0.0919
121-01D	2.2	98.2715	0.5702	5.7310	0.0371	0.1782	0.0035	29.7588	0.3299	0.0120	0.0011	0.75	9.8	64.7	10.178	0.132	98.7	106.92	1.01	1.03	0.00004	26.36	0.05824	0.90	0.0283
121-01E	2.4	57.2450	0.1708	3.2835	0.0141	0.0978	0.0046	17.9063	0.1840	0.0075	0.0010	0.43	5.6	61.9	10.689	0.120	98.5	108.44	0.82	0.85	0.00005	35.28	0.05728	0.57	0.0185
121-01F	2.6	16.0334	0.0582	0.9345	0.0079	0.0132	0.0069	5.9310	0.0616	0.0030	0.0010	0.12	1.6	52.2	12.440	0.168	97.4	105.60	2.11	2.12	0.00009	67.78	0.05819	0.95	0.0085
SN08HH07 - biotite - irradiation:DT-2																									
115-01A	0.1	192.5962	0.4402	12.2944	0.0521	0.2032	0.0064	0.0717	0.0108	0.0522	0.0014	1.61	5.5	0.0	0.011	0.002	92.0	91.27	0.55	0.57	0.00027	2.87	0.06385	0.53	0.2193
115-01B	0.1	251.2826	0.3802	16.9058	0.0511	0.2805	0.0096	0.0450	0.0125	0.0052	0.0010	2.21	7.6	0.2	0.005	0.001	99.4	93.50	0.38	0.42	0.00002	18.66	0.06729	0.40	0.0341
115-01C	0.2	515.6562	0.3702	34.6345	0.1101	0.4978	0.0038	0.0456	0.0104	0.0090	0.0011	4.52	15.6	0.1	0.003	0.001	99.5	93.74	0.36	0.40	0.00002	12.02	0.06718	0.38	0.0516
115-01D	0.3	448.1419	0.6501	30.0241	0.1401	0.4284	0.0041	0.0152	0.0139	0.0026	0.0011	3.92	13.5	0.1	0.001	0.001	99.8	94.29	0.49	0.53	0.00001	40.80	0.06701	0.53	0.0147
115-01E	0.4	317.0534	0.4002	21.4071	0.1001	0.2991	0.0094	0.0793	0.0130	0.0032	0.0008	2.80	9.6	0.6	0.007	0.001	99.7	93.46	0.49	0.52	0.00001	24.76	0.06753	0.53	0.0241
115-01F	0.5	267.3530	0.7201	17.9559	0.0511	0.3026	0.0095	0.0971	0.0149	0.0031	0.0010	2.34	8.1	0.8	0.011	0.002	99.7	93.92	0.42	0.46	0.00001	32.39	0.06718	0.44	0.0207
115-01G	0.7	222.8872	0.3802	14.9040	0.0391	0.2546	0.0095	0.0431	0.0144	0.0027	0.0010	1.95	6.7	0.4	0.006	0.002	99.6	94.30	0.37	0.41	0.00001	36.16	0.06688	0.37	0.0179
115-01H	0.9	202.4367	0.4702	13.6623	0.0411	0.2044	0.0077	0.0233	0.0130	0.0021	0.0010	1.78	6.1	0.3	0.003	0.002	99.7	93.50	0.42	0.45	0.00001	46.89	0.06750	0.43	0.0140
115-01I	1.0	153.4915	0.5002	10.2531	0.0391	0.1629	0.0040	0.0000	0.0126	0.0032	0.0010	1.34	4.6	0.0	0.000	0.002	99.4	94.16	0.53	0.56	0.00002	30.72	0.06681	0.54	0.0220
115-01J	1.1	154.4596	0.4302	10.4646	0.0441	0.1685	0.0053	0.0367	0.0130	0.0020	0.0010	1.37	4.7	0.5	0.007	0.002	99.6	93.07	0.53	0.55	0.00001	47.30	0.06776	0.55	0.0137
115-01K	1.2	166.5920	0.4102	11.3571	0.0601	0.1732	0.0065	0.0347	0.0112	0.0015	0.0009	1.48	5.1	0.6	0.006	0.002	99.7	92.63	0.58	0.61	0.00001	64.25	0.06819	0.62	0.0095
115-01L	1.3	100.4350	0.1805	6.7443	0.0291	0.1027	0.0032	0.0000	0.0117	0.0025	0.0009	0.88	3.0	0.0	0.000	0.003	99.3	93.56	0.53	0.56	0.00003	36.46	0.06716	0.51	0.0169
115-01M	1.4	78.6800	0.1705	5.3039	0.0231	0.0777	0.0026	0.0000	0.0113	0.0034	0.0010	0.69	2.4	0.0	0.000	0.004	98.7	92.72	0.59	0.61	0.00004	28.82	0.06742	0.53	0.0217
115-01N	1.5	56.9473	0.1406	3.8237	0.0231	0.0616	0.0020	0.0139	0.0131	0.0003	0.0010	0.50	1.7	1.2	0.007	0.007	99.8	94.11	0.79	0.81	0.00001	338.13	0.06716	0.69	0.0018
115-01O	1.6	63.0099	0.1605	4.3082	0.0221	0.0619	0.0025	0.0000	0.0117	0.0011	0.0009	0.56	1.9	0.0	0.000	0.005	99.5	92.14	0.67	0.70	0.00002	84.92	0.06839	0.61	0.0073
115-01P	1.8	48.8725	0.1207	3.3285	0.0191	0.0520	0.0019	0.0208	0.0135	0.0016	0.0009	0.43	1.5	0.3	0.012	0.008	99.0	92.06	0.78	0.80	0.00003	57.00	0.06812	0.66	0.0106
115-01Q	2.0	30.3642	0.0999	2.0887	0.0131	0.0231	0.0092	0.0005	0.0113	0.0012	0.0008	0.27	0.9	0.0	0.000	0.011	98.9	91.05	0.98	0.99	0.00004	71.70	0.06880	0.74	0.0086
115-01S	3.0	43.4203	0.0979	2.8934	0.0151	0.0486	0.0024	0.0595	0.0122	0.0015	0.0009	0.38	1.3	1.1	0.040	0.008	99.0	94.03	0.81	0.83	0.00003	63.37	0.06665	0.61	0.0096
SN08TD04 - biotite - irradiation:DT-2																									
114-02A	0.1	240.0401	0.5601	14.3541	0.0551	0.2605	0.0080	0.2437	0.0130	0.2467	0.0028	1.88	9.9	0.0	0.033	0.002	69.6	74.11	0.65	0.67	0.00103	1.40	0.05981	0.50	0.4570
114-02B	0.2	351.9970	0.3302	24.6648	0.1101	0.3440	0.0032	0.2200	0.0145	0.0878	0.0017	3.22	17.0	0.1	0.017	0.001	92.6	83.90	0.45	0.48	0.00025	2.11	0.07009	0.50	0.2828
114-02C	0.3	329.5669	0.6001	23.7560	0.1101	0.3306	0.0029	0.1866	0.0155	0.0612	0.0016	3.11	16.4	0.1	0.015	0.001	94.5	83.23	0.48	0.50	0.00019	2.76	0.07210	0.54	0.2203
114-02D	0.4	263.9653	0.6601	18.7021	0.0911	0.2846	0.0099	0.2161	0.0186	0.0484	0.0011	2.45	12.9	0.1	0.023	0.002	94.6	84.71	0.52	0.54	0.00018	2.49	0.07087	0.59	0.2504
114-02E	0.5	226.2585	0.3901	15.8400	0.0481	0.2527	0.0093	0.2000	0.0155	0.0518	0.0014	2.07	10.9	0.1	0.025	0.002	93.2	84.51	0.40	0.43	0.00023	2.89	0.07002	0.41	0.2215
114-02F	0.7	182.3217	0.6501	12.9060	0.0611	0.2026	0.0072	0.2346	0.0145	0.0411	0.0013	1.69	8.9	0.1	0.036	0.002	93.3	83.69	0.58	0.60	0.00023	3.38	0.07080	0.63	0.1973
114-02G	0.9	140.2187	0.3601	10.0262	0.0461	0.1503	0.0049	0.2135	0.0155	0.0311	0.0011	1.31	6.9	0.2	0.042	0.003	93.5	82.97	0.53	0.55	0.00022	3.74	0.07152	0.57	0.1689
114-02H	1.0	119.7561	0.6301	8.5713	0.0591	0.1166	0.0036	0.1624	0.0140	0.0245	0.0011	1.12	5.9	0.2	0.037	0.003	94.0	83.33	0.80	0.81	0.00020	4.66	0.07159	0.90	0.1505
114-02I	1.2	152.3430	0.5001	10.9397	0.0531	0.1700	0.0063	0.2952	0.0136	0.0321	0.0013	1.43	7.5	0.2	0.053	0.002	93.8	82.91	0.57	0.59	0.00021	4.01	0.07182	0.63	0.1629
114-02J	1.4	26.0895	0.0945	1.8724	0.0102	0.0144	0.0093	0.0956	0.0145	0.0079	0.0009	0.24	1.3	0.3	0.100	0.015	91.0	80.57	1.09	1.10	0.00030	11.87	0.07178	0.69	0.0551
114-02K	1.6	16.9261	0.0403	1.2030	0.0102	0.0091	0.0057	0.1252	0.0114	0.0056	0.0010	0.16	0.8	0.6	0.204	0.019	90.4	80.75	1.65	1.66	0.00033	17.56	0.07109	0.91	0.0302
114-02L	1.8	32.4442	0.1105	2.3492	0.0131	0.0317	0.0023	0.2238	0.0181	0.0047	0.0009	0.31	1.6	1.2	0.187	0.015	95.7	83.92	0.93	0.94	0.00014	19.78	0.07242	0.69	0.0324

Supplemental Table SP2.1. $^{40}Ar/^{39}Ar$ Isotopic Data (continued)

		Relative Isotopic Abundances										Derived Results									Inverse Isochron Data				
Lab ID#	Watts	^{40}Ar ±1σ		^{39}Ar ±1σ		^{38}Ar ±1σ		^{37}Ar ±1σ		^{36}Ar ±1σ		^{39}Ar Mol × 10^{-14}	^{39}Ar % of total	$\%(^{36}Ar)_{Ca}$	Ca/K ±1σ		$\%^{40}Ar^{*}$	Age (Ma) ±1σ		w/±J ±1σ	$^{36}Ar/^{40}Ar$ ±%1σ		$^{39}Ar/^{40}Ar$ ±%1σ		$^{36}Ar/^{39}Ar$ Er. Corr.
SN08YH05 - amphibole - irradiation:DT-2																									
123-02A	0.7	33.0387	0.1110	2.0299	0.0101	0.0121	0.0150	10.9573	0.1568	0.0105	0.0010	0.27	6.5	27.1	10.580	0.161	93.2	96.05	1.09	1.10	0.00023	12.88	0.06136	0.64	0.0507
123-02B	0.9	39.8149	0.2105	2.6140	0.0141	0.0500	0.0044	16.6975	0.1266	0.0084	0.0010	0.34	8.4	51.5	12.520	0.118	97.0	93.65	1.01	1.03	0.00010	24.32	0.06555	0.79	0.0305
123-02C	1.0	52.0578	0.1508	3.4677	0.0161	0.0767	0.0042	23.1067	0.2176	0.0104	0.0010	0.45	11.2	57.7	13.060	0.138	97.5	92.84	0.74	0.76	0.00008	21.82	0.06650	0.59	0.0295
123-02D	1.1	58.5057	0.1408	3.8741	0.0191	0.0878	0.0045	25.1304	0.2026	0.0155	0.0010	0.51	12.5	42.2	12.714	0.121	95.5	91.50	0.72	0.75	0.00015	11.34	0.06611	0.59	0.0546
123-02E	1.2	53.6736	0.1508	3.5380	0.0161	0.0728	0.0031	23.3721	0.0713	0.0141	0.0010	0.46	11.4	43.2	12.948	0.073	95.6	92.01	0.76	0.78	0.00015	12.85	0.06581	0.58	0.0499
123-02F	1.3	47.3910	0.1309	3.0786	0.0131	0.0653	0.0037	20.8215	0.1117	0.0110	0.0009	0.40	9.9	49.2	13.256	0.092	96.5	94.20	0.76	0.78	0.00012	16.73	0.06485	0.55	0.0386
123-02G	1.4	46.8588	0.1806	3.0812	0.0171	0.0616	0.0047	22.0099	0.2992	0.0104	0.0010	0.40	9.9	55.3	14.001	0.207	97.1	93.63	0.89	0.91	0.00010	21.49	0.06564	0.71	0.0308
123-02H	1.5	57.6583	0.1508	3.8318	0.0181	0.0805	0.0028	26.7841	0.1625	0.0135	0.0010	0.50	12.3	51.6	13.700	0.107	96.7	92.27	0.71	0.73	0.00011	14.97	0.06634	0.58	0.0421
123-02I	1.6	32.5562	0.1110	2.1692	0.0121	0.0180	0.0160	17.3296	0.1373	0.0081	0.0009	0.28	7.0	55.5	15.659	0.153	96.7	92.12	1.02	1.04	0.00011	26.27	0.06649	0.69	0.0244
123-02J	1.7	17.0267	0.0503	1.1295	0.0088	0.0088	0.0084	11.5301	0.0866	0.0054	0.0009	0.15	3.6	55.1	20.008	0.219	95.8	91.68	1.64	1.65	0.00014	36.26	0.06616	0.87	0.0156
123-02K	1.8	9.3604	0.0465	0.6177	0.0066	0.0058	0.0045	6.6968	0.0423	0.0033	0.0009	0.08	2.0	52.5	21.249	0.265	95.0	91.48	2.80	2.80	0.00017	55.22	0.06580	1.20	0.0105
123-02L	2.0	19.3911	0.0863	1.2623	0.0121	0.0078	0.0098	11.2995	0.3255	0.0087	0.0011	0.16	4.1	33.8	17.546	0.535	91.2	89.03	1.85	1.86	0.00030	18.76	0.06494	1.09	0.0311
123-02M	2.5	6.0650	0.0300	0.3877	0.0051	0.0035	0.0029	3.6606	0.0458	0.0014	0.0009	0.05	1.2	66.3	18.507	0.339	97.6	96.85	4.27	4.28	0.00008	177.50	0.06376	1.44	0.0029
SN08YH05 - biotite - irradiation:DT-2																									
117-01A	0.1	103.5097	0.5801	6.8623	0.0581	0.1169	0.0041	0.0341	0.0127	0.0344	0.0014	0.90	3.8	0.0	0.010	0.004	90.2	86.26	1.00	1.01	0.00033	4.25	0.06631	1.05	0.1595
117-01B	0.1	187.9631	0.5101	12.9038	0.0481	0.2038	0.0077	0.0522	0.0110	0.0122	0.0011	1.69	7.1	0.1	0.008	0.002	98.1	90.50	0.48	0.51	0.00007	8.87	0.06866	0.51	0.0740
117-01C	0.2	268.3305	0.3302	18.3746	0.0811	0.2842	0.0084	0.0519	0.0131	0.0075	0.0006	2.40	10.0	0.2	0.006	0.001	99.2	91.72	0.46	0.49	0.00003	8.69	0.06849	0.50	0.0693
117-01D	0.3	273.1362	0.5501	18.7425	0.0661	0.2873	0.0090	0.0480	0.0118	0.0031	0.0006	2.45	10.2	0.4	0.005	0.001	99.7	91.97	0.42	0.45	0.00001	20.59	0.06863	0.46	0.0310
117-01E	0.4	217.8709	0.6601	14.9837	0.0861	0.2149	0.0067	0.0207	0.0141	0.0023	0.0006	1.96	8.2	0.2	0.003	0.002	99.7	91.79	0.62	0.64	0.00001	27.00	0.06879	0.69	0.0230
117-01F	0.5	225.3020	0.3002	15.4250	0.0451	0.2398	0.0096	0.0586	0.0146	0.0040	0.0010	2.02	8.4	0.4	0.007	0.002	99.5	92.00	0.36	0.40	0.00002	24.05	0.06848	0.38	0.0264
117-01G	0.7	204.0984	0.3702	13.9338	0.0541	0.2134	0.0075	0.1166	0.0132	0.0042	0.0010	1.82	7.6	0.7	0.016	0.002	99.4	92.18	0.45	0.48	0.00002	23.31	0.06828	0.48	0.0269
117-01H	0.9	177.0785	0.6101	12.1403	0.0501	0.1863	0.0061	0.0918	0.0156	0.0015	0.0010	1.59	6.6	1.6	0.015	0.003	99.8	92.13	0.54	0.57	0.00001	68.69	0.06857	0.58	0.0098
117-01I	1.0	227.9821	0.3302	15.5670	0.0421	0.2418	0.0065	0.2410	0.0107	0.0019	0.0009	2.04	8.5	3.2	0.030	0.001	99.8	92.50	0.35	0.39	0.00001	50.74	0.06830	0.37	0.0126
117-01J	1.1	181.5325	0.5501	12.5267	0.0531	0.1826	0.0057	0.2735	0.0166	0.0019	0.0009	1.64	6.9	3.8	0.043	0.003	99.7	91.51	0.52	0.55	0.00001	53.21	0.06902	0.56	0.0123
117-01K	1.2	185.7969	0.5601	12.7085	0.0521	0.1929	0.0080	0.3942	0.0197	0.0023	0.0009	1.66	7.0	4.5	0.061	0.003	99.7	92.25	0.52	0.55	0.00001	43.88	0.06841	0.55	0.0150
117-01L	1.3	147.3663	0.3902	10.1163	0.0411	0.1470	0.0050	0.4036	0.0161	0.0001	0.0009	1.32	5.5	79.5	0.078	0.003	100.0	92.23	0.50	0.53	0.00000	3835.52	0.06866	0.53	0.0002
117-01M	1.4	152.7022	0.3402	10.4317	0.0341	0.1551	0.0051	0.8060	0.0171	0.0016	0.0009	1.36	5.7	12.8	0.151	0.003	99.7	92.43	0.43	0.47	0.00001	64.26	0.06833	0.45	0.0101
117-01N	1.5	84.7206	0.1804	5.8270	0.0261	0.0836	0.0023	1.3967	0.0251	0.0008	0.0008	0.76	3.2	48.1	0.470	0.009	99.9	91.95	0.54	0.57	0.00000	197.81	0.06879	0.54	0.0031
117-01O	1.6	34.1252	0.1306	2.3132	0.0171	0.0312	0.0021	0.9020	0.0176	0.0004	0.0007	0.30	1.3	66.8	0.764	0.016	99.9	93.30	0.98	1.00	0.00000	641.76	0.06779	0.86	0.0010
SN08YH11 - biotite - irradiation:DT-2																									
120-01A	0.1	74.8530	0.1605	3.7971	0.0201	0.0776	0.0023	0.3064	0.0175	0.1063	0.0017	0.50	2.2	0.1	0.158	0.009	58.1	72.87	1.10	1.11	0.00142	1.81	0.05073	0.61	0.3319
120-01B	0.2	166.8805	0.3202	12.0460	0.0411	0.1817	0.0065	0.2077	0.0146	0.0268	0.0013	1.58	6.8	0.2	0.034	0.002	95.3	83.76	0.43	0.46	0.00016	4.77	0.07220	0.44	0.1336
120-01C	0.3	421.1105	0.4202	30.6553	0.1301	0.4166	0.0032	0.2583	0.0167	0.0173	0.0007	4.01	17.4	0.4	0.017	0.001	98.8	86.07	0.41	0.44	0.00004	4.14	0.07281	0.48	0.1456
120-01D	0.4	329.0080	0.3902	24.1796	0.1001	0.3290	0.0032	0.3342	0.0150	0.0070	0.0008	3.16	13.7	1.2	0.027	0.001	99.4	85.77	0.41	0.44	0.00002	11.58	0.07351	0.48	0.0525
120-01E	0.5	280.9751	0.3602	20.7388	0.0741	0.3200	0.0110	0.7426	0.0213	0.0090	0.0011	2.71	11.8	2.1	0.070	0.002	99.1	85.15	0.38	0.41	0.00003	12.37	0.07383	0.43	0.0502
120-01F	0.7	229.6853	0.7901	17.0521	0.0881	0.2531	0.0110	0.9564	0.0218	0.0068	0.0010	2.23	9.7	3.6	0.110	0.003	99.2	84.74	0.56	0.58	0.00003	15.25	0.07426	0.66	0.0428
120-01G	0.9	219.6157	0.7501	16.2004	0.0701	0.2208	0.0051	2.0586	0.0253	0.0074	0.0007	2.12	9.2	7.3	0.249	0.003	99.1	85.21	0.50	0.53	0.00003	9.77	0.07378	0.59	0.0687
120-01H	1.0	189.8012	1.2001	13.9176	0.1001	0.1964	0.0072	3.1428	0.0294	0.0044	0.0007	1.82	7.9	18.8	0.443	0.005	99.5	86.03	0.84	0.85	0.00002	19.68	0.07334	0.99	0.0387
120-01I	1.1	186.8565	0.8401	13.8566	0.0911	0.2084	0.0078	4.0747	0.0289	0.0048	0.0011	1.81	7.9	21.9	0.576	0.006	99.4	85.05	0.71	0.72	0.00002	28.80	0.07417	0.83	0.0232
120-01J	1.2	98.2816	0.3002	7.3203	0.0421	0.0958	0.0032	2.3621	0.0483	0.0013	0.0006	0.96	4.2	48.0	0.632	0.013	99.8	85.01	0.59	0.62	0.00001	97.71	0.07449	0.69	0.0064
120-01K	1.3	97.9623	0.1904	7.3474	0.0291	0.1012	0.0039	2.1243	0.0374	0.0025	0.0007	0.96	4.2	21.9	0.567	0.010	99.4	84.11	0.44	0.46	0.00002	33.59	0.07501	0.49	0.0187
120-01L	1.4	79.9081	0.1405	5.9590	0.0261	0.0876	0.0032	2.0901	0.0223	0.0017	0.0010	0.78	3.4	32.7	0.687	0.008	99.6	84.74	0.53	0.55	0.00001	89.29	0.07458	0.52	0.0069
120-01M	1.5	38.0990	0.1107	2.8779	0.0151	0.0369	0.0016	1.8147	0.0214	0.0004	0.0009	0.38	1.6	105.0	1.236	0.016	100.0	84.04	0.78	0.79	0.00000	0.00	0.07554	0.64	0.0002
SN08YH13 - amphibole - irradiation:DT-2																									
128-02A	0.2	81.6837	0.2104	4.4701	0.0191	0.0825	0.0057	1.3174	0.0405	0.0380	0.0014	0.58	8.5	0.9	0.578	0.018	86.4	99.73	0.82	0.85	0.00046	3.78	0.05473	0.54	0.1690
128-02B	0.4	126.3331	0.2204	8.4660	0.0311	0.1551	0.0110	10.9020	0.0495	0.0193	0.0010	1.11	16.1	14.7	2.524	0.015	96.2	90.92	0.47	0.50	0.00013	6.05	0.06700	0.46	0.1040
128-02C	0.5	105.4762	0.1705	7.2744	0.0271	0.1266	0.0027	12.1836	0.1309	0.0111	0.0009	0.95	13.8	28.6	3.283	0.038	97.8	89.87	0.47	0.50	0.00008	11.53	0.06895	0.46	0.0542
128-02D	0.7	205.0563	0.4502	13.9966	0.0441	0.2669	0.0170	36.3619	0.3043	0.0260	0.0014	1.83	26.6	36.3	5.092	0.046	97.6	90.65	0.44	0.47	0.00008	8.45	0.06822	0.44	0.0770
128-02E	0.9	138.6287	0.2603	9.8985	0.0271	0.1654	0.0041	9.5522	0.1372	0.0082	0.0008	1.29	18.8	30.3	1.891	0.028	98.8	87.73	0.37	0.41	0.00004	13.57	0.07140	0.39	0.0478
128-02F	1.1	75.2693	0.1406	5.2854	0.0171	0.0984	0.0030	7.9535	0.0696	0.0039	0.0008	0.69	10.0	53.2	2.949	0.028	99.3	89.63	0.47	0.50	0.00002	43.39	0.07021	0.43	0.0147
128-02G	1.2	19.7440	0.0634	1.3438	0.0102	0.0238	0.0009	3.5148	0.0309	0.0021	0.0010	0.18	2.6	43.7	5.126	0.060	98.2	91.48	1.59	1.60	0.00006	87.30	0.06803	0.86	0.0066
128-02H	1.4	15.6811	0.0459	1.0710	0.0112	0.0196	0.0012	3.3212	0.0372	0.0016	0.0009	0.14	2.0	55.9	6.078	0.094	98.7	91.61	1.77	1.78	0.00004	125.53	0.06825	1.11	0.0040
128-02K	1.7	12.1475	0.0624	0.8674	0.0082	0.0132	0.0037	3.0367	0.0820	0.0034	0.0010	0.11	1.6	23.5	6.862	0.197	93.7	83.41	2.33	2.34	0.00021	39.32	0.07135	1.11	0.0158

Supplemental Table SP2.1. $^{40}Ar/^{39}Ar$ Isotopic Data (continued)

		Relative Isotopic Abundances										Derived Results									Inverse Isochron Data				
Lab ID#	**Watts**	**^{40}Ar**	**±1σ**	**^{39}Ar**	**±1σ**	**^{38}Ar**	**±1σ**	**^{37}Ar**	**±1σ**	**^{36}Ar**	**±1σ**	**^{39}Ar Mol**	**^{39}Ar %**	**%(^{36}Ar)$_{Ca}$**	**Ca/K**	**±1σ**	**%$^{40}Ar^{*}$**	**Age (Ma)**	**±1σ**	**w/±J**	**±1σ**	**$^{36}Ar/^{40}Ar$**	**±%1σ**	**$^{39}Ar/^{40}Ar$**	**±%1σ**	**$^{36}Ar/^{39}Ar$**
												× 10^{-14}	**of total**													**Er. Corr.**
SN08YH13 - biotite - irradiation:DT-2																										
118-01A	0.1	89.6696	0.3302	4.6496	0.0291	0.0948	0.0025	0.3380	0.0146	0.1149	0.0021	0.61	1.7	0.1	0.142	0.006	62.2	76.24	1.17	1.17	0.00128	2.01	0.05186	0.76	0.3159
118-01B	0.2	113.1407	0.3502	7.9163	0.0371	0.1395	0.0036	0.1828	0.0126	0.0338	0.0012	1.04	3.0	0.1	0.045	0.003	91.2	82.74	0.60	0.62	0.00030	3.73	0.06998	0.60	0.1739
118-01C	0.3	261.3173	0.3902	18.6303	0.0651	0.3317	0.0080	0.2918	0.0151	0.0363	0.0013	2.44	7.0	0.2	0.031	0.002	95.9	85.33	0.40	0.43	0.00014	3.72	0.07131	0.43	0.1683
118-01D	0.4	286.7945	0.2902	20.8252	0.0721	0.3351	0.0070	0.2848	0.0126	0.0219	0.0011	2.72	7.8	0.3	0.027	0.001	97.8	85.40	0.37	0.40	0.00008	5.28	0.07263	0.42	0.1171
118-01E	0.5	511.8131	0.8401	37.1529	0.1601	0.5424	0.0057	0.4206	0.0131	0.0299	0.0013	4.86	13.9	0.4	0.022	0.001	98.3	85.87	0.44	0.47	0.00006	4.49	0.07261	0.51	0.1364
118-01F	0.7	445.2779	0.5001	32.1290	0.1301	0.4823	0.0044	0.4266	0.0126	0.0207	0.0011	4.20	12.1	0.5	0.026	0.001	98.6	86.68	0.41	0.44	0.00005	5.28	0.07217	0.47	0.1152
118-01G	0.9	384.9677	0.4901	28.1977	0.1201	0.4174	0.0056	0.4956	0.0194	0.0103	0.0010	3.69	10.6	1.3	0.034	0.001	99.2	85.92	0.42	0.45	0.00003	10.31	0.07326	0.49	0.0588
118-01H	1.0	338.9854	0.4002	24.9605	0.1001	0.3699	0.0037	1.1276	0.0205	0.0088	0.0010	3.27	9.4	3.3	0.089	0.002	99.3	85.51	0.40	0.43	0.00003	11.64	0.07365	0.47	0.0524
118-01I	1.2	505.9886	0.4401	37.2561	0.1401	0.5501	0.0057	6.2506	0.0484	0.0101	0.0011	4.87	14.0	16.1	0.329	0.003	99.5	85.73	0.37	0.41	0.00002	12.46	0.07364	0.44	0.0491
118-01J	1.4	405.2813	0.3802	29.7636	0.1201	0.4528	0.0034	7.2868	0.0589	0.0054	0.0011	3.89	11.2	35.3	0.480	0.004	99.7	86.15	0.40	0.43	0.00001	31.15	0.07345	0.46	0.0195
118-01K	1.6	159.1808	0.5301	11.7442	0.0461	0.1980	0.0064	3.9146	0.0415	0.0052	0.0009	1.54	4.4	19.6	0.653	0.007	99.2	85.33	0.49	0.52	0.00003	22.25	0.07379	0.56	0.0304
118-01L	1.8	77.8352	0.1504	5.7394	0.0241	0.0902	0.0029	1.7287	0.0195	0.0026	0.0009	0.75	2.2	17.6	0.590	0.007	99.2	85.35	0.52	0.54	0.00003	43.19	0.07375	0.51	0.0144
118-01M	2.0	41.3062	0.1205	3.0786	0.0171	0.0446	0.0025	0.8094	0.0217	0.0025	0.0007	0.40	1.2	8.6	0.515	0.014	98.4	83.79	0.70	0.72	0.00005	32.23	0.07454	0.66	0.0193
118-01N	2.5	60.6903	0.1305	4.4794	0.0231	0.0749	0.0018	1.5258	0.0178	0.0026	0.0009	0.59	1.7	15.3	0.668	0.009	98.9	85.04	0.62	0.64	0.00004	40.93	0.07382	0.60	0.0148
SN08YV03 - amphibole - irradiation:DT-2																										
126-02A	0.7	85.8303	0.2203	5.0749	0.0221	0.0925	0.0026	9.2548	0.1727	0.0653	0.0019	0.66	24.3	3.7	3.574	0.069	78.3	84.13	0.90	0.91	0.00073	3.17	0.05911	0.55	0.2007
126-02B	0.8	57.7673	0.1504	3.0287	0.0151	0.0608	0.0020	12.1631	0.0991	0.0217	0.0015	0.40	14.5	14.5	7.871	0.076	90.5	108.91	1.11	1.13	0.00032	7.95	0.05238	0.60	0.0785
126-02C	0.9	28.1743	0.0986	1.5117	0.0088	0.0286	0.0013	5.6108	0.0992	0.0089	0.0009	0.20	7.2	16.4	7.275	0.136	92.2	108.42	1.36	1.37	0.00026	12.40	0.05361	0.72	0.0515
126-02D	1.0	23.9987	0.1006	1.3087	0.0112	0.0211	0.0067	6.0602	0.0686	0.0049	0.0011	0.17	6.3	31.9	9.077	0.130	95.9	110.88	1.81	1.83	0.00014	31.53	0.05447	0.98	0.0190
126-02E	1.1	15.6014	0.0532	0.8788	0.0081	0.0130	0.0044	4.1521	0.0473	0.0032	0.0009	0.11	4.2	33.9	9.261	0.137	96.0	107.61	2.08	2.09	0.00014	40.96	0.05626	1.01	0.0133
126-02F	1.3	30.0622	0.1106	1.7154	0.0112	0.0237	0.0022	8.6587	0.1794	0.0038	0.0011	0.22	8.2	58.8	9.893	0.216	98.5	108.89	1.45	1.46	0.00005	71.22	0.05699	0.78	0.0088
126-02G	1.5	118.2023	0.2003	6.5744	0.0221	0.1273	0.0023	39.2255	0.1486	0.0223	0.0013	0.86	31.4	45.6	11.694	0.061	97.0	110.02	0.60	0.63	0.00010	10.70	0.05554	0.43	0.0592
126-02H	1.6	10.4176	0.0348	0.6015	0.0079	0.0125	0.0010	2.7162	0.0313	0.0014	0.0008	0.08	2.9	51.5	8.851	0.156	98.1	107.28	2.93	2.93	0.00006	126.90	0.05767	1.39	0.0036
126-02I	2.0	3.8000	0.0237	0.2316	0.0051	0.0049	0.0010	1.2496	0.0499	0.0000	0.0008	0.03	1.1	0.0	10.575	0.485	110.7	114.45	6.89	6.90	0.00000	0.00	0.06087	2.34	0.0069
SN08YV03 - biotite - irradiation:DT-2																										
125-01A	0.2	217.3842	0.4502	12.6095	0.0491	0.2134	0.0066	0.1846	0.0139	0.1178	0.0018	1.65	5.0	0.0	0.029	0.002	84.0	91.69	0.58	0.61	0.00054	1.74	0.05802	0.49	0.3626
125-01B	0.3	656.0420	0.5501	40.3295	0.1201	0.5518	0.0040	0.3506	0.0189	0.0421	0.0013	5.27	16.1	0.2	0.017	0.001	98.1	100.81	0.38	0.42	0.00006	3.09	0.06149	0.37	0.2022
125-01C	0.4	459.3794	0.4102	28.0829	0.1201	0.3990	0.0038	0.3778	0.0179	0.0271	0.0013	3.67	11.2	0.4	0.026	0.001	98.3	101.51	0.49	0.53	0.00006	4.71	0.06114	0.48	0.1275
125-01D	0.5	397.4280	0.5301	24.2164	0.1101	0.3442	0.0029	0.4542	0.0163	0.0226	0.0011	3.17	9.7	0.5	0.037	0.001	98.3	101.90	0.53	0.56	0.00006	5.14	0.06094	0.52	0.1169
125-01E	0.7	368.2977	0.6101	22.5310	0.0881	0.2990	0.0049	0.4195	0.0189	0.0208	0.0012	2.95	9.0	0.5	0.036	0.002	98.3	101.52	0.48	0.52	0.00006	5.66	0.06119	0.47	0.1098
125-01F	0.9	289.5987	0.3602	17.6947	0.0681	0.2751	0.0099	0.4351	0.0139	0.0198	0.0011	2.31	7.1	0.6	0.048	0.002	98.0	101.30	0.47	0.51	0.00007	5.87	0.06111	0.45	0.1048
125-01G	1.0	276.3351	0.3802	17.1055	0.0891	0.2683	0.0087	0.3851	0.0164	0.0183	0.0011	2.24	6.8	0.5	0.044	0.002	98.1	100.08	0.58	0.61	0.00007	6.09	0.06191	0.58	0.0963
125-01H	1.2	276.2936	0.5601	17.0826	0.0440	0.2618	0.0092	0.4700	0.0179	0.0152	0.0011	2.23	6.8	0.8	0.054	0.002	98.4	100.53	0.40	0.45	0.00005	7.36	0.06184	0.39	0.0890
125-01I	1.4	276.4588	0.4302	17.0039	0.0460	0.2626	0.0092	0.7893	0.0217	0.0188	0.0011	2.22	6.8	1.1	0.091	0.003	98.0	100.66	0.39	0.44	0.00007	6.01	0.06152	0.37	0.1067
125-01J	1.6	227.9018	0.5801	14.0440	0.0521	0.2221	0.0078	0.6652	0.0154	0.0160	0.0011	1.84	5.6	1.1	0.093	0.002	98.0	100.42	0.51	0.55	0.00007	6.90	0.06163	0.50	0.0942
125-01K	1.8	200.6629	0.6101	12.3720	0.0581	0.1946	0.0072	0.5935	0.0169	0.0152	0.0011	1.62	4.9	1.0	0.094	0.003	97.8	100.20	0.62	0.64	0.00007	7.38	0.06167	0.60	0.0877
125-01L	2.0	219.5554	0.5101	13.5228	0.0460	0.2169	0.0077	0.9901	0.0223	0.0207	0.0011	1.77	5.4	1.2	0.144	0.003	97.3	99.77	0.49	0.52	0.00009	5.53	0.06160	0.46	0.1173
125-01M	2.5	173.1109	0.2503	10.5747	0.0370	0.1618	0.0051	1.0139	0.0250	0.0204	0.0011	1.38	4.2	1.3	0.188	0.005	96.6	99.87	0.47	0.51	0.00012	5.51	0.06110	0.43	0.1135
125-01N	3.0	39.2674	0.0968	2.4209	0.0131	0.0365	0.0020	0.6033	0.0149	0.0066	0.0010	0.32	1.0	2.4	0.488	0.012	95.2	97.61	0.98	1.00	0.00016	15.87	0.06166	0.63	0.0384
125-01O	3.5	17.9510	0.0524	1.1189	0.0095	0.0089	0.0057	0.6220	0.0175	0.0016	0.0009	0.15	0.4	10.2	1.089	0.032	97.6	99.02	1.72	1.73	0.00008	63.02	0.06233	0.93	0.0087
SN08YV07 - biotite - irradiation:DT-2																										
116-01A	0.1	144.4537	0.4002	9.8299	0.0421	0.1675	0.0049	0.1702	0.0148	0.0859	0.0017	1.28	6.0	0.1	0.034	0.003	82.4	77.02	0.59	0.61	0.00059	2.15	0.06806	0.55	0.3004
116-01B	0.1	278.7758	0.4201	20.1769	0.1201	0.2940	0.0100	0.0840	0.0139	0.0089	0.0011	2.64	12.4	0.2	0.008	0.001	99.1	86.79	0.56	0.59	0.00003	12.57	0.07239	0.65	0.0455
116-01C	0.2	387.0348	0.5101	27.5056	0.1201	0.3827	0.0035	0.1326	0.0135	0.0062	0.0010	3.59	16.9	0.6	0.009	0.001	99.5	88.76	0.44	0.47	0.00002	16.62	0.07108	0.50	0.0364
116-01D	0.3	338.9046	0.3602	24.0540	0.0941	0.3181	0.0028	0.1366	0.0163	0.0042	0.0009	3.14	14.8	0.8	0.011	0.001	99.6	88.97	0.40	0.44	0.00001	21.22	0.07099	0.46	0.0288
116-01E	0.4	227.0978	0.3702	16.1502	0.0471	0.2454	0.0093	0.0896	0.0135	0.0039	0.0009	2.11	9.9	0.6	0.011	0.002	99.5	88.67	0.36	0.39	0.00002	23.27	0.07113	0.39	0.0275
116-01F	0.5	227.8986	0.5701	16.2417	0.0501	0.2556	0.0097	0.2130	0.0126	0.0035	0.0010	2.12	10.0	1.6	0.026	0.002	99.6	88.54	0.41	0.44	0.00002	29.33	0.07128	0.45	0.0225
116-01G	0.7	190.5668	0.5301	13.5859	0.0481	0.2026	0.0074	0.3072	0.0154	0.0046	0.0009	1.78	8.3	1.7	0.044	0.002	99.3	88.29	0.45	0.48	0.00002	19.83	0.07131	0.50	0.0334
116-01H	0.9	149.2929	0.4301	10.6285	0.0451	0.1559	0.0061	0.4255	0.0149	0.0050	0.0010	1.39	6.5	2.2	0.078	0.003	99.0	88.18	0.51	0.54	0.00003	20.62	0.07121	0.56	0.0316
116-01I	1.0	118.7779	0.3902	8.4219	0.0451	0.1192	0.0040	0.6828	0.0179	0.0050	0.0010	1.10	5.2	3.6	0.159	0.004	98.8	88.33	0.62	0.64	0.00004	20.33	0.07092	0.67	0.0315
116-01J	1.1	77.3094	0.1404	5.4824	0.0251	0.0730	0.0019	0.8118	0.0205	0.0044	0.0009	0.72	3.4	4.8	0.290	0.007	98.4	87.95	0.56	0.58	0.00005	21.97	0.07093	0.54	0.0278
116-01K	1.2	59.9182	0.1604	4.2398	0.0231	0.0594	0.0024	1.2198	0.0237	0.0032	0.0010	0.55	2.6	10.0	0.564	0.011	98.6	88.32	0.69	0.71	0.00005	33.36	0.07077	0.64	0.0185
116-01L	1.3	31.5248	0.1106	2.2590	0.0121	0.0279	0.0022	1.0964	0.0190	0.0035	0.0006	0.30	1.4	8.2	0.951	0.017	97.0	85.86	0.77	0.78	0.00010	19.39	0.07166	0.68	0.0336
116-01M	1.4	35.3884	0.1006	2.4334	0.0141	0.0314	0.0028	1.1451	0.0195	0.0044	0.0010	0.32	1.5	6.8	0.922	0.017	96.6	89.04	0.95	0.96	0.00012	23.77	0.06877	0.68	0.0258
116-01N	1.5	11.3944	0.0348	0.7840	0.0076	0.0078	0.0036	0.5170	0.0145	0.0013	0.0007	0.10	0.5	10.4	1.292	0.038	97.0	89.36	1.91	1.92	0.00010	62.37	0.06880	1.05	0.0083
116-01O	1.6	16.7701	0.0473	1.2017	0.0101	0.0096	0.0055	0.9174	0.0303	0.0011	0.0009	0.16	0.7	22.4	1.496	0.051	98.5	87.21	1.64	1.65	0.00005	113.93	0.07166	0.92	0.0048

Supplemental Table SP2.1. $^{40}Ar/^{39}Ar$ Isotopic Data (continued)

		Relative Isotopic Abundances										Derived Results									Inverse Isochron Data				
Lab ID#	Watts	^{40}Ar ±1σ		^{39}Ar ±1σ		^{38}Ar ±1σ		^{37}Ar ±1σ		^{36}Ar ±1σ		^{39}Ar Mol × 10^{-14}	^{39}Ar % of total	$\%(^{36}Ar)_{Ca}$	Ca/K ±1σ		$\%^{40}Ar^{*}$	Age (Ma) ±1σ		w/±J ±1σ	$^{36}Ar/^{40}Ar$ ±%1σ		$^{39}Ar/^{40}Ar$ ±%1σ		$^{36}Ar/^{39}Ar$ Er. Corr.
SN08YV07 - amphibole - irradiation:DT-2																									
122-01A	1.0	8.0945	0.0318	0.2675	0.0051	0.0034	0.0022	1.3808	0.0181	0.0133	0.0010	0.03	1.2	2.7	10.118	0.237	52.7	100.81	7.20	7.20	0.00160	7.81	0.03300	2.00	0.0466
122-01B	1.2	8.4036	0.0327	0.4818	0.0063	0.0024	0.0035	8.1045	0.0399	0.0075	0.0010	0.06	2.1	28.1	32.968	0.467	81.1	90.03	3.96	3.96	0.00064	18.29	0.05707	1.40	0.0257
122-01C	1.4	19.9577	0.0863	1.3268	0.0082	0.0018	0.0099	21.0103	0.1097	0.0095	0.0011	0.17	5.9	57.3	31.037	0.255	94.0	89.95	1.62	1.63	0.00020	25.72	0.06620	0.79	0.0259
122-01D	1.6	38.4643	0.1309	2.6311	0.0161	0.0405	0.0047	36.5699	0.2003	0.0200	0.0012	0.34	11.7	47.5	27.242	0.227	91.9	85.59	1.05	1.06	0.00027	11.13	0.06815	0.74	0.0563
122-01E	1.8	59.9284	0.2904	4.1831	0.0230	0.0712	0.0038	55.4340	0.5724	0.0192	0.0013	0.55	18.6	74.9	25.974	0.307	97.6	88.96	0.89	0.90	0.00008	26.26	0.06956	0.77	0.0272
122-01F	2.0	69.8389	0.3603	4.8470	0.0260	0.0795	0.0032	63.4819	0.8113	0.0244	0.0014	0.63	21.6	67.7	25.671	0.358	96.7	88.61	0.87	0.89	0.00011	17.39	0.06916	0.78	0.0423
122-01G	2.2	56.3847	0.1707	3.8806	0.0201	0.0591	0.0039	50.0492	0.2770	0.0284	0.0014	0.51	17.3	45.8	25.279	0.194	91.9	85.05	0.89	0.91	0.00027	9.39	0.06859	0.64	0.0676
122-01H	2.4	40.7089	0.1608	2.8072	0.0171	0.0451	0.0048	38.8706	0.2822	0.0162	0.0013	0.37	12.5	62.2	27.139	0.260	95.5	88.17	1.11	1.12	0.00015	21.66	0.06870	0.76	0.0301
122-01I	2.6	29.5750	0.1156	2.0333	0.0097	0.0065	0.0150	28.8608	0.2297	0.0086	0.0012	0.27	9.1	87.5	27.820	0.261	98.9	91.49	1.22	1.24	0.00004	109.76	0.06849	0.66	0.0062
SN08YV07 - amphibole - irradiation:DT-2																									
122-02B	0.7	14.7529	0.0522	0.9658	0.0076	0.0117	0.0044	19.0181	0.1650	0.0068	0.0010	0.13	16.1	72.7	38.597	0.457	96.3	93.62	2.10	2.10	0.00013	54.57	0.06511	0.90	0.0107
122-02C	0.9	15.8327	0.0454	1.0689	0.0078	0.0163	0.0010	21.4070	0.2322	0.0085	0.0010	0.14	17.8	65.5	39.253	0.517	94.5	89.23	1.83	1.84	0.00019	33.09	0.06715	0.82	0.0173
122-02D	1.0	16.4813	0.0492	1.1297	0.0121	0.0169	0.0012	22.8678	0.2384	0.0081	0.0009	0.15	18.8	73.4	39.674	0.599	96.1	89.38	1.83	1.84	0.00013	43.22	0.06817	1.15	0.0114
122-02E	1.1	20.4735	0.0571	1.3899	0.0102	0.0221	0.0008	27.2251	0.3608	0.0110	0.0010	0.18	23.1	64.4	38.393	0.585	94.3	88.57	1.55	1.56	0.00019	26.34	0.06753	0.82	0.0217
122-02F	1.2	18.2449	0.0415	1.1920	0.0075	0.0196	0.0010	32.1757	0.2326	0.0139	0.0009	0.16	19.8	60.3	52.907	0.513	91.1	89.04	1.49	1.50	0.00030	15.69	0.06485	0.71	0.0370
122-02G	1.3	4.1080	0.0178	0.2618	0.0045	0.0029	0.0007	7.7965	0.0860	0.0018	0.0008	0.03	4.4	111.9	58.364	1.210	101.5	101.47	5.56	5.56	0.00000	0.00	0.06321	1.83	0.0012
SN08YV07 - amphibole - irradiation:DT-2																									
122-03C	0.3	5.3291	0.0228	0.3001	0.0051	0.0035	0.0009	4.3494	0.1202	0.0058	0.0009	0.04	6.0	19.6	28.405	0.926	74.3	84.07	5.83	5.84	0.00087	19.82	0.05610	1.78	0.0209
122-03D	0.5	22.5715	0.0778	1.4425	0.0101	0.0251	0.0017	19.0528	0.4166	0.0136	0.0010	0.19	28.7	36.5	25.889	0.597	88.7	88.31	1.50	1.51	0.00038	11.84	0.06368	0.82	0.0511
122-03E	0.7	29.1858	0.0877	1.9488	0.0101	0.0322	0.0011	25.6173	0.2332	0.0106	0.0010	0.25	38.7	62.7	25.765	0.272	96.0	91.39	1.14	1.15	0.00014	26.11	0.06654	0.64	0.0243
122-03F	0.9	12.9770	0.0415	0.8755	0.0082	0.0123	0.0010	17.6573	0.2899	0.0068	0.0010	0.11	17.4	67.9	39.531	0.752	95.1	89.78	2.36	2.36	0.00017	47.53	0.06709	1.03	0.0112
122-03G	1.0	2.6849	0.0220	0.1775	0.0035	0.0020	0.0010	4.4191	0.0419	0.0009	0.0009	0.02	3.5	121.8	48.803	1.068	102.3	98.47	9.84	9.84	0.00000	0.00	0.06565	2.16	0.0012
122-03H	1.2	4.3668	0.0246	0.2880	0.0045	0.0048	0.0012	9.2788	0.0713	0.0030	0.0009	0.04	5.7	79.2	63.153	1.110	95.7	92.74	6.21	6.22	0.00014	148.99	0.06536	1.70	0.0033
SN08YV07 - amphibole - irradiation:DT-2																									
122-04B	0.3	7.3639	0.0264	0.2737	0.0050	0.0050	0.0012	3.9689	0.0472	0.0106	0.0010	0.04	5.0	9.8	28.422	0.623	61.7	105.17	7.07	7.07	0.00130	10.68	0.03702	1.89	0.0345
122-04C	0.4	13.1720	0.0355	0.8387	0.0076	0.0083	0.0040	11.6196	0.0709	0.0082	0.0011	0.11	15.2	36.8	27.154	0.301	88.4	88.31	2.48	2.48	0.00039	20.41	0.06344	0.98	0.0256
122-04D	0.5	35.5205	0.1108	2.4679	0.0131	0.0397	0.0023	30.8902	0.1511	0.0113	0.0010	0.32	44.8	71.2	24.533	0.180	97.3	89.06	0.92	0.94	0.00009	29.53	0.06925	0.65	0.0215
122-04E	0.7	18.5576	0.0383	1.2941	0.0101	0.0135	0.0062	15.3949	0.1512	0.0069	0.0010	0.17	23.5	58.3	23.317	0.295	95.4	87.08	1.56	1.56	0.00015	33.82	0.06951	0.84	0.0159
122-04F	0.9	1.6263	0.0214	0.1156	0.0036	0.0004	0.0008	1.8210	0.0333	0.0011	0.0008	0.02	2.1	44.9	30.889	1.135	89.4	80.33	13.85	13.85	0.00036	146.25	0.07075	3.47	0.0046
122-04G	1.0	0.7358	0.0170	0.0482	0.0025	0.0000	0.0007	0.9662	0.0221	0.0001	0.0008	0.01	0.9	302.5	39.267	2.224	106.7	103.37	32.62	32.62	0.00000	0.00	0.06518	5.72	0.0021
122-04H	1.1	0.9538	0.0184	0.0645	0.0024	0.0005	0.0007	1.3567	0.0342	0.0005	0.0009	0.01	1.2	74.9	41.205	1.859	96.3	90.71	24.90	24.90	0.00012	729.77	0.06728	4.24	0.0014
122-04I	1.2	2.5426	0.0199	0.1852	0.0036	0.0013	0.0009	3.1900	0.0333	0.0012	0.0008	0.02	3.4	70.4	33.760	0.744	95.9	84.00	8.34	8.35	0.00014	234.96	0.07250	2.11	0.0023
122-04J	1.3	2.9845	0.0230	0.2180	0.0039	0.0018	0.0009	3.5583	0.0439	0.0025	0.0009	0.03	4.0	37.4	31.991	0.704	84.7	74.11	7.50	7.50	0.00052	55.92	0.07273	2.00	0.0101
SN08MD01 - biotite - irradiation:DT-3																									
175-01A	0.1	1927.9110	2.8000	82.0350	0.1902	1.1826	0.0036	0.5313	0.0132	0.4603	0.0021	1.81	18.3	0.0	0.013	0.000	92.9	156.89	0.45	0.65	0.00024	0.54	#####	0.28	0.3665
175-01B	0.3	1931.8010	2.6000	87.3675	0.2002	1.1633	0.0035	0.8307	0.0154	0.0803	0.0014	1.93	19.5	0.3	0.019	0.000	98.8	156.87	0.42	0.63	0.00004	1.79	#####	0.28	0.1073
175-01C	0.5	1541.8170	1.0001	69.5747	0.1201	0.9316	0.0033	1.7181	0.0187	0.0459	0.0012	1.54	15.6	1.0	0.048	0.001	99.1	157.74	0.30	0.56	0.00003	2.63	#####	0.20	0.0678
175-01D	0.6	1298.1050	1.4001	58.7059	0.2302	0.7877	0.0031	5.0813	0.0274	0.0421	0.0013	1.30	13.1	3.1	0.170	0.001	99.1	157.33	0.63	0.79	0.00003	3.21	#####	0.42	0.0434
175-01E	0.7	842.8016	1.4001	37.9349	0.1401	0.5088	0.0027	3.7794	0.0257	0.0242	0.0013	0.84	8.5	4.1	0.195	0.002	99.2	158.22	0.63	0.79	0.00003	5.50	#####	0.42	0.0312
175-01F	0.8	733.9923	0.4602	33.2660	0.0821	0.4439	0.0022	5.7191	0.0275	0.0254	0.0011	0.74	7.4	5.8	0.337	0.002	99.0	156.95	0.41	0.62	0.00003	4.64	#####	0.26	0.0342
175-01G	0.9	424.4130	0.7401	19.0565	0.0261	0.2632	0.0018	4.7745	0.0257	0.0146	0.0011	0.42	4.3	8.5	0.491	0.003	99.1	158.41	0.38	0.60	0.00003	8.11	#####	0.23	0.0296
175-01H	1.1	505.7876	0.5602	22.9529	0.0611	0.3015	0.0022	1.8374	0.0171	0.0092	0.0011	0.51	5.1	5.2	0.157	0.002	99.5	157.44	0.46	0.66	0.00002	13.01	#####	0.30	0.0131
175-01I	1.2	356.4967	0.6302	16.1609	0.0531	0.2190	0.0018	1.9348	0.0213	0.0089	0.0011	0.36	3.6	5.7	0.235	0.003	99.3	157.32	0.60	0.76	0.00002	13.21	#####	0.38	0.0143
175-01J	1.4	263.7774	0.4802	11.8805	0.0171	0.1591	0.0017	1.2450	0.0171	0.0100	0.0011	0.26	2.7	3.2	0.205	0.003	98.9	157.70	0.42	0.63	0.00004	11.44	#####	0.24	0.0213
175-01M	2.0	180.0276	0.3603	8.1735	0.0281	0.1093	0.0014	1.4940	0.0188	0.0052	0.0011	0.18	1.8	7.4	0.358	0.005	99.2	156.94	0.68	0.82	0.00003	23.45	#####	0.41	0.0085

Supplemental Table SP2.1. $^{40}Ar/^{39}Ar$ Isotopic Data (continued)

		Relative Isotopic Abundances										Derived Results									Inverse Isochron Data				
Lab ID#	Watts	^{40}Ar ±1σ		^{39}Ar ±1σ		^{38}Ar ±1σ		^{37}Ar ±1σ		^{36}Ar ±1σ		^{39}Ar Mol × 10^{-14}	^{39}Ar % of total	$\%(^{36}Ar)_{Ca}$	Ca/K ±1σ		$\%^{40}Ar^{*}$	Age (Ma) ±1σ		w/±J ±1σ	$^{36}Ar/^{40}Ar$ ±%1σ		$^{39}Ar/^{40}Ar$ ±%1σ		$^{36}Ar/^{39}Ar$ Er. Corr.
SN08MD01 - amphibole - irradiation:DT-3																									
180-02B	0.7	59.9124	0.1510	2.5514	0.0141	0.0432	0.0009	8.2114	0.0394	0.0154	0.0011	0.06	2.3	13.9	6.308	0.047	93.5	157.75	1.30	1.38	0.00022	8.38	#####	0.62	0.0217
180-02C	0.8	310.2384	0.3704	12.7790	0.0271	0.2233	0.0015	55.6090	0.1221	0.0496	0.0012	0.28	11.7	29.1	8.529	0.026	96.7	168.20	0.46	0.68	0.00011	3.36	#####	0.25	0.0562
180-02D	0.9	701.5924	2.0001	28.7248	0.1001	0.5156	0.0025	129.6041	0.1743	0.1131	0.0014	0.64	26.3	29.8	8.843	0.034	96.7	169.20	0.77	0.92	0.00011	1.83	#####	0.46	0.1432
180-02E	1.0	723.2575	1.5001	30.7144	0.1801	0.5520	0.0024	136.7658	0.2091	0.1086	0.0016	0.68	28.1	32.7	8.728	0.054	97.0	163.96	1.01	1.12	0.00010	2.18	#####	0.63	0.0679
180-02F	1.1	408.8432	0.6202	17.2899	0.0421	0.3103	0.0019	74.3175	0.1571	0.0476	0.0013	0.38	15.8	40.6	8.425	0.028	98.0	166.14	0.50	0.71	0.00007	4.57	#####	0.30	0.0432
180-02G	1.2	113.7097	0.2306	4.9270	0.0201	0.0827	0.0010	24.4049	0.0747	0.0124	0.0011	0.11	4.5	51.2	9.709	0.050	98.4	163.10	0.87	1.00	0.00005	18.93	#####	0.47	0.0097
180-02H	1.3	90.1142	0.1609	3.8932	0.0211	0.0680	0.0012	20.5193	0.0515	0.0088	0.0012	0.09	3.6	60.6	10.330	0.062	98.9	164.26	1.10	1.20	0.00004	33.37	#####	0.58	0.0042
180-02I	1.5	128.1229	0.2306	5.4360	0.0201	0.0980	0.0013	29.6109	0.0713	0.0099	0.0011	0.12	5.0	77.5	10.676	0.048	99.5	168.14	0.79	0.93	0.00002	48.08	#####	0.42	0.0037
180-02J	1.7	69.9131	0.1808	2.9941	0.0151	0.0494	0.0010	16.3391	0.0396	0.0077	0.0011	0.07	2.7	55.5	10.696	0.061	98.6	165.17	1.18	1.28	0.00005	32.25	#####	0.58	0.0061
SN08MD07 - biotite - irradiation:DT-3																									
174-01A	0.1	1356.9250	1.5001	95.8162	0.2102	1.3057	0.0040	0.2307	0.0144	0.1156	0.0016	2.12	25.8	0.1	0.005	0.000	97.5	100.72	0.26	0.40	0.00009	1.44	#####	0.26	0.1267
174-01B	0.3	1459.1830	3.7000	101.9013	0.2502	1.3663	0.0043	0.2311	0.0130	0.0322	0.0014	2.25	27.4	0.2	0.004	0.000	99.3	103.71	0.37	0.49	0.00002	4.35	#####	0.36	0.0615
174-01C	0.5	779.1341	1.3001	53.7876	0.1802	0.7227	0.0030	0.1565	0.0144	0.0181	0.0013	1.19	14.5	0.2	0.006	0.001	99.3	104.84	0.40	0.51	0.00002	7.08	#####	0.38	0.0256
174-01D	0.6	550.6474	0.9201	38.0773	0.1401	0.5145	0.0023	0.2449	0.0144	0.0099	0.0012	0.84	10.3	0.6	0.013	0.001	99.5	104.83	0.43	0.53	0.00002	12.54	#####	0.41	0.0138
174-01E	0.7	408.3783	0.5501	28.1711	0.1201	0.3780	0.0022	0.4327	0.0152	0.0092	0.0012	0.62	7.6	1.2	0.030	0.001	99.3	104.94	0.48	0.57	0.00002	13.69	#####	0.46	0.0104
174-01F	0.8	239.1774	0.6001	16.5405	0.0391	0.2236	0.0018	0.4761	0.0138	0.0068	0.0012	0.37	4.5	1.8	0.056	0.002	99.2	104.52	0.39	0.51	0.00003	18.38	#####	0.36	0.0146
174-01G	0.9	164.5345	0.3202	11.4585	0.0371	0.1530	0.0015	0.5759	0.0159	0.0030	0.0012	0.25	3.1	5.1	0.099	0.003	99.5	104.14	0.45	0.55	0.00002	42.26	#####	0.39	0.0048
174-01H	1.1	129.3704	0.3302	8.8897	0.0261	0.1221	0.0014	1.8044	0.0199	0.0054	0.0012	0.20	2.4	8.6	0.398	0.005	98.9	104.86	0.49	0.59	0.00004	23.73	#####	0.40	0.0107
174-01I	1.2	168.5621	0.1804	11.6660	0.0211	0.1591	0.0017	3.4317	0.0233	0.0073	0.0012	0.26	3.1	12.3	0.577	0.004	98.9	104.15	0.31	0.44	0.00004	18.10	#####	0.22	0.0106
174-01J	1.4	74.9143	0.1904	5.1522	0.0191	0.0681	0.0011	1.0586	0.0167	0.0000	0.0012	0.11	1.4	0.0	0.403	0.007	100.5	106.44	0.67	0.75	0.00000	0.00	#####	0.46	0.0024
SN08MD07 - amphibole - irradiation:DT-3																									
179-01A	0.6	45.8247	0.1207	1.4925	0.0100	0.0425	0.0007	0.3541	0.0145	0.1058	0.0011	0.03	1.8	0.1	0.465	0.019	31.8	71.86	1.75	1.77	0.00231	1.07	#####	0.73	0.1540
179-01B	0.7	26.6584	0.0959	1.6250	0.0098	0.0245	0.0007	0.6550	0.0158	0.0240	0.0009	0.04	1.9	0.7	0.790	0.020	73.6	88.35	1.33	1.36	0.00090	3.69	#####	0.72	0.0675
179-01C	0.8	59.7859	0.2104	3.8533	0.0230	0.0698	0.0011	13.7952	0.0359	0.0249	0.0010	0.09	4.5	14.4	7.017	0.046	89.5	101.36	0.91	0.96	0.00036	4.76	#####	0.71	0.0513
179-01D	0.9	172.8732	0.2503	11.0227	0.0250	0.2541	0.0015	68.1563	0.1012	0.0654	0.0010	0.24	13.0	27.1	12.119	0.033	91.8	105.15	0.36	0.48	0.00028	2.14	#####	0.28	0.0925
179-01E	1.0	209.3924	0.3003	14.0138	0.0310	0.3158	0.0020	90.5222	0.1943	0.0506	0.0010	0.31	16.5	46.5	12.661	0.040	96.2	104.93	0.33	0.46	0.00013	3.74	#####	0.27	0.0532
179-01F	1.1	196.5512	0.2205	13.3436	0.0310	0.2986	0.0016	87.3939	0.2230	0.0376	0.0009	0.29	15.7	60.5	12.837	0.045	97.8	105.14	0.32	0.45	0.00008	6.22	#####	0.27	0.0289
179-01G	1.2	221.2014	0.3403	15.1320	0.0240	0.3333	0.0019	92.8494	0.2375	0.0417	0.0011	0.33	17.8	57.9	12.027	0.037	97.7	104.23	0.29	0.43	0.00008	6.18	#####	0.23	0.0359
179-01H	1.3	98.3681	0.0950	6.6850	0.0140	0.1241	0.0013	28.8486	0.0487	0.0183	0.0008	0.15	7.9	40.9	8.458	0.023	96.7	103.90	0.35	0.47	0.00011	7.25	#####	0.24	0.0247
179-01I	1.4	76.1620	0.1507	5.1718	0.0180	0.0993	0.0010	29.6730	0.0466	0.0121	0.0008	0.11	6.1	63.7	11.245	0.044	98.3	105.64	0.54	0.63	0.00006	18.56	#####	0.41	0.0106
179-01J	1.5	136.3775	0.2404	9.1480	0.0220	0.1593	0.0014	31.3308	0.0445	0.0193	0.0008	0.20	10.8	42.2	6.713	0.019	97.6	106.09	0.38	0.50	0.00008	7.55	#####	0.31	0.0282
179-01K	1.6	37.6579	0.1206	2.5439	0.0120	0.0500	0.0009	13.9977	0.0396	0.0051	0.0009	0.06	3.0	70.9	10.785	0.060	98.8	106.73	0.94	0.99	0.00004	58.15	#####	0.58	0.0043
179-01L	1.7	15.3496	0.0380	1.0538	0.0078	0.0233	0.0006	8.1249	0.0312	0.0007	0.0009	0.02	1.2	282.7	15.111	0.128	102.6	109.05	1.91	1.94	0.00000	0.00	#####	0.80	0.0023
SN08MD10 - biotite - irradiation:DT-3																									
184-01A	0.1	153.5088	0.2502	10.9271	0.0281	0.1944	0.0018	0.1504	0.0132	0.1055	0.0014	0.24	2.9	0.0	0.027	0.002	79.7	82.12	0.39	0.47	0.00069	1.35	#####	0.31	0.1487
184-01B	0.1	345.0172	0.5701	26.3893	0.1001	0.4040	0.0021	0.1146	0.0132	0.0256	0.0012	0.58	7.0	0.1	0.009	0.001	97.8	93.49	0.40	0.49	0.00007	4.71	#####	0.42	0.0358
184-01C	0.3	878.1893	0.8101	67.4993	0.1802	1.0207	0.0035	0.2792	0.0140	0.0295	0.0013	1.49	17.8	0.2	0.008	0.000	99.0	94.16	0.27	0.40	0.00003	4.54	#####	0.29	0.0359
184-01D	0.5	670.6448	0.6301	51.2432	0.1401	0.7734	0.0029	0.2492	0.0148	0.0191	0.0012	1.13	13.5	0.3	0.010	0.001	99.2	94.84	0.28	0.40	0.00003	6.51	#####	0.30	0.0249
184-01E	0.6	666.1265	0.4901	50.8374	0.1101	0.7703	0.0027	0.4174	0.0132	0.0187	0.0013	1.12	13.4	0.6	0.016	0.001	99.2	94.96	0.23	0.37	0.00003	6.86	#####	0.24	0.0247
184-01F	0.7	665.6795	0.6401	50.9734	0.1501	0.7464	0.0026	1.0581	0.0156	0.0132	0.0012	1.13	13.5	2.1	0.041	0.001	99.4	94.89	0.30	0.42	0.00002	9.64	#####	0.32	0.0163
184-01G	0.8	669.3874	0.4401	51.0778	0.1401	0.7676	0.0029	4.9906	0.0271	0.0213	0.0012	1.13	13.5	6.1	0.192	0.001	99.1	94.93	0.28	0.40	0.00003	6.09	#####	0.29	0.0251
184-01H	0.9	487.6955	0.5601	37.2064	0.1101	0.5549	0.0027	8.2822	0.0336	0.0116	0.0012	0.82	9.8	18.6	0.436	0.002	99.4	95.24	0.31	0.43	0.00002	12.90	#####	0.33	0.0128
184-01I	1.1	181.8709	0.3001	13.8013	0.0281	0.2037	0.0020	5.0459	0.0289	0.0042	0.0011	0.31	3.6	31.6	0.717	0.004	99.5	95.84	0.31	0.42	0.00002	40.07	#####	0.27	0.0054
184-01J	1.2	128.6020	0.2102	9.7300	0.0221	0.1462	0.0014	7.7540	0.0345	0.0041	0.0012	0.22	2.6	49.1	1.562	0.008	99.5	96.11	0.37	0.47	0.00002	56.37	#####	0.29	0.0037
184-01K	1.4	44.7412	0.2502	3.3538	0.0241	0.0514	0.0008	0.9814	0.0120	0.0054	0.0010	0.07	0.9	4.7	0.574	0.008	96.6	94.19	1.08	1.12	0.00012	20.18	#####	0.93	0.0195
184-01L	1.5	67.8745	0.1802	5.1664	0.0191	0.0774	0.0010	0.9431	0.0157	0.0022	0.0012	0.11	1.4	10.9	0.358	0.006	99.1	95.17	0.64	0.70	0.00003	58.13	#####	0.47	0.0041

Supplemental Table SP2.1. $^{40}Ar/^{39}Ar$ Isotopic Data (continued)

		Relative Isotopic Abundances										Derived Results									Inverse Isochron Data				
Lab ID#	**Watts**	**^{40}Ar ±1σ**		**^{39}Ar ±1σ**		**^{38}Ar ±1σ**		**^{37}Ar ±1σ**		**^{36}Ar ±1σ**		**^{39}Ar Mol × 10^{-14}**	**^{39}Ar % of total**	**%(^{36}Ar)$_{Ca}$**	**Ca/K ±1σ**		**%$^{40}Ar^{*}$**	**Age (Ma) ±1σ**		**w/±J ±1σ**	**$^{36}Ar/^{40}Ar$ ±%1σ**		**$^{39}Ar/^{40}Ar$ ±%1σ**		**$^{36}Ar/^{39}Ar$ Er. Corr.**
SN08MD10 - amphibole - irradiation:DT-3																									
183-02A	0.6	91.8133	0.2715	5.5175	0.0241	0.1391	0.0014	25.3740	0.0600	0.0401	0.0012	0.12	14.8	16.4	9.014	0.045	89.2	108.22	0.74	0.81	0.00037	3.56	#####	0.54	0.0685
183-02B	0.7	262.1869	0.3810	17.3687	0.0351	0.4442	0.0026	95.3416	0.2100	0.0477	0.0012	0.38	46.4	52.0	10.759	0.033	97.4	107.27	0.32	0.45	0.00009	5.38	#####	0.26	0.0382
183-02C	0.8	164.5564	0.3013	11.0447	0.0311	0.2744	0.0021	59.0986	0.1402	0.0299	0.0011	0.24	29.5	51.5	10.488	0.039	97.4	105.89	0.42	0.53	0.00009	7.85	#####	0.35	0.0262
183-02D	0.9	24.1565	0.1921	1.5600	0.0101	0.0377	0.0010	8.5227	0.0301	0.0060	0.0011	0.03	4.2	37.2	10.708	0.080	95.4	107.76	1.82	1.85	0.00015	28.48	#####	1.04	0.0231
183-02E	1.0	21.3619	0.1232	1.4976	0.0121	0.0307	0.0009	6.4951	0.0211	0.0024	0.0011	0.03	4.0	69.3	8.501	0.075	99.0	103.06	1.80	1.83	0.00003	143.12	#####	1.01	0.0027
183-02F	1.1	3.7302	0.0635	0.2181	0.0050	0.0039	0.0009	1.0938	0.0150	0.0000	0.0011	0.00	0.6	768.3	9.829	0.263	102.0	126.49	10.85	10.85	0.00000	0.00	#####	2.88	0.0024
183-02G	1.2	2.8185	0.0488	0.1714	0.0044	0.0042	0.0009	0.7892	0.0164	0.0020	0.0011	0.00	0.5	10.4	9.024	0.300	81.5	98.01	13.34	13.34	0.00063	59.91	#####	3.13	0.0168
183-02H	1.3	0.5362	0.0418	0.0133	0.0027	0.0000	0.0008	0.0099	0.0143	0.0000	0.0011	0.00	0.0	0.0	1.460	2.141	390.5	911.17	183.97	183.99	0.00000	0.00	#####	22.01	0.1294
183-02I	1.5	2.0994	0.0472	0.0027	0.0023	0.0000	0.0008	0.0000	0.0129	0.0039	0.0011	0.00	0.0	0.0	0.000	10.687	45.2	#####	974.27	974.28	0.00185	28.63	#####	84.13	0.0022
183-02J	1.7	0.1669	0.0382	0.0000	0.0024	0.0000	0.0007	0.0000	0.0119	0.0000	0.0011	0.00	0.0	0.4	40.058	35.323	840.5		0.00	0.00	0.00000	0.00	#####	0.00	0.1766
SN08MH01 - biotite - irradiation:DT-3																									
176-01A	0.1	158.1217	0.2306	6.0396	0.0171	0.1420	0.0016	0.2550	0.0147	0.3066	0.0018	0.13	2.9	0.0	0.083	0.005	42.7	82.01	0.79	0.83	0.00194	0.65	#####	0.33	0.2819
176-01B	0.1	245.8930	0.3604	17.5040	0.0361	0.2549	0.0021	0.1021	0.0133	0.0772	0.0013	0.39	8.4	0.0	0.011	0.001	90.7	93.18	0.30	0.41	0.00031	1.73	#####	0.26	0.1185
176-01C	0.3	489.9322	0.6502	36.5959	0.1201	0.5126	0.0024	0.1949	0.0147	0.0409	0.0013	0.81	17.5	0.1	0.010	0.001	97.5	95.41	0.35	0.45	0.00008	3.17	#####	0.36	0.0520
176-01D	0.5	478.1732	0.5503	35.7035	0.1001	0.4841	0.0024	0.4411	0.0147	0.0301	0.0013	0.79	17.1	0.4	0.024	0.001	98.1	96.02	0.30	0.42	0.00006	4.16	#####	0.31	0.0406
176-01E	0.6	399.5129	0.4303	29.9813	0.1301	0.4175	0.0022	0.9689	0.0170	0.0260	0.0012	0.66	14.4	1.0	0.063	0.001	98.1	95.51	0.44	0.52	0.00006	4.63	#####	0.46	0.0282
176-01F	0.7	446.2171	0.5603	33.8602	0.1201	0.4712	0.0024	2.5643	0.0170	0.0171	0.0012	0.75	16.2	3.9	0.148	0.001	98.9	95.25	0.37	0.47	0.00004	7.09	#####	0.39	0.0219
176-01G	0.8	263.9999	0.3404	20.1222	0.0431	0.2788	0.0018	2.9221	0.0203	0.0079	0.0012	0.45	9.6	9.6	0.285	0.002	99.2	95.10	0.27	0.40	0.00003	16.48	#####	0.26	0.0117
176-01H	0.9	167.4230	0.2506	12.7500	0.0271	0.1794	0.0017	2.7794	0.0211	0.0062	0.0011	0.28	6.1	11.7	0.427	0.003	99.0	95.04	0.31	0.43	0.00003	20.67	#####	0.27	0.0099
176-01I	1.1	89.7330	0.1709	6.9038	0.0241	0.0962	0.0014	1.2467	0.0170	0.0041	0.0011	0.15	3.3	7.8	0.354	0.005	98.7	93.82	0.51	0.58	0.00004	29.70	#####	0.41	0.0065
176-01J	1.2	74.1968	0.1908	5.7746	0.0191	0.0791	0.0013	1.5858	0.0163	0.0033	0.0012	0.13	2.8	12.3	0.538	0.006	98.8	92.86	0.57	0.64	0.00004	39.26	#####	0.43	0.0062
176-01K	1.4	44.3736	0.1410	3.4495	0.0241	0.0477	0.0014	1.4176	0.0163	0.0042	0.0012	0.08	1.7	8.8	0.805	0.011	97.5	91.72	1.00	1.04	0.00009	30.68	#####	0.78	0.0064
SN08MH01 - amphibole - irradiation:DT-3																									
181-02A	0.6	80.4274	0.1109	4.7925	0.0111	0.0781	0.0011	3.8575	0.0220	0.0645	0.0015	0.11	5.0	1.6	1.578	0.010	76.7	94.09	0.70	0.76	0.00079	2.30	#####	0.28	0.0841
181-02B	0.7	154.0492	0.1805	11.3294	0.0201	0.1684	0.0014	17.1833	0.0664	0.0165	0.0014	0.25	11.8	27.1	2.973	0.013	97.7	97.06	0.33	0.44	0.00008	11.40	#####	0.22	0.0173
181-02C	0.8	222.8187	0.1805	16.2400	0.0251	0.2583	0.0020	56.7000	0.1300	0.0319	0.0015	0.36	17.0	46.2	6.843	0.019	97.7	98.00	0.26	0.40	0.00008	8.45	#####	0.19	0.0222
181-02D	0.9	344.4968	0.6402	25.2902	0.0381	0.4142	0.0022	125.2757	0.2165	0.0635	0.0015	0.56	26.4	51.3	9.709	0.023	97.3	96.98	0.28	0.40	0.00009	4.97	#####	0.25	0.0492
181-02E	1.0	256.2225	0.3903	18.8937	0.0271	0.2999	0.0018	66.7071	0.1302	0.0345	0.0015	0.42	19.7	50.2	6.920	0.017	98.0	97.17	0.27	0.40	0.00007	8.92	#####	0.22	0.0252
181-02F	1.1	128.7260	0.1507	9.4457	0.0191	0.1536	0.0015	36.3693	0.1044	0.0201	0.0014	0.21	9.9	47.1	7.547	0.027	97.6	97.21	0.39	0.49	0.00008	12.88	#####	0.24	0.0148
181-02G	1.2	43.1745	0.0675	3.1808	0.0089	0.0489	0.0011	9.5595	0.0520	0.0058	0.0013	0.07	3.3	42.9	5.891	0.036	97.7	96.97	0.91	0.95	0.00008	38.92	#####	0.33	0.0049
181-02H	1.3	29.9603	0.1010	2.1881	0.0069	0.0355	0.0009	6.8962	0.0402	0.0062	0.0012	0.05	2.3	28.7	6.177	0.041	95.6	95.73	1.24	1.27	0.00015	26.91	#####	0.47	0.0118
181-02I	1.5	40.3765	0.1208	2.9893	0.0085	0.0475	0.0010	10.9754	0.0658	0.0048	0.0013	0.07	3.1	59.5	7.196	0.048	98.6	97.34	0.98	1.03	0.00005	65.43	#####	0.42	0.0045
181-02J	1.7	17.5560	0.0568	1.3163	0.0077	0.0198	0.0009	5.0419	0.0512	0.0019	0.0012	0.03	1.4	67.9	7.507	0.089	99.0	96.51	2.07	2.09	0.00004	198.94	#####	0.68	0.0011
SN08MH05 - biotite - irradiation:DT-3																									
177-01A	0.1	132.9631	0.2303	8.4051	0.0211	0.1291	0.0015	0.1628	0.0229	0.0743	0.0013	0.19	2.3	0.1	0.038	0.005	83.5	96.47	0.46	0.54	0.00056	1.73	#####	0.31	0.1202
177-01B	0.1	340.3273	0.4401	24.0133	0.0841	0.3263	0.0023	0.1827	0.0238	0.0163	0.0012	0.53	6.7	0.3	0.015	0.002	98.6	101.90	0.40	0.50	0.00005	7.50	#####	0.38	0.0210
177-01C	0.3	1069.9810	2.5000	75.5706	0.1501	1.0330	0.0030	0.6217	0.0238	0.0254	0.0013	1.67	21.1	0.6	0.016	0.001	99.3	102.53	0.32	0.45	0.00002	5.12	#####	0.32	0.0520
177-01D	0.5	749.4085	0.6301	52.5609	0.1101	0.7116	0.0030	4.8122	0.0369	0.0204	0.0012	1.16	14.7	6.1	0.179	0.001	99.2	103.17	0.24	0.40	0.00003	6.30	#####	0.24	0.0278
177-01E	0.6	694.0188	0.5601	49.2135	0.1501	0.6658	0.0025	1.9170	0.0276	0.0148	0.0013	1.09	13.7	3.4	0.076	0.001	99.4	102.22	0.33	0.45	0.00002	8.90	#####	0.33	0.0168
177-01F	0.7	661.0294	0.6101	46.5954	0.1201	0.6341	0.0031	3.7557	0.0324	0.0171	0.0012	1.03	13.0	5.7	0.158	0.001	99.3	102.70	0.29	0.43	0.00002	7.54	#####	0.28	0.0219
177-01G	0.8	431.8463	0.4901	30.2693	0.1301	0.4148	0.0029	1.1106	0.0259	0.0085	0.0012	0.67	8.4	3.4	0.072	0.002	99.4	103.43	0.47	0.56	0.00002	15.20	#####	0.45	0.0088
177-01H	0.9	388.6646	0.4901	27.3236	0.1201	0.3721	0.0022	1.2929	0.0248	0.0060	0.0012	0.60	7.6	5.6	0.093	0.002	99.6	103.26	0.48	0.57	0.00001	21.41	#####	0.47	0.0064
177-01I	1.1	205.4425	0.2702	14.4680	0.0320	0.2018	0.0017	1.8891	0.0265	0.0033	0.0012	0.32	4.0	14.7	0.256	0.004	99.6	103.11	0.32	0.45	0.00001	41.86	#####	0.27	0.0046
177-01J	1.2	212.2913	0.3802	14.8644	0.0320	0.2015	0.0015	3.8455	0.0296	0.0009	0.0012	0.33	4.1	117.2	0.507	0.004	100.0	104.13	0.34	0.46	0.00000	0.00	#####	0.29	0.0003
177-01K	1.4	215.6021	0.2303	15.1419	0.0260	0.2090	0.0016	1.5568	0.0386	0.0003	0.0015	0.33	4.2	124.1	0.202	0.005	100.0	103.81	0.30	0.43	0.00000	0.00	#####	0.21	0.0001

Supplemental Table SP2.1. $^{40}Ar/^{39}Ar$ Isotopic Data (continued)

		Relative Isotopic Abundances										Derived Results									Inverse Isochron Data				
Lab ID#	Watts	^{40}Ar ±1σ		^{39}Ar ±1σ		^{38}Ar ±1σ		^{37}Ar ±1σ		^{36}Ar ±1σ		^{39}Ar Mol × 10^{-14}	^{39}Ar % of total	$\%(^{36}Ar)_{Ca}$	Ca/K ±1σ		$\%^{40}Ar^{*}$	Age (Ma) ±1σ		w/±J ±1σ	$^{36}Ar/^{40}Ar$ ±%1σ		$^{39}Ar/^{40}Ar$ ±%1σ		$^{36}Ar/^{39}Ar$ Er. Corr.
SN08MH05 - amphibole - irradiation:DT-3																									
182-01A	0.6	19.0535	0.1008	1.0578	0.0100	0.0192	0.0007	0.6547	0.0125	0.0170	0.0009	0.02	2.1	1.0	1.213	0.026	73.9	97.21	2.18	2.20	0.00088	5.56	#####	1.10	0.0550
182-01B	0.7	32.5989	0.1207	2.3392	0.0160	0.0461	0.0009	11.3830	0.0356	0.0066	0.0010	0.05	4.7	44.6	9.538	0.073	96.7	98.48	1.16	1.20	0.00011	26.48	#####	0.79	0.0090
182-01C	0.8	122.6141	0.2404	8.5321	0.0260	0.1962	0.0015	59.3187	0.0894	0.0289	0.0010	0.19	17.0	53.4	13.627	0.047	96.8	101.63	0.45	0.55	0.00011	7.56	#####	0.37	0.0274
182-01D	0.9	138.0709	0.1904	9.5671	0.0310	0.2140	0.0016	61.4373	0.1265	0.0287	0.0009	0.21	19.1	55.7	12.587	0.049	97.3	102.57	0.42	0.52	0.00009	7.35	#####	0.36	0.0229
182-01E	1.0	48.8997	0.1406	3.3617	0.0160	0.0807	0.0009	24.1728	0.0444	0.0135	0.0009	0.07	6.7	46.6	14.094	0.073	95.6	101.68	0.81	0.87	0.00015	12.76	#####	0.57	0.0177
182-01F	1.1	49.2105	0.1326	3.3759	0.0190	0.0878	0.0010	26.4247	0.0623	0.0127	0.0009	0.07	6.7	54.3	15.342	0.095	96.5	102.83	0.84	0.90	0.00012	15.03	#####	0.64	0.0127
182-01G	1.2	105.8483	0.2017	7.3080	0.0250	0.1837	0.0013	55.6221	0.1194	0.0310	0.0009	0.16	14.6	46.6	14.918	0.061	95.4	101.00	0.48	0.57	0.00016	5.42	#####	0.40	0.0357
182-01H	1.3	130.0048	0.2414	9.1353	0.0270	0.2017	0.0016	54.0655	0.1343	0.0267	0.0009	0.20	18.3	52.7	11.600	0.045	97.1	101.02	0.42	0.52	0.00010	7.22	#####	0.36	0.0281
182-01I	1.4	43.4165	0.1424	3.1085	0.0170	0.0661	0.0010	17.8435	0.0389	0.0071	0.0008	0.07	6.2	65.1	11.251	0.067	98.3	100.35	0.85	0.90	0.00006	33.04	#####	0.65	0.0072
182-01J	1.5	31.8764	0.1228	2.2615	0.0170	0.0522	0.0010	14.6428	0.0375	0.0050	0.0009	0.05	4.5	76.5	12.691	0.102	98.9	101.88	1.17	1.21	0.00004	73.45	#####	0.86	0.0032
SN08MH11 - biotite - irradiation:DT-3																									
173-01A	0.1	1224.0920	2.1001	67.5119	0.1902	0.9548	0.0030	0.1738	0.0131	0.1797	0.0015	1.49	22.7	0.0	0.005	0.000	95.7	125.67	0.42	0.57	0.00015	0.90	#####	0.34	0.2204
173-01B	0.3	1133.4100	0.4402	62.9642	0.1001	0.8608	0.0030	0.1460	0.0131	0.0318	0.0011	1.39	21.2	0.1	0.005	0.000	99.2	129.21	0.22	0.45	0.00003	3.57	#####	0.18	0.0492
173-01C	0.5	654.7805	0.9501	36.1969	0.1101	0.5065	0.0027	0.1515	0.0132	0.0138	0.0011	0.80	12.2	0.3	0.008	0.001	99.4	130.09	0.44	0.59	0.00002	7.92	#####	0.35	0.0224
173-01D	0.6	677.5055	1.5001	37.6941	0.1301	0.5140	0.0024	0.1980	0.0139	0.0151	0.0011	0.83	12.7	0.3	0.010	0.001	99.3	129.24	0.53	0.66	0.00002	7.30	#####	0.42	0.0293
173-01E	0.7	570.6958	0.6002	31.6343	0.1101	0.4346	0.0024	0.4731	0.0154	0.0115	0.0012	0.70	10.6	1.1	0.029	0.001	99.4	129.79	0.47	0.62	0.00002	10.13	#####	0.37	0.0146
173-01F	0.8	457.8517	0.7201	25.2979	0.0981	0.3487	0.0020	0.8299	0.0146	0.0112	0.0011	0.56	8.5	1.9	0.064	0.001	99.3	130.04	0.55	0.67	0.00002	10.31	#####	0.43	0.0158
173-01G	0.9	368.4169	0.6302	20.5684	0.0411	0.2879	0.0022	0.8767	0.0154	0.0079	0.0011	0.45	6.9	2.9	0.084	0.001	99.4	128.87	0.36	0.53	0.00002	14.50	#####	0.27	0.0153
173-01H	1.1	140.3099	0.2304	7.8252	0.0270	0.1093	0.0012	0.4589	0.0125	0.0005	0.0010	0.17	2.6	21.8	0.115	0.003	99.9	129.65	0.56	0.68	0.00000	232.60	#####	0.39	0.0008
173-01I	1.2	61.2107	0.1805	3.4256	0.0171	0.0518	0.0012	0.4476	0.0124	0.0014	0.0010	0.08	1.2	8.6	0.256	0.007	99.4	128.59	0.95	1.02	0.00002	79.63	#####	0.59	0.0028
173-01J	1.4	73.5593	0.1905	4.1029	0.0211	0.0563	0.0012	0.7780	0.0154	0.0016	0.0010	0.09	1.4	12.7	0.372	0.008	99.4	129.06	0.89	0.97	0.00002	72.17	#####	0.59	0.0027
SN08MH11 - amphibole - irradiation:DT-3																									
178-01B	0.7	23.4893	0.1205	1.1138	0.0067	0.0215	0.0007	1.1517	0.0128	0.0219	0.0008	0.02	1.8	1.4	2.027	0.026	72.8	111.73	1.82	1.85	0.00092	3.75	#####	0.81	0.1030
178-01C	0.8	54.4415	0.1704	2.6865	0.0160	0.0529	0.0009	10.5197	0.0314	0.0253	0.0009	0.06	4.3	10.8	7.675	0.052	87.8	128.90	1.11	1.18	0.00041	3.92	#####	0.69	0.0548
178-01D	0.9	186.7454	0.2802	9.7465	0.0230	0.2398	0.0012	83.0944	0.1424	0.0626	0.0009	0.22	15.6	34.5	16.710	0.050	93.5	129.98	0.43	0.58	0.00022	2.32	#####	0.29	0.0856
178-01E	1.0	193.9526	0.3002	10.3322	0.0330	0.2540	0.0016	98.7845	0.1709	0.0563	0.0010	0.23	16.6	45.6	18.739	0.069	95.3	129.87	0.52	0.65	0.00016	3.39	#####	0.37	0.0525
178-01F	1.1	116.2776	0.2022	6.2006	0.0220	0.1549	0.0011	54.9555	0.0928	0.0306	0.0009	0.14	9.9	46.6	17.371	0.069	95.8	130.39	0.61	0.72	0.00014	5.64	#####	0.41	0.0319
178-01G	1.2	126.9015	0.2320	6.8455	0.0230	0.1693	0.0014	70.2237	0.1854	0.0297	0.0009	0.15	11.0	61.4	20.107	0.087	97.3	130.92	0.58	0.70	0.00009	7.86	#####	0.39	0.0242
178-01H	1.3	129.2635	0.2320	6.9390	0.0260	0.1785	0.0013	68.7210	0.1926	0.0313	0.0009	0.15	11.1	57.0	19.411	0.092	96.9	131.00	0.61	0.73	0.00010	6.46	#####	0.43	0.0276
178-01I	1.4	105.2435	0.1334	5.6710	0.0110	0.1418	0.0011	53.5912	0.1428	0.0246	0.0009	0.13	9.1	56.7	18.522	0.062	97.0	130.62	0.46	0.61	0.00010	8.54	#####	0.24	0.0231
178-01J	1.5	72.6377	0.0883	3.9329	0.0110	0.0986	0.0011	36.8051	0.0596	0.0157	0.0008	0.09	6.3	60.9	18.342	0.060	97.5	130.64	0.60	0.72	0.00008	13.68	#####	0.32	0.0125
178-01K	1.6	36.6266	0.0735	2.0202	0.0072	0.0485	0.0008	17.9996	0.0343	0.0049	0.0009	0.04	3.2	96.3	17.463	0.071	99.9	131.29	1.03	1.11	0.00000	486.98	#####	0.42	0.0004
178-01L	1.7	23.0131	0.0591	1.2995	0.0095	0.0298	0.0007	9.2280	0.0308	0.0012	0.0009	0.03	2.1	209.5	13.919	0.114	101.6	130.47	1.72	1.77	0.00000	0.00	#####	0.79	0.0021
178-01M	1.9	53.7245	0.1711	2.9014	0.0170	0.0700	0.0009	21.9110	0.0506	0.0078	0.0009	0.06	4.6	73.3	14.802	0.095	98.9	132.66	1.07	1.14	0.00004	41.87	#####	0.68	0.0053
178-01N	2.1	49.1970	0.1314	2.7223	0.0130	0.0788	0.0009	27.2670	0.0372	0.0077	0.0009	0.06	4.4	91.8	19.632	0.099	99.6	130.63	1.00	1.07	0.00001	147.49	#####	0.56	0.0014
SN08DW01 - biotite - irradiation:DT-6c																									
433-01B	0.0	367.5457	0.2602	12.9524	0.0221	0.1912	0.0017	0.2586	0.0034	0.0618	0.0013	0.29	2.5	0.1	0.039	0.001	95.0	101.51	0.23	0.69	0.00017	2.13	#####	0.20	0.0849
433-01C	1.2	910.9650	0.3401	32.7797	0.0520	0.4538	0.0021	0.4993	0.0041	0.0147	0.0015	0.73	6.2	0.9	0.030	0.000	99.5	104.04	0.18	0.69	0.00002	10.24	#####	0.18	0.0171
433-01D	1.6	1727.9720	0.6001	61.9577	0.0640	0.8549	0.0029	0.8290	0.0066	0.0279	0.0019	1.37	11.8	0.8	0.026	0.000	99.5	104.40	0.13	0.68	0.00002	6.78	#####	0.13	0.0276
433-01E	2.0	2492.5080	0.8601	89.5656	0.0790	1.2179	0.0031	0.9894	0.0044	0.0180	0.0024	1.99	17.1	1.5	0.022	0.000	99.8	104.44	0.12	0.68	0.00001	13.32	#####	0.11	0.0142
433-01F	2.8	1951.7020	0.7904	70.0382	0.0680	0.9527	0.0032	1.0566	0.0049	0.0000	0.0022	1.55	13.4	0.0	0.030	0.000	100.1	104.89	0.13	0.69	0.00000	0.00	#####	0.12	0.0053
433-01G	3.2	2499.9420	0.8904	89.1943	0.0850	1.2189	0.0037	1.5230	0.0074	0.0052	0.0025	1.98	17.0	8.1	0.033	0.000	99.9	105.33	0.13	0.69	0.00000	52.36	#####	0.12	0.0036
433-01H	3.6	2466.5300	0.8804	87.9421	0.0800	1.1840	0.0032	1.8823	0.0098	0.0000	0.0024	1.95	16.8	0.0	0.042	0.000	100.1	105.56	0.12	0.69	0.00000	0.00	#####	0.12	0.0068
433-01I	4.0	2237.9360	0.7205	80.1037	0.0860	1.0830	0.0034	2.5794	0.0062	0.0000	0.0024	1.78	15.3	0.0	0.063	0.000	100.2	105.27	0.14	0.69	0.00000	0.00	#####	0.13	0.0120

Supplemental Table SP2.1. $^{40}Ar/^{39}Ar$ Isotopic Data (continued)

		Relative Isotopic Abundances										Derived Results									Inverse Isochron Data				
Lab ID#	Watts	^{40}Ar ±1σ		^{39}Ar ±1σ		^{38}Ar ±1σ		^{37}Ar ±1σ		^{36}Ar ±1σ		^{39}Ar Mol × 10^{-14}	^{39}Ar % of total	$\%(^{36}Ar)_{Ca}$	Ca/K ±1σ		$\%^{40}Ar^{*}$	Age (Ma) ±1σ		w/±J ±1σ	$^{36}Ar/^{40}Ar$ ±%1σ		$^{39}Ar/^{40}Ar$ ±%1σ		$^{36}Ar/^{39}Ar$ Er. Corr.
SN08DW01 - amphibole - irradiation:DT-6b																									
408-01B	1.0	52.9189	0.1102	1.8030	0.0071	0.0291	0.0015	0.6698	0.0054	0.0361	0.0010	0.04	3.0	0.5	0.728	0.007	79.9	89.27	0.73	0.74	0.00068	2.71	#####	0.46	0.0705
408-01C	1.5	92.6207	0.1202	3.2340	0.0090	0.0572	0.0013	4.8460	0.0250	0.0474	0.0010	0.07	5.4	2.8	2.937	0.017	85.3	92.96	0.46	0.48	0.00050	2.25	#####	0.32	0.0782
408-01D	1.8	110.5015	0.1402	3.7618	0.0120	0.0796	0.0016	25.9039	0.0608	0.0423	0.0009	0.08	6.3	17.0	13.497	0.054	90.6	101.40	0.45	0.47	0.00032	2.69	#####	0.36	0.0607
408-01E	2.1	266.5149	0.4700	8.9919	0.0210	0.2391	0.0020	93.9387	0.2766	0.0869	0.0012	0.20	15.0	29.9	20.476	0.078	93.2	105.43	0.36	0.38	0.00023	2.02	#####	0.30	0.1062
408-01F	2.4	345.1732	0.6100	11.7244	0.0270	0.3343	0.0024	123.1852	0.3042	0.1116	0.0015	0.26	19.6	30.6	20.593	0.070	93.4	104.88	0.35	0.38	0.00022	1.95	#####	0.30	0.1105
408-01G	2.7	342.3409	0.4800	11.8693	0.0400	0.3258	0.0025	118.4519	0.2679	0.0975	0.0014	0.26	19.8	33.6	19.560	0.080	94.4	103.89	0.41	0.43	0.00019	2.18	#####	0.38	0.0758
408-01H	3.0	129.0635	0.1202	4.6708	0.0089	0.1085	0.0017	43.2194	0.0579	0.0271	0.0010	0.10	7.8	44.2	18.136	0.043	96.5	101.78	0.33	0.36	0.00012	6.69	#####	0.22	0.0273
408-01I	3.5	88.3153	0.1002	3.2860	0.0100	0.0710	0.0016	29.7480	0.0580	0.0200	0.0009	0.07	5.5	41.2	17.744	0.065	96.1	98.59	0.44	0.46	0.00013	7.38	#####	0.34	0.0218
408-01J	4.0	72.0191	0.0793	2.6122	0.0110	0.0640	0.0016	26.7844	0.0916	0.0143	0.0010	0.06	4.4	52.0	20.097	0.110	97.2	102.29	0.60	0.62	0.00010	13.99	#####	0.45	0.0095
408-01K	4.5	61.5721	0.1002	2.2018	0.0083	0.0524	0.0014	22.0487	0.0794	0.0094	0.0010	0.05	3.7	64.7	19.628	0.104	98.4	104.96	0.65	0.67	0.00005	29.53	#####	0.42	0.0057
408-01L	5.0	116.1890	0.0982	4.4337	0.0079	0.0829	0.0012	24.6771	0.0398	0.0141	0.0008	0.10	7.4	48.6	10.909	0.027	98.2	98.00	0.29	0.32	0.00006	11.54	#####	0.21	0.0158
408-01M	5.5	33.1811	0.0862	1.2258	0.0079	0.0145	0.0014	5.0898	0.0337	0.0000	0.0008	0.03	2.0	0.0	8.138	0.076	102.2	105.04	1.02	1.03	0.00000	0.00	#####	0.71	0.0050
SN08AR04 - biotite - irradiation:DT-6b																									
407-01B	0.9	859.5529	0.3034	32.8862	0.0681	0.4668	0.0026	0.2111	0.0033	0.0690	0.0020	0.73	4.4	0.1	0.013	0.000	97.6	96.87	0.22	0.26	0.00008	2.95	#####	0.22	0.0553
407-01C	1.2	1538.8920	0.6660	59.2000	0.0591	0.8016	0.0033	0.3745	0.0035	0.0353	0.0022	1.31	7.9	0.3	0.012	0.000	99.3	97.99	0.13	0.18	0.00002	6.28	#####	0.13	0.0301
407-01D	1.6	1848.9580	0.6660	70.7935	0.0691	0.9524	0.0028	0.5343	0.0039	0.0207	0.0024	1.57	9.4	0.7	0.015	0.000	99.7	98.77	0.12	0.18	0.00001	11.66	#####	0.12	0.0162
407-01E	2.0	2305.6460	0.9940	87.5266	0.0911	1.1833	0.0034	0.9542	0.0046	0.0350	0.0028	1.94	11.7	0.8	0.021	0.000	99.6	99.49	0.13	0.19	0.00002	7.96	#####	0.13	0.0237
407-01F	2.4	2574.3140	1.6025	98.0024	0.0821	1.3315	0.0031	1.7772	0.0056	0.0281	0.0029	2.17	13.1	1.8	0.036	0.000	99.7	99.34	0.12	0.18	0.00001	10.34	#####	0.12	0.0190
407-01G	2.8	2686.1420	1.1036	102.1763	0.0991	1.3814	0.0042	3.0004	0.0081	0.0171	0.0030	2.27	13.6	4.9	0.058	0.000	99.8	99.55	0.12	0.18	0.00001	18.19	#####	0.12	0.0104
407-01H	3.2	2613.0020	1.1036	99.2765	0.0791	1.3425	0.0035	5.2149	0.0091	0.0154	0.0027	2.20	13.2	9.4	0.103	0.000	99.8	99.69	0.11	0.17	0.00001	19.10	#####	0.11	0.0101
407-01I	3.6	2159.0070	0.7156	82.1477	0.0851	1.1068	0.0033	5.3589	0.0083	0.0120	0.0024	1.82	11.0	12.4	0.128	0.000	99.9	99.56	0.13	0.18	0.00000	22.79	#####	0.13	0.0082
407-01J	4.0	1850.5480	1.2033	70.3081	0.0861	0.9564	0.0025	5.8417	0.0088	0.0157	0.0019	1.56	9.4	10.3	0.163	0.000	99.8	99.62	0.15	0.20	0.00001	13.77	#####	0.15	0.0138
407-01K	4.5	1247.6790	0.4587	47.5663	0.0551	0.6364	0.0024	6.1564	0.0117	0.0000	0.0022	1.05	6.3	0.0	0.254	0.001	100.1	99.64	0.14	0.19	0.00000	0.00	#####	0.14	0.0048
SN08AR04 - amphibole - irradiation:DT-6b																									
413-01B	1.0	73.8137	0.0779	2.6979	0.0051	0.0447	0.0013	0.3757	0.0041	0.0274	0.0012	0.06	4.3	0.4	0.273	0.003	89.1	92.63	0.54	0.56	0.00037	4.49	#####	0.23	0.0421
413-01C	1.5	105.2701	0.1146	3.7278	0.0070	0.0526	0.0013	0.4220	0.0041	0.0201	0.0013	0.08	6.0	0.6	0.222	0.002	94.4	101.07	0.45	0.47	0.00019	6.58	#####	0.23	0.0289
413-01D	1.8	107.4573	0.1031	3.8813	0.0064	0.0616	0.0012	1.8205	0.0060	0.0408	0.0013	0.09	6.2	1.2	0.919	0.003	88.9	93.57	0.42	0.44	0.00038	3.28	#####	0.20	0.0582
413-01E	2.1	86.0731	0.0815	3.0728	0.0070	0.0498	0.0014	8.6844	0.0143	0.0186	0.0012	0.07	4.9	12.9	5.539	0.016	94.4	100.52	0.51	0.52	0.00019	7.57	#####	0.26	0.0230
413-01F	2.4	75.9869	0.0797	2.7177	0.0062	0.0560	0.0013	15.5912	0.0341	0.0173	0.0012	0.06	4.4	25.0	11.244	0.036	95.0	101.09	0.56	0.58	0.00017	9.48	#####	0.26	0.0187
413-01G	2.7	90.9719	0.1146	3.2892	0.0080	0.0777	0.0013	23.4678	0.0426	0.0164	0.0012	0.07	5.3	39.7	13.984	0.043	96.8	101.98	0.50	0.52	0.00011	12.40	#####	0.28	0.0148
413-01H	3.0	108.1828	0.1242	3.8550	0.0086	0.0844	0.0014	29.1852	0.0710	0.0154	0.0012	0.09	6.2	52.4	14.839	0.050	98.0	104.71	0.44	0.46	0.00007	16.69	#####	0.26	0.0110
413-01I	3.5	145.1968	0.2520	5.1385	0.0101	0.1170	0.0016	45.1308	0.1193	0.0303	0.0014	0.11	8.2	41.3	17.214	0.057	96.4	103.81	0.41	0.43	0.00012	7.92	#####	0.27	0.0282
413-01J	4.0	201.2035	0.6308	7.1857	0.0210	0.1603	0.0017	64.5193	0.1592	0.0362	0.0015	0.16	11.5	49.4	17.599	0.068	97.3	103.88	0.51	0.53	0.00009	8.23	#####	0.44	0.0368
413-01K	4.5	223.2025	0.7107	7.9174	0.0181	0.1889	0.0017	71.1925	0.1423	0.0461	0.0014	0.18	12.7	42.8	17.624	0.054	96.5	103.74	0.46	0.48	0.00012	5.36	#####	0.40	0.0611
413-01L	5.0	261.2367	0.3216	9.3519	0.0190	0.2084	0.0019	78.2864	0.2079	0.0508	0.0013	0.21	15.0	42.7	16.408	0.056	96.7	102.97	0.30	0.33	0.00011	4.53	#####	0.25	0.0425
413-01M	5.5	262.1937	0.2322	9.5367	0.0131	0.2038	0.0017	81.4720	0.2109	0.0393	0.0016	0.21	15.3	57.4	16.744	0.050	98.1	102.84	0.26	0.29	0.00006	9.55	#####	0.18	0.0203
SN08AR06 -biotite - irradiation:DT-6b																									
404-01C	0.9	1032.1280	0.3601	37.3039	0.0520	0.5196	0.0023	0.2958	0.0032	0.0423	0.0017	0.83	5.5	0.2	0.016	0.000	98.8	103.57	0.17	0.22	0.00004	3.99	#####	0.16	0.0450
404-01D	1.2	1407.6740	0.5001	50.6656	0.0490	0.6929	0.0025	0.3004	0.0034	0.0181	0.0015	1.12	7.5	0.5	0.012	0.000	99.6	104.84	0.13	0.19	0.00001	8.30	#####	0.12	0.0227
404-01E	1.6	1907.9520	0.5901	67.8725	0.0870	0.9297	0.0036	0.4489	0.0034	0.0151	0.0019	1.50	10.1	0.8	0.013	0.000	99.8	106.19	0.15	0.21	0.00001	12.48	#####	0.15	0.0145
404-01F	2.0	2312.6110	0.7601	82.5168	0.0740	1.1249	0.0029	0.7707	0.0044	0.0417	0.0022	1.83	12.3	0.5	0.018	0.000	99.5	105.57	0.12	0.18	0.00002	5.22	#####	0.11	0.0362
404-01G	2.4	2415.4570	0.9300	86.0254	0.1601	1.1607	0.0033	1.4195	0.0046	0.0408	0.0024	1.91	12.8	1.0	0.032	0.000	99.5	105.80	0.21	0.25	0.00002	5.84	#####	0.20	0.0289
404-01H	2.8	2567.5770	0.8700	91.7906	0.0870	1.2392	0.0030	2.4970	0.0060	0.0070	0.0023	2.03	13.6	9.8	0.053	0.000	99.9	105.85	0.12	0.19	0.00000	35.61	#####	0.12	0.0053
404-01I	3.2	2587.1110	0.8900	92.1289	0.0800	1.2604	0.0037	2.6965	0.0060	0.0269	0.0023	2.04	13.7	2.8	0.057	0.000	99.7	106.02	0.12	0.18	0.00001	8.65	#####	0.11	0.0220
404-01J	3.6	1778.3860	0.6901	63.4681	0.0700	0.8563	0.0025	1.8241	0.0058	0.0260	0.0020	1.41	9.4	1.9	0.056	0.000	99.6	105.66	0.14	0.20	0.00001	7.73	#####	0.13	0.0241
404-01K	4.0	1499.7970	0.5801	53.4136	0.0580	0.7167	0.0029	2.8163	0.0080	0.0379	0.0016	1.18	7.9	2.1	0.103	0.000	99.3	105.56	0.14	0.20	0.00002	4.27	#####	0.13	0.0437
404-01L	4.5	1346.5210	0.4201	47.8941	0.0620	0.6538	0.0030	2.7488	0.0058	0.0328	0.0014	1.06	7.1	2.3	0.112	0.000	99.3	105.72	0.16	0.21	0.00002	4.37	#####	0.15	0.0415

Supplemental Table SP2.1. $^{40}Ar/^{39}Ar$ Isotopic Data (continued)

		Relative Isotopic Abundances										Derived Results									Inverse Isochron Data				
Lab ID#	Watts	^{40}Ar	±1σ	^{39}Ar	±1σ	^{38}Ar	±1σ	^{37}Ar	±1σ	^{36}Ar	±1σ	^{39}Ar Mol $\times 10^{-14}$	^{39}Ar % of total	$\%(^{36}Ar)_{Ca}$	Ca/K	±1σ	$\%^{40}Ar^{*}$	Age (Ma)	±1σ	w/±J	±1σ	$^{36}Ar/^{40}Ar$	±%1σ	$^{39}Ar/^{40}Ar$	±%1σ	$^{36}Ar/^{39}Ar$ Er. Corr.
SN08AR06 - amphibole - irradiation:DT-6b																										
410-01C	1.2	48.8808	0.0894	1.6871	0.0077	0.0241	0.0013	0.7411	0.0054	0.0135	0.0018	0.04	2.0	1.5	0.861	0.007	92.0	101.08	1.25	1.26	0.00027	13.41	#####	0.50	0.0120
410-01D	1.5	75.0657	0.0924	2.6383	0.0101	0.0389	0.0013	1.9664	0.0073	0.0185	0.0018	0.06	3.1	2.9	1.461	0.008	92.9	100.34	0.84	0.85	0.00024	9.92	#####	0.41	0.0149
410-01E	1.8	76.4285	0.1203	2.6994	0.0101	0.0466	0.0013	6.9926	0.0140	0.0119	0.0018	0.06	3.1	16.3	5.077	0.022	96.2	103.35	0.83	0.84	0.00013	17.88	#####	0.42	0.0093
410-01F	2.1	97.0745	0.1802	3.4375	0.0100	0.0692	0.0014	18.4068	0.0600	0.0108	0.0018	0.08	4.0	47.3	10.495	0.046	98.3	105.49	0.67	0.69	0.00006	31.30	#####	0.36	0.0065
410-01G	2.4	152.7034	0.2202	5.4139	0.0171	0.1327	0.0016	37.5751	0.1337	0.0221	0.0021	0.12	6.3	47.1	13.603	0.065	97.7	104.92	0.56	0.57	0.00008	17.70	#####	0.36	0.0098
410-01H	2.7	197.6514	0.2502	6.9049	0.0181	0.1762	0.0021	53.3475	0.2075	0.0364	0.0023	0.15	8.0	40.6	15.143	0.072	96.8	105.47	0.48	0.50	0.00011	10.47	#####	0.30	0.0170
410-01I	3.0	343.8310	0.5601	11.9764	0.0340	0.3173	0.0022	91.7830	0.2213	0.0610	0.0021	0.27	13.9	41.6	15.021	0.057	96.9	105.94	0.40	0.42	0.00010	5.82	#####	0.34	0.0330
410-01J	3.5	487.6802	1.4000	17.1398	0.0440	0.4506	0.0026	131.0284	0.4375	0.0629	0.0016	0.38	19.9	57.7	14.984	0.064	98.4	106.55	0.43	0.45	0.00005	6.01	#####	0.40	0.0485
410-01K	4.0	719.0228	1.4000	25.3149	0.0450	0.6092	0.0035	171.0545	0.3557	0.0858	0.0020	0.56	29.3	55.2	13.244	0.037	98.4	106.34	0.30	0.33	0.00005	5.14	#####	0.27	0.0472
410-01L	4.5	257.5961	0.2901	9.0608	0.0260	0.2488	0.0018	76.8410	0.3013	0.0344	0.0020	0.20	10.5	61.8	16.622	0.082	98.5	106.63	0.41	0.43	0.00005	15.01	#####	0.32	0.0110
SN08AR11 - biotite - irradiation:DT-6b																									
406-01C	1.2	2332.1150	2.5000	68.2070	0.1001	0.9487	0.0032	5.6468	0.0147	0.1606	0.0036	1.51	6.3	1.0	0.162	0.000	98.0	126.15	0.25	0.30	0.00007	2.31	#####	0.19	0.0867
406-01D	1.6	3405.8010	2.7000	96.8087	0.2501	1.3193	0.0048	6.7670	0.0130	0.1085	0.0043	2.15	8.9	1.7	0.137	0.000	99.1	131.07	0.36	0.40	0.00003	4.08	#####	0.28	0.0394
406-01E	2.0	3895.7210	3.3000	110.4282	0.1901	1.5173	0.0056	9.5583	0.0168	0.1860	0.0053	2.45	10.2	1.4	0.170	0.000	98.6	130.82	0.26	0.31	0.00005	2.92	#####	0.20	0.0633
406-01F	2.4	4158.3900	4.1000	117.3785	0.1901	1.6155	0.0042	9.4878	0.0155	0.1690	0.0056	2.60	10.8	1.6	0.158	0.000	98.8	131.62	0.26	0.31	0.00004	3.39	#####	0.20	0.0568
406-01G	2.8	4843.1120	4.9000	136.7610	0.1701	1.8779	0.0067	12.7622	0.0284	0.1301	0.0062	3.03	12.6	2.7	0.183	0.000	99.2	132.10	0.23	0.29	0.00003	4.93	#####	0.17	0.0411
406-01H	3.2	6323.0610	8.3000	177.0611	0.2201	2.4212	0.0071	16.8758	0.0191	0.3075	0.0073	3.93	16.3	1.5	0.187	0.000	98.6	132.34	0.25	0.31	0.00005	2.43	#####	0.19	0.0892
406-01I	3.6	7351.7480	8.9000	206.6910	0.2301	2.8377	0.0064	21.2014	0.0284	0.2094	0.0100	4.58	19.0	2.8	0.201	0.000	99.2	132.60	0.23	0.29	0.00003	4.93	#####	0.18	0.0435
406-01J	3.5	3298.0150	2.0000	92.4157	0.1401	1.2490	0.0036	8.7609	0.0161	0.1018	0.0060	2.05	8.5	2.4	0.186	0.000	99.1	132.93	0.24	0.29	0.00003	6.07	#####	0.18	0.0300
406-01K	3.5	2811.8220	1.6000	79.2706	0.1401	1.0573	0.0045	8.4843	0.0182	0.0344	0.0047	1.76	7.3	6.8	0.210	0.001	99.7	132.87	0.26	0.31	0.00001	14.77	#####	0.20	0.0119
SN08AR11 - amphibole - irradiation:DT-6b																									
412-01F	2.1	41.3164	0.0525	0.9868	0.0026	0.0226	0.0011	8.5930	0.0127	0.0201	0.0008	0.02	3.0	11.8	17.068	0.052	87.3	137.99	0.93	0.95	0.00043	4.29	#####	0.30	0.0416
412-01G	2.4	58.6130	0.0631	1.4683	0.0035	0.0329	0.0011	13.7634	0.0308	0.0213	0.0008	0.03	4.5	17.9	18.373	0.061	91.2	137.49	0.68	0.71	0.00030	4.44	#####	0.27	0.0396
412-01H	2.7	91.2763	0.0826	2.4687	0.0055	0.0517	0.0013	26.2282	0.0364	0.0150	0.0008	0.05	7.6	48.3	20.824	0.056	97.5	136.32	0.47	0.51	0.00009	9.78	#####	0.25	0.0177
412-01I	3.0	102.5192	0.0826	2.7194	0.0060	0.0635	0.0013	29.3751	0.0392	0.0212	0.0007	0.06	8.4	38.4	21.172	0.056	96.2	137.22	0.45	0.48	0.00013	5.73	#####	0.25	0.0296
412-01J	3.5	104.1727	0.0875	2.6759	0.0072	0.0632	0.0012	28.4321	0.0449	0.0346	0.0012	0.06	8.2	22.7	20.826	0.066	92.4	136.09	0.62	0.65	0.00026	4.50	#####	0.29	0.0353
412-01K	4.0	148.9132	0.1112	3.9465	0.0072	0.0902	0.0015	45.4563	0.0673	0.0324	0.0008	0.09	12.2	38.8	22.576	0.054	96.1	137.15	0.35	0.40	0.00013	3.89	#####	0.21	0.0458
412-01L	4.5	145.3900	0.1013	3.7804	0.0083	0.0831	0.0015	41.2404	0.0870	0.0400	0.0008	0.08	11.7	28.5	21.382	0.066	94.2	137.00	0.41	0.45	0.00020	2.98	#####	0.24	0.0561
412-01M	5.0	151.8209	0.1310	4.0326	0.0070	0.0851	0.0012	41.6417	0.1011	0.0345	0.0009	0.09	12.4	33.4	20.239	0.061	95.5	136.00	0.37	0.41	0.00015	3.88	#####	0.21	0.0475
412-01N	5.5	195.5492	0.1409	5.2366	0.0097	0.0997	0.0013	54.5425	0.1518	0.0394	0.0009	0.12	16.1	38.3	20.414	0.069	96.3	136.04	0.34	0.38	0.00012	3.75	#####	0.21	0.0471
412-01O	6.0	194.6228	0.1409	5.1243	0.0090	0.0971	0.0016	55.7869	0.1406	0.0473	0.0009	0.11	15.8	32.6	21.338	0.066	95.2	136.71	0.33	0.37	0.00016	2.71	#####	0.20	0.0663
SN08PV11 - biotite - irradiation:DT-6b																									
414-01B	0.9	534.8211	0.2027	22.0556	0.0550	0.3155	0.0025	0.3690	0.0036	0.0709	0.0016	0.49	5.5	0.1	0.033	0.000	96.1	88.66	0.24	0.27	0.00013	2.33	#####	0.26	0.0655
414-01C	1.2	1613.3270	0.5211	67.7541	0.0650	0.9068	0.0031	0.7180	0.0039	0.0116	0.0018	1.50	17.0	1.7	0.021	0.000	99.8	90.37	0.11	0.16	0.00001	16.10	#####	0.12	0.0117
414-01D	1.6	1591.8430	0.5610	66.4204	0.0710	0.8861	0.0029	0.7507	0.0050	0.0061	0.0020	1.47	16.7	3.4	0.022	0.000	99.9	91.03	0.12	0.17	0.00000	34.41	#####	0.13	0.0054
414-01E	2.0	1543.0180	0.5710	64.5953	0.0790	0.8630	0.0028	0.7642	0.0041	0.0000	0.0018	1.43	16.2	0.0	0.023	0.000	100.0	90.88	0.13	0.18	0.00000	0.00	#####	0.14	0.0023
414-01F	2.4	1682.0640	0.4911	70.3382	0.0660	0.9361	0.0032	0.8133	0.0043	0.0083	0.0019	1.56	17.7	2.7	0.023	0.000	99.9	90.81	0.11	0.16	0.00000	23.75	#####	0.12	0.0079
414-01G	2.8	1403.5950	0.6708	58.5704	0.0500	0.7767	0.0035	1.0590	0.0043	0.0000	0.0018	1.30	14.7	0.0	0.035	0.000	100.1	91.22	0.11	0.16	0.00000	0.00	#####	0.12	0.0055
414-01H	3.2	1158.5240	0.3914	48.3438	0.0580	0.6405	0.0025	1.8722	0.0066	0.0000	0.0019	1.07	12.1	0.0	0.076	0.000	100.1	91.22	0.13	0.18	0.00000	0.00	#####	0.14	0.0039
SN08PV11 - amphibole - irradiation:DT-6b																									
415-01B	1.0	122.8084	0.0893	4.8862	0.0079	0.0723	0.0013	0.4397	0.0038	0.0475	0.0014	0.11	2.9	0.3	0.176	0.002	88.6	84.84	0.35	0.37	0.00039	2.92	#####	0.19	0.0627
415-01C	1.8	347.3326	0.1602	14.0517	0.0141	0.1972	0.0019	13.8232	0.0317	0.0208	0.0014	0.31	8.3	18.4	1.928	0.005	98.6	92.66	0.16	0.20	0.00005	8.30	#####	0.13	0.0229
415-01D	2.1	335.4158	0.1601	13.5178	0.0130	0.1963	0.0016	32.2501	0.0494	0.0228	0.0013	0.30	8.0	39.1	4.676	0.009	98.8	93.29	0.16	0.20	0.00004	9.29	#####	0.12	0.0205
415-01E	2.4	423.7878	0.2901	17.0034	0.0220	0.2535	0.0019	48.0042	0.0756	0.0270	0.0014	0.38	10.1	49.2	5.534	0.011	99.0	93.97	0.17	0.21	0.00003	10.07	#####	0.16	0.0188
415-01F	2.7	457.1479	0.2501	18.3905	0.0240	0.2640	0.0023	52.2172	0.1164	0.0299	0.0017	0.41	10.9	48.4	5.565	0.015	99.0	93.69	0.17	0.21	0.00003	10.81	#####	0.16	0.0171
415-01G	3.0	538.1142	0.2301	21.5095	0.0330	0.3192	0.0020	66.6872	0.0990	0.0368	0.0016	0.48	12.7	50.1	6.077	0.013	99.0	94.29	0.18	0.22	0.00003	8.57	#####	0.17	0.0207
415-01H	3.5	585.0322	0.2401	23.4410	0.0360	0.3404	0.0022	76.9550	0.1923	0.0329	0.0016	0.52	13.9	64.8	6.435	0.019	99.4	94.47	0.18	0.22	0.00002	13.60	#####	0.17	0.0130
415-01I	4.0	889.7267	0.3301	35.9447	0.0520	0.5229	0.0028	83.9098	0.1895	0.0450	0.0016	0.80	21.3	51.6	4.575	0.012	99.3	93.53	0.16	0.20	0.00002	7.22	#####	0.16	0.0247
415-01J	4.5	491.9006	0.2801	20.0795	0.0220	0.2796	0.0020	35.8657	0.0526	0.0344	0.0015	0.45	11.9	28.9	3.501	0.007	98.5	91.88	0.15	0.19	0.00005	6.05	#####	0.14	0.0314

Supplemental Table SP2.1. $^{40}Ar/^{39}Ar$ Isotopic Data (continued)

		Relative Isotopic Abundances										Derived Results									Inverse Isochron Data				
Lab ID#	Watts	^{40}Ar ±1σ		^{39}Ar ±1σ		^{38}Ar ±1σ		^{37}Ar ±1σ		^{36}Ar ±1σ		^{39}Ar Mol × 10^{-14}	^{39}Ar % of total	$\%(^{36}Ar)_{Ca}$	Ca/K ±1σ		$\%^{40}Ar^{*}$	Age (Ma) ±1σ		w/±J ±1σ	$^{36}Ar/^{40}Ar$ ±%1σ		$^{39}Ar/^{40}Ar$ ±%1σ		$^{36}Ar/^{39}Ar$ Er. Corr.
SN08RM01 - biotite - irradiation:DT-6b																									
416-01B	0.9	69.6819	0.1116	2.8114	0.0101	0.0396	0.0014	0.1805	0.0033	0.0045	0.0018	0.06	1.9	1.1	0.126	0.002	98.1	92.45	0.79	0.80	0.00006	40.69	#####	0.40	0.0042
416-01C	1.2	241.5461	0.2109	9.9178	0.0231	0.1367	0.0018	0.3248	0.0040	0.0000	0.0020	0.22	6.8	0.0	0.064	0.001	100.6	93.10	0.32	0.34	0.00000	0.00	#####	0.26	0.0041
416-01D	1.6	332.3463	0.2906	13.6393	0.0251	0.1875	0.0023	0.9687	0.0058	0.0000	0.0020	0.30	9.3	0.0	0.139	0.001	100.0	92.65	0.25	0.28	0.00000	0.00	#####	0.21	0.0004
416-01E	2.2	531.6889	0.3106	21.6259	0.0350	0.3094	0.0022	17.4964	0.0370	0.0099	0.0022	0.48	14.8	48.9	1.586	0.004	99.7	93.22	0.20	0.24	0.00001	43.15	#####	0.18	0.0041
416-01F	2.8	746.5138	0.3206	29.9715	0.0470	0.4564	0.0024	77.2006	0.1214	0.0295	0.0016	0.66	20.5	72.6	5.049	0.011	99.7	94.48	0.17	0.21	0.00001	19.98	#####	0.18	0.0088
416-01G	3.2	707.9849	0.5204	28.4095	0.0530	0.4431	0.0026	84.1375	0.1427	0.0367	0.0019	0.63	19.4	63.5	5.805	0.015	99.4	94.34	0.21	0.24	0.00002	14.14	#####	0.21	0.0125
416-01H	3.8	679.8243	0.3505	27.6624	0.0480	0.3962	0.0023	38.0779	0.0767	0.0178	0.0015	0.61	18.9	59.4	2.698	0.007	99.7	93.19	0.19	0.22	0.00001	21.09	#####	0.19	0.0083
416-01I	4.3	199.6605	0.2109	8.0560	0.0181	0.1112	0.0016	17.6361	0.0318	0.0019	0.0018	0.18	5.5	262.1	4.291	0.013	100.4	94.71	0.34	0.36	0.00000	0.00	#####	0.26	0.0030
416-01J	4.7	98.9217	0.1314	3.9768	0.0098	0.0618	0.0015	16.2489	0.0292	0.0000	0.0019	0.09	2.7	0.0	8.008	0.025	101.7	96.28	0.59	0.60	0.00000	0.00	#####	0.29	0.0054
SN08RM01 - amphibole - irradiation:DT-6b																									
417-01C	1.5	7.6340	0.0141	0.2717	0.0022	0.0000	0.0011	0.1443	0.0036	0.0000	0.0008	0.01	1.0	0.0	1.041	0.027	107.5	114.12	3.37	3.37	0.00000	0.00	#####	0.84	0.0025
417-01D	1.8	7.7543	0.0150	0.2878	0.0024	0.0067	0.0011	0.2635	0.0055	0.0035	0.0007	0.01	1.0	2.1	1.794	0.041	87.0	89.23	2.84	2.84	0.00044	21.02	#####	0.86	0.0051
417-01E	2.1	15.0353	0.0150	0.5674	0.0032	0.0058	0.0010	1.7101	0.0055	0.0001	0.0007	0.01	2.0	648.7	5.908	0.039	100.8	101.48	1.44	1.45	0.00000	0.00	#####	0.58	0.0006
417-01F	2.4	60.3388	0.0585	2.3086	0.0060	0.0439	0.0011	18.5654	0.0329	0.0134	0.0007	0.05	8.1	38.4	15.762	0.050	96.0	95.78	0.43	0.45	0.00014	8.63	#####	0.29	0.0192
417-01G	2.7	172.0590	0.1901	6.5524	0.0121	0.1148	0.0016	63.2035	0.0686	0.0315	0.0009	0.15	22.9	55.6	18.906	0.041	97.6	97.92	0.26	0.29	0.00008	6.19	#####	0.23	0.0310
417-01H	3.0	265.0093	0.3601	9.9791	0.0210	0.1734	0.0014	86.3056	0.2149	0.0524	0.0009	0.22	34.9	45.6	16.951	0.056	96.8	98.16	0.28	0.30	0.00011	3.23	#####	0.26	0.0610
417-01I	3.5	50.8735	0.0547	1.9781	0.0048	0.0334	0.0013	11.7850	0.0284	0.0053	0.0007	0.04	6.9	61.7	11.677	0.040	98.8	96.88	0.49	0.51	0.00004	36.97	#####	0.28	0.0047
417-01J	4.0	51.5047	0.0567	2.0135	0.0088	0.0382	0.0011	13.7809	0.0261	0.0074	0.0008	0.04	7.0	51.8	13.415	0.065	98.0	95.62	0.60	0.61	0.00007	21.56	#####	0.46	0.0061
417-01K	4.5	60.5124	0.0577	2.3359	0.0047	0.0381	0.0012	17.2975	0.0267	0.0070	0.0008	0.05	8.2	68.7	14.514	0.037	98.9	97.77	0.42	0.44	0.00004	35.04	#####	0.23	0.0052
417-01L	5.0	37.3449	0.0459	1.4475	0.0050	0.0264	0.0011	12.2107	0.0424	0.0061	0.0007	0.03	5.1	55.3	16.534	0.082	97.8	96.40	0.66	0.67	0.00007	26.70	#####	0.38	0.0058
417-01M	5.5	22.0936	0.0429	0.8467	0.0041	0.0156	0.0011	8.0809	0.0514	0.0039	0.0007	0.02	3.0	56.9	18.706	0.151	97.7	97.44	1.07	1.08	0.00008	42.55	#####	0.54	0.0038
SN08RM04 - biotite - irradiation:DT-6b																									
405-01B	9.0	826.0523	0.3603	35.2256	0.0510	0.4904	0.0024	0.1511	0.0024	0.0634	0.0011	0.78	5.1	0.1	0.008	0.000	97.7	87.24	0.15	0.19	0.00008	1.75	#####	0.16	0.1029
405-01C	1.2	1916.5340	0.5702	78.8176	0.0780	1.0794	0.0028	0.2385	0.0028	0.0629	0.0014	1.75	11.5	0.1	0.006	0.000	99.0	91.55	0.11	0.16	0.00003	2.18	#####	0.12	0.0859
405-01D	1.6	2112.3450	0.9001	86.2694	0.0920	1.1658	0.0029	0.3092	0.0035	0.0568	0.0017	1.91	12.6	0.2	0.007	0.000	99.2	92.33	0.12	0.17	0.00003	3.05	#####	0.13	0.0616
405-01E	2.0	2434.2120	0.7601	98.8392	0.0930	1.3477	0.0036	0.4745	0.0039	0.0517	0.0015	2.19	14.4	0.3	0.009	0.000	99.4	93.01	0.11	0.16	0.00002	2.82	#####	0.12	0.0666
405-01F	2.4	2563.1920	0.8701	103.5712	0.0800	1.4036	0.0040	1.0437	0.0046	0.0506	0.0015	2.30	15.1	0.6	0.020	0.000	99.4	93.50	0.10	0.16	0.00002	3.07	#####	0.10	0.0623
405-01G	2.8	2136.1330	0.7201	86.4601	0.0840	1.1696	0.0031	2.4475	0.0063	0.0369	0.0016	1.92	12.6	1.8	0.055	0.000	99.5	93.41	0.11	0.17	0.00002	4.50	#####	0.12	0.0417
405-01H	3.2	1727.6100	0.5002	69.5287	0.0740	0.9481	0.0026	4.8384	0.0093	0.0437	0.0014	1.54	10.1	3.1	0.136	0.000	99.3	93.73	0.12	0.17	0.00002	3.22	#####	0.13	0.0576
405-01I	3.6	1457.0400	0.5502	58.6061	0.0770	0.7948	0.0032	5.0092	0.0101	0.0481	0.0015	1.30	8.5	2.9	0.168	0.000	99.1	93.58	0.14	0.19	0.00003	3.30	#####	0.15	0.0550
405-01J	4.0	1014.4360	0.3103	40.7445	0.0520	0.5497	0.0021	4.4098	0.0088	0.0275	0.0012	0.90	5.9	4.4	0.212	0.001	99.2	93.88	0.14	0.19	0.00003	4.46	#####	0.15	0.0406
405-01K	4.5	727.1155	0.2404	29.2825	0.0500	0.3990	0.0018	5.1406	0.0099	0.0181	0.0011	0.65	4.3	7.9	0.344	0.001	99.3	93.72	0.18	0.22	0.00002	6.79	#####	0.19	0.0253
SN08RM04 - amphibole - irradiation:DT-6b																									
411-01G	2.4	33.8784	0.0499	1.2785	0.0027	0.0206	0.0010	4.0626	0.0080	0.0088	0.0007	0.03	1.8	12.8	6.228	0.018	93.3	94.16	0.67	0.68	0.00023	9.42	#####	0.27	0.0216
411-01H	2.7	34.0248	0.0558	1.2577	0.0028	0.0189	0.0010	3.9430	0.0094	0.0100	0.0008	0.03	1.8	10.9	6.145	0.020	92.2	94.98	0.75	0.76	0.00026	8.90	#####	0.29	0.0236
411-01I	3.0	34.5922	0.0450	1.3163	0.0028	0.0220	0.0010	4.5478	0.0107	0.0041	0.0008	0.03	1.9	30.9	6.772	0.022	97.6	97.58	0.68	0.70	0.00008	27.14	#####	0.26	0.0071
411-01J	3.5	83.3465	0.0470	3.1279	0.0039	0.0565	0.0011	16.0403	0.0143	0.0163	0.0008	0.07	4.5	27.2	10.051	0.016	95.8	97.23	0.30	0.33	0.00014	6.39	#####	0.15	0.0293
411-01K	4.0	132.8033	0.0548	5.0287	0.0078	0.0956	0.0012	28.8579	0.0306	0.0208	0.0008	0.11	7.2	38.4	11.248	0.022	97.2	97.76	0.25	0.28	0.00010	6.59	#####	0.17	0.0268
411-01L	4.5	177.4908	0.1104	6.6793	0.0096	0.1382	0.0014	41.3320	0.0333	0.0275	0.0009	0.15	9.6	41.6	12.129	0.021	97.3	98.56	0.22	0.25	0.00009	5.35	#####	0.17	0.0344
411-01M	5.0	218.2436	0.1004	8.2537	0.0100	0.1632	0.0015	51.9777	0.0833	0.0324	0.0009	0.18	11.8	44.5	12.343	0.025	97.6	98.33	0.19	0.23	0.00008	5.06	#####	0.14	0.0366
411-01N	5.5	253.2312	0.1603	9.5387	0.0110	0.2051	0.0015	61.4530	0.0556	0.0353	0.0015	0.21	13.7	48.2	12.627	0.019	97.9	99.01	0.22	0.26	0.00007	8.16	#####	0.15	0.0234
411-01O	6.0	297.0999	0.1714	11.2320	0.0160	0.2399	0.0017	74.8120	0.1268	0.0411	0.0009	0.25	16.1	50.4	13.055	0.029	98.0	98.78	0.19	0.23	0.00007	4.29	#####	0.17	0.0427
411-01P	6.5	327.5319	0.2709	12.2774	0.0190	0.2754	0.0017	85.4468	0.1100	0.0514	0.0015	0.27	17.6	46.0	13.641	0.028	97.5	99.15	0.23	0.26	0.00008	5.32	#####	0.19	0.0353
411-01Q	6.5	256.8748	0.1414	9.7748	0.0131	0.2025	0.0015	65.9302	0.0742	0.0289	0.0009	0.22	14.0	63.1	13.220	0.024	98.8	98.94	0.19	0.23	0.00004	8.70	#####	0.16	0.0212

Supplemental Table SP2.1. $^{40}Ar/^{39}Ar$ Isotopic Data (continued)

		Relative Isotopic Abundances										Derived Results									Inverse Isochron Data				
Lab ID#	Watts	^{40}Ar	±1σ	^{39}Ar	±1σ	^{38}Ar	±1σ	^{37}Ar	±1σ	^{36}Ar	±1σ	^{39}Ar Mol × 10^{-14}	^{39}Ar % of total	%($^{36}Ar)_{Ca}$	Ca/K	±1σ	%$^{40}Ar^{*}$	Age (Ma)	±1σ	w/±J ±1σ	$^{36}Ar/^{40}Ar$	±%1σ	$^{39}Ar/^{40}Ar$	±%1σ	$^{36}Ar/^{39}Ar$ Er. Corr.
SN08RM10 - biotite - irradiation:DT-6b																									
403-01C	0.9	490.1685	0.2301	19.7388	0.0210	0.2889	0.0016	0.4253	0.0035	0.0813	0.0015	0.44	2.8	0.1	0.042	0.000	95.1	89.83	0.15	0.19	0.00017	1.82	#####	0.13	0.1036
403-01D	1.2	941.3022	0.4500	38.4968	0.0560	0.5311	0.0026	0.5576	0.0040	0.0508	0.0017	0.85	5.4	0.3	0.028	0.000	98.4	91.49	0.16	0.20	0.00005	3.28	#####	0.17	0.0550
403-01E	1.5	1441.3640	0.4700	59.4505	0.0590	0.8193	0.0029	0.8053	0.0042	0.0395	0.0018	1.32	8.4	0.6	0.027	0.000	99.2	91.44	0.11	0.17	0.00003	4.47	#####	0.12	0.0419
403-01F	1.8	1731.6280	0.5500	70.8716	0.0650	0.9668	0.0033	1.0640	0.0047	0.0439	0.0019	1.57	10.0	0.7	0.029	0.000	99.3	92.19	0.11	0.16	0.00003	4.26	#####	0.12	0.0443
403-01G	2.1	1658.0310	0.5600	68.5043	0.0730	0.9429	0.0029	1.1244	0.0042	0.0435	0.0019	1.52	9.7	0.7	0.032	0.000	99.2	91.32	0.12	0.17	0.00003	4.29	#####	0.13	0.0434
403-01H	2.4	1644.9750	0.5400	67.5433	0.0780	0.9257	0.0027	1.3078	0.0056	0.0404	0.0017	1.50	9.5	0.9	0.038	0.000	99.3	91.92	0.13	0.17	0.00002	4.15	#####	0.14	0.0444
403-01I	2.7	1839.3300	0.6300	75.2964	0.0700	1.0347	0.0034	1.9016	0.0054	0.0403	0.0019	1.67	10.6	1.3	0.049	0.000	99.4	92.26	0.11	0.16	0.00002	4.67	#####	0.12	0.0405
403-01J	3.0	1835.0070	0.5200	75.0144	0.0780	1.0369	0.0031	3.1281	0.0079	0.0486	0.0020	1.66	10.6	1.8	0.082	0.000	99.2	92.27	0.12	0.17	0.00003	4.09	#####	0.12	0.0454
403-01K	3.3	1782.4360	0.4900	73.2414	0.0730	0.9936	0.0031	5.5989	0.0094	0.0358	0.0018	1.62	10.3	4.3	0.150	0.000	99.4	91.99	0.11	0.17	0.00002	5.13	#####	0.12	0.0364
403-01L	3.6	1555.7990	0.4700	63.6235	0.0640	0.8654	0.0025	8.5610	0.0111	0.0318	0.0018	1.41	9.0	7.5	0.264	0.000	99.4	92.44	0.11	0.17	0.00002	5.97	#####	0.12	0.0313
403-01M	3.9	1193.6620	0.3201	48.3715	0.0660	0.6657	0.0022	11.7381	0.0148	0.0243	0.0023	1.07	6.8	13.4	0.476	0.001	99.5	93.30	0.15	0.19	0.00002	11.12	#####	0.15	0.0161
403-01N	4.2	736.8772	0.3001	30.0174	0.0470	0.4147	0.0019	10.5543	0.0146	0.0142	0.0015	0.67	4.2	20.6	0.689	0.001	99.5	92.90	0.17	0.21	0.00002	12.99	#####	0.17	0.0136
403-01O	4.5	443.1944	0.1601	18.0041	0.0260	0.2571	0.0017	8.5938	0.0116	0.0107	0.0013	0.40	2.5	22.3	0.936	0.002	99.4	93.06	0.17	0.21	0.00002	15.39	#####	0.16	0.0116
SN08RM10 - amphibole - irradiation:DT-6b																									
409-01B	0.9	101.1159	0.1432	2.7528	0.0101	0.0612	0.0015	0.9078	0.0057	0.1384	0.0026	0.06	1.4	0.2	0.646	0.005	59.6	83.47	1.11	1.12	0.00137	1.90	#####	0.40	0.0840
409-01C	1.2	145.6038	0.1530	4.6338	0.0111	0.0863	0.0017	1.0326	0.0052	0.1181	0.0028	0.10	2.4	0.2	0.437	0.002	76.1	90.93	0.71	0.72	0.00081	2.38	#####	0.27	0.0736
409-01D	1.5	278.9971	0.2617	8.7253	0.0181	0.1660	0.0017	2.3121	0.0078	0.2342	0.0032	0.19	4.6	0.3	0.519	0.002	75.3	91.52	0.47	0.49	0.00084	1.38	#####	0.24	0.1294
409-01E	1.8	328.3005	0.2419	11.8795	0.0261	0.1919	0.0020	6.3895	0.0139	0.1117	0.0025	0.26	6.2	1.6	1.054	0.003	90.1	94.62	0.33	0.35	0.00034	2.28	#####	0.24	0.0740
409-01F	2.1	334.3684	0.2320	12.5932	0.0221	0.2153	0.0020	26.4792	0.0378	0.0560	0.0024	0.28	6.6	13.1	4.121	0.009	95.7	96.61	0.28	0.31	0.00015	4.94	#####	0.20	0.0362
409-01G	2.4	449.4797	0.4410	17.1995	0.0341	0.3137	0.0028	69.9601	0.2319	0.0686	0.0026	0.38	9.0	28.3	7.972	0.031	96.8	96.29	0.28	0.30	0.00011	5.28	#####	0.23	0.0347
409-01H	2.7	537.3009	0.3214	20.3706	0.0361	0.3707	0.0023	72.6152	0.1430	0.0791	0.0025	0.45	10.7	25.4	6.987	0.019	96.8	97.12	0.23	0.27	0.00011	4.24	#####	0.20	0.0414
409-01I	3.0	711.9700	0.5009	27.7680	0.0710	0.4754	0.0029	91.1014	0.1405	0.0782	0.0032	0.62	14.5	32.3	6.430	0.020	97.8	95.45	0.29	0.31	0.00007	6.00	#####	0.28	0.0264
409-01J	3.5	920.2546	0.5109	36.5529	0.0810	0.6030	0.0031	99.7865	0.1892	0.0874	0.0031	0.81	19.1	31.6	5.351	0.016	98.1	93.99	0.24	0.27	0.00006	5.16	#####	0.24	0.0316
409-01K	4.0	938.6934	0.7606	37.6894	0.0971	0.5734	0.0031	73.7616	0.1569	0.0519	0.0030	0.84	19.7	39.4	3.836	0.013	99.0	93.82	0.27	0.30	0.00003	9.48	#####	0.28	0.0170
409-01L	4.5	142.0119	0.2022	5.6112	0.0171	0.0900	0.0016	17.0877	0.0407	0.0000	0.0021	0.12	2.9	0.0	5.969	0.023	102.4	98.58	0.53	0.54	0.00000	0.00	#####	0.35	0.0097
409-01M	5.0	60.3830	0.0958	2.3953	0.0096	0.0392	0.0015	6.7176	0.0153	0.0000	0.0018	0.05	1.3	0.0	5.497	0.026	107.2	102.65	0.94	0.95	0.00000	0.00	#####	0.44	0.0129
409-01N	5.5	69.7939	0.0949	2.7901	0.0101	0.0445	0.0012	7.4783	0.0180	0.0000	0.0018	0.06	1.5	0.0	5.253	0.023	104.2	99.07	0.81	0.82	0.00000	0.00	#####	0.40	0.0085

Supplemental Table SP2.2. Irradiation Data and Nucleogenic production ratios

Irradiation package	Irr. Time (hours)	*J* (X 10^{-3}) ± 1σ		Nucleogenic production ratios										
				$(^{36}Ar/^{37}Ar)_{Ca}$ (x10^{-4}) ±1σ		$(^{39}Ar/^{37}Ar)_{Ca}$ (x10^{-4}) ±1σ		$(^{38}Ar/^{37}Ar)_{Ca}$ (x10^{-4}) ±1σ		$(^{40}Ar/^{39}Ar)_{K}$ (x10^{-4}) ±1σ		$(^{38}Ar/^{39}Ar)_{K}$ (x10^{-2}) ±1σ		$(^{36}Ar/^{38}Ar)_{Cl}$ (x10^{-2})	$^{37}Ar/^{39}Ar$ to Ca/K
DT-2	20	3.602	0.007	2.599	0.034	2.818	0.392	0.196	0.0082	29.938	25.967	1.29	0.03	3.2	1.96
DT-3	20	4.16	0.013	2.599	0.034	2.818	0.392	0.196	0.0082	29.938	25.967	1.29	0.03	3.2	1.96
DT-6b	10	2.162	0.003	2.769	0.0229	6.889	0.0387	0.196	0.0082	29.938	25.967	1.29	0.03	3.2	1.96
DT-6c	10	2.146	0.014	2.769	0.0229	6.889	0.0387	0.196	0.0082	29.938	25.967	1.29	0.03	3.2	1.96
DT-14	30	6.516	0.008	2.599	0.034	2.818	0.392	0.196	0.0082	29.938	25.967	1.29	0.03	3.2	1.96

Samples were irradiated in the central thimble position of the USGS TRIGA reactor in Denver, Colorado while being rotated at 1 rpm. Sanidine from the Fish Canyon Tuff was used as the neutron fluence monitor with a reference age of 28.201 Ma (Kuiper et al, 2008).

Isotopic constants and decay rates:

$\lambda(^{40}K)/yr = 5.81 \pm 0.17 \times 10^{-11}$ $\lambda(^{37}Ar)/d = 1.975 \times 10^{-2}$ $\lambda(^{36}Cl)/d = 6.308 \times 10^{-9}$ $(^{40}Ar/^{38}Ar)_{ATM} = 1575 \pm 2$

$\lambda(^{40}K_{\beta-})/yr = 4.962 \pm 0.086 \times 10^{-10}$ $\lambda(^{39}Ar)/d = 7.068 \times 10^{-6}$ $(^{40}Ar/^{36}Ar)_{ATM} = 295.5 \pm 0.5$ $^{40}K/Ar_{Total} = 0.01167$

Supplemental Table 2.3. U-Pb Analytical Data

				Isotopic ratios						Corrected ages (Ma)					
Spot Name	U (ppm)	Th (ppm)	Th/U	207Pb/ 206Pb	± (%)	207Pb/ 235U	± (%)	206Pb/ 238U	± (%)	206Pb 238U	± (1σ)	207Pb 206Pb	± (1σ)	Best Age (Ma)	± (1σ)
MH01-12.1	228	139	0.61	.0491	4.0	0.11	4.1	.0159	1.0	101.8	1.1	150	94	101.8	1.1
MH01-5.1	128	88	0.69	.0566	9.9	0.13	10.0	.0161	1.5	102.0	1.4	478	219	102.0	1.4
MH01-7.1	233	182	0.78	.0501	3.8	0.11	4.0	.0161	1.0	102.9	1.1	197	89	102.9	1.1
MH01-8.1	229	189	0.82	.0416	11.1	0.09	11.1	.0160	1.1	103.4	1.1	-252	281	103.4	1.1
MH01-4.1	154	100	0.65	.0322	18.2	0.07	18.3	.0161	1.4	105.1	1.3	-945	533	105.1	1.3
MH01-10.1	339	166	0.49	.0485	3.1	0.11	3.2	.0165	0.8	105.1	0.9	122	74	105.1	0.9
MH01-11.1	435	205	0.47	.0433	5.7	0.10	5.7	.0164	0.8	105.6	0.8	-150	141	105.6	0.8
MH01-2.1	148	82	0.55	.0457	8.6	0.10	8.7	.0165	1.3	105.9	1.4	-17	208	105.9	1.4
MH01-9.1	372	179	0.48	.0494	3.3	0.11	3.4	.0166	0.8	106.2	0.8	166	78	106.2	0.8
MH01-6.1	489	208	0.43	.0491	2.6	0.11	2.7	.0167	0.7	106.6	0.8	152	61	106.6	0.8
MH01-3.1	327	161	0.49	.0500	4.3	0.12	4.4	.0167	0.9	106.7	0.9	195	101	106.7	0.9
MH01-1.1	395	200	0.51	.0467	3.4	0.11	3.5	.0168	0.8	107.4	0.8	35	82	107.4	0.8
YV07-13.1	503	246	0.49	.0436	7.2	0.08	7.2	.0137	0.8	88.4	0.6	-132	178	88.4	0.6
YV07-3.1	502	226	0.45	.0454	5.3	0.09	5.4	.0140	0.8	89.7	0.7	-36	129	89.7	0.7
YV07-5.1	549	244	0.44	.0435	5.7	0.08	5.8	.0140	0.7	90.3	0.6	-141	142	90.3	0.6
YV07-6.1	620	216	0.35	.0439	4.7	0.09	4.8	.0140	0.7	90.4	0.6	-117	117	90.4	0.6
YV07-8.1	591	335	0.57	.0453	3.2	0.09	3.3	.0141	0.7	90.6	0.6	-37	79	90.6	0.6
YV07-4.1	752	363	0.48	.0463	3.5	0.09	3.6	.0141	0.6	90.7	0.5	12	84	90.7	0.5
YV07-12.1	336	116	0.35	.0465	5.0	0.09	5.1	.0142	0.9	90.9	0.8	23	121	90.9	0.8
YV07-1.1	617	254	0.41	.0467	4.6	0.09	4.6	.0142	0.7	91.2	0.6	35	110	91.2	0.6
YV07-2.1	562	247	0.44	.0478	3.1	0.09	3.2	.0143	0.7	91.7	0.6	89	73	91.7	0.6
YV07-16.1	370	170	0.46	.0446	5.5	0.09	5.6	.0143	0.9	91.7	0.8	-78	135	91.7	0.8
YV07-7.1	539	178	0.33	.0490	4.1	0.10	4.2	.0144	0.7	92.2	0.7	146	96	92.2	0.7
YV07-11.1	457	201	0.44	.0514	3.9	0.10	4.0	.0147	0.8	93.7	0.7	260	89	93.7	0.7
YV07-9.1	844	338	0.40	.0463	3.3	0.09	3.4	.0146	0.6	93.7	0.5	16	79	93.7	0.5
YV07-15.1	729	305	0.42	.0466	2.4	0.09	2.5	.0146	0.6	93.9	0.6	31	57	93.9	0.6
YV07-10.1	387	166	0.43	.0453	4.0	0.09	4.1	.0148	0.8	94.9	0.8	-40	97	94.9	0.8
YV07-14.1	951	456	0.48	.0462	2.3	0.09	2.4	.0149	0.5	95.5	0.5	6	56	95.5	0.5
MH05-9.1	163	154	0.95	.0505	7.3	0.11	7.4	.0163	1.3	104.1	1.3	219	169	104.1	1.3
MH05-3.1	145	130	0.89	.0572	10.7	0.13	10.8	.0166	1.5	104.8	1.4	500	236	104.8	1.4
MH05-2.1	156	150	0.96	.0550	7.8	0.13	7.9	.0165	1.3	104.9	1.3	413	174	104.9	1.3
MH05-4.1	167	160	0.96	.0364	20.3	0.08	20.3	.0162	1.5	105.1	1.3	-603	552	105.1	1.3
MH05-1.1	194	171	0.88	.0433	8.5	0.10	8.5	.0164	1.2	105.3	1.2	-148	210	105.3	1.2
MH05-6.1	193	187	0.97	.0562	7.6	0.13	7.7	.0167	1.2	105.5	1.2	462	168	105.5	1.2
MH05-10.1	164	153	0.93	.0416	9.3	0.09	9.3	.0165	1.3	106.6	1.3	-248	234	106.6	1.3
MH05-8.1	159	143	0.90	.0463	4.8	0.11	5.0	.0167	1.2	106.8	1.4	11	117	106.8	1.4
MH05-7.1	151	138	0.92	.0334	18.2	0.08	18.2	.0166	1.4	108.4	1.4	-838	520	108.4	1.4
MH05-5.1	207	193	0.93	.0456	5.5	0.11	5.6	.0169	1.1	108.5	1.2	-21	132	108.5	1.2

Supplemental Table 2.3. U-Pb Analytical Data (continued)

				Isotopic ratios						Corrected ages (Ma)					
Spot Name	U (ppm)	Th (ppm)	Th/U	207Pb/ 206Pb	± (%)	207Pb/ 235U	± (%)	206Pb/ 238U	± (%)	206Pb 238U	± (1σ)	207Pb 206Pb	± (1σ)	Best Age (Ma)	± (1σ)
MH11-18.1	84	52	0.62	.0433	9.5	0.12	9.7	.0203	1.8	130.3	2.4	-149	236	130.3	2.4
MH11-20.1	186	79	0.43	.0470	6.0	0.13	6.1	.0204	1.1	130.7	1.4	48	143	130.7	1.4
MH11-3.1	100	62	0.62	.0421	13.3	0.12	13.3	.0204	1.6	131.5	1.9	-222	333	131.5	1.9
MH11-2.1	150	61	0.41	.0614	12.0	0.18	12.1	.0210	1.4	131.6	1.7	654	258	131.6	1.7
MH11-9.1	87	47	0.53	.0411	11.0	0.12	11.1	.0205	1.6	132.4	2.1	-282	280	132.4	2.1
MH11-5.1	157	72	0.46	.0407	8.6	0.12	8.7	.0205	1.2	132.4	1.6	-306	219	132.4	1.6
MH11-13.1	83	55	0.65	.0538	5.5	0.16	5.7	.0210	1.6	133.1	2.1	361	124	133.1	2.1
MH11-11.1	180	79	0.44	.0466	5.2	0.13	5.4	.0209	1.1	133.9	1.4	31	126	133.9	1.4
MH11-10.1	166	73	0.44	.0519	4.0	0.15	4.1	.0211	1.1	134.1	1.5	282	91	134.1	1.5
MH11-16.1	93	58	0.63	.0458	8.1	0.13	8.2	.0209	1.5	134.1	2.0	-15	195	134.1	2.0
MH11-7.1	161	67	0.41	.0565	9.6	0.17	9.7	.0212	1.3	134.2	1.5	471	213	134.2	1.5
MH11-6.1	90	57	0.64	.0387	12.8	0.11	12.9	.0208	1.6	134.2	2.0	-438	336	134.2	2.0
MH11-1.1	221	98	0.45	.0365	12.2	0.10	12.3	.0207	1.1	134.3	1.3	-596	332	134.3	1.3
MH11-17.1	214	112	0.52	.0458	6.0	0.13	6.0	.0210	1.0	134.4	1.3	-14	144	134.4	1.3
MH11-4.1	97	59	0.60	.0248	38.9	0.07	38.9	.0205	1.8	134.7	2.0			134.7	2.0
MH11-12.1	85	54	0.64	.0390	16.3	0.11	16.4	.0209	1.7	134.9	2.1	-419	426	134.9	2.1
MH11-8.1	175	100	0.57	.0485	4.1	0.14	4.2	.0212	1.1	135.3	1.5	125	96	135.3	1.5
MH11-14.1	172	68	0.39	.0376	12.6	0.11	12.6	.0210	1.2	135.5	1.5	-511	335	135.5	1.5
MH11-15.1	191	100	0.53	.0477	4.8	0.14	5.0	.0214	1.2	136.5	1.7	84	114	136.5	1.7
MH11-19.1	129	55	0.43	.0426	6.7	0.13	6.8	.0213	1.3	137.1	1.7	-190	167	137.1	1.7
YV03-13.1	140	90	0.64	.0391	22.8	0.09	22.9	.0169	2.0	109.0	1.9	-409	596	109.0	1.9
YV03-1.1	92	72	0.78	.0478	9.1	0.11	9.3	.0171	2.0	109.1	2.1	87	216	109.1	2.1
YV03-2.1	266	146	0.55	.0431	5.9	0.10	6.1	.0171	1.5	109.8	1.6	-164	147	109.8	1.6
YV03-11.1	360	185	0.51	.0462	4.6	0.11	4.8	.0172	1.4	110.3	1.5	11	111	110.3	1.5
YV03-15.1	511	296	0.58	.0485	2.8	0.12	3.1	.0173	1.3	110.6	1.5	126	66	110.6	1.5
YV03-3.1	358	170	0.47	.0478	4.5	0.11	4.8	.0174	1.4	110.9	1.6	89	108	110.9	1.6
YV03-8.1	222	162	0.73	.0461	3.9	0.11	4.2	.0174	1.5	111.5	1.7	2	95	111.5	1.7
YV03-5.1	229	117	0.51	.0468	4.6	0.11	4.8	.0174	1.5	111.5	1.7	40	110	111.5	1.7
YV03-4.1	345	216	0.63	.0467	3.1	0.11	3.4	.0174	1.4	111.7	1.6	33	74	111.7	1.6
YV03-14.1	188	94	0.50	.0476	4.3	0.11	4.6	.0175	1.6	111.7	1.8	81	102	111.7	1.8
YV03-12.1	308	154	0.50	.0487	3.6	0.12	3.8	.0175	1.4	111.7	1.6	133	84	111.7	1.6
YV03-6.1	141	125	0.88	.0429	9.6	0.10	9.7	.0174	1.8	112.2	2.0	-175	239	112.2	2.0
YV03-9.1	273	125	0.46	.0419	6.6	0.10	6.7	.0174	1.5	112.2	1.6	-233	166	112.2	1.6
YV03-10.1	448	296	0.66	.0505	2.5	0.12	2.8	.0178	1.3	113.2	1.5	218	58	113.2	1.5
YV03-7.1	224	81	0.36	.0440	7.0	0.11	7.2	.0183	1.6	117.2	1.8	-109	172	117.2	1.8
AR11-13.1	120	45	0.37	.0403	12.4	0.11	12.5	.0203	1.8	130.8	2.2	-332	318	130.8	2.2
AR11-12.1	124	40	0.32	.0503	4.5	0.15	4.8	.0209	1.7	133.1	2.3	209	103	133.1	2.3
AR11-4.1	103	57	0.55	.0512	7.4	0.15	7.7	.0211	1.8	134.3	2.5	248	171	134.3	2.5
AR11-14.1	132	34	0.26	.0486	5.6	0.14	5.8	.0211	1.6	134.7	2.2	126	132	134.7	2.2
AR11-9.1	163	97	0.60	.0513	6.0	0.15	6.2	.0212	1.6	134.7	2.1	255	137	134.7	2.1
AR11-16.1	119	66	0.55	.0341	16.4	0.10	16.5	.0210	1.8	136.5	2.3	-779	464	136.5	2.3
AR11-3.1	106	41	0.38	.0458	14.9	0.13	15.1	.0213	2.0	136.6	2.5	-12	361	136.6	2.5
AR11-8.1	107	58	0.54	.0498	4.9	0.15	5.2	.0215	1.8	136.8	2.5	187	114	136.8	2.5
AR11-15.1	351	282	0.80	.0478	4.8	0.14	5.0	.0215	1.4	137.0	1.9	90	114	137.0	1.9
AR11-5.1	105	58	0.56	.0424	13.0	0.12	13.2	.0213	1.9	137.0	2.5	-201	326	137.0	2.5
AR11-7.1	151	62	0.41	.0452	6.4	0.13	6.6	.0215	1.7	137.6	2.3	-43	156	137.6	2.3
AR11-1.1	169	97	0.57	.0371	11.6	0.11	11.7	.0213	1.6	137.7	2.2	-549	311	137.7	2.2
AR11-2.1	126	70	0.55	.0459	9.6	0.14	9.8	.0216	1.8	137.9	2.4	-9	233	137.9	2.4
AR11-6.1	118	68	0.57	.0604	10.0	0.18	10.2	.0222	1.8	139.5	2.4	619	217	139.5	2.4
AR11-11.1	120	30	0.25	.0440	6.7	0.13	6.9	.0218	1.7	139.6	2.4	-113	164	139.6	2.4
AR11-10.1	173	102	0.59	.0493	4.5	0.15	4.8	.0224	1.5	142.5	2.2	164	106	142.5	2.2

Supplemental Table 2.3. U-Pb Analytical Data (continued)

				Isotopic ratios						Corrected ages (Ma)					
Spot Name	U (ppm)	Th (ppm)	Th/U	207Pb/ 206Pb	± (%)	207Pb/ 235U	± (%)	206Pb/ 238U	± (%)	206Pb 238U	± (1σ)	207Pb 206Pb	± (1σ)	Best Age (Ma)	± (1σ)
AR06-7.1	391	155	0.40	.0463	3.7	0.10	4.0	.0161	1.4	103.3	1.4	11	90	103.3	1.4
AR06-12.1	480	257	0.54	.0488	3.3	0.11	3.5	.0164	1.4	104.5	1.4	139	76	104.5	1.4
AR06-10.1	533	224	0.42	.0491	2.6	0.11	2.9	.0166	1.3	105.9	1.4	152	61	105.9	1.4
AR06-13.1	420	136	0.32	.0480	3.8	0.11	4.1	.0167	1.4	106.9	1.5	97	90	106.9	1.5
AR06-3.1	536	225	0.42	.0456	3.2	0.10	3.5	.0167	1.3	106.9	1.4	-25	77	106.9	1.4
AR06-16.1	715	381	0.53	.0495	2.1	0.11	2.4	.0168	1.3	107.1	1.4	171	49	107.1	1.4
AR06-9.1	397	149	0.37	.0455	5.8	0.10	6.0	.0167	1.4	107.2	1.5	-31	141	107.2	1.5
AR06-1.1	583	254	0.44	.0479	3.3	0.11	3.6	.0168	1.4	107.5	1.5	95	78	107.5	1.5
AR06-8.1	353	163	0.46	.0464	5.2	0.11	5.4	.0168	1.4	107.9	1.5	17	124	107.9	1.5
AR06-6.1	649	258	0.40	.0481	2.5	0.11	2.8	.0169	1.3	108.2	1.4	105	59	108.2	1.4
AR06-4.1	463	220	0.48	.0454	5.7	0.11	5.8	.0169	1.4	108.4	1.5	-36	138	108.4	1.5
AR06-15.1	646	246	0.38	.0472	2.4	0.11	2.7	.0170	1.3	108.7	1.4	61	57	108.7	1.4
AR06-14.1	712	319	0.45	.0479	2.2	0.11	2.6	.0170	1.3	108.9	1.4	96	53	108.9	1.4
AR06-2.1	944	575	0.61	.0488	1.8	0.12	2.2	.0171	1.3	109.5	1.4	140	43	109.5	1.4
AR06-5.1	423	176	0.42	.0474	3.4	0.11	3.7	.0172	1.5	109.9	1.6	69	81	109.9	1.6
AR06-11.1	855	526	0.62	.0486	2.4	0.12	2.7	.0173	1.3	110.4	1.4	131	56	110.4	1.4
AR04-11.1	383	139	0.36	.0553	4.6	0.12	4.9	.0163	1.4	103.3	1.4	426	104	103.3	1.4
AR04-5.1	559	225	0.40	.0510	2.7	0.12	3.0	.0165	1.3	105.3	1.4	242	61	105.3	1.4
AR04-7.1	496	270	0.54	.0473	3.4	0.11	3.6	.0165	1.3	105.6	1.4	63	81	105.6	1.4
AR04-3.1	572	267	0.47	.0457	3.0	0.10	3.3	.0165	1.3	105.7	1.4	-20	74	105.7	1.4
AR04-12.1	795	401	0.50	.0479	2.2	0.11	2.5	.0165	1.3	105.8	1.3	94	51	105.8	1.3
AR04-10.1	507	258	0.51	.0492	2.5	0.11	2.9	.0166	1.3	105.8	1.4	159	59	105.8	1.4
AR04-2.1	487	195	0.40	.0481	2.6	0.11	2.9	.0166	1.3	106.3	1.4	105	61	106.3	1.4
AR04-4.1	388	156	0.40	.0507	4.3	0.12	4.5	.0167	1.4	106.6	1.5	227	99	106.6	1.5
AR04-9.1	445	163	0.37	.0456	3.7	0.10	4.0	.0167	1.6	106.8	1.7	-23	89	106.8	1.7
AR04-8.1	397	116	0.29	.0432	4.7	0.10	4.9	.0170	1.5	109.1	1.6	-156	116	109.1	1.6
AR04-6.1	400	139	0.35	.0471	3.6	0.11	3.9	.0171	1.4	109.4	1.5	55	86	109.4	1.5
AR04-1.1	566	300	0.53	.0467	4.0	0.11	4.3	.0171	1.3	109.8	1.5	35	97	109.8	1.5
YH05-4.1	167	142	0.85	.0485	8.7	0.10	9.0	.0144	2.3	92.0	2.2	124	205	92.0	2.2
YH05-8.1	178	147	0.82	.0497	5.8	0.10	5.9	.0152	1.2	96.8	1.2	180	135	96.8	1.2
YH05-3.1	116	90	0.78	.0525	8.8	0.11	9.1	.0153	2.3	97.3	2.3	308	200	97.3	2.3
YH05-13.1	191	155	0.81	.0453	6.3	0.10	6.4	.0153	1.2	98.3	1.2	-40	153	98.3	1.2
YH05-10.1	189	155	0.82	.0440	6.9	0.09	7.0	.0154	1.2	98.9	1.1	-110	169	98.9	1.1
YH05-11.1	124	62	0.50	.0343	21.4	0.07	21.4	.0152	1.6	98.9	1.4	-766	602	98.9	1.4
YH05-9.1	118	93	0.79	.0420	14.3	0.09	14.3	.0154	1.6	99.3	1.5	-225	359	99.3	1.5
YH05-6.1	137	112	0.81	.0320	21.0	0.07	21.1	.0153	1.5	100.0	1.3	-961	618	100.0	1.3
YH05-5.1	127	102	0.80	.0401	9.7	0.09	9.8	.0155	1.4	100.1	1.4	-347	251	100.1	1.4
YH05-12.1	150	122	0.81	.0430	7.6	0.09	7.7	.0156	1.3	100.2	1.3	-170	190	100.2	1.3
YH05-7.1	110	85	0.77	.0392	15.4	0.08	15.5	.0156	1.6	100.8	1.6	-404	402	100.8	1.6
YH05-1.1	152	121	0.80	.0385	11.5	0.08	11.6	.0156	1.4	101.1	1.4	-453	304	101.1	1.4
YH11-5.1	1545	879	0.57	.0478	2.3	0.09	2.4	.0136	0.4	86.8	0.4	90	55	86.8	0.4
YH11-1.1	1063	477	0.45	.0490	2.0	0.09	2.1	.0136	0.5	86.9	0.5	148	47	86.9	0.5
YH11-9.1	1360	778	0.57	.0486	1.8	0.09	1.8	.0136	0.5	87.1	0.4	130	42	87.1	0.4
YH11-2.1	854	384	0.45	.0480	2.3	0.09	2.3	.0136	0.6	87.2	0.5	99	54	87.2	0.5
YH11-3.1	611	172	0.28	.0466	4.3	0.09	4.3	.0137	0.7	88.0	0.6	30	102	88.0	0.6
YH11-10.1	579	168	0.29	.0492	5.0	0.09	5.1	.0138	0.8	88.1	0.7	158	117	88.1	0.7
YH11-11.1	1413	621	0.44	.0510	2.3	0.10	2.3	.0139	0.5	88.7	0.4	242	52	88.7	0.4
YH11-7.1	1376	708	0.51	.0473	2.2	0.09	2.3	.0139	0.5	88.8	0.4	63	53	88.8	0.4
YH11-8.1	690	194	0.28	.0453	3.1	0.09	3.2	.0138	0.7	88.9	0.6	-38	75	88.9	0.6
YH11-4.1	1246	627	0.50	.0471	2.0	0.09	2.1	.0139	0.5	89.4	0.4	53	48	89.4	0.4
YH11-6.1	961	365	0.38	.0449	2.4	0.09	2.5	.0139	0.5	89.4	0.5	-64	59	89.4	0.5

Supplemental Table 2.3. U-Pb Analytical Data (continued)

				Isotopic ratios						Corrected ages (Ma)					
Spot Name	U (ppm)	Th (ppm)	Th/U	207Pb/ 206Pb	± (%)	207Pb/ 235U	± (%)	206Pb/ 238U	± (%)	206Pb 238U	± (1σ)	207Pb 206Pb	± (1σ)	Best Age (Ma)	± (1σ)
MD01-13.1	543	356	0.66	.0464	4.0	0.11	4.1	.0170	0.7	108.9	0.8	20	97	108.9	0.8
MD01-1.1	456	45	0.10	.0466	3.3	0.16	3.4	.0252	0.7	161.2	1.1	28	79	161.2	1.1
MD01-7.1	473	113	0.24	.0453	3.1	0.16	3.2	.0253	0.7	161.6	1.1	-42	75	161.6	1.1
MD01.14.1	699	232	0.33	.0491	2.2	0.17	2.2	.0256	0.5	163.1	0.8	154	50	163.1	0.8
MD01-12.1	435	162	0.37	.0506	2.6	0.18	2.7	.0258	0.7	163.7	1.1	223	60	163.7	1.1
MD01-4.1	249	175	0.70	.0459	6.4	0.16	6.5	.0257	0.9	164.2	1.5	-10	154	164.2	1.5
MD01-3.1	799	312	0.39	.0521	2.0	0.19	2.1	.0261	0.5	165.4	0.8	290	46	165.4	0.8
MD01.15.1	415	119	0.29	.0519	3.0	0.19	3.1	.0263	0.7	166.6	1.2	281	70	166.6	1.2
MD01-2.1	317	66	0.21	.0486	2.8	0.18	2.9	.0262	0.8	166.8	1.3	129	66	166.8	1.3
MD01-6.1	903	331	0.37	.0486	2.3	0.18	2.4	.0262	0.5	166.9	0.8	127	55	166.9	0.8
MD01-5.1	650	213	0.33	.0485	3.7	0.18	3.7	.0263	0.6	167.6	0.9	125	86	167.6	0.9
MD01-16.1	1020	219	0.22	.0490	2.4	0.18	2.4	.0264	0.5	168.4	0.8	148	55	168.4	0.8
MD01-10.1	529	15	0.03	.0456	3.3	0.17	3.3	.0263	0.6	168.4	1.0	-22	79	168.4	1.0
MD01-9.1	718	43	0.06	.0496	1.9	0.18	1.9	.0265	0.5	168.5	0.9	175	44	168.5	0.9
MD01-11.1	782	135	0.17	.0488	2.0	0.18	2.0	.0267	0.5	169.8	0.9	138	46	169.8	0.9
MD01-8.1	192	146	0.76	.0411	7.5	0.15	7.5	.0266	1.0	170.8	1.7	-280	190	170.8	1.7
YH13-3.1	36	30	0.81					.0130	5.5	91.2	2.6			91.2	2.6
YH13-15.1	350	147	0.42	.0452	5.0	0.09	5.1	.0147	0.9	94.5	0.8	-46	122	94.5	0.8
YH13-8.1	329	172	0.52	.0484	5.7	0.10	5.8	.0149	1.0	95.1	0.9	117	135	95.1	0.9
YH13-12.1	359	401	1.12	.0426	8.2	0.09	8.3	.0148	1.0	95.2	0.9	-188	205	95.2	0.9
YH13.11.1	305	122	0.40	.0420	7.4	0.09	7.5	.0148	1.0	95.7	0.9	-227	187	95.7	0.9
YH13-9.1	388	148	0.38	.0506	4.3	0.10	4.4	.0150	0.9	95.8	0.9	224	99	95.8	0.9
YH13-7.1	401	171	0.43	.0438	3.9	0.09	4.0	.0149	0.8	95.9	0.8	-120	97	95.9	0.8
YH13-10.1	650	251	0.39	.0469	3.0	0.10	3.1	.0150	0.7	96.0	0.7	46	73	96.0	0.7
YH13-13.1	266	187	0.71	.0425	8.5	0.09	8.6	.0149	1.1	96.0	1.0	-196	213	96.0	1.0
YH13-16.1	402	308	0.77	.0461	4.4	0.10	4.5	.0150	0.9	96.2	0.8	0	106	96.2	0.8
YH13-5.1	396	147	0.37	.0446	5.4	0.09	5.4	.0151	0.9	97.0	0.8	-75	131	97.0	0.8
YH13-2.1	279	118	0.42	.0448	4.0	0.09	4.1	.0151	1.0	97.0	1.0	-65	97	97.0	1.0
YH13-14.1	977	968	0.99	.0476	2.4	0.10	2.5	.0152	0.5	97.1	0.5	81	58	97.1	0.5
YH13-6.1	418	165	0.40	.0463	4.8	0.10	4.9	.0152	0.8	97.2	0.8	15	116	97.2	0.8
YH13-4.1	337	236	0.70	.0466	4.3	0.10	4.4	.0153	0.9	97.8	0.9	27	102	97.8	0.9
YH13-1.1	240	172	0.72	.0442	6.7	0.09	6.8	.0154	1.1	99.0	1.1	-102	165	99.0	1.1
HH06-3.1	674	640	0.95	.0482	2.2	0.16	2.2	.0236	0.6	150.7	0.9	112	51	150.7	0.9
HH06-4.1	728	699	0.96	.0482	2.6	0.16	2.6	.0238	0.6	151.5	0.9	107	60	151.5	0.9
HH06-5.1	516	416	0.81	.0480	2.6	0.16	2.7	.0239	0.7	152.2	1.0	98	62	152.2	1.0
HH06-6.1	207	133	0.64	.0465	6.2	0.15	6.3	.0239	1.1	152.6	1.6	24	149	152.6	1.6
HH06-1.1	388	123	0.32	.0491	3.2	0.16	3.3	.0240	0.8	152.7	1.2	153	74	152.7	1.2
HH06-7.1	570	280	0.49	.0466	3.0	0.15	3.1	.0240	0.6	153.5	1.0	31	73	153.5	1.0
HH06-8.1	342	243	0.71	.0472	4.1	0.16	4.2	.0241	0.8	153.8	1.3	57	97	153.8	1.3
HH06-2.1	399	273	0.68	.0466	4.4	0.16	4.5	.0241	0.8	154.1	1.2	31	106	154.1	1.2
MD07-11.1	337	121	0.36	.0458	4.4	0.10	4.5	.0165	0.9	105.7	1.0	-11	105	105.7	1.0
MD07-2.1	270	87	0.32	.0430	9.1	0.10	9.1	.0164	1.1	105.8	1.1	-168	226	105.8	1.1
MD07-9.1	210	73	0.35	.0479	4.6	0.11	4.7	.0166	1.2	105.9	1.3	92	108	105.9	1.3
MD07-4.1	670	297	0.44	.0493	3.1	0.11	3.2	.0167	0.8	106.6	0.8	163	73	106.6	0.8
MD07-10.1	288	114	0.40	.0496	4.8	0.11	4.9	.0167	1.0	106.8	1.1	175	111	106.8	1.1
MD07-3.1	194	78	0.40	.0467	6.3	0.11	6.4	.0167	1.2	106.9	1.3	36	151	106.9	1.3
MD07-1.1	400	150	0.37	.0526	5.9	0.12	6.0	.0170	0.9	107.9	0.9	311	135	107.9	0.9
MD07-7.1	327	159	0.49	.0454	4.4	0.11	4.5	.0168	0.9	108.1	1.0	-35	108	108.1	1.0
MD07-6.1	397	142	0.36	.0495	3.7	0.12	3.8	.0171	0.8	108.8	0.9	171	86	108.8	0.9
MD07-12.1	276	127	0.46	.0497	3.8	0.12	3.9	.0172	1.0	109.6	1.1	180	88	109.6	1.1
MD07-5.1	451	180	0.40	.0472	3.5	0.11	3.6	.0172	0.8	110.1	0.9	60	84	110.1	0.9
MD07-8.1	240	95	0.40	.0393	7.5	0.09	7.6	.0171	1.1	110.8	1.2	-398	195	110.8	1.2

Supplemental Table 2.3. U-Pb Analytical Data (continued)

				Isotopic ratios						Corrected ages (Ma)					
Spot Name	U (ppm)	Th (ppm)	Th/U	207Pb/ 206Pb	± (%)	207Pb/ 235U	± (%)	206Pb/ 238U	± (%)	206Pb 238U	± (1σ)	207Pb 206Pb	± (1σ)	Best Age (Ma)	± (1σ)
HH07-2.1	260	178	0.68	.0381	14.4	0.09	14.5	.0166	1.3	107.3	1.3	-479	383	107.3	1.3
HH07-3.1	134	102	0.77	.0406	13.7	0.09	13.8	.0167	1.5	108.0	1.5	-312	351	108.0	1.5
HH07-6.1	97	65	0.67	.0475	8.4	0.11	8.5	.0170	1.7	108.4	1.8	76	199	108.4	1.8
HH07-9.1	215	183	0.85	.0423	9.3	0.10	9.4	.0169	1.2	108.8	1.2	-209	235	108.8	1.2
HH07-7.1	166	95	0.57	.0417	11.3	0.10	11.3	.0170	1.3	109.7	1.4	-242	284	109.7	1.4
HH07-10.1	561	283	0.50	.0459	3.5	0.11	3.5	.0171	0.7	109.9	0.8	-6	84	109.9	0.8
HH07-8.1	402	189	0.47	.0489	3.0	0.12	3.1	.0173	0.8	110.2	0.9	144	70	110.2	0.9
HH07-4.1	426	179	0.42	.0449	4.4	0.11	4.5	.0172	0.8	110.5	0.9	-61	107	110.5	0.9
HH07-5.1	326	117	0.36	.0459	4.2	0.11	4.3	.0173	0.9	110.6	1.0	-8	102	110.6	1.0
HH07-11.1	274	202	0.73	.0406	6.0	0.10	6.0	.0172	1.0	110.9	1.1	-312	153	110.9	1.1
HH07-12.1	348	223	0.64	.0490	3.3	0.12	3.4	.0175	0.9	112.0	1.0	148	77	112.0	1.0
HH07-1.1	317	163	0.51	.0473	3.3	0.12	3.4	.0177	0.9	113.1	1.0	63	79	113.1	1.0
TD04-6.1	614	217	0.35	.0432	14.9	0.09	15.0	.0157	1.8	100.7	1.7	-154	369	100.7	1.7
TD04-15.1	875	275	0.31	.0469	2.5	0.10	2.6	.0157	0.5	100.8	0.6	42	60	100.8	0.6
TD04-11.1	674	172	0.26	.0460	3.8	0.10	3.9	.0158	0.6	101.6	0.6	0	93	101.6	0.6
TD04-10.1	566	192	0.34	.0479	3.2	0.11	3.3	.0160	0.7	102.1	0.7	95	77	102.1	0.7
TD04-9.1	948	808	0.85	.0460	4.0	0.10	4.1	.0160	0.5	102.9	0.5	-3	98	102.9	0.5
TD04-5.1	779	242	0.31	.0474	71.0	0.11	71.2	.0162	4.2	103.4	3.8	69	1690	103.4	3.8
TD04-13.1	2278	672	0.29	.0480	1.8	0.11	1.8	.0163	0.3	103.9	0.3	100	43	103.9	0.3
TD04-14.1	621	212	0.34	.0440	3.8	0.10	3.9	.0162	0.6	104.0	0.7	-110	94	104.0	0.7
TD04-4.1	1087	397	0.37	.0430	2.8	0.10	2.8	.0162	0.5	104.2	0.5	-168	69	104.2	0.5
TD04-2.1	607	109	0.18	.0460	3.3	0.10	3.4	.0162	0.7	104.2	0.7	-1	80	104.2	0.7
TD04-1.1	1101	404	0.37	.0475	2.7	0.11	2.7	.0163	0.5	104.2	0.5	75	64	104.2	0.5
TD04-12.1	817	176	0.22	.0464	2.6	0.11	2.7	.0164	0.7	105.2	0.7	20	63	105.2	0.7
TD04-3.1	766	293	0.38	.0454	3.9	0.10	3.9	.0165	0.6	105.7	0.6	-34	94	105.7	0.6
TD04-7.1	1057	327	0.31	.0502	3.5	0.12	3.7	.0166	0.9	105.9	1.0	206	82	105.9	1.0
TD04-8.1	1262	260	0.21	.0467	3.0	0.11	3.1	.0166	0.8	106.5	0.8	34	71	106.5	0.8
EW35-9.1	104	63	0.61	.0428	12.6	0.10	12.8	.0178	1.7	114.2	1.9	-178	315	114.2	1.9
EW35-10.1	81	75	0.94	.0548	6.2	0.14	6.5	.0181	1.8	114.9	2.2	402	139	114.9	2.2
EW35-5.1	59	34	0.57	.0607	15.0	0.15	15.2	.0184	2.4	115.6	2.5	629	323	115.6	2.5
EW35-6.1	103	59	0.57	.0610	13.8	0.16	13.9	.0185	1.9	116.4	1.9	639	296	116.4	1.9
EW35-1.1	140	86	0.61	.0540	7.3	0.14	7.4	.0185	1.4	117.4	1.7	370	164	117.4	1.7
EW35-7.1	80	44	0.55	.0334	27.5	0.08	27.6	.0182	2.1	118.2	2.2	-836	786	118.2	2.2
EW35-4.1	103	62	0.60	.0368	15.7	0.09	15.8	.0183	1.7	118.3	1.9	-569	425	118.3	1.9
EW35-2.1	143	141	0.99	.0375	14.3	0.10	14.4	.0185	1.5	119.4	1.7	-520	383	119.4	1.7
EW35-3.1	108	104	0.97	.0308	29.5	0.08	29.6	.0185	1.9	120.5	2.0	-1074	889	120.5	2.0
EW35-8.1	86	56	0.65	.0224	36.0	0.06	36.0	.0185	2.0	122.2	2.2			122.2	2.2
EW39-7.1	1421	714	0.50	.0478	1.9	0.09	2.0	.0139	0.5	88.8	0.5	90	45	88.8	0.5
EW39-3.1	536	175	0.33	.0467	4.1	0.09	4.2	.0140	0.8	89.6	0.8	32	99	89.6	0.8
EW39-1.1	760	330	0.43	.0492	2.5	0.10	2.6	.0140	0.7	89.6	0.6	157	59	89.6	0.6
EW39-5.1	615	221	0.36	.0452	4.3	0.09	4.4	.0140	0.8	90.2	0.7	-43	105	90.2	0.7
EW39-4.1	932	405	0.43	.0457	3.9	0.09	4.0	.0141	0.6	90.3	0.6	-19	95	90.3	0.6
EW39-8.1	732	371	0.51	.0466	2.8	0.09	2.9	.0141	0.7	90.3	0.6	28	68	90.3	0.6
EW39-2.1	650	257	0.39	.0516	4.4	0.10	4.5	.0143	0.8	90.9	0.7	269	101	90.9	0.7
EW39-6.1	749	343	0.46	.0439	4.7	0.09	4.7	.0142	0.7	91.3	0.6	-119	115	91.3	0.6

Supplemental Table 2.3. U-Pb Analytical Data (continued)

				Isotopic ratios						Corrected ages (Ma)					
Spot Name	U (ppm)	Th (ppm)	Th/U	207Pb/ 206Pb	± (%)	207Pb/ 235U	± (%)	206Pb/ 238U	± (%)	206Pb 238U	± (1σ)	207Pb 206Pb	± (1σ)	Best Age (Ma)	± (1σ)
RM01-5.1	285	10	0.04	.0452	7.6	0.10	7.7	.0155	1.1	99.2	1.1	-46	186	99.2	1.1
RM01-6.1	173	87	0.50	.0470	5.3	0.10	5.5	.0156	1.4	99.8	1.5	47	127	99.8	1.5
RM01-8.1	847	554	0.65	.0448	5.1	0.10	5.2	.0156	0.7	100.4	0.6	-67	125	100.4	0.6
RM01-12.1	279	124	0.45	.0428	6.7	0.09	6.8	.0156	1.1	100.6	1.1	-182	168	100.6	1.1
RM01-11.1	654	72	0.11	.0465	3.1	0.10	3.1	.0158	0.7	101.1	0.7	26	73	101.1	0.7
RM01-9.1	723	41	0.06	.0520	3.9	0.11	3.9	.0159	0.7	101.2	0.7	284	88	101.2	0.7
RM01-10.1	354	141	0.40	.0461	5.0	0.10	5.1	.0160	1.0	102.4	1.0	4	121	102.4	1.0
RM01-2.1	879	527	0.60	.0499	2.4	0.11	2.4	.0161	0.6	102.4	0.6	192	55	102.4	0.6
RM01-1.1	1096	955	0.87	.0478	2.3	0.11	2.4	.0160	0.5	102.6	0.6	92	55	102.6	0.6
RM01-3.1	302	120	0.40	.0483	3.7	0.11	3.9	.0162	1.0	103.8	1.1	116	88	103.8	1.1
RM01-13.1	1362	1318	0.97	.0441	3.9	0.10	3.9	.0163	0.6	104.4	0.6	-103	96	104.4	0.6
RM01-4.1	1268	528	0.42	.0476	2.3	0.11	2.4	.0164	0.5	105.0	0.5	77	55	105.0	0.5
RM10-10.1	759	223	0.29	.0362	17.5	0.07	17.5	.0137	1.2	89.2	0.8	-617	477	89.2	0.8
RM10-6.1	541	223	0.41	.0450	4.6	0.10	4.6	.0159	0.8	102.0	0.8	-55	111	102.0	0.8
RM10-5.1	234	82	0.35	.0589	7.5	0.13	7.6	.0163	1.3	102.5	1.3	563	163	102.5	1.3
RM10-11.1	793	272	0.34	.0472	2.9	0.10	3.0	.0161	0.6	103.0	0.7	58	70	103.0	0.7
RM10-4.1	592	148	0.25	.0456	5.5	0.10	5.5	.0161	0.8	103.4	0.8	-25	133	103.4	0.8
RM10-9.1	741	287	0.39	.0487	3.1	0.11	3.1	.0163	0.7	104.2	0.7	131	72	104.2	0.7
RM10-12.1	700	449	0.64	.0503	2.5	0.11	2.6	.0164	0.7	104.4	0.7	209	57	104.4	0.7
RM10-7.1	353	207	0.59	.0414	7.9	0.09	8.0	.0162	1.0	104.5	1.0	-261	201	104.5	1.0
RM10-3.1	656	389	0.59	.0458	2.8	0.10	2.9	.0163	0.7	104.5	0.7	-15	67	104.5	0.7
RM10-2.1	527	171	0.32	.0474	4.6	0.11	4.7	.0164	0.8	104.7	0.9	70	110	104.7	0.9
RM10-1.1	403	165	0.41	.0410	6.5	0.09	6.6	.0163	0.9	105.0	1.0	-286	166	105.0	1.0
RM10-8.1	760	263	0.35	.0456	2.7	0.10	2.7	.0164	0.6	105.0	0.7	-21	64	105.0	0.7
RM10-13.1	393	318	0.81	.0444	4.1	0.10	4.2	.0164	0.9	105.4	1.0	-89	101	105.4	1.0
RM10-14.1	283	122	0.43	.0491	3.9	0.11	4.1	.0166	1.1	106.2	1.2	152	91	106.2	1.2
RM10-15.1	289	614	2.12	.0466	5.2	0.11	5.3	.0167	1.1	106.7	1.2	27	125	106.7	1.2

THIS PAGE INTENTIONALLY LEFT BLANK

CHAPTER 3

Zircon Rare Earth Element Patterns in Cretaceous Plutonic Rocks of the Sierra Nevada Batholith, California: Implications for Cyclical Flare-up Models

Abstract

We present new zircon trace element data for 20 surface samples collected in the northern and central Sierra Nevada batholith. We use this dataset to assess the patterns of fractionation in Cretaceous magmas as indicated by U, Th, Hf and REE abundances in zircon. The variation of trace element ratios and abundances with time offer an opportunity to assess aspects of the cyclical magmatic flare-ups proposed for the Cordilleran convergent margin; specifically the late-Cretaceous flare-up event in California. Decreasing Ce/Gd, U/Yb and Hf concentration trends in zircon indicate a decrease in fractionation from 160 Ma until about 120 Ma. At 120 Ma a significant reversal occurs in which Ce/Gd, U/Yb and Hf concentration indicate an increasing degree of fractionation during the late-Cretaceous flare-up event. Hf concentration in zircon varies by about 6000ppm where the minimum observed Hf concentration occurs in samples ~120 Ma. U/Yb varies systematically with time from >10 to <0.2 where minimum values correspond to samples with ages of ~120 Ma. The patterns of fractionation, as interpreted by the trace element data presented here, are in agreement with previously published εNd, $^{87}Sr/^{86}Sr$, and $\delta^{18}O$ data, which also indicate that as much as 50% of melts produced during the late-Cretaceous flare-up event were sourced from anatexis of the continental lithosphere. These findings support models of cyclical

processes in continental convergent margins which hypothesize that crustal thickening leads to flare-up magmatic events through the partial melting of the base of a thickened continental lithosphere.

Previously published U-Pb ages from the central and northern Sierra Nevada batholith show considerable mismatch with published intrusive flux calculations and corresponding time windows for the late-Cretaceous flare-up event. Our data, in combination with previously published zircon U-Pb age data indicate that the Cretaceous flare-up event in the northern Sierra Nevada batholith occurred 10-15 my earlier than previously reported. We find that fractionation markers (i.e. U/Yb, [Hf], Ce/Gd) temporally correspond tightly with the assertion that the late Cretaceous flare-up initiated in the north 10-15 my earlier than in the southern Sierra Nevada. As a result, the find that 'late' Cretaceous flare-up event appears to have initiated in the northern Sierra Nevada at ~120 Ma and finished by ~90 Ma. The late Cretaceous flare-up of the southern Sierra Nevada, however, is reported to have started at ~105 Ma and finished at ~85 Ma. We suggest that the late Cretaceous flare-up started in the northern Sierra Nevada and swept southward over a period of 10-15 my.

INTRODUCTION

Magmatic flare-up events have been well documented at convergent plate margins throughout the world (Armstrong, 1988; Paterson et al, 2011; Paterson and Ducea, 2015; de Silva et al, 2015; Turnbull et al, 2016; Kirsch et al, 2016; Moghadam et a, 2017; Riley et al, 2018, Alonso et al, 2018). In the North American cordillera, a majority of batholith construction occurred during these short-lived events (Ducea, 2001; DeCelles et al, 2009; DeCelles and Grahm, 2015; Ducea et al, 2015). Specifically, in the California arc the late Cretaceous flare-up resulted in >78% percent of the batholithic volume being emplaced in as little as 15 my of the arc's ~140 my history (Ducea, 2001). Identifying the processes that lead to flare-up events is critical to understanding the larger structure of batholithic systems and the nature of convergent margins. Efforts to explain the conditions leading to flare-up events have included a variety of mechanisms including (1) increased melt production from the subducted slab and/or pelagic sediment (e.g. Drummond and Defant, 1990), (2) increased asthenosphere melt input from thinned lithosphere as a result of extension, delamination or slab rollback (Kay and Kay, 1991; Ferrari et al., 2007), and (3) fractional melting of thickened lithosphere due to forearc and/or retroarc thrusting (Ducea, 2001; DeCelles et al., 2009). The source and subsequent makeup of magmas generated by each of these models is unique and, as a result, should impart discernable differences on the trace element patterns of the melts (DePaolo, 1981; Spera et al., 2007; Grimes et al. 2015).

Zircon's ability to incorporate a variety of trace elements into its structure allows an opportunity to track changes in parental melt trace element abundance and ratios with

time (Hoskin and Schaltegger, 2003; Belousova et al., 2002; Trail et al., 2012). Specifically, U/Yb and Hf have been proposed as markers for tracers of melt fractionation in granitic magmas (Bath and Wooden, 2010). Hf and U/Yb show and overall increase with magmatic differentiation, although small variations in the trends can reflect dynamic processes within the system (Claiborne et al., 2006; 2010). Relative concentrations of U, Yb, Hf and Y in zircons have also been proposed as tools to indicate the tectonic setting of a zircon as being sourced from continental crust, oceanic crust or kimberlite (e.g. Hoskin and Ireland, 2000; Grimes et al. 2007; Barth and Wooden, 2010; Grimes et al., 2015).

Long-term fractionation patterns have important implications for the interpretation of processes contributing to episodic magmatic flare-up events. Such models (Ducea, 2001; Ducea and Barton, 2007; DeCelles et al., 2009; 2015; Ducea et al., 2015) hypothesize that episodic thickening of the continental lithosphere through structural means leads to partial melting of the base of the thickened lithosphere. We hypothesize that investigation of trace element ratios in zircon should indicate changes in the parental melt fractionation and, therefore, help establish the rock type source for the magmas (i.e subducted slab, asthenosphere or continental crust) as well as increased contribution of fractional melts generated in thickened continental crust.

SIERRA NEVADA BATHOLITHIC ROCKS AND MAGMATIC CYCLICITY

The magmatic system that comprises the Sierra Nevada range experienced two major flare-up events: one in the late Jurassic (160-150 Ma) and a second event in the late Cretaceous (105-85 Ma) (Ducea, 2001; Ducea and Barton, 2007; Paterson et al. 2011;

Cecil et al., 2012). It was this later event, commonly referred to as the late-Cretaceous flare-up, during which >78% of the Sierra Nevada arc was formed within 20 m.y. (Ducea, 2001; Chapman et al., 2012). During these flare-up events, production rates of granitoid rocks increased significantly over average production rates (DeCelles and Graham, 2015, Patterson et al., 2011). Such flare-up events are not unique to the California arc system and have been observed and/or speculated elsewhere in the North and South American Cordillera systems (DeCelles et al., 2009, Patterson et al., 2011).

Understanding the mechanisms that drive flare-up events and the source of the voluminous magmas generated during such events have been a topics of debate among geologist for decades (e.g. Armstrong, 1988; Ducea and Barton, 2007; Paterson et al., 2011; Decelles and Graham, 2015; Ducea et al., 2015). Because of the close association between subduction and arc construction, it would be natural to correlate the flare-up events observed in the Sierra Nevada range with increased subductive/convergence rates. However, investigation of convergence rates between the North American and Farallon plates reveals no such correlation (Ducea, 2001; Page and Engebretson, 1985). Furthermore, an investigation between intrusive flux rates and the angle of plate convergence also fails to yield clear correlations (Ducea, 2001; Page and Engebretson, 1985).

In the absence of direct causality between convergence rate/angle variation and flare-up magmatic events, studies have explored processes in the overriding continental lithospheric/asthenospheric wedge for driving mechanisms in episodic and punctuated magmatic production. It has been proposed that lithospheric extension and/or delamination could be a driving mechanism in increased magmatic production (Lee et al.,

2006). In such a scenario, delamination or lithospheric extension should lead to the introduction of "fresh" asthenospheric mantle at the lithospheric base (Kay and Kay, 1991) and provide a source of mantle-derived melt. However, it has been noted that batholithic rocks of the Sierra Nevada have systematically low ε_{Nd} values during periods of flare-up magmatism (Ducea, 2001). The low ε_{Nd} values (-20>5 for the late Cretaceous flare-up) are incompatible with values generally found in mantle-sourced melts as well as slab derived melts, whose values do not typically depart from MORB values of +12 ± 3 (Gregory and Taylor, 1981). These results indicate that lithospheric thinning and/or lower crust removal are unlikely to be a direct cause of the flare-up magmatic events observed in the Sierra Nevada (Ducea and Barton, 2007).

It has also been suggested that crustal thickening might play a role in creating the voluminous melts generated during magmatic flare-up events (Burchfiel et al., 1992; Ducea, 2001). Both the late-Jurassic and late-Cretaceous flare-up events observed in the Sierra Nevada temporally coincide with periods of regional compression (Dickinson, 2004; DeCelles, 2004). Specifically, the late-Cretaceous flare-up event correlates with the Sevier orogeny and crustal thickening driven by subduction-erosion and retro-arc thrusting (DeCelles, 2004). The speculation that crustal thickening and the subsequent sourcing of flare-up magmas from lower crustal sources seems to be supported by isotopic data. As previously mentioned, low ε_{Nd} values observed in plutonic rocks emplaced during flare-up events indicate a more evolved source for the magmas. Furthermore, positive δO^{18} values and high $^{87}Sr/^{86}Sr$ also indicate that the source of magmas during flare-up events in the Sierra Nevada batholith were likely sourced in

greater amounts by melts generated in overlying continental crust and mantle lithosphere (Ducea and Barton, 2007 and references therein; Lackey et al., 2008).

Trace elements in zircons offer an opportunity to test the cyclical flare-up models by helping establish the source and degree of fractionation of the melts that produced them (Profeta et al, 2015; Kirsch et al, 2016; Shea et al, 2018). Recent flare-up models predict that melts produced during flare-up events are largely produced by the structural thickening of continental crust and the melting of lower crust materials (DeCelles, et al 2009; DeCelles and Grahm, 2015). It also stands to reason that as this lower crustal material is progressively melted, resulting melt should become increasingly fractionated over time. We test these trends by investigating the trace element patterns in zircons of the Sierra Nevada batholith. Specifically, we examine variations of U, Hf, Y and REEs with time. Zircons ability to incorporate these trace elements during crystallization offer a way to view changing trace element abundances in melts. Such changes reflect the processes involved in the melt genesis and evolution (Claiborne et al, 2006; 2010; Barth and Wooden, 2010).

SAMPLE PREPARATION AND ANALYTICAL METHODOLOGY

Twenty samples of the plutonic rocks of the central Sierra Nevada batholithic system were collected, prepared and analyzed for U-Pb and REE concentrations (figure 1, table 1). Samples profiles were arranged in East-West oriented transects. The northernmost samples were collected along the South Fork of the American River, near California State Highway 50 and the Desolation Wilderness, just north of Hwy 50. The southernmost samples were collected from near the Merced River in Yosemite Valley.

Additional East-West transects include Hwy 120, the Tuolumne River, Hwy 108, the Mokelumne River, and Hwy 88.

All samples were collected in-situ, from outcrops. Any weathered surfaces were removed or excluded from sample preparation. The samples were crushed, milled and processed for zircon separation using standard techniques as outlined in chapter 1 of this thesis (i.e. density separation on a water table, magnetic separation on a Frantz device, and further density separation in MEI and bromoform). The zircon separates were then mounted in epoxy and polished to reveal grain interiors. These mounts were then imaged using a cathodoluminescence (CL) detector on a scanning electron microscope at the USGS microbeam laboratory in Denver, CO. The grains were then analyzed using the USGS/Stanford Sensitive High Resolution Ion Microprobe - Reverse Geometry (SHRIMP-RG). The ion microprobe technique allowed the minimally destructive, high resolution, and spatially constrained analysis (~25 μm spot size) of particular zones of the zircon grains for U, Th, Pb, Y, Hf and rare earth element (REE) concentrations. Spot locations were selected using CL imagery to avoid large inclusions and areas of complicated or non-concentric zoning. Supplemental file 1 includes imagery and spot locations for a selection of representative samples. The SQUID2 software (Ludwig, 2009) was used to reduce the raw data into isotopic ratios for the calculation of U/Pb ages and are reported in chapter 2 of this thesis (chapter 2, table 1). Ages were standardized against the R33 zircon reference material from the Braintree Complex of Madagascar (Black et al., 2004). Trace element concentrations were standardized against Madagascar Green (MAD) zircons (Mazdab and Wooden, 2006). Plots of REE concentrations were standardized against C1-chrondrite values (McDonough and Sun, 1995) and plotted using

the software package Isoplot v. 4.1? (Ludwig, ????) and using the procedures outlined in Barth and Wooden (2006).

RESULTS

In zircons, the chondrite-normalized REE patterns are typically enriched in heavy REE (HREE) relative to light REE (LREE) owing to the increase in compatibility of the heavy REEs as ionic radii decrease (e.g. Shannon 1976, Hoskin and Schaltegger, 2003). The ionic radius of Zr^{4+} is 0.84 Å and the ionic radii of the trivalent REE decrease from 1.160 Å (light REE $La^{3+)}$ to 0.977 Å (heavy REE Lu^{3+}). This pattern is observed in all analyses presented in this study (figure 2). Two common exceptions to the chrondrite-normalized REE pattern are found in Cerium and Europium as discussed below.

Cerium and Europium

The decrease in ionic radius of REEs from La^{3+} to Lu^{3+} (Shannon 1976) makes the substitution into the zircon structure progressively easier for the REE of higher atomic number (Nagasawa 1970, Watson 1980; Fujimaki 1986; Heaman et al. 1990; Hinton and Upton 1991; Hanchar et al. 2001). This behavior typically leads to a general abundance increase from light to heavy REEs in zircon. In most rock types (i.e. non-mantle affinity), zircons exhibit variations in this general trend commonly occur for Ce, as a positive anomaly, and in Eu, as a negative anomaly. In oxidizing conditions Ce^{3+} is oxidized to Ce^{4+} where it behaves more like Zr or Hf and is preferred by zircon over other LREE. The preferential inclusion of Ce^{4+} leads to the positive Ce anomaly observed in crustal-affinity rocks. Conversely, the absence of a positive Ce anomaly has been used to speculate about conditions of low oxidation state in parental magmas (e.g.

Hoskin and Schaltegger, 2003; Trail et al., 2012). As shown in figure 2, all samples in this study show a positive Ce anomaly, thus indicating the lack of especially low oxidative state conditions during zircon formation.

The Eu anomaly is calculated as: $\frac{Eu}{Eu*} = \frac{Eu_N}{\sqrt{Sm_N \times Gd_N}}$, where the subscript N denotes chrondrite-normalized concentrations. Europium may exist in magmas as both a divalent and trivalent cation. In conditions with low oxygen fugacity, Eu^{2+} substitutes for Ca in plagioclase. However, fO_2conditions where Eu^{2+} is stable should be incompatible with the presence of Ce^{4+}. As discussed by Maas et al. (1992), this consideration results in a paradox in which most crustal zircons exhibit both positive Ce anomalies (indicator of oxidative conditions) and negative Eu anomalies (indicator of reducing conditions). However, it has been speculated that plagioclase fractionation that depletes Eu from magma prior to the crystallization of zircon could result in both observed anomalies (Hoskin and Schaltegger, 2003 and references therein). Titanite, which occurs extensively throughout the plutonic rocks of the Sierra Nevada batholith (Ross, 1989, Dodge et al., 1982) also serves as a Eu sink and it has been demonstrated that co-crystallization of titanite and zircon can impart a negative Eu/Eu* (Loader et al., 2017).

All zircons analyzed in this study display this pattern of positive Ce and negative Eu anomalies. As illustrated in figure 3, we do recognize a time/(Eu/Eu*) correlation where decreasing Eu/Eu* with time leads to a minimum Eu/Eu* of 0.2-0.3 between 120 and 110 Ma. This is followed by an increase in Eu/Eu* values to 0.8 at about 90 Ma.

Uranium, Thorium and Hafnium

Zircons crystallized from granitoid melts typically exhibit Th-U ratios from 0.1 to 1, showing that the zircon structure incorporates Uranium more easily than Thorium (e.g.

Hurley and Fairbairn, 1956; Belousova et al., 2002; Hanchar and Hoskin, 2003). This pattern is consistent with this data set where a minimum Th/U of 0.3 and a maximum of 1.0 is observed. A maximum U concentration of 1679 ppm is observed in the youngest sample, SN08YH11 and a minimum of 83ppm is observed in SN08EW35.

In zircon, Hf^{4+} can enter as a simple substitution for Zr (Hoskin and Schaltegger, 2003) creating the zircon-hafnon solid solution $(Zr,Hf)SiO_4$ where Hf commonly makes up 1-2 weight percent in granitoid zircons (e.g. Claiborne et al., 2006). It has been suggested that Zr/Hf in zircon serves as a marker for magmatic evolution (Claiborne et al., 2006; 2010). The underlying principle of this system relies upon the relative increase in Hf content in granitoid melts as crystallization of zircon proceeds in magmas where Si is saturated (otherwise Zr is incorporated into baddeleyite, augite or amphibole). To this end, decreased Zr/Hf ratios concentrations can be interpreted as conditions of increased fractionation of the magma source (Claiborne et al., 2006; 2010). Hafnium concentrations presented here range from a low of 6247 ppm (SN08HH06, excluding an anomalously low value of 15 ppm in SN08YV03) to a high of 17135 ppm (SN08YH13). A characteristic trend in the data illustrated in figure 4 shows that Hf concentrations start at relatively high values (13917 ppm) in the oldest samples (168.4±1.6 Ma; SN08MD01) and systematically decrease to a minimum of about 7229 ppm (152.4±0.9 Ma; HH06) before increasing to higher values of about 15079 ppm in the youngest sample (88.8±0.8 Ma; SN08YH11).

DISCUSSION

Melt Sources during the late-Cretaceous Flare-up

Overall REE abundances and chondrite-normalized patterns have been shown to have little utility in differentiating non-MORB source terrains (Hoskin and Ireland, 2000). However, the ratios of certain trace element and REE have demonstrated usefulness in determining the source rock's tectonic setting. U/Yb, Hf, and Y, in particular, have been shown to be particularly useful in differentiating between MORB and continental and island arc systems (Grimes et al., 2007; 2015; Barth and Wooden, 2010). U and Yb share nearly equivalent compatibility in zircon with partition coefficients of 254 and 278 respectively (Bea et al., 1994). However, U and Yb demonstrate disparate behavior in magmatic systems where U concentrations are typically enriched in continental environments and are depleted in MORB (Klein, 2003, Grimes et al, 2015). The enrichment of U in continental rocks is due, in part, to the incorporation of subducted sediments, re-melting of subducted oceanic crust, and slab derived fluids that preferentially mobilize U and LREEs (Keleman et al., 2003). As a result, trace elements in zircon such as heavy REE (e.g. Yb), Hf and Y can be relatively depleted in arc magmas. Zircon's ability to incorporate U, Yb, Hf and REE during crystallization provides an opportunity to model the relative abundances of U, Yb, Hf and REE in the melts. In this way, zircon U/Yb plotted against Hf and Y concentrations have been demonstrated to help identify the tectono-magmatic setting of the zircons (Grimes et al., 2007; 2015).

It is well understood that the Sierra Nevada batholithic rocks were formed in a continental arc tectonic setting. Therefore, the data presented here offers an opportunity

to supplement and possibly further validate the geochemical models of Grimes et al. (2015). We recognize the ability of our dataset to validate the Grimes et al. (2015) models only extends as far as supporting the continental field and does not directly test the validity of the MORB fields. Figure 5 is based on the zircon discrimination diagrams proposed in Grimes et al. (2007). The data collected in this study shows (figure 5) that our samples lie entirely (with the exception of one analysis in each plot) within the continental fields of Grimes et al. (2007). These results indicate that the melts from which the zircons crystallized were largely sourced by continental-affinity rocks rather than MORB basalts or asthenospheric mantle.

These results are in agreement with other studies indicating that a significant proportion (~50% by mass or more) of Cretaceous melts produced in the California were sourced from recycled crust and lithospheric mantle. This evidence comes from three distinct isotopic indicators:

(1) Systematically low ε_{Nd} values have been observed throughout the Cretaceous portions of the Sierra Nevada batholith, particularly during flare-up events (DePaolo, 1981; Ducea and Barton, 2007; Cecil et al., 2012). Downward excursions in ε_{Nd} values (i.e. increasingly negative values) are well correlated with the late-Jurassic and late-Cretaceous flare-up events (DePaolo, 1981; Ducea, 2001) and indicate a higher degree of melt sourcing from the overlying continental crust and less input from primitive mantle sources.

(2) Strontium isotopes have been extensively measured in the Sierra Nevada (e.g. Kistler and Peterman, 1973; 1978; DePaolo, 1981; Cecil et al., 2012). There is a regional trend in the Sierra Nevada with higher $^{87}Sr/^{86}Sr$ observed towards the east, identifying the

boundary between plutonic development in the Panthalassan accreted terranes to the west and Proterozoic lithosphere of North America to the east (Kistler and Peterman, 1973; 1978). Magmas emplaced during the late-Cretaceous flare-up have higher $^{87}Sr/^{86}Sr$ and indicate that they were either sourced within the Precambrian basement of the overlying lithosphere or incorporated a significant of more evolved lithosphere.

(3) Oxygen isotope ratios (i.e. $\delta^{18}O$) are well suited to identify supracrustal signatures in magmatic sources owing to the low-temperature fractionation of $^{18}O/^{16}O$, especially in the presence of water. It has been demonstrated that melts generated during the late-Cretaceous flare-up show general increases in $\delta^{18}O$ (figure 13 in Lackey et al., 2008), thus indicating an increased input of rocks influenced by near surface conditions (e.g. metasedimentary rocks of the overlying continental lithosphere).

Temporal Variation of Fractionation Patterns

It has been demonstrated that magmatic arc systems often undergo multi-phase emplacement histories with complex interplay of replenishment and fractionation. (Coleman et al., 2004; Glazner et al., 2004; Claiborne et al., 2010; Memeti et al., 2010; Schwartz et al., 2014). In these systems, variations in temperature and chemistry can result in complex zonation within single zircon grains (Hanchar and Miller, 1993; Claiborne et al, 2006). Such variations can mask the long-term changes that occur during the construction of larger, regional-scale magmatic systems such as the Sierra Nevada batholith. Our attempt here is to identify changes in magmatic fractionation patterns throughout the Cretaceous. To accomplish this, our analysis of trace elements in zircon avoided grain cores and rims, which can complicate the interpretation of data due to the presence of inherited cores (antecrysts) and the refractory (i.e. late) stages of batholithic

construction. Our sample set also covers a relatively large region and incorporates samples from several intrusive suites. As a result, we are able to assess the long-term fractionation trends associated with construction of the central Sierra Nevada batholithic system. Figure 4 shows decreasing Hf concentration and decreasing Ce/Gd with with from ~170 Ma to ~125 Ma. In these plots, individual analyses were divided into 10 my groups and differentiated by plot symbols. The highest observed Ce/Gd and Hf concentrations were observed in the youngest and oldest samples (i.e. (<100 Ma and >139 Ma). Figure 6 outlines the U/Yb trend with time, where a trend reversal is observed at ~120 Ma. We interpret these results to indicate a trend of decreasing fractionation of magmas from ~170 Ma to ~125 Ma and an increase in fractionation from ~125 Ma until ~87 Ma.

Implications for Episodic Flare-up models

It has been suggested that cordillera-style magmatic systems undergo episodic flare-up events in response to cyclical changes in subduction mechanics and the structural evolution of the region (Ducea, 2001; Ducea and Barton, 2007; Ducea et al., 2015, DeCelles et al., 2009; DeCelles and Graham, 2015). As discussed earlier, it is apparent that the magmas generated during flare-up events incorporate higher amounts of crustal material (this study; Ducea, 2001). We also understand that flare-up events typically occur in compressive convergent tectonic regimes (DeCelles et al., 2009). These observations have led to the postulation that structural thickening, driven primarily by thrusting in the foreland, is responsible for the thickening of the lithosphere and subsequent anatexis of the lower crust of the overriding plate (DeCelles et al. 2009, DeCelles and Graham, 2015; Ducea et al., 2015).

Anatexis, as a result of crustal thickening, has been well documented in multiple orogenic regimes where lithosphere-scale thrusting leads to structural burial of the lower crust (e.g. Sawyer et al., 2011; Jamieson et al., 2011, Schwindinger and Weinberg, 2017). Such environments are well documented in continental collision environments (e.g. Dabie-Sulu of China, Western Gneiss Region of Norway, Himalaya of South Asia, Alps of western Europe) (Acosta-Vigil et al., 2010; Chen et al., 2015; Zheng et al., 2001 and references therein) but are less documented in the overlying lithosphere of continental arcs. In these environments, elevated temperatures as a result of structural burial lead to the partial melting of lower crust rocks. In the absence of continued structural displacement or the continuous addition of volatiles (e.g. H_2O), the relatively stable reservoir of the lower crust would be expected to produce melts that display trends toward higher fractionation as melts are progressively extracted from the lower crust (Kay and Kay, 1991). In the central Sierra Nevada, it has been suggested that the eventual exhaustion of lower-crust volatiles in the final stages of the late Cretaceous flare-up led to an infertile and melt drained lower crust, thus ending the flare-up event at ~85Ma. (Ducea, 2001).

Our interpretation of the zircon trace element patterns presented in this study is that change in fractionation of the various melts of the Sierra Nevada arc that occurred at about 120 Ma and represents a trend towards increasing amounts of lower-crust derived melts through the late Cretaceous flare-up. As figures 4 and 6 demonstrate, zircon trace element data show a trend that indicates increasing fractionation of the parental melts starting at 120 Ma and continuing through the late-Cretaceous magmatic flare-up until the end of magmatic emplacement at about 85 Ma. Although it is difficult to quantify the

amount of fractionation of the melts produced from trace element patterns presented here, the dataset offers qualitative evidence of the increasing fractionation in melts throughout the late-Cretaceous flare-up.

Timing of the 'late' Cretaceous Flare-up

DeCelles (2004) points out that the periods of most rapid shortening were during the Early Cretaceous (~140-110 Ma) and the Late Cretaceous-Eocene (~85-55 Ma) and outlines a poor correlation between magmatic flare-up events (at 160-150 Ma and 100-85 Ma) and periods of rapid shortening. It is apparent, therefore, that the link, if any, between crustal shortening/thickening and flare-up events is indirect. The data presented here indicate that magma fractionation, as indicated by an inflection of the U/Yb vs age (figure 6) trend, began during the magmatic lull about 15-20 m.y. before the initiation of the commonly reported (i.e. Ducea et al, 2001) late-Cretaceous magmatic flare-up ages for the Sierra Nevada. It has been suggested that the delayed onset of voluminous magmatic production post-dates rapid thickening due to the relaxation of geotherms in the cooler underthrust lithosphere (Glazner and Bartley, 1985). They calculate that the time to restore 'normal' geothermal gradients to a 35 km thick thrust sheet with characteristics of the California Arc would be ~10-35 m.y., thus providing a mechanism for the delayed onset of magmatism of about 15-20 m.y. However, this explanation does not account for the delayed onset of voluminous magmatism that would be excepted as a result of structural thickening in the >25 m.y. of rapid shortening that occurred since the initiation of rapid shortening.

In an effort to further understand the relationship between timing of the late-Cretaceous flare-up and the end of rapid shortening and crustal thickening, we compiled

zircon U-Pb ages from the central Sierra Nevada (this study, chapter 2) and Cecil et al. (2012) and inspected the frequency of ages relative to the apparent intrusive flux of Ducea (2001). We find significant mismatch between the age histograms of the northern Sierra Nevada and the flux calculations (Figure 7). Specifically, the histogram of northern Sierra Nevada ages indicates that the Cretaceous flare-up event was initiated about 15-20 m.y. earlier than in the southern Sierra Nevada. While the time span of the late-Cretaceous flare-up event is certainly well understood in the southern Sierra Nevada, we suggest that a sample bias exists, owing to the greater sample density in the southern Sierra Nevada. When considering the data presented here from the northern Sierra Nevada, it appears that the Cretaceous flare-up event started in the northern Sierra Nevada at ~120 Ma and spread south over a 10-15 m.y. time span before ending in the south at ~85 Ma. These findings agree with fractionation indicators discussed above. The inflection point between early Cretaceous patterns of decreasing fractionation to late Cretaceous patterns of higher fractionation occurs at ~120 Ma; precisely the time at which the age histogram of the central/northern samples indicates the initiation of rapid emplacement in that region (figure 7). We therefore suggest that the 'late' Cretaceous flare-up occurred over longer time span and in more spatially complicated fashion than previously appreciated.

CONCLUSIONS

It has been well documented that the plutonic rocks of the Sierra Nevada were sourced by a mixture of melts from the asthenospheric mantle and the overlying lithosphere as indicated by trace element and isotopic studies (e.g. Kistler and Peterman,

1973; 1978; DePaolo, 1981; Ducea, 2001; Cecil et al., 2012). The balance of input from each of these sources has been shown to vary with time and location, such that the Jurassic plutons on the western flanks of the batholith exhibit more primitive isotopic signatures and the portions of the batholithic system along the modern range crest exhibit more evolved, crustal, signatures (DePaolo, 1981, Cecil et al., 2012). We augment these finding by investigating the trace element abundances in zircon from surface samples in the central Sierra Nevada. Our data reveal that the magmas generated throughout the Cretaceous show trace element ratios indicative of evolved arc-sourced melts with variable degrees of fractionation. Our data also indicate a systematic change in fractionation of the melts with time. From the early Cretaceous until ~120Ma, trace element markers indicate decreased fractionation and indicate the increasing addition of less evolved, asthenosphere-sourced melts. However, after ~120Ma, our data indicate an increasing trend of fractionation in melts. Fractionation increased throughout the late-Cretaceous flare-up. We interpret these results as a system of increased production of melts in the lower crust.

These findings support the hypothesis (see DeCelles and Graham, 2015) that structural thickening of the lithosphere in the middle Cretaceous drove anatexis of the thickened crust and resulted in voluminous magmatic production in the late Cretaceous. We also find that the 'late' Cretaceous flare-up event occurred over a longer time period than previously described; initiating at ~120 Ma in the northern Sierra Nevada before initiation in the southern Sierra Nevada at ~105 Ma. These results indicate a southern 'sweep' of the late-Cretaceous flare-up event over the span of 15-20 m.y.

References Cited

Acosta-Vigil, A., Buick, I., Hermann, J., Cesare, B., Rubatto, D., London, D., Morgan, GB., 2010, Mechanisms of Crustal Anatexis: a Geochemical Study of Partially Melted Metapelitic Enclaves and Host Dacite, SE Spain: Journal of Petrology: v. 51, no. 4, p 785-821. Doi: 10.1093/petrology/egp095

Armstrong, R.L., 1988, Mesozoic and early Cenozoic magmatic evolution of the Canadian Cordillera, in Clark, S.P., Burchfiel, B.C., and Supper, J., eds., Processes in continental lithosphere deformation: A symposium to honor John Rodgers: Geological Society of America, Special Papers, v. 218, p. 55-91.

Bea, F., Pereira, M.D., Stroh, A., 1994, Mineral/leucosome trace element partitioning in a peraluminous migmatite (a laser ablation-ICP-MS study): Chemical Geology, v. 177, p. 291–312, doi: 10.1016/0009–2541(94)90133–3.

Barth, A.P., Wooden, J.L., 2006, Timing of magmatism following initial convergence at a passive margin, southwestern U.S. Cordillera, and ages of lower crustal magma sources: The Journal of Geology, v. 114, p. 231–245, doi: 10.1086/499573

Barth A.P., Wooden J.L., 2010, Coupled elemental and isotopic analyses of polygenetic zircons from granitic rocks by ion microprobe, with implications for melt evolution and the sources of granitic magmas: Chemical Geology, v. 277, p. 149–159

Belousova, E.A., Griffin, W.L., O'Reilly, S.Y., Fisher, N.J., 2002, Igneous zircon: Trace element composition as an indicator of source rock type: Contributions to Mineralogy and Petrology, v. 143, p. 602–622, doi: 10.1007/s00410–002–0364–7.

Black, L.P., Kamo, S.L., Allen, C.M., Davis, D.W., Aleinikoff, J.N., Valley, J.W., Mundil, R.M., Campbell, I.H., Korsch, R.J., Williams, I.S., Foudoulis, C., 2004. Improved 206Pb/238U microprobe geochronology by the monitoring of a trace-element-related matrix effect: SHRIMP, ID-TIMS, ELA-ICP-MS, and oxygen isotope documentation for a series of zircon standards: Chemical Geology v. 205, p. 115–140.

Burchfiel, B. C., Cowan, D. S., and Davis, G. A., 1992, Tectonic overview of the Cordilleran orogen in the western United States, *in* Burchfiel, B. C., Lipman, P. W., and Zoback, M. L., editors., The Cordilleran Orogen: Conterminous U. S.: Geological Society of America, The Geology of North America, v. G-3, p. 407– 480.

Cecil, M.R., Rotberg, G., Ducea, M.N., Saleeby, J.B., and Gehrels, G.E., 2012, Magmatic growth and batho- lithic root development in the northern Sierra Nevada, California: Geosphere, v. 8, p. 592–606, doi:10.1130 /GES00729.1.

Chapman, A.D., Saleeby, J.B., Wood, D.J., Piasecki, A., Kidder, S., Ducea, M.N., Farley, K.A., 2012, Late Cretaceous gravitational collapse of the southern Sierra Nevada batholith, California: Geosphere, v. 8, no. 2, p. 314–341. doi: https://doi-org.www2.lib.ku.edu/10.1130/GES00740.1

Chen, RX., Ding, B., Zheng, YF., Hu, Z., 2015, Multiple episodes of anatexis in a collisional orogen: Zircon evidence from migmatite in the Dabie orogeny: Lithos, v. 212, p. 247-265. Doi: 10.1016/j.lithos.2014.11.004

Claiborne, L. L., Miller, C. F., Walker, B. A., Wooden, J. L., Mazdab, F. K., Bea, F., 2006, Tracking magmatic processes through Zr/Hf ratios in rocks and Hf and Ti zoning in zircons: an example from the Spirit Mountain batholith, Nevada: Mineralogical Magazine, v. 70, no. 5, p. 517-543.

Claiborne, L. L., Miller, C. F., Wooden, J. L., 2010, Trace element composition of igneous zircon: a thermal and compositional record of the accumulation and evolution of a large silicic batholith, Spirit Mountain, Nevada: Contributions to Mineralogy and Petrology, v. 160, no. 4, p 511-531.

Coleman D.S., Gray W., Glazner A.F., 2004, Rethinking the emplacement and evolution of zoned plutons: Geochronologic evidence for incremental assembly of the Tuolumne Intrusive Suite, California: Geology, v. 32, p. 433–436

DeCelles, P.G., Ducea, M.N., Kapp, P., and Zandt, G., 2009, Cyclicity in Cordilleran orogenic systems: Nature Geoscience, v. 2, p. 251–257. doi:10.1038/ngeo469.

DeCelles, P.G., Zandt, G., Beck, S.L., Currie, C.A., Ducea, M.N., Kapp, P., Gehrels, G.E., Carrapa, B., Quade, J., and Schoenbohm, L.M., 2015, Cyclical orogenic processes in the Cenozoic central Andes. In P.G. DeCelles, M.N. Ducea, B. Carrapa, and P.A. Kapp, Eds., Geodynamics of a Cordilleran Orogenic System: The Central Andes of Argentina and Northern Chile. Geological Society of America Memoirs, v. 212, p. 459–490. doi:10.1130/2015.1212(22).

DeCelles, P.G. Graham, S.A., 2015, Cyclical processes in the North American Cordilleran orogenic system: Geology, v. 43, no. 6, p. 499–502. doi: https://doi.org/10.1130/G36482.1

DePaolo, D.J., 1981, A neodymium and strontium study of the Mesozoic calc-alkaline granitic batholiths of the Sierra Nevada and Peninsular Ranges: Journal of Geophysical Research, v. 86, p. 10470–10488.

De Silva, S.L., Riggs, N.R., Barth, A.P., 2015, Quickening the pulse: Fractal tempos in continental arc magmatism: Elements, v. 11, p. 113-118.

Dickinson, W.R., 2004, Evolution of the North American Cordillera: Annual Review of Earth and Planetary Sciences, v. 32, p. 13–45, doi: 10.1146/annurev.earth.32.101802.120257.

Dodge, F.C.W., Millard, H.T., Elsheimer, H. N., 1982, Compositional variations and abundances of selected elements in granitoid rocks and constituent minerals, central Sierra Nevada Batholith, California: U. S. Geological Survey Professional Paper, v. 1248, 24 pp.

Drummond, M.S., and Defant, M.J., 1990, A model for trondhjemite-tonalite-dacite genesis and crustal growth via slab melting, Archean to modern comparisons: Journal of Geophysical Research, v. 95, p. 21503–21521.

Ducea, M.N., 2001, The California Arc; thick granitic batholiths, eclogitic residues, lithospheric-scale thrusting, and magmatic flare-ups: GSA Today, v.11, p. 4-10.

Ducea, M.N., and Barton, M.D., 2007, Igniting flare-up events in Cordilleran arcs: Geology, v. 35, p. 1047–1050, doi:10.1130/G23898A.1.

Ducea, M.N., Paterson, S.R., DeCelles, P.G., 2015, High-volume magmatic events in subduction systems: Elements, v. 11, no. 2, p. 99–104.

Ferrari L, Valencia-Moreno M, Bryan S., 2007, Magmatism and tectonics of the Sierra Madre Occidental and its relation with the evolution of the western margin of North America: Geological Society of America Special Paper, v. 422, p. 1-39

Fujimaki H., 1986, Partition coefficients of Hf, Zr, and REE between zircon, apatite, and liquid: Contributions to Mineral Petrology, v. 94, p. 42-45

Gehrels, G., 2014, Detrital Zircon U-Pb Geochronology Applied to Tectonics: Annual Review of Earth and Planetary Sciences, v. 42, no. 1, p. 127-149

Glazner, A.F., Bartley, JM, 1985, Evolution of lithospheric strength after thrusting: Geology, v. 13, no. 1, p. 42–45. doi: https://doi-org.www2.lib.ku.edu/10.1130/0091-7613(1985)13<42:EOLSAT>2.0.CO;2

Glazner A.F., Bartley J.M., Coleman D.S., Gray W., Taylor R.Z., 2004, Are plutons assembled over millions of years by amalgamation from small magma chambers: GSA Today, v. 14, p. 4–11

Gregory, R.T., and Taylor, H.P., 1981, An oxygen isotope profile in a section of Cretaceous oceanic-crust, Samail ophiolite, Oman—Evidence for $\delta^{18}O$ buffering of the oceans by deep (<5 km) seawater-hydrothermal circulation at mid-ocean ridges: Journal of Geophysical Research, v. 86, no. B4, p. 2737–2755.

Grimes, C.B., John, B.E., Kelemen, P.B., Mazdab, F., Wooden, J.L., Cheadle, MJ, Hanghøj, K., Schwartz, J.J., 2007, The trace element chemistry of zircons from oceanic crust: a method for distinguishing detrital zircon provenance: Geology, v. 35, p. 643–646. doi:10.1130/ G23603A.1

Grimes, C.B., Wooden, J.L., Cheadle, M.J., John, B.E., 2015, "Fingerprinting" tectono-magnetic provenance using trace elements in igneous zircon: Contributions to Mineral Petrology, v. 170, p.46 Doi: 10.1007/s00410-015-119903

Gutierrez-Alonso, G., Fernandez-Suarez, J., Lopez-Carmona, A., Gartner, A., 2018, Exhuming a cold case: The early granodiorites of the northwest Iberian Variscan belt—A Visean magmatic flare□up?, Lithosphere, v. 10, no. 2, p. 194-216.

Hanchar, J.M., Miller, C.F., 1993, Zircon zonation patterns as revealed by cathodoluminescence and backscatteres electron images: Implications for interpretation of complex crustal histories: Chemical Geology, v. 110, p. 1-13.

Hanchar, J.M., and Hoskin, .W.O., 2003, Zircon: Reviews in Mineralogy and geochemistry, v. 53, +500pp.

Hanchar, J.M., Finch R.J., Hoskin, P.W.O., Watson, E.B., Cherniak, D.J., Mariano, A.N., 2001, Rare earth elements in synthetic zircon: Part I. Synthesis, and rare-earth element and phosphorous doping of zircon: Am Mineral, v. 86, p. 667-680

Heaman, L.M., Bowins, R., Crocket, J., 1990, The chemical composition of igneous zircon suites: implications for geochemical tracer studies: Geochim Cosmochim Acta, v. 54, p. 1597-1607

Hinton, R.W., Upton, B.G.J., 1991, The chemistry of zircon: variations within and between large crystals from syenite and alkali basalt xenoliths: Geochim Cosmochim Acta, v. 55, p. 3287-3302

Hoskin, P.W.O., and Ireland, T.R., 2000, Rare earth element chemistry of zircon and its use as a provenance indicator: Geology, v. 28, p. 627–630.

Hoskin, P.W.O., Ireland, T.R., 2000, Rare earth element chemistry of zircon and its use as a provenance indicator: Geology, v. 28, p. 627–630

Hoskin, P.W., Schaltegger, U., 2003, The Composition of Zircon and Igneous and Metamorphic Petrogenesis: Reviews in Mineralogy and Geochemistry, v. 53, no. 1, p. 27–62. doi: https://doi-org.www2.lib.ku.edu/10.2113/0530027

Hurley, P.M., and Fairbairn, H.W., 1956, Abundance and distribution of Uranium and Thorium in zircon, sphene, apatite, epidote and monazite in granitic rocks: USGS Proffesional Papers, no 636

Jamieson, R.A., Unsworth, M.J., Harris, N.B.W., Rosenberg, C.L., Schulmann, K., 2011, Crustal melting and the flow of mountains: Elements, v. 7, p. 253-260

Kay, R.W., and Kay, S.M., 1991, Creation and destruction of the lower continental crust: Geologische Rundschau, v. 80, p. 259–270, doi: 10.1007/ BF01829365.

Kelemen, P.B., Hanghoj, K., and Greene, A.R., 2003, One view of geochemistry of subduction-related magmatic arcs, with an emphasis on primitive andesite and lower crust, *in* Rudnick, R.L., ed., The crust: Oxford, Elsevier- Pergamon, Treatise on Geochemistry, v. 3, p. 593–650.

Kirsch, M., Paterson, S.R., Wobbe, F., Martinez Ardila, A.M., Clausen, B.L., and Alasion, P.H., 2016, Temporal histories of Cordilleran continental arcs: Testing models for magmatic episodicity: American Mineralogist, v. 101, p. 2133–2154.

Kistler, R.W.,and Peterman, Z.E., 1973, Variations in Sr, Rb, K, Na, and initial St87/Sr86 in Mesozoic granitic rocks and intruded wall rocks in Central California: Geol. Soc. Am. Bull., v. 84, p. 3489-3512

Kistler,R.W.,and Peterman,Z.E., 1978, A study of regional variation of initial strontium isotopic composition of Mesozoic granitic rocks in California, U.S. Geol. Surv. Prof. Pap. 1071

Klein, E.M., 2003, Geochemistry of the igneous oceanic crust, *in* Rudnick, R.L., ed., The crust: Oxford, Elsevier-Pergamon, Treatise on Geochemistry, v. 3, p. 433–464.

Lee, C-TA., Cheng, X., Horodyskyi, U., 2006, The development and refinement of continental arcs by primary basaltic magmatism, garnet pyroxenite accumulation, basaltic recharge and delamination: insights from the Sierra Nevada, California: Contributions to Mineralogy and Petrology, v. 151, p. 222-242

Loader, M.A., Wilkinson, J.J., Armstrong, R.N., 2017, The effect of titanite crystallisation on Eu and Ce anomalies in zircon and its implications for the assessment of porphyry Cu deposit fertility: Earth and Planetary Science Letters, v. 472, p. 107-119

Ludwig, K.R., 2009. Squid 2, version 2.50, A user's manual: Berkeley Geochronology Center, Special Publication, No. 5, 110 p.

Maas R., Kinny, P.D., Wiliams, I.S., Froude, D.O., Compston, W., 1992, The Earth's Oldest known crust: a geochronological and geochemical study of 3900-4200 Ma old detrital zircons from Mt. Narryer and Jack Hills, Western Austrlia: Geochim Cosmochim Acta, v. 56, p. 1281-1300

Loader, M.A., Wilkinson, J.J., Armstrong, R.N., 2017, The effect of titanite crystallisation on Eu and Ce anomalies in zircon and its implications for the assessment of porphyry Cu deposit fertility: Earth and Planetary Science Letters, v. 472, p. 107-119

Mazdab, F.K., Wooden, J.L., 2006. Trace element analysis in zircon by ion microprobe (SHRIMP-RG): technique and applications: Geochimica et Cosmochimica Acta, v. 70, no. 18, p. 405.

Memeti, V./, Paterson, S., Matzel, J., Mundil, R., Okaya, D,. 2010, Magmatic lobes as "snapshots" of magma chamber growth and evolution in large, composite batholiths: An example from the Tuolumne intrusion, Sierra Nevada, California. *GSA Bulletin*, v. 122, p. 11-12. doi: https://doi-org.www2.lib.ku.edu/10.1130/B30004.1

McDonough, W.F., Sun S-S., 1995, The composition of the Earth: Chemical Geology, v. 120, p. 223-253

Moghadam, H.S., Li, X-H., Santos, J.F., Stern, R.J., Griffin, W.L., Ghorbani, G., Sarebani, N., 2017, Neoproterozoic magmatic flare-up along the N. margin of Gondwana: The Taknar complex, NE Iran: Earth and Planetary Sience Letters, v. 474, p. 83-96.

Nagasawa, H., 1970, Rare earth concentrations in zircon and their host dacites and granites: Earth Planet Sci Letters, v. 9, p. 359-364

Page, B.M., and Engebretson, D.C., 1985, Correlation between the geologic record and computed plate motions for central California: Tectonics, v. 2, p. 133–155.

Paterson, S.R., Okaya, D., Memeti, V., Economos, R., and Miller, R.B., 2011, Magma addition and flux calculations of incrementally constructed magma chambers in continental margin arcs: Combined field, geochronologic, and thermal modeling studies: Geosphere, v. 7, p. 1439–1468, doi:10.1130 /GES00696.1.

Riley, T.R., Burton-Johnson, A., Flowerdew, M.J., Whitehouse, M.J., 2018, Episodicity within a mid-Cretaceous magmatic flare-up in West Antarctica: U-Pb ages of the Lassiter Coast intrusive suite, Antarctic Peninsula, and correlations along the Gondwana margin: GSA Bulletin, v. 130, no. 7-8, p. 1177-1196.

Ross, D.C., 1989, The metamorphic and plutonic rocks of the southernmost Sierra Nevada, California, and their tectonic framework. U. S. Geological Survey Professional Paper: P 1381 159 pp.

Schwartz, J.J., Johnson, K., Mueller, P., Valley, J., Strickland, A., Wooden, J.L., 2014, Time scales and processes of Cordilleran batholith construction and high-Sr/Y magmatic pulses: Evidence from the Bald Mountain batholith, northeastern Oregon: *Geosphere, v*. 10, no. 6, p. 1456–1481. doi: https://doi-org.www2.lib.ku.edu/10.1130/GES01033.1

Shannon, R.D., 1976, Revised effective ionic radii and systematic studies of inter-atomic distances in halides and chalcogenides: Acta Crystallography, v., A32, p. 751-767

Sawyer, E.W., Cesare, B., Brown, M., 2011. When the continental crust melts: Elements, v. 7, p. 229–234.

Spera, F.J., Bohrson, W.A., Till, C.B., Ghiorso, M.S., 2007, Partitioning of trace elements among coexisting crystals, melt, and supercritical fluid during isobaric crystallization and melting: *American Mineralogist, v*. 92, p. 1881–1898. doi: https://doi-org.www2.lib.ku.edu/10.2138/am.2007.2326

Schwindinger, M., and Weinberg, RF, 2017, A felsic MASH zone of crustal magmas — Feedback between granite magma intrusion and in situ crustal anatexis: Lithos, v. 284-285, p. 109-121. Doi:10.1016/j.lithos.2017.03.030

Turnbull, R., Tulloch, A., Ramenzani, J., Jongens, R., 2016, Extension-facilitated pulsed S-I-A-type "flare-up" magmatism at 370 Ma along the southeast Gondwana margin in New Zealand: Insights from U-Pb geochronology and geochemistry: GSA Bulletin, v. 128, no. 9-10, p. 1500-1520.

Watson, E.B., 1980, Some experimentally determined zircon/liquid partition coefficients for the rare earth elements: Geochim Cosmochim Acta, v. 44, p. 895-897

Zheng, Y.F., Xia, Q.X., Chen, R.X., Gao, X.Y., 2011, Partial melting, fluid supercriticality and element mobility in ultrahigh-pressure metamorphic rocks during continental collision: Earth-Science Reviews, v. 107, p. 342-374. Doi: 10.1016/j.earscirev.2011.04.004

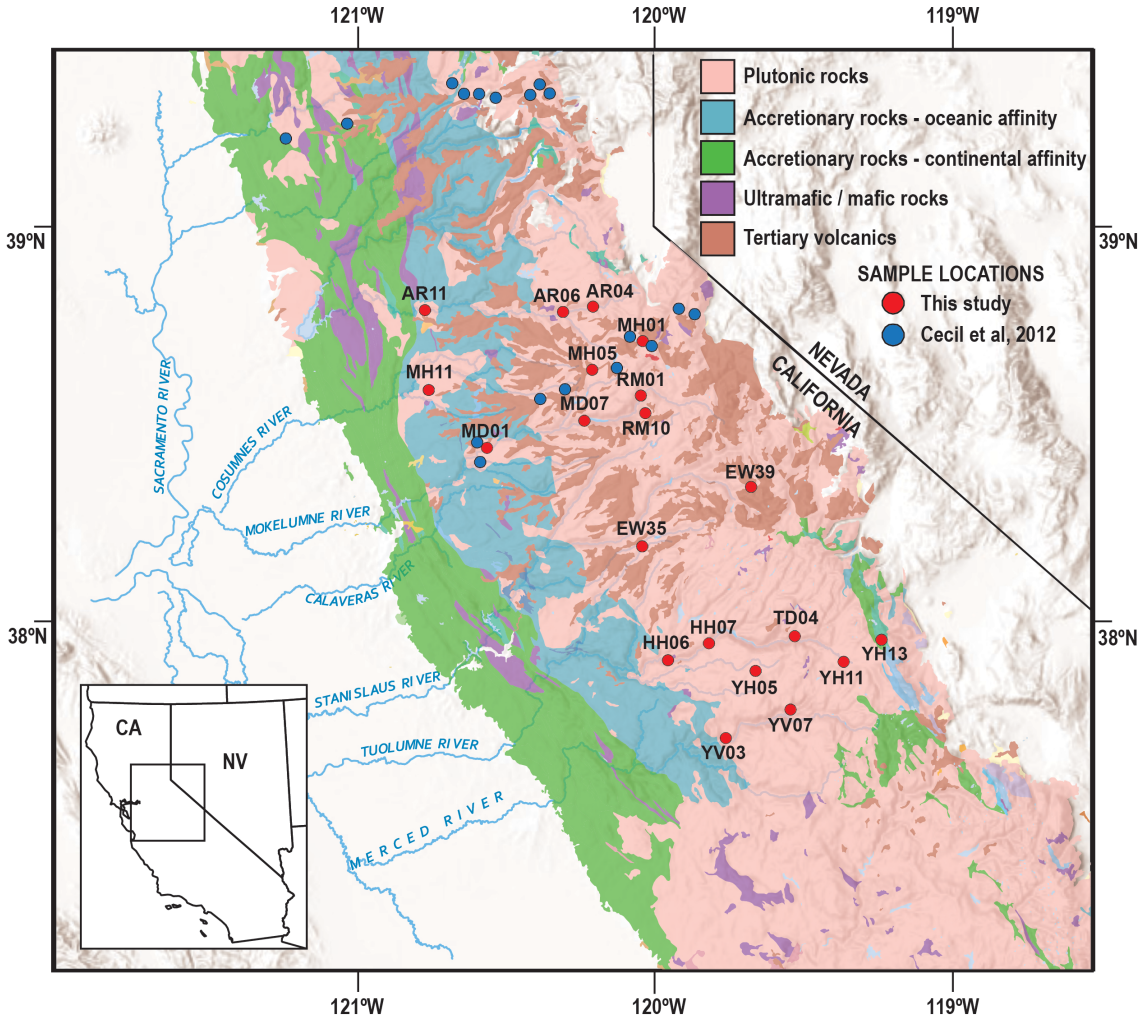
121°W
120°W
119°W
39°N
38°N
Plutonic rocks
Accretionary rocks - oceanic affinity
Accretionary rocks - continental affinity
Ultramafic / mafic rocks
Tertiary volcanics
SAMPLE LOCATIONS
This study
Cecil et al, 2012
NEVADA
CALIFORNIA
AR11
AR06
AR04
MH01
MH05
MH11
RM01
MD07
RM10
MD01
EW39
EW35
HH07
HH06
TD04
YH13
YH11
YH05
YV07
YV03
SACRAMENTO RIVER
COSUMNES RIVER
MOKELUMNE RIVER
CALAVERAS RIVER
STANISLAUS RIVER
TUOLUMNE RIVER
MERCED RIVER
CA
NV

Figure 3.1

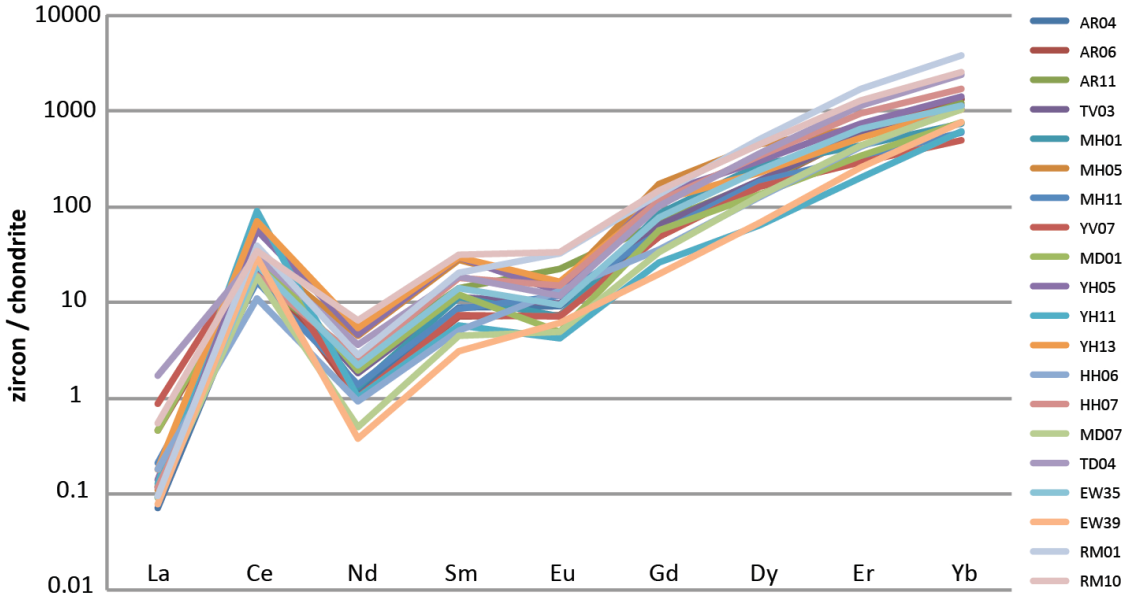
10000
1000
100
10
1
0.1
0.01
zircon / chondrite
La
Ce
Nd
Sm
Eu
Gd
Dy
Er
Yb
AR04
AR06
AR11
TV03
MH01
MH05
MH11
YV07
MD01
YH05
YH11
YH13
HH06
HH07
MD07
TD04
EW35
EW39
RM01
RM10

Figure 3.2

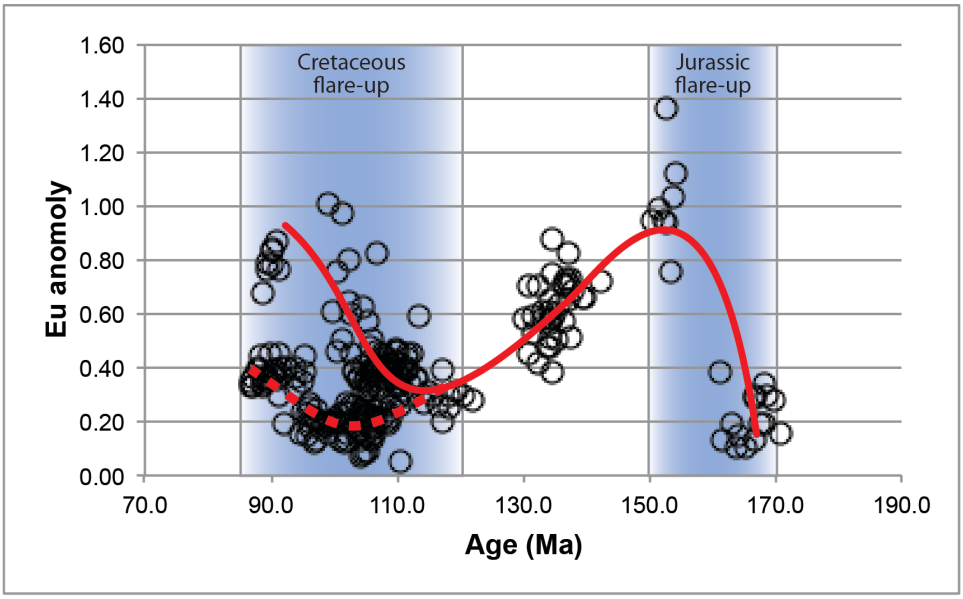
Cretaceous flare-up
Jurassic flare-up
Eu anomoly
1.60
1.40
1.20
1.00
0.80
0.60
0.40
0.20
0.00
70.0
90.0
110.0
130.0
150.0
170.0
190.0
Age (Ma)

Figure 3.3

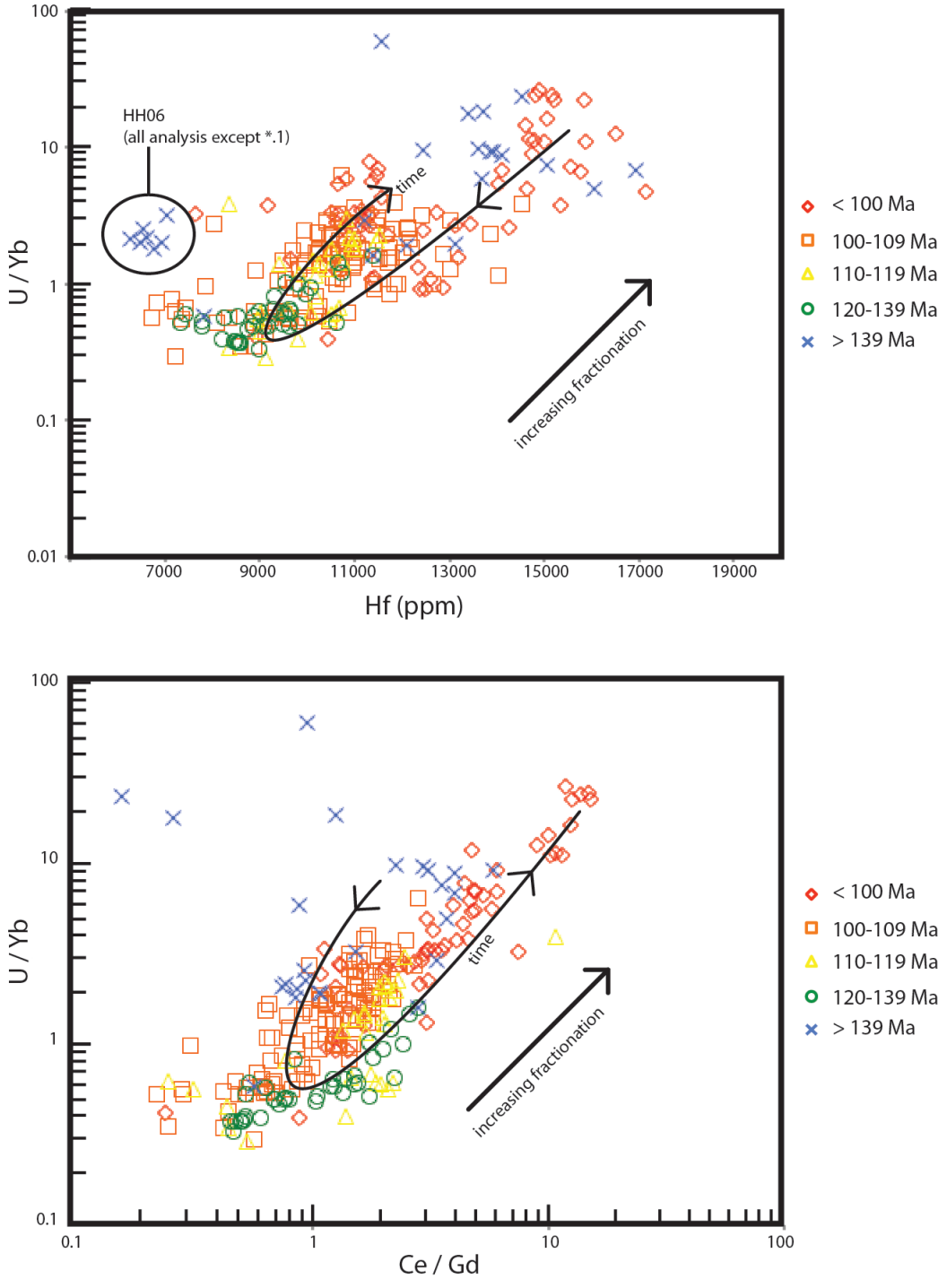
100
10
1
0.1
0.01
U / Yb
HH06
(all analysis except *.1)
time
increasing fractionation
7000
9000
11000
13000
15000
17000
19000
Hf (ppm)
< 100 Ma
100-109 Ma
110-119 Ma
120-139 Ma
> 139 Ma
100
10
1
0.1
U / Yb
time
increasing fractionation
0.1
1
10
100
Ce / Gd
< 100 Ma
100-109 Ma
110-119 Ma
120-139 Ma
> 139 Ma

Figure 3.4

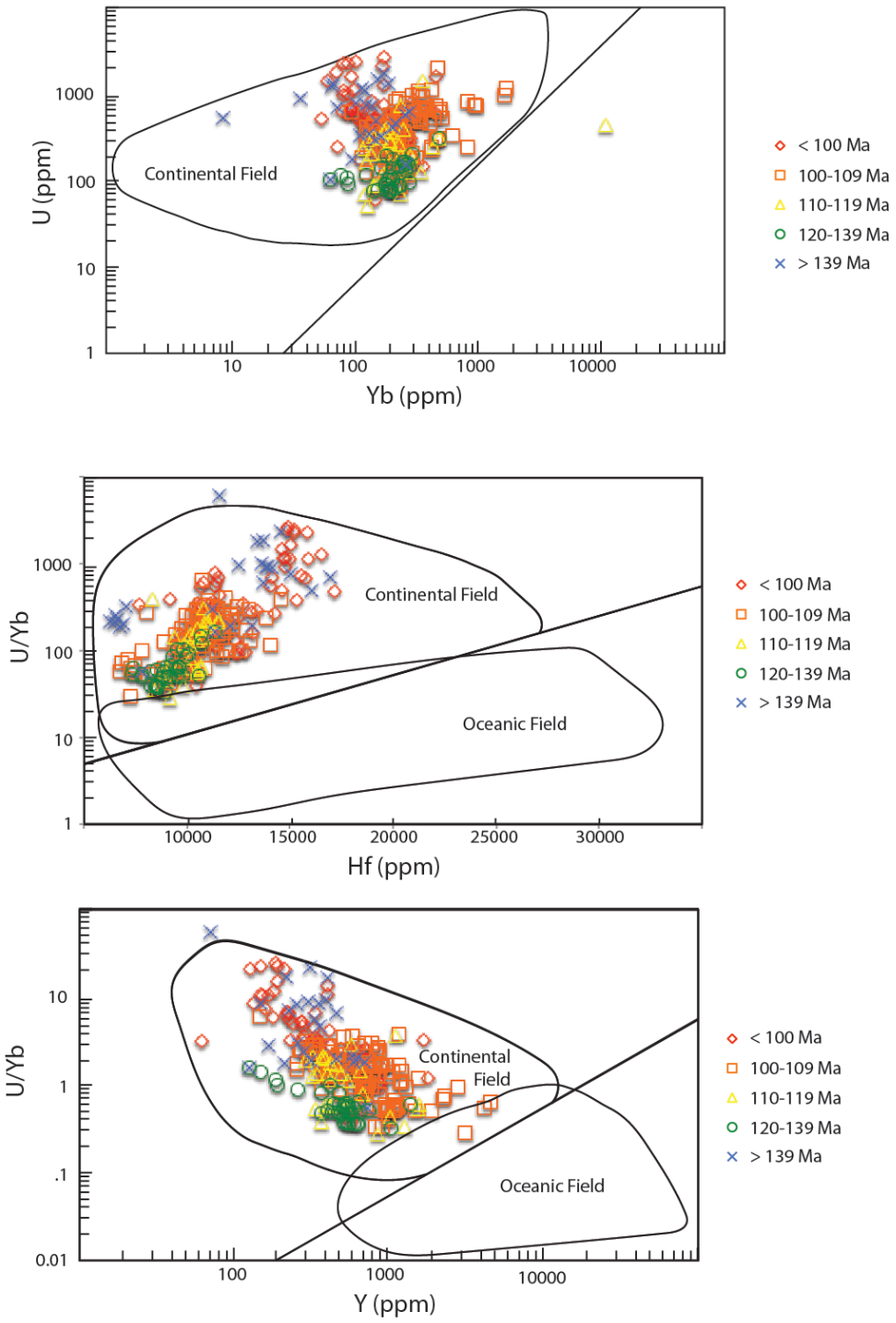
U (ppm)
1000
100
10
1
Continental Field
10
100
1000
10000
Yb (ppm)
< 100 Ma
100-109 Ma
110-119 Ma
120-139 Ma
> 139 Ma
U/Yb
1000
100
10
1
Continental Field
Oceanic Field
10000
15000
20000
25000
30000
Hf (ppm)
< 100 Ma
100-109 Ma
110-119 Ma
120-139 Ma
> 139 Ma
U/Yb
10
1
.1
0.01
Continental
Field
Oceanic Field
100
1000
10000
Y (ppm)
< 100 Ma
100-109 Ma
110-119 Ma
120-139 Ma
> 139 Ma

Figure 3.5

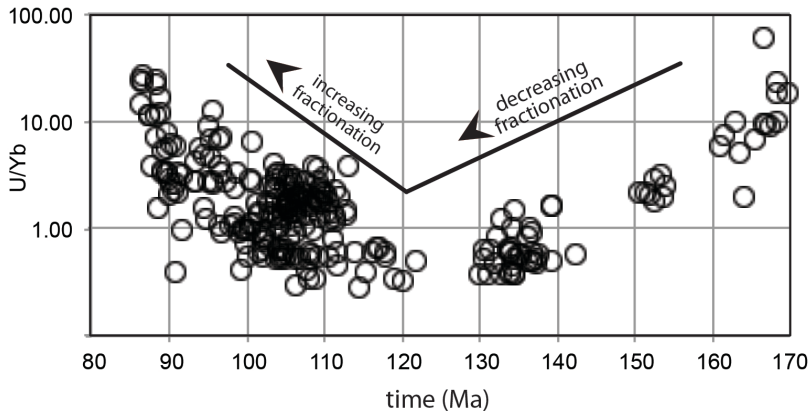
100.00
10.00
1.00
U/Yb
80
90
100
110
120
130
140
150
160
170
time (Ma)
increasing fractionation
decreasing fractionation

Figure 3.6

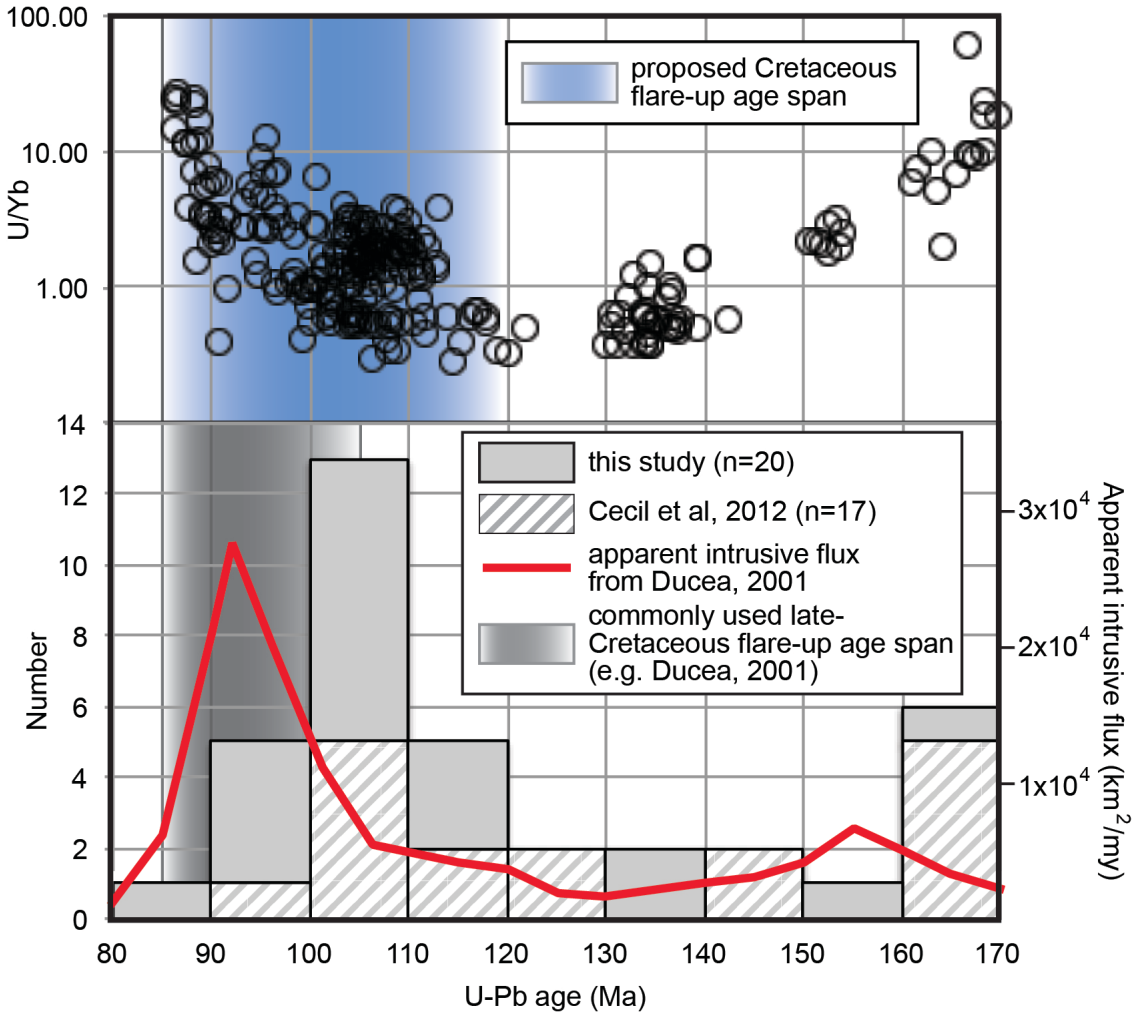
100.00
10.00
1.00
U/Yb
proposed Cretaceous flare-up age span
14
12
10
8
6
4
2
0
Number
this study (n=20)
Cecil et al, 2012 (n=17)
apparent intrusive flux from Ducea, 2001
commonly used late-Cretaceous flare-up age span (e.g. Ducea, 2001)
3x10^4
2x10^4
1x10^4
Apparent intrusive flux (km^2/my)
80
90
100
110
120
130
140
150
160
170
U-Pb age (Ma)

Figure 3.7

Table 3.1: Sample-Averaged Trace Element Abundances

	*YH11	06W39	*YV07	*YH13	*YH05	*RM01	*RM10	*TD04	*MH05	*AR04	*MH01	*MD07	*AR06	*HH07	*YV03	06EW35	*MH11	*AR11	*HH06	*MD01
number of analyses	11	8	16	16	13	13	15	15	10	12	12	12	16	12	15	10	20	16	8	16
U (ppm)	1678.9	660.86	500.34	604.08	237.54	623.59	439.07	780.40	146.22	411.75	248.25	283.24	470.93	246.90	226.84	83.40	121.72	118.99	395.94	907.51
Th (ppm)	789.46	297.71	222.89	376.42	191.79	317.44	219.34	268.57	138.94	184.62	138.33	115.42	225.49	141.91	131.27	61.49	62.11	64.20	295.22	270.23
Y (ppm)	212.94	242.13	453.01	563.56	742.06	1488	1183	1027	1048	534.29	690.78	387.02	525.25	880.71	485.84	608.77	513.30	520.29	365.07	359.81
La (ppm)	0.03	0.02	0.21	0.04	0.03	32.07	0.13	0.41	0.03	0.02	0.02	0.02	0.11	0.03	1.32	0.02	0.05	0.03	0.04	0.11
Ce (ppm)	54.61	17.94	23.18	43.39	34.79	67.51	21.27	18.93	19.80	13.91	18.56	11.25	16.22	11.77	14.09	15.02	10.05	10.65	6.82	19.74
Nd (ppm)	0.46	0.18	0.47	2.44	2.10	10.35	3.02	1.64	2.03	0.56	0.60	0.23	0.46	1.16	0.89	1.00	0.63	1.21	0.42	0.89
Sm (ppm)	0.84	0.45	1.09	4.33	4.44	4.95	4.60	2.72	4.08	1.33	1.68	0.67	1.05	2.70	1.61	2.07	1.26	2.10	0.75	1.79
Eu (ppm)	0.24	0.34	0.40	0.93	0.72	2.27	1.89	0.66	0.85	0.52	0.40	0.28	0.42	0.85	1.24	0.53	0.67	1.26	0.74	0.28
Gd (ppm)	5.21	3.93	9.62	22.76	26.51	29.17	29.20	20.41	34.14	11.24	16.73	6.76	9.57	22.90	14.97	15.28	10.66	13.63	7.07	11.26
Dy (ppm)	15.60	17.02	39.59	55.90	73.37	120.34	111.69	89.48	110.34	44.64	66.74	31.70	42.34	84.56	50.20	59.42	44.48	45.29	30.85	32.76
Er (ppm)	32.1	41.5	79.3	83.2	117.9	258.7	207.0	182.3	167.6	93.6	119.1	68.8	92.8	151.4	97.4	105.0	94.3	88.8	68.3	53.8
Yb (ppm)	99.6	121.1	180.9	166.2	228.4	584.0	406.1	383.9	258.4	216.3	210.1	164.4	216.2	277.0	877.0	183.0	211.0	196.4	170.4	120.6
Hf (ppm)	15079	11089	10875	14055	12099	8364	10480	11493	9689	10718	10623	11047	10549	9727	9572	9838	9060	9085	7229	13917
Th/U	0.47	0.45	0.45	0.62	0.81	0.51	0.50	0.34	0.95	0.45	0.56	0.41	0.48	0.57	0.58	0.74	0.51	0.54	0.75	0.30
U/Yb	16.86	5.46	2.77	3.64	1.04	1.07	1.08	2.03	0.57	1.90	1.18	1.72	2.18	0.89	0.26	0.46	0.58	0.61	2.32	7.53
Ce/Gd	3.41	1.48	0.78	0.62	0.43	0.75	0.24	0.30	0.19	0.40	0.36	0.54	0.55	0.17	0.32	0.32	0.31	0.25	0.31	0.57
Eu_A	0.36	0.79	0.38	0.23	0.20	0.64	0.26	0.19	0.22	0.39	0.23	0.40	0.40	0.33	0.36	0.28	0.55	0.70	1.01	0.21
Ce_A	247.88	169.13	39.92	72.63	70.98	1.99	18.31	12.43	46.14	76.42	87.16	85.48	38.74	35.29	9.92	53.79	30.37	30.76	27.07	34.03
La (ch)	0.13	0.08	0.88	0.18	0.14	135.32	0.54	1.71	0.11	0.07	0.09	0.09	0.46	0.12	2.22	0.10	0.21	0.12	0.18	0.46
Ce (ch)	89.08	29.27	37.82	70.79	56.76	110.13	34.70	30.87	32.31	22.69	30.28	18.35	26.47	19.21	23.00	24.50	16.39	17.37	11.12	32.21
Nd (ch)	1.00	0.38	1.02	5.33	4.59	22.65	6.61	3.60	4.43	1.23	1.32	0.51	1.01	2.54	2.43	2.18	1.39	2.65	0.93	1.94
Sm (ch)	5.68	3.07	7.39	29.27	30.01	33.46	31.11	18.35	27.54	8.99	11.33	4.51	7.11	18.27	11.31	13.99	8.52	14.16	5.04	12.11
Eu (ch)	4.26	6.10	7.08	16.51	12.75	40.27	33.50	11.65	15.02	9.18	7.09	4.90	7.41	15.18	12.64	9.49	11.87	22.40	13.17	5.00
Gd (ch)	26.16	19.76	48.34	114.36	133.20	146.59	146.72	102.57	171.55	56.49	84.05	33.99	48.11	115.07	72.22	76.81	53.56	68.52	35.55	56.56
Dy (chn)	63.41	69.17	160.92	227.24	298.25	489.18	454.03	363.75	448.56	181.47	271.32	128.86	172.11	343.75	202.15	241.54	180.81	184.09	125.42	133.18
Y (ch)	135.6	154.2	288.5	359.0	472.7	947.5	753.4	654.3	667.6	340.3	440.0	246.5	334.6	561.0	348.9	387.8	326.9	331.4	232.5	229.2
Er (ch)	200.9	259.6	495.9	520.0	736.7	1617.1	1293.8	1139.1	1047.7	585.2	744.7	430.2	579.7	946.2	608.0	656.4	589.5	555.0	426.6	336.3
Yb (ch)	618.7	752.2	1123.4	1032.1	1418.9	3627.5	2522.2	2384.6	1604.8	1343.2	1305.0	1021.1	1342.9	1720.5	1133.7	1136.9	1310.6	1220.0	1058.1	749.0

Subscript A: Anamolies

* : Sample Prefix is SN08

(ch) : chondrite normalized values (C1; McDonough and Sun, 1995)

Chapter 3 Figure Captions

Figure 3.1. Generalized geologic map of the central Sierra Nevada Range, showing sample locations for this study. Samples extend from the south fork of the American River drainage in the North to the Merced River drainage in the South. All samples were collected from surface exposure of plutonic rocks of the Sierra Nevada batholithic complex. Samples presented in this study are shown as red circles; age data from samples presented by Cecil et al (2012) are designated by blue circles.

Figure 3.2. Sample averaged chondrite-normalized REE plots. REE abundances were collected from single spots on multiple grains per sample. All samples showed typical continental zircon REE behavior where positive REE slope with the heavier REEs occurring in higher concentrations than the light REES. All REE patterns exhibit a positive Ce anomaly and negative Eu anomaly. REE concentrations were standardized against C1-chrondrite values (McDonough and Sun, 1995).

Figure 3.3. Plot of Europium anomaly against age. Two hundred sixty seven individual analyses, representing 20 samples, are shown. The red line indicates a qualitative representation of data trends. The dashed red line illustrates a possible secondary trend in the late Cretaceous. The Cretaceous and Jurassic flare-up events are represented by blue fields.

Figure 3.4. Fractionation markers (U/Yb vs Ce/Gd and [Hf]). Different symbols denote 10 my age brackets for the 267 analyses shown. As figure 5 illustrates a trend of decreasing U/Yb and Hf reverses at ~120Ma towards increasing U/Yb. An analogous reversal occurs in Hafnium concentration and Ce/Gd (a measure of REE slope from light REE to midweight REE). Greater Hafnium concentrations and greater Ce/Gd indicate greater fractionation (Barth and Wooden, 2010).

Figure 3.5. Geochemical discriminant diagrams for zircon from Grimes et al. (2007). 267 individual analyses from 20 samples are shown. The data presented in this study show consistent affinity for continental-type parental melts during crystallization of zircon. These results are in agreement with the Grimes et al. (2007) provenance models insofar as the continental arc fields are defined.

Figure 3.6. U/Yb trends with time for 267 analyses from 20 samples. Two systematic trends in the data are observed: (1) a pre-120Ma trend towards less fractionated melts and (2) a post-120Ma trend towards increasing fractionation of melts.

Figure 3.7. Compiled age, fractionation and apparent intrusive flux data. U-Pb ages from the central and northern Sierra Nevada batholith are compiled into a histogram. In total, 37 samples are included and show a contrasting profile to the apparent intrusive flux of Ducea (2001). Increased U/Yb in the central Sierra Nevada temporally corresponds with an increased occurrence of U-Pb ages in the central to northern extents of the Sierra Nevada batholith. We suspect a sampling bias is responsible for the mismatch observed between the histogram of central/northern Sierra Nevada ages and the apparent intrusive flux. A greater number of ages are available from the southern extents of the range. We suggest that the late-Cretaceous flare-up was initiated in the north about 10-15 my before the flare-up in the southern portions of the range and migrated southward.

Chapter 3 - Supplemental tables

Supplemental Table SP3.1. Individual analysis trace element data

Spot	Concentrations (ppm)													Ratios							
	U	Th	Y	La	Ce	Nd	Sm	Eu	Gd	Dy	Er	Yb	Hf	Hf/Yb	Yb/Gd	Ce/Sm	Y/Yb	Sm/Nd	Yb/Sm	Yb/Ce	Eu*
SN08AR04																					
1	470.3	255.8	769.6	0.02	13.63	1.56	2.89	1.17	20.97	69.28	130.1	280	10219	36.47	13.36	4.72	2.75	1.85	97.0	20.55	0.46
10	419.2	218.0	591.1	0.02	15.06	0.70	1.71	0.55	14.02	51.41	102.4	229	11086	48.38	16.34	8.82	2.58	2.46	134.1	15.21	0.34
11	315.2	117.1	421.8	0.01	11.80	0.26	0.78	0.30	7.13	31.77	75.4	185	10628	57.41	25.97	15.21	2.28	2.98	238.7	15.69	0.38
12	662.5	342.7	974.2	0.03	21.50	1.30	2.66	1.02	19.84	80.37	168.1	376	9701	25.78	18.97	8.10	2.59	2.04	141.7	17.50	0.43
2	401.2	163.8	328.1	0.03	13.06	0.20	0.61	0.24	5.94	26.42	58.4	137	11481	84.00	23.02	21.31	2.40	3.03	222.9	10.46	0.38
3	460.9	217.3	724.6	0.03	14.74	0.88	1.97	0.88	15.97	61.97	127.6	298	11032	37.03	18.65	7.49	2.43	2.24	151.4	20.21	0.48
4	319.9	131.0	545.9	0.01	14.30	0.33	1.14	0.41	9.84	43.03	97.6	224	10433	46.51	22.81	12.53	2.43	3.47	196.5	15.69	0.37
5	458.6	187.3	427.9	0.01	16.90	0.30	0.95	0.30	8.69	34.84	75.7	183	11769	64.16	21.11	17.77	2.33	3.13	192.9	10.86	0.31
6	331.3	118.2	268.0	0.01	11.10	0.16	0.44	0.16	4.08	22.00	48.9	123	11454	93.50	30.05	25.40	2.19	2.81	280.3	11.04	0.37
7	414.2	231.6	415.0	0.02	14.87	0.41	1.07	0.36	10.37	38.15	70.5	142	10413	73.16	13.72	13.85	2.92	2.62	132.6	9.57	0.33
8	328.3	98.3	383.3	0.01	8.81	0.22	0.58	0.26	6.76	29.43	68.6	176	10929	62.21	25.98	15.31	2.18	2.60	305.2	19.93	0.41
9	359.5	134.3	562.2	0.02	11.12	0.43	1.17	0.55	11.28	47.04	100.4	241	9470	39.22	21.40	9.46	2.33	2.74	205.5	21.72	0.46
avg	**411.7**	**184.6**	**534.3**	**0.02**	**13.91**	**0.56**	**1.33**	**0.52**	**11.24**	**44.64**	**93.6**	**216**	**10718**	**55.65**	**20.95**	**13.33**	**2.45**	**2.66**	**191.6**	**15.70**	**0.39**
SN08AR06																					
1	490.2	220.9	564.9	0.02	16.90	0.45	0.96	0.43	9.04	41.28	94.4	223	10485	46.96	24.68	17.67	2.53	2.11	233.4	13.21	0.45
10	438.9	188.6	340.2	0.01	12.35	0.21	0.60	0.33	6.49	27.61	58.8	141	11479	81.33	21.76	20.61	2.41	2.88	235.5	11.43	0.51
11	699.2	435.8	579.4	1.37	28.22	1.24	1.41	0.48	11.47	49.79	103.0	233	10825	46.50	20.29	20.04	2.49	1.14	165.3	8.25	0.36
12	401.3	223.3	299.9	0.03	11.47	0.31	0.68	0.26	5.79	24.72	51.4	122	10648	87.57	21.01	16.94	2.47	2.16	179.6	10.60	0.41
13	349.8	116.1	409.2	0.02	13.18	0.25	0.64	0.27	6.74	31.94	75.0	193	11132	57.57	28.69	20.74	2.12	2.54	304.3	14.67	0.40
14	591.0	270.7	724.5	0.02	20.71	0.50	1.26	0.51	12.39	57.00	128.9	306	9944	32.51	24.68	16.42	2.37	2.51	242.5	14.77	0.39
15	535.1	207.8	744.7	0.02	17.38	0.44	1.33	0.52	12.10	57.16	135.6	318	10188	32.04	26.27	13.08	2.34	3.00	239.3	18.30	0.39
16	584.6	314.8	749.5	0.02	21.26	0.58	1.50	0.62	12.88	63.61	134.0	302	10642	35.21	23.46	14.20	2.48	2.58	201.8	14.21	0.43
2	782.6	488.9	519.6	0.04	23.77	0.42	1.15	0.39	9.52	43.50	91.5	211	11009	52.10	22.19	20.61	2.46	2.76	183.2	8.89	0.36
3	446.6	191.9	533.6	0.02	15.46	0.40	1.03	0.43	10.23	42.16	91.9	214	10836	50.73	20.88	15.05	2.50	2.58	207.9	13.82	0.41
4	379.4	183.7	465.0	0.02	13.30	0.35	0.89	0.32	8.52	37.47	81.0	184	10697	58.04	21.63	14.92	2.52	2.57	206.7	13.85	0.36
5	351.6	150.1	343.7	0.06	11.63	0.35	0.77	0.29	6.55	27.85	60.9	147	10204	69.45	22.44	15.01	2.34	2.18	189.7	12.63	0.39
6	539.9	219.8	714.4	0.01	18.54	0.44	1.19	0.47	11.17	53.78	129.5	300	10261	34.25	26.82	15.56	2.38	2.72	251.3	16.16	0.39
7	323.5	131.3	313.0	0.07	10.57	0.27	0.67	0.26	6.24	25.89	55.4	130	9925	76.50	20.79	15.87	2.41	2.43	194.8	12.27	0.39
8	291.6	137.8	723.8	0.02	11.25	1.00	2.20	0.84	17.61	63.01	124.6	268	9553	35.60	15.24	5.12	2.70	2.19	122.1	23.86	0.41
9	329.5	126.3	378.6	0.01	13.58	0.16	0.58	0.26	6.43	30.63	68.1	167	10954	65.52	25.98	23.48	2.26	3.55	289.1	12.31	0.41
avg	**470.9**	**225.5**	**525.2**	**0.11**	**16.22**	**0.46**	**1.05**	**0.42**	**9.57**	**42.34**	**92.8**	**216**	**10549**	**53.87**	**22.93**	**16.58**	**2.42**	**2.49**	**215.4**	**13.70**	**0.40**

Supplemental Table SP3.1. Individual analysis trace element data

Spot	*Concentrations (ppm)*													*Ratios*							
	U	*Th*	*Y*	*La*	*Ce*	*Nd*	*Sm*	*Eu*	*Gd*	*Dy*	*Er*	*Yb*	*Hf*	*Hf/Yb*	*Yb/Gd*	*Ce/Sm*	*Y/Yb*	*Sm/Nd*	*Yb/Sm*	*Yb/Ce*	*Eu**
SN08AR11																					
1	140.1	81.5	660.7	0.02	15.55	0.97	2.05	0.93	14.81	57.42	117.6	272	10597	38.99	18.35	7.57	2.43	2.11	132.3	17.47	0.52
10	147.4	89.8	729.0	0.04	11.13	2.18	3.19	1.88	19.70	63.77	120.2	255	7818	30.66	12.94	3.49	2.86	1.47	79.8	22.91	0.72
11	100.0	26.1	126.2	0.01	5.50	0.08	0.19	0.13	1.97	9.70	22.8	62	11386	182.83	31.64	29.61	2.03	2.40	335.0	11.31	0.66
12	103.7	34.1	186.1	0.01	7.29	0.10	0.36	0.22	3.38	15.12	33.4	85	10727	125.79	25.21	20.26	2.18	3.51	236.9	11.70	0.61
13	100.4	38.5	405.8	0.08	8.21	0.37	0.93	0.55	6.12	30.26	74.1	188	7782	41.48	30.65	8.86	2.16	2.47	202.4	22.86	0.71
14	110.0	28.9	151.7	0.02	6.13	0.13	0.19	0.20	2.37	12.33	28.4	76	10645	140.45	31.92	31.79	2.00	1.53	392.9	12.36	0.88
15	288.4	236.5	1401.8	0.06	25.50	4.87	7.83	5.23	47.70	133.77	235.5	476	7421	15.58	9.99	3.26	2.94	1.61	60.8	18.68	0.82
16	98.4	55.6	552.3	0.04	10.62	1.71	2.50	1.46	15.41	48.91	95.0	200	9177	45.95	12.96	4.25	2.77	1.46	80.0	18.80	0.72
2	107.0	61.3	535.0	0.03	9.36	1.41	2.27	1.30	14.79	45.36	88.4	188	8251	43.82	12.73	4.12	2.84	1.61	82.8	20.11	0.68
3	88.0	34.4	192.9	0.02	7.97	0.10	0.32	0.24	3.30	14.94	34.1	88	9781	111.78	26.55	24.83	2.20	3.18	272.5	10.97	0.70
4	85.6	48.5	516.3	0.02	10.24	1.28	2.30	1.23	14.32	45.89	86.2	184	8720	47.33	12.86	4.46	2.80	1.80	80.2	17.98	0.65
5	87.1	49.5	491.0	0.02	10.52	1.09	2.29	1.32	14.00	45.11	82.8	177	9606	54.23	12.65	4.59	2.77	2.11	77.3	16.83	0.71
6	98.7	57.8	569.5	0.02	11.50	1.57	2.67	1.44	16.65	50.32	94.9	200	8831	44.12	12.02	4.31	2.85	1.70	75.0	17.41	0.66
7	124.5	52.4	580.7	0.02	10.22	0.58	1.10	0.79	9.85	42.59	102.0	256	7799	30.45	26.01	9.29	2.27	1.89	232.8	25.07	0.73
8	88.6	48.8	471.1	0.02	9.50	0.81	1.68	1.09	12.33	41.00	79.3	176	9492	53.78	14.32	5.67	2.67	2.07	105.3	18.58	0.73
9	136.0	83.7	754.6	0.04	11.12	2.16	3.67	2.18	21.46	68.09	126.1	259	7328	28.31	12.07	3.03	2.91	1.70	70.5	23.28	0.75
avg	**119.0**	**64.2**	**520.3**	**0.03**	**10.65**	**1.21**	**2.10**	**1.26**	**13.63**	**45.29**	**88.8**	**196**	**9085**	**64.72**	**18.93**	**10.59**	**2.54**	**2.04**	**157.3**	**17.90**	**0.70**
06-EW35																					
1	116.0	72.6	521.2	0.01	18.77	0.35	1.42	0.26	10.61	48.29	92.7	172	10663	62.10	16.18	13.22	3.04	4.09	121.0	9.15	0.20
2	117.9	119.0	1280.1	0.07	16.61	3.94	6.22	1.56	37.73	130.77	216.5	343	8361	24.35	9.10	2.67	3.73	1.58	55.2	20.68	0.31
3	90.4	90.3	1045.4	0.02	14.81	2.63	4.95	1.24	32.20	109.53	174.1	276	8967	32.49	8.57	2.99	3.79	1.88	55.8	18.64	0.30
4	85.6	52.8	415.4	0.03	15.99	0.27	0.83	0.22	8.55	38.06	73.1	140	10076	72.18	16.33	19.32	2.98	3.09	168.6	8.73	0.25
5	49.1	28.5	368.3	0.02	10.48	0.29	0.76	0.23	7.59	32.92	65.5	125	9786	78.40	16.44	13.72	2.95	2.66	163.4	11.91	0.30
6	84.9	49.7	399.3	0.01	15.74	0.22	0.77	0.20	7.22	36.49	72.6	139	10617	76.48	19.23	20.46	2.88	3.56	180.5	8.82	0.26
7	66.3	37.4	340.0	0.02	13.08	0.24	0.67	0.20	6.32	30.32	60.5	119	10473	87.87	18.87	19.42	2.85	2.83	176.9	9.11	0.30
8	71.2	47.2	430.5	0.01	15.45	0.29	0.91	0.26	8.87	39.78	75.8	140	9793	69.95	15.78	17.06	3.08	3.11	154.5	9.06	0.28
9	85.9	53.3	423.6	0.01	15.76	0.24	0.85	0.23	8.05	39.19	75.8	144	10509	72.94	17.91	18.50	2.94	3.56	169.1	9.14	0.27
10	66.8	64.1	863.9	0.02	13.49	1.50	3.32	0.94	25.71	88.83	143.5	233	9129	39.22	9.06	4.06	3.71	2.21	70.1	17.26	0.31
avg	**83.4**	**61.5**	**608.8**	**0.02**	**15.02**	**1.00**	**2.07**	**0.53**	**15.28**	**59.42**	**105.0**	**183**	**9838**	**61.60**	**14.75**	**13.14**	**3.19**	**2.86**	**131.5**	**12.25**	**0.28**

Supplemental Table SP3.1. Individual analysis trace element data

Spot	*Concentrations (ppm)*													*Ratios*							
	U	*Th*	*Y*	*La*	*Ce*	*Nd*	*Sm*	*Eu*	*Gd*	*Dy*	*Er*	*Yb*	*Hf*	*Hf/Yb*	*Yb/Gd*	*Ce/Sm*	*Y/Yb*	*Sm/Nd*	*Yb/Sm*	*Yb/Ce*	*Eu**
06-EW39																					
1	628.8	279.4	245.4	0.02	17.98	0.19	0.49	0.35	3.79	17.67	41.4	117	10649	90.94	30.92	36.54	2.10	2.62	238.0	6.51	0.79
2	539.3	217.2	179.1	0.01	14.12	0.13	0.35	0.29	3.04	12.43	30.3	87	11441	131.92	28.53	40.27	2.06	2.71	247.3	6.14	0.86
3	444.1	148.5	235.0	0.01	11.24	0.13	0.37	0.27	3.11	15.86	41.2	127	11157	87.66	40.87	30.03	1.85	2.88	340.1	11.33	0.76
4	766.0	338.6	271.1	0.02	20.23	0.17	0.44	0.34	3.51	18.35	47.0	137	11342	82.75	39.00	46.45	1.98	2.59	314.6	6.77	0.83
5	499.6	183.6	278.9	0.03	14.25	0.18	0.48	0.41	4.62	19.67	49.2	147	10502	71.35	31.83	29.41	1.89	2.68	303.8	10.33	0.84
6	624.5	293.2	227.0	0.02	18.62	0.22	0.54	0.40	4.69	17.76	39.2	106	10812	101.92	22.61	34.59	2.14	2.43	197.0	5.70	0.77
7	1182.8	611.1	338.6	0.02	31.77	0.23	0.60	0.39	5.24	21.90	55.8	170	11477	67.59	32.38	52.65	1.99	2.58	281.4	5.34	0.67
8	601.9	310.0	162.0	0.02	15.31	0.15	0.36	0.29	3.45	12.49	28.1	78	11328	145.94	22.50	42.39	2.09	2.38	214.9	5.07	0.78
avg	**660.9**	**297.7**	**242.1**	**0.02**	**17.94**	**0.18**	**0.45**	**0.34**	**3.93**	**17.02**	**41.5**	**121**	**11089**	**97.51**	**31.08**	**39.04**	**2.01**	**2.61**	**267.2**	**7.15**	**0.79**
SN08HH06																					
1	319.4	101.9	168.9	0.02	6.40	0.11	0.15	0.24	1.90	11.02	31.7	110	11204	101.82	57.85	42.23	1.53	1.39	726.6	17.20	1.36
2	331.1	230.7	282.0	0.04	5.55	0.49	0.74	0.78	5.98	24.94	52.0	130	6562	50.45	21.73	7.46	2.17	1.52	174.8	23.44	1.12
3	556.7	536.7	585.0	0.03	10.15	0.37	0.93	0.98	10.87	48.95	107.2	251	6618	26.38	23.08	10.96	2.33	2.47	270.8	24.71	0.95
4	598.2	583.1	626.7	0.05	9.02	0.69	1.13	1.18	11.75	54.25	117.0	276	6247	22.60	23.51	7.99	2.27	1.63	244.9	30.65	0.99
5	430.0	352.8	467.0	0.07	7.51	0.54	0.99	0.98	10.08	40.99	87.2	210	6477	30.80	20.86	7.60	2.22	1.82	212.9	28.02	0.95
6	173.0	113.5	212.0	0.04	4.31	0.42	0.73	0.59	5.09	18.90	39.1	95	6749	70.83	18.72	5.91	2.23	1.73	130.6	22.12	0.94
7	474.0	236.6	262.3	0.03	5.09	0.08	0.27	0.24	3.33	19.23	53.0	147	7055	47.86	44.25	18.54	1.78	3.61	537.1	28.97	0.75
8	285.0	206.5	316.7	0.06	6.51	0.69	1.02	0.94	7.58	28.57	58.8	143	6918	48.54	18.81	6.38	2.22	1.49	139.6	21.88	1.03
avg	**395.9**	**295.2**	**365.1**	**0.04**	**6.82**	**0.42**	**0.75**	**0.74**	**7.07**	**30.85**	**68.3**	**170**	**7229**	**49.91**	**28.60**	**13.38**	**2.09**	**1.96**	**304.7**	**24.62**	**1.01**
SN08HH07																					
1	265.0	139.5	495.9	0.02	13.44	0.37	0.94	0.35	8.97	41.09	88.8	192	9395	48.94	21.40	14.23	2.58	2.58	203.4	14.29	0.37
2	217.8	151.9	1494.6	0.05	9.52	2.53	5.28	1.58	43.51	156.67	257.2	416	8893	21.38	9.56	1.80	3.59	2.09	78.8	43.68	0.32
3	112.9	89.0	999.3	0.02	12.62	1.12	3.11	0.85	28.41	101.15	164.7	269	9139	34.04	9.45	4.05	3.72	2.79	86.2	21.28	0.28
4	356.4	152.4	375.1	0.03	12.05	0.21	0.64	0.22	6.30	29.27	68.7	173	11468	66.36	27.44	18.80	2.17	2.99	269.7	14.34	0.34
5	275.0	101.6	407.0	0.02	9.72	0.17	0.62	0.16	5.83	29.23	74.9	193	10761	55.80	33.06	15.59	2.11	3.70	309.2	19.83	0.26
6	80.9	55.0	812.9	0.02	6.26	1.36	3.21	1.30	25.64	85.91	140.0	234	8592	36.78	9.11	1.95	3.48	2.35	72.8	37.34	0.44
7	138.0	80.8	736.3	0.03	5.79	1.50	2.89	1.20	20.61	68.99	130.0	246	8361	33.92	11.96	2.00	2.99	1.92	85.3	42.60	0.47
8	337.9	163.6	467.5	0.02	14.84	0.32	0.84	0.24	7.69	37.08	81.8	190	10498	55.39	24.66	17.57	2.47	2.66	224.4	12.78	0.29
9	179.0	155.6	1149.5	0.03	16.97	1.31	3.30	0.78	31.92	113.64	193.0	316	9970	31.55	9.90	5.15	3.64	2.52	95.9	18.63	0.23
10	475.0	246.3	475.6	0.03	15.67	0.28	0.87	0.29	7.83	36.99	85.2	204	11677	57.19	26.08	17.92	2.33	3.12	233.4	13.03	0.33
11	234.4	177.9	1548.5	0.02	13.39	2.15	5.28	1.53	42.99	152.11	257.9	423	8956	21.18	9.84	2.53	3.66	2.45	80.0	31.58	0.31
12	290.5	189.4	1606.4	0.04	11.04	2.61	5.46	1.76	45.09	162.60	274.6	469	9014	19.21	10.41	2.02	3.42	2.09	86.0	42.51	0.34
avg	**246.9**	**141.9**	**880.7**	**0.03**	**11.77**	**1.16**	**2.70**	**0.85**	**22.90**	**84.56**	**151.4**	**277**	**9727**	**40.15**	**16.90**	**8.64**	**3.01**	**2.61**	**152.1**	**25.99**	**0.33**

Supplemental Table SP3.1. Individual analysis trace element data

Spot	*Concentrations (ppm)*													*Ratios*							
	U	*Th*	*Y*	*La*	*Ce*	*Nd*	*Sm*	*Eu*	*Gd*	*Dy*	*Er*	*Yb*	*Hf*	*Hf/Yb*	*Yb/Gd*	*Ce/Sm*	*Y/Yb*	*Sm/Nd*	*Yb/Sm*	*Yb/Ce*	*Eu**
SN08MD01																					
1	722.6	73.8	329.3	0.02	6.38	0.17	0.70	0.28	7.23	26.06	49.1	123	13676	111.04	17.04	9.12	2.67	4.22	176.1	19.31	0.38
2	507.0	109.9	71.2	0.02	5.05	0.30	0.96	0.21	5.35	8.65	6.8	9	11568	#####	1.59	5.24	8.38	3.25	8.8	1.68	0.29
3	1249.5	496.3	462.2	0.02	40.96	0.43	1.39	0.13	10.22	38.47	75.3	183	16947	92.57	17.92	29.47	2.52	3.20	131.7	4.47	0.10
4	391.4	280.0	706.8	0.03	32.64	2.60	5.75	0.64	30.49	73.49	107.3	201	13110	65.13	6.60	5.67	3.51	2.21	35.0	6.17	0.15
5	1029.7	343.8	254.0	0.02	21.39	0.26	0.80	0.13	5.33	19.66	41.8	118	14119	119.95	22.07	26.74	2.16	3.09	147.2	5.50	0.19
6	1406.9	522.6	357.4	0.03	25.23	0.43	1.02	0.13	8.19	28.87	59.3	152	13918	91.28	18.63	24.66	2.34	2.39	149.0	6.04	0.13
7	749.4	183.4	229.9	0.14	16.75	0.46	0.71	0.08	4.77	18.32	38.5	100	15074	150.95	20.93	23.74	2.30	1.53	141.5	5.96	0.13
8	303.0	236.8	607.5	0.04	31.91	3.58	6.55	0.71	29.35	65.34	87.7	160	12083	75.65	5.44	4.88	3.80	1.83	24.4	5.01	0.16
9	1141.7	70.4	406.0	0.02	3.61	0.28	1.36	0.42	13.96	41.24	45.3	64	13409	208.81	4.60	2.65	6.32	4.91	47.1	17.81	0.29
10	838.3	23.7	309.3	0.02	1.81	0.16	0.93	0.37	11.72	34.42	30.6	36	14529	404.84	3.06	1.94	8.62	6.03	38.4	19.79	0.34
11	1223.4	214.2	219.4	0.02	8.47	0.31	0.97	0.23	6.73	20.70	30.6	66	13730	206.75	9.86	8.78	3.30	3.15	68.8	7.84	0.28
12	682.7	259.9	363.4	0.02	31.27	0.30	1.09	0.10	8.46	30.30	58.6	137	16053	116.89	16.23	28.71	2.65	3.60	126.1	4.39	0.10
13	850.2	568.2	591.5	0.03	31.31	1.72	3.06	0.54	18.73	51.47	93.2	223	14527	65.20	11.89	10.24	2.65	1.78	72.9	7.12	0.22
14	1100.1	373.6	302.2	1.09	23.83	2.48	1.89	0.25	8.12	25.97	48.4	114	12456	109.16	14.05	12.64	2.65	0.76	60.5	4.79	0.19
15	659.7	193.1	150.8	0.03	15.12	0.13	0.39	0.10	2.60	11.30	25.1	72	13868	193.03	27.67	39.08	2.10	2.87	185.7	4.75	0.29
16	1664.5	373.9	396.0	0.19	20.17	0.60	1.11	0.20	8.84	29.92	63.1	171	13603	79.47	19.37	18.24	2.31	1.85	154.8	8.49	0.19
avg	**907.5**	**270.2**	**359.8**	**0.11**	**19.74**	**0.89**	**1.79**	**0.28**	**11.26**	**32.76**	**53.8**	**121**	**13917**	**215.69**	**13.56**	**15.74**	**3.64**	**2.92**	**98.0**	**8.07**	**0.21**
SN08MD07																					
1	337.4	129.7	271.3	0.03	10.61	0.22	0.49	0.22	4.65	21.29	46.8	122	11011	90.30	26.24	21.57	2.23	2.19	247.9	11.49	0.44
2	226.0	97.5	256.4	0.01	7.72	0.12	0.35	0.15	4.36	19.76	45.7	122	12193	100.29	27.86	21.82	2.11	3.07	343.5	15.74	0.38
3	163.9	99.8	494.3	0.02	10.04	0.23	0.87	0.31	9.45	43.38	87.5	177	9880	55.70	18.77	11.56	2.79	3.74	204.4	17.68	0.33
4	553.0	108.4	409.4	0.02	15.85	0.29	0.70	0.29	6.97	33.00	73.3	189	13019	68.86	27.14	22.74	2.17	2.43	271.3	11.93	0.40
5	383.4	74.5	384.3	0.02	11.89	0.22	0.68	0.30	5.74	28.75	67.8	181	10983	60.76	31.50	17.53	2.13	3.14	266.5	15.20	0.46
6	335.1	68.1	434.6	0.02	10.66	0.23	0.71	0.30	6.73	32.39	78.5	203	10515	51.85	30.13	14.99	2.14	3.03	285.1	19.02	0.42
7	272.6	247.5	594.9	0.01	15.92	0.51	1.25	0.49	13.11	56.04	103.6	203	10248	50.57	15.46	12.77	2.94	2.43	162.6	12.73	0.37
8	202.7	157.1	423.9	0.03	9.86	0.25	0.67	0.29	7.40	33.96	73.4	172	9836	57.21	23.22	14.74	2.47	2.71	257.0	17.44	0.39
9	175.9	123.0	253.8	0.02	7.64	0.11	0.40	0.17	4.26	20.73	45.4	112	11778	104.78	26.37	19.19	2.26	3.60	282.2	14.70	0.39
10	240.5	134.7	413.5	0.02	10.76	0.23	0.65	0.27	6.25	31.38	74.4	183	10684	58.45	29.23	16.45	2.26	2.84	279.5	16.99	0.41
11	276.9	82.4	368.4	0.02	9.81	0.17	0.53	0.22	5.74	29.83	68.3	178	11753	66.09	30.97	18.45	2.07	3.13	334.5	18.13	0.39
12	231.5	62.4	339.5	0.03	14.20	0.20	0.72	0.30	6.49	29.88	61.4	132	10661	80.95	20.29	19.85	2.58	3.64	184.1	9.27	0.42
avg	**283.2**	**115.4**	**387.0**	**0.02**	**11.25**	**0.23**	**0.67**	**0.28**	**6.76**	**31.70**	**68.8**	**164**	**11047**	**70.48**	**25.60**	**17.64**	**2.34**	**3.00**	**259.9**	**15.03**	**0.40**

Supplemental Table SP3.1. Individual analysis trace element data

Spot	*Concentrations (ppm)*													*Ratios*							
	U	***Th***	***Y***	***La***	***Ce***	***Nd***	***Sm***	***Eu***	***Gd***	***Dy***	***Er***	***Yb***	***Hf***	***Hf/Yb***	***Yb/Gd***	***Ce/Sm***	***Y/Yb***	***Sm/Nd***	***Yb/Sm***	***Yb/Ce***	***Eu****
SN08MH01																					
1	338.4	175.6	614.8	0.02	22.46	0.49	1.28	0.28	13.49	56.47	106.2	194	10688	55.01	14.41	17.50	3.16	2.61	151.4	8.65	0.21
2	126.6	145.6	491.7	0.03	14.89	0.29	1.04	0.26	10.44	45.46	86.3	154	10184	66.00	14.78	14.37	3.19	3.59	148.9	10.37	0.24
3	281.4	179.1	545.4	0.01	19.99	0.45	1.09	0.25	12.01	51.16	96.1	174	10541	60.59	14.49	18.41	3.14	2.40	160.2	8.70	0.21
4	131.5	120.7	716.1	0.01	12.85	0.33	1.17	0.47	14.81	68.91	124.6	210	10178	48.38	14.21	11.00	3.40	3.55	180.2	16.37	0.35
5	105.9	71.7	633.1	0.02	12.21	0.55	1.80	0.50	18.10	66.75	108.8	178	9500	53.52	9.81	6.80	3.57	3.28	98.9	14.53	0.27
6	419.2	141.3	562.9	0.01	23.47	0.35	1.01	0.18	11.19	51.32	99.5	195	12178	62.59	17.39	23.18	2.89	2.93	192.1	8.29	0.16
7	198.5	86.6	874.9	0.05	17.60	1.15	2.94	0.75	26.45	89.92	146.8	245	10193	41.67	9.25	5.99	3.58	2.55	83.2	13.90	0.26
8	196.6	74.7	1101.1	0.01	19.53	1.51	3.62	0.75	33.40	115.97	182.6	285	10260	35.98	8.54	5.39	3.86	2.40	78.7	14.60	0.21
9	321.0	182.5	686.9	0.01	22.59	0.28	1.11	0.23	13.75	60.36	118.2	226	11701	51.71	16.45	20.31	3.04	4.04	203.5	10.02	0.18
10	291.8	158.7	705.8	0.03	18.21	0.60	1.50	0.36	15.93	63.56	122.9	227	9840	43.34	14.25	12.11	3.11	2.51	151.0	12.47	0.23
11	373.5	165.2	647.7	0.02	23.06	0.50	1.37	0.26	12.78	59.27	113.5	219	10783	49.22	17.15	16.85	2.96	2.76	160.1	9.50	0.19
12	194.5	158.3	708.9	0.02	15.86	0.74	2.20	0.49	18.36	71.79	124.3	214	11426	53.39	11.66	7.20	3.31	2.97	97.2	13.49	0.24
avg	**248.2**	**138.3**	**690.8**	**0.02**	**18.56**	**0.60**	**1.68**	**0.40**	**16.73**	**66.74**	**119.1**	**210**	**10623**	**51.78**	**13.53**	**13.26**	**3.27**	**2.97**	**142.1**	**11.74**	**0.23**
SN08MH05																					
1	168.3	152.8	1139.4	0.06	19.73	4.08	5.69	1.14	41.65	118.98	178.7	270	8884	32.96	6.47	3.47	4.23	1.40	47.3	13.66	0.23
2	134.9	135.1	1076.9	0.03	19.19	2.47	4.94	0.96	36.76	114.74	169.3	255	9171	36.00	6.93	3.89	4.23	2.00	51.6	13.28	0.22
3	125.3	133.1	888.4	0.03	17.05	1.15	2.52	0.59	26.66	93.33	142.2	228	9628	42.16	8.57	6.76	3.89	2.18	90.6	13.40	0.22
4	143.8	114.6	1069.2	0.02	20.15	2.63	5.03	1.00	37.45	114.45	167.3	252	9234	36.65	6.73	4.01	4.24	1.91	50.1	12.51	0.22
5	177.7	141.6	1125.7	0.03	23.65	1.34	3.38	0.70	34.73	117.00	186.1	288	10843	37.68	8.29	6.99	3.91	2.53	85.0	12.17	0.20
6	165.9	169.0	1168.9	0.01	23.16	1.93	4.49	0.89	38.51	123.63	185.1	282	10221	36.23	7.33	5.16	4.14	2.33	62.9	12.18	0.21
7	128.9	163.8	951.3	0.02	17.88	0.91	2.78	0.58	28.55	98.00	153.3	243	9843	40.51	8.51	6.43	3.91	3.06	87.4	13.59	0.20
8	135.7	120.6	969.7	0.01	19.40	1.20	2.89	0.71	27.74	100.66	160.0	253	10476	41.43	9.12	6.71	3.83	2.41	87.5	13.04	0.24
9	139.5	123.7	1090.8	0.04	18.54	3.14	5.67	1.16	38.35	118.72	175.2	265	9014	34.07	6.90	3.27	4.12	1.81	46.7	14.27	0.24
10	142.1	135.1	1000.6	0.02	19.30	1.43	3.37	0.72	31.00	103.95	159.0	249	9581	38.52	8.03	5.72	4.02	2.36	73.8	12.89	0.22
avg	**146.2**	**138.9**	**1048.1**	**0.03**	**19.80**	**2.03**	**4.08**	**0.85**	**34.14**	**110.34**	**167.6**	**258**	**9689**	**37.62**	**7.69**	**5.24**	**4.05**	**2.20**	**68.3**	**13.10**	**0.22**

Supplemental Table SP3.1. Individual analysis trace element data

Spot	Concentrations (ppm)													Ratios							
	U	Th	Y	La	Ce	Nd	Sm	Eu	Gd	Dy	Er	Yb	Hf	Hf/Yb	Yb/Gd	Ce/Sm	Y/Yb	Sm/Nd	Yb/Sm	Yb/Ce	Eu*
SN08MH11																					
1	190.0	86.9	643.1	0.02	13.52	0.43	0.83	0.46	9.03	48.32	119.6	288	9249	32.13	31.87	16.26	2.23	1.95	346.1	21.29	0.51
2	129.8	63.5	438.4	0.49	15.20	1.20	1.05	0.52	6.82	34.35	81.8	201	9604	47.72	29.51	14.42	2.18	0.88	191.0	13.24	0.59
3	85.9	70.6	649.9	0.02	8.08	1.31	2.37	1.14	18.04	62.06	116.2	229	8541	37.29	12.70	3.42	2.84	1.81	96.8	28.34	0.53
4	83.2	47.1	607.5	0.02	8.08	1.33	2.27	1.15	16.10	59.11	109.5	222	8591	38.70	13.78	3.57	2.74	1.70	98.0	27.49	0.58
5	135.6	48.4	374.3	0.02	11.41	0.24	0.51	0.25	6.36	29.39	69.3	162	9959	61.44	25.50	22.46	2.31	2.10	319.1	14.21	0.42
6	77.1	59.6	557.0	0.01	7.88	0.88	1.91	1.07	15.11	52.54	97.7	196	8205	41.94	12.95	4.13	2.85	2.17	102.5	24.84	0.61
7	138.1	91.0	487.6	0.01	11.32	0.29	0.75	0.37	7.30	36.32	91.7	225	9460	41.98	30.87	15.13	2.16	2.61	301.0	19.90	0.48
8	152.6	51.1	606.5	0.05	12.26	0.54	1.21	0.58	10.26	50.17	114.7	263	8866	33.74	25.60	10.15	2.31	2.25	217.5	21.43	0.51
9	74.7	99.0	373.8	0.01	6.37	0.28	0.82	0.59	8.06	33.11	70.2	153	9087	59.27	19.02	7.81	2.44	2.89	188.0	24.07	0.70
10	142.3	45.4	515.2	0.02	12.02	0.38	0.76	0.45	7.99	41.37	96.4	237	9506	40.05	29.71	15.78	2.17	2.01	311.5	19.74	0.56
11	156.4	49.2	530.0	0.02	11.18	0.37	0.98	0.47	9.21	42.77	101.9	245	8991	36.64	26.65	11.37	2.16	2.66	249.5	21.95	0.48
12	72.5	54.3	548.1	0.02	7.55	0.84	1.81	1.03	15.24	53.69	98.1	195	8555	43.77	12.82	4.17	2.80	2.16	108.0	25.88	0.60
13	71.9	68.9	518.5	0.02	7.82	0.62	1.64	0.88	13.05	47.94	90.8	187	8442	45.24	14.29	4.76	2.78	2.64	113.6	23.86	0.58
14	147.9	54.3	555.0	0.02	10.47	0.36	0.83	0.55	8.41	44.28	106.0	254	8539	33.63	30.20	12.61	2.19	2.29	305.7	24.25	0.63
15	168.1	50.8	481.0	0.12	9.16	0.67	1.25	0.70	10.92	42.06	85.6	203	9285	45.69	18.60	7.35	2.37	1.86	163.0	22.17	0.58
16	79.4	63.0	623.5	0.03	7.63	1.17	2.34	1.18	16.33	60.62	110.4	215	8549	39.81	13.15	3.27	2.90	1.99	91.9	28.13	0.58
17	185.4	50.6	422.5	0.02	12.92	0.27	0.81	0.31	7.46	35.68	79.0	182	9542	52.51	24.35	15.89	2.32	3.03	223.5	14.06	0.38
18	72.5	58.5	525.7	0.02	7.22	0.88	1.80	0.96	14.20	50.93	93.5	189	8489	44.82	13.33	4.00	2.78	2.05	104.9	26.25	0.58
19	112.3	89.3	262.2	0.01	8.66	0.18	0.40	0.28	4.33	21.88	49.0	121	10073	83.39	27.92	21.42	2.17	2.31	298.8	13.95	0.65
20	158.9	40.6	546.2	0.02	12.22	0.44	0.87	0.41	8.91	43.03	104.6	252	9665	38.32	28.29	14.11	2.17	1.97	291.3	20.64	0.45
avg	**121.7**	**62.1**	**513.3**	**0.05**	**10.05**	**0.63**	**1.26**	**0.67**	**10.66**	**44.48**	**94.3**	**211**	**9060**	**44.90**	**22.06**	**10.60**	**2.44**	**2.17**	**206.1**	**21.78**	**0.55**
SN08RM01																					
1	902.6	800.2	4225.9	0.03	62.49	3.45	8.58	5.06	76.59	343.22	738.7	1613	6733	4.18	21.06	7.28	2.62	2.49	187.9	25.80	0.60
2	722.6	441.4	2296.1	0.02	34.04	1.64	4.40	2.69	37.55	181.41	403.2	933	7133	7.64	24.85	7.73	2.46	2.68	211.9	27.42	0.64
3	249.9	101.7	408.5	0.01	10.65	0.32	0.85	0.28	6.97	33.02	74.4	185	9945	53.88	26.50	12.55	2.21	2.62	217.6	17.33	0.36
4	1043.7	443.3	794.2	0.02	29.58	0.42	1.17	0.47	13.48	65.11	140.6	326	12421	38.14	24.16	25.35	2.44	2.75	279.1	11.01	0.36
5	236.5	8.8	62.0	0.02	1.60	0.01	0.02	0.02	0.21	3.26	16.1	73	7646	104.84	339.44	90.05	0.85	1.96	4095.8	45.48	1.00
6	142.0	72.3	999.2	0.02	6.21	2.03	3.76	1.99	26.35	96.84	173.9	346	8907	25.74	13.13	1.65	2.89	1.85	92.0	55.70	0.61
7	1348.2	388.5	1127.2	416.65	587.60	118.99	27.52	7.48	54.59	75.86	146.2	349	8346	23.95	6.38	21.35	3.23	0.23	12.7	0.59	0.59
8	696.1	462.9	2283.3	0.02	36.56	1.69	3.65	2.87	36.78	176.78	404.0	949	6819	7.19	25.79	10.03	2.41	2.16	260.2	25.95	0.75
9	593.5	33.9	148.4	0.03	3.81	0.04	0.11	0.13	1.35	9.60	29.9	94	10724	114.04	69.53	33.23	1.58	2.79	820.8	24.70	0.97
10	289.3	117.4	949.9	0.02	12.55	0.53	1.42	1.13	13.19	69.49	174.7	460	7230	15.70	34.90	8.84	2.06	2.68	324.3	36.69	0.80
11	541.0	60.4	324.1	0.02	4.57	0.28	0.66	0.29	4.69	20.87	66.4	199	8021	40.38	42.35	6.88	1.63	2.35	299.4	43.50	0.50
12	228.3	104.1	1124.7	0.02	9.84	0.94	2.46	1.15	23.29	101.55	203.1	417	7375	17.69	17.90	4.00	2.70	2.63	169.3	42.36	0.46
13	1112.8	1091.8	4595.2	0.02	78.10	4.22	9.77	5.92	84.18	387.39	792.3	1650	7439	4.51	19.60	7.99	2.78	2.32	168.9	21.13	0.63
avg	**623.6**	**317.4**	**1487.6**	**32.07**	**67.51**	**10.35**	**4.95**	**2.27**	**29.17**	**120.34**	**258.7**	**584**	**8364**	**35.22**	**51.20**	**18.23**	**2.30**	**2.27**	**549.2**	**29.05**	**0.64**

Supplemental Table SP3.1. Individual analysis trace element data

Spot	Concentrations (ppm)													Ratios							
	U	Th	Y	La	Ce	Nd	Sm	Eu	Gd	Dy	Er	Yb	Hf	Hf/Yb	Yb/Gd	Ce/Sm	Y/Yb	Sm/Nd	Yb/Sm	Yb/Ce	Eu*
SN08RM10																					
1	333.1	138.5	656.8	0.02	15.05	0.36	1.20	0.18	11.27	57.87	122.7	248	10970	44.15	22.04	12.56	2.64	3.33	207.3	16.51	0.15
2	435.7	144.8	1184.0	0.01	14.19	0.48	1.91	0.17	21.03	107.42	218.7	400	10751	26.86	19.04	7.41	2.96	4.01	209.1	28.21	0.08
3	501.8	311.4	1303.0	0.10	21.54	1.34	3.03	0.86	25.02	118.17	240.9	500	10593	21.20	19.97	7.10	2.61	2.26	164.6	23.20	0.30
4	492.5	125.9	790.0	0.01	8.61	0.15	0.85	0.14	9.43	59.59	147.5	344	10990	31.98	36.44	10.08	2.30	5.59	402.3	39.92	0.15
5	195.9	70.3	673.2	0.02	9.81	0.57	1.66	0.35	13.22	59.05	116.3	230	11736	50.95	17.42	5.90	2.92	2.94	138.7	23.49	0.23
6	449.3	189.1	865.9	0.02	16.51	0.40	1.43	0.24	14.43	75.83	164.9	336	10976	32.64	23.30	11.50	2.58	3.59	234.3	20.37	0.16
7	285.1	170.8	1366.6	-0.02	19.78	2.17	4.50	0.96	32.18	129.70	239.0	451	9333	20.69	14.02	4.39	3.03	2.08	100.2	22.81	0.24
8	623.9	219.8	898.4	0.02	14.99	0.26	1.12	0.11	12.99	73.21	167.6	365	12011	32.90	28.10	13.35	2.46	4.36	325.1	24.35	0.09
9	612.0	241.4	828.3	0.02	14.49	0.29	1.07	0.19	11.43	67.12	152.9	331	11725	35.42	28.97	13.50	2.50	3.76	308.5	22.85	0.17
10	623.7	187.1	944.9	1.23	24.25	7.04	4.32	1.01	16.96	70.14	162.5	397	13202	33.25	23.42	5.61	2.38	0.61	91.9	16.37	0.36
11	656.9	230.3	911.2	0.02	16.29	0.29	1.17	0.22	12.05	73.84	168.4	372	11296	30.34	30.91	13.93	2.45	4.06	318.4	22.85	0.18
12	583.5	383.2	1574.7	0.03	29.48	1.26	3.83	0.51	37.01	162.68	283.1	469	8912	18.99	12.68	7.70	3.36	3.03	122.6	15.92	0.13
13	322.4	264.0	1915.6	0.08	16.62	5.18	9.44	4.43	58.63	190.97	317.2	617	8085	13.09	10.53	1.76	3.10	1.82	65.4	37.15	0.57
14	233.2	102.7	672.1	0.02	13.06	0.58	1.54	0.29	13.22	67.32	123.1	223	9384	42.10	16.86	8.51	3.01	2.65	145.2	17.06	0.20
15	237.0	510.7	3158.8	0.36	84.40	24.96	31.98	18.60	149.11	362.47	480.3	806	7231	8.97	5.41	2.64	3.92	1.28	25.2	9.55	0.82
avg	**439.1**	**219.3**	**1182.9**	**0.13**	**21.27**	**3.02**	**4.60**	**1.89**	**29.20**	**111.69**	**207.0**	**406**	**10480**	**29.57**	**20.61**	**8.40**	**2.81**	**3.03**	**190.6**	**22.71**	**0.26**
SN08TD04																					
1	930.2	351.5	857.1	1.84	28.14	5.83	4.97	0.72	18.76	70.13	149.5	330	10411	31.59	17.56	5.66	2.60	0.85	66.3	11.71	0.23
2	508.5	93.3	479.9	0.01	7.74	0.08	0.31	0.03	5.14	36.06	92.5	216	13866	64.06	42.13	24.58	2.22	4.14	687.7	27.98	0.07
3	642.5	250.7	1165.8	0.02	24.58	0.85	2.29	0.33	23.10	106.85	203.7	370	10271	27.74	16.03	10.72	3.15	2.70	161.5	15.06	0.14
4	911.7	340.4	707.9	0.03	17.06	0.29	0.99	0.22	11.86	57.93	127.0	287	11242	39.11	24.24	17.15	2.46	3.43	289.0	16.85	0.20
5	631.2	192.9	977.7	0.06	16.74	0.55	1.70	0.41	13.50	73.79	179.0	489	13028	26.62	36.25	9.82	2.00	3.10	287.3	29.24	0.26
6	499.7	176.5	1227.4	0.03	22.01	0.48	2.32	0.29	20.66	107.48	221.5	439	14053	31.98	21.27	9.48	2.79	4.84	189.2	19.96	0.13
7	876.3	274.3	842.7	0.01	19.18	0.38	1.16	0.16	12.02	66.53	153.8	349	12124	34.74	29.03	16.48	2.41	3.03	299.9	18.20	0.13
8	1057.3	222.1	887.1	0.04	13.16	0.21	0.87	0.16	9.23	64.68	161.7	408	12128	29.69	44.25	15.08	2.17	4.24	468.2	31.05	0.17
9	788.8	682.5	2838.9	0.13	30.26	8.46	15.55	5.89	100.77	297.00	457.1	809	7848	9.70	8.03	1.95	3.51	1.84	52.0	26.72	0.45
10	474.2	164.4	1066.6	0.03	18.81	0.75	2.60	0.34	24.15	103.78	188.7	328	9972	30.40	13.58	7.22	3.25	3.48	125.9	17.44	0.13
11	569.7	148.7	821.3	0.03	11.71	0.15	0.80	0.11	10.22	64.12	152.3	340	12859	37.81	33.27	14.69	2.41	5.28	426.6	29.05	0.12
12	681.3	149.6	1218.5	0.38	11.54	0.85	1.84	0.16	18.38	104.57	227.8	448	11512	25.70	24.36	6.26	2.72	2.17	243.0	38.79	0.09
13	1880.2	564.3	1165.5	3.43	35.18	5.24	3.55	0.47	20.59	96.99	211.2	468	11842	25.32	22.72	9.91	2.49	0.68	131.8	13.30	0.17
14	519.0	180.7	524.5	0.02	12.61	0.26	0.82	0.31	8.19	41.39	94.7	221	10490	47.38	27.02	15.29	2.37	3.14	268.5	17.56	0.36
15	735.3	236.4	628.0	0.03	15.18	0.30	0.94	0.22	9.59	50.92	113.2	255	10745	42.16	26.58	16.20	2.46	3.18	272.0	16.79	0.22
avg	**780.4**	**268.6**	**1027.3**	**0.41**	**18.93**	**1.64**	**2.72**	**0.66**	**20.41**	**89.48**	**182.3**	**384**	**11493**	**33.60**	**25.76**	**12.03**	**2.60**	**3.07**	**264.6**	**21.98**	**0.19**

Supplemental Table SP3.1. Individual analysis trace element data

Spot	*Concentrations (ppm)*													*Ratios*							
	U	*Th*	*Y*	*La*	*Ce*	*Nd*	*Sm*	*Eu*	*Gd*	*Dy*	*Er*	*Yb*	*Hf*	*Hf/Yb*	*Yb/Gd*	*Ce/Sm*	*Y/Yb*	*Sm/Nd*	*Yb/Sm*	*Yb/Ce*	*Eu**
SN08YH05																					
1	242.1	199.7	748.7	0.05	33.52	2.52	4.85	0.70	26.76	70.39	114.9	217	10547	48.52	8.12	6.91	3.44	1.92	44.8	6.48	0.19
2	325.2	276.7	821.1	0.03	34.55	2.71	5.64	1.10	31.91	89.98	150.4	295	13475	45.63	9.25	6.12	2.78	2.08	52.3	8.55	0.25
3	181.3	143.6	670.7	0.03	31.54	1.52	4.16	0.71	25.22	65.68	105.2	199	12485	62.59	7.91	7.58	3.36	2.74	47.9	6.32	0.21
4	258.4	221.7	889.0	0.05	38.11	2.66	5.33	0.83	32.78	90.54	142.7	271	12874	47.51	8.27	7.15	3.28	2.00	50.8	7.11	0.19
5	200.1	164.5	688.3	0.02	33.12	1.68	4.01	0.66	25.63	67.67	106.0	204	11400	55.99	7.94	8.26	3.38	2.39	50.8	6.15	0.20
6	216.7	180.3	743.6	0.03	35.27	2.04	4.62	0.70	27.12	73.33	114.2	218	11901	54.67	8.03	7.63	3.42	2.27	47.1	6.17	0.19
7	174.4	137.0	585.4	0.03	30.54	1.14	3.20	0.52	20.54	56.45	90.1	176	11853	67.46	8.56	9.54	3.33	2.80	54.9	5.75	0.20
8	281.3	237.4	876.9	0.04	36.47	3.07	5.37	0.86	29.89	86.69	137.8	259	11353	43.86	8.66	6.79	3.39	1.75	48.2	7.10	0.21
9	182.7	146.4	661.6	0.02	32.54	1.25	3.39	0.59	23.20	65.31	102.6	199	12381	62.37	8.56	9.61	3.33	2.71	58.6	6.10	0.20
10	298.5	249.1	886.9	0.04	40.54	2.82	5.52	0.77	31.12	87.91	137.7	268	11418	42.62	8.61	7.34	3.31	1.96	48.5	6.61	0.18
11	193.3	97.3	376.4	0.02	29.41	0.47	1.42	0.24	9.62	32.19	63.6	147	12350	83.98	15.29	20.66	2.56	3.06	103.3	5.00	0.20
12	235.7	194.5	792.6	0.03	36.65	2.09	4.68	0.80	30.01	78.88	123.1	238	12664	53.19	7.93	7.83	3.33	2.24	50.9	6.50	0.20
13	298.3	245.0	905.6	0.06	40.02	3.30	5.55	0.84	30.79	88.78	144.0	279	12585	45.07	9.07	7.21	3.24	1.68	50.3	6.98	0.20
avg	**237.5**	**191.8**	**742.1**	**0.03**	**34.79**	**2.10**	**4.44**	**0.72**	**26.51**	**73.37**	**117.9**	**228**	**12099**	**54.88**	**8.94**	**8.67**	**3.24**	**2.28**	**54.5**	**6.52**	**0.20**
SN08YH11																					
1	1691.2	780.8	148.8	0.03	52.94	0.30	0.48	0.15	3.55	11.18	22.3	70	14828	212.38	19.66	111.45	2.13	1.57	147.0	1.32	0.35
2	1353.5	625.4	127.5	0.03	44.29	0.27	0.48	0.14	2.92	9.50	19.1	60	15214	253.59	20.55	92.86	2.13	1.75	125.8	1.35	0.36
3	962.7	278.2	154.7	0.03	28.31	0.15	0.38	0.12	2.48	9.79	24.0	87	14981	172.69	35.01	74.14	1.78	2.63	227.2	3.06	0.39
4	1961.9	1010.7	403.8	0.05	59.04	1.49	2.40	0.65	12.44	30.76	58.9	167	14684	87.80	13.45	24.58	2.41	1.61	69.6	2.83	0.36
5	2488.5	1456.0	402.9	0.03	91.91	0.64	1.28	0.37	9.11	29.27	59.4	172	14587	84.72	18.90	71.99	2.34	2.00	134.9	1.87	0.33
6	1491.6	580.5	192.6	0.02	52.11	0.30	0.58	0.19	4.21	13.12	29.1	92	15057	163.24	21.90	89.36	2.09	1.94	158.2	1.77	0.36
7	2151.5	1125.0	190.7	0.03	67.52	0.42	0.80	0.23	4.96	14.65	29.2	89	15153	170.29	17.95	84.13	2.14	1.91	110.9	1.32	0.36
8	1079.7	308.9	166.7	0.03	30.33	0.15	0.41	0.12	2.98	10.93	26.5	97	15876	163.30	32.61	74.30	1.71	2.69	238.2	3.21	0.34
9	2141.3	1245.4	188.2	0.04	75.96	0.73	1.27	0.31	6.41	16.00	28.3	81	14870	184.01	12.60	59.99	2.33	1.74	63.8	1.06	0.33
10	918.7	274.4	151.3	0.03	28.91	0.21	0.36	0.13	2.68	10.25	23.6	80	14792	184.44	29.92	81.27	1.89	1.72	225.5	2.77	0.40
11	2227.6	998.7	215.1	0.02	69.34	0.39	0.83	0.23	5.52	16.13	33.2	100	15829	157.90	18.15	84.04	2.15	2.10	121.5	1.45	0.33
avg	**1678.9**	**789.5**	**212.9**	**0.03**	**54.61**	**0.46**	**0.84**	**0.24**	**5.21**	**15.60**	**32.1**	**100**	**15079**	**166.76**	**21.88**	**77.10**	**2.10**	**1.97**	**147.5**	**2.00**	**0.36**

Supplemental Table SP3.1. Individual analysis trace element data

Spot	Concentrations (ppm)													Ratios							
	U	Th	Y	La	Ce	Nd	Sm	Eu	Gd	Dy	Er	Yb	Hf	Hf/Yb	Yb/Gd	Ce/Sm	Y/Yb	Sm/Nd	Yb/Sm	Yb/Ce	Eu*
SN08YH13																					
1	379.8	278.7	579.7	0.02	29.09	2.29	5.09	0.62	26.95	61.44	85.1	156	12462	79.89	5.79	5.71	3.72	2.23	30.6	5.36	0.16
2	440.5	190.6	338.2	0.03	32.77	0.34	1.13	0.12	8.00	28.98	53.7	118	15352	130.39	14.71	28.92	2.87	3.29	103.9	3.59	0.12
3	57.2	47.4	577.2	0.06	32.18	4.31	7.75	2.47	36.50	65.56	81.9	146	10429	71.30	4.01	4.15	3.95	1.80	18.9	4.55	0.45
4	532.9	382.1	705.8	0.04	37.74	2.93	5.39	0.69	28.60	71.64	106.0	198	13134	66.42	6.91	7.00	3.57	1.84	36.7	5.24	0.17
5	621.0	236.1	217.6	0.02	26.56	0.22	0.65	0.13	5.01	17.32	33.4	93	15766	170.42	18.48	40.60	2.35	2.91	141.4	3.48	0.22
6	661.3	267.9	225.7	0.02	30.13	0.27	0.78	0.18	6.21	18.54	34.4	93	15571	167.42	14.98	38.46	2.43	2.92	118.7	3.09	0.24
7	632.6	276.0	228.6	0.02	30.51	0.49	1.20	0.23	6.20	20.18	35.9	92	14102	153.37	14.82	25.32	2.49	2.46	76.3	3.01	0.25
8	516.7	276.6	275.5	0.03	24.19	0.46	1.30	0.25	8.00	23.58	42.5	105	14625	139.30	13.13	18.60	2.62	2.81	80.7	4.34	0.24
9	610.7	238.3	333.6	0.03	32.56	0.26	0.81	0.12	7.44	28.72	54.3	131	17135	130.75	17.62	40.42	2.55	3.13	162.7	4.03	0.15
10	1029.2	407.5	182.0	0.02	41.81	0.25	0.63	0.15	4.65	14.83	28.9	81	16525	202.93	17.52	66.17	2.24	2.57	128.9	1.95	0.27
11	484.7	199.3	134.8	0.01	22.80	0.16	0.54	0.11	3.80	11.38	20.8	53	14744	277.32	14.00	42.38	2.54	3.29	98.8	2.33	0.23
12	566.9	650.1	1835.7	0.17	168.99	16.63	24.65	7.25	101.76	194.85	247.6	451	10592	23.50	4.43	6.86	4.07	1.48	18.3	2.67	0.44
13	419.3	302.4	561.4	0.04	40.43	0.95	2.74	0.44	19.96	57.19	85.2	161	14237	88.53	8.06	14.74	3.49	2.88	58.6	3.98	0.18
14	1534.5	1543.6	1720.5	0.09	67.25	5.34	9.10	1.02	59.59	170.76	257.0	455	12727	27.95	7.64	7.39	3.78	1.70	50.0	6.77	0.13
15	546.9	234.0	275.9	0.03	32.38	0.38	1.01	0.13	6.64	24.59	43.6	100	14051	141.19	14.98	32.05	2.77	2.67	98.5	3.07	0.16
16	631.1	492.2	824.7	0.04	44.92	3.71	6.51	0.97	34.81	84.85	121.0	227	13434	59.30	6.51	6.90	3.64	1.76	34.8	5.04	0.20
avg	**604.1**	**376.4**	**563.6**	**0.04**	**43.39**	**2.44**	**4.33**	**0.93**	**22.76**	**55.90**	**83.2**	**166**	**14055**	**120.62**	**11.48**	**24.10**	**3.07**	**2.48**	**78.6**	**3.91**	**0.23**
SN08YV03																					
1	76.2	61.0	926.2	0.03	14.11	2.95	5.00	1.10	33.34	97.19	148.9	221	8869	40.16	6.62	2.82	4.19	1.69	44.2	15.66	0.26
10	369.6	248.3	658.2	0.08	22.33	0.76	1.57	0.54	13.42	55.69	115.8	247	10124	41.02	18.39	14.21	2.67	2.07	157.1	11.05	0.36
11	306.8	162.8	377.4	0.01	16.57	0.40	0.91	0.33	8.16	31.66	62.6	139	10905	78.31	17.06	18.13	2.71	2.28	152.4	8.41	0.37
12	254.8	130.3	548.2	0.02	17.20	0.53	1.36	0.48	10.20	44.05	97.2	222	10169	45.80	21.77	12.66	2.47	2.54	163.5	12.91	0.39
13	117.6	77.8	367.3	0.03	11.99	0.50	0.95	0.38	8.32	32.12	61.0	124	9723	78.58	14.87	12.67	2.97	1.89	130.8	10.32	0.41
14	155.6	79.4	323.0	0.02	12.72	0.28	0.75	0.28	6.27	27.20	55.7	122	10479	86.01	19.44	16.86	2.65	2.69	161.5	9.58	0.40
15	421.5	248.0	0.0	19.35	0.68	1.59	0.59	11.03	46.63	94.58	208.3	10599	51	18.88	12.18	2.68	2.33	131.16	10.8	0.43	0.05
2	219.1	122.5	432.0	0.07	16.29	0.57	1.08	0.42	9.02	36.31	75.3	168	10730	63.98	18.60	15.12	2.58	1.90	155.6	10.29	0.41
3	297.1	144.5	425.6	0.03	17.72	0.38	0.86	0.35	8.37	34.79	73.5	164	10996	67.23	19.54	20.52	2.60	2.28	189.4	9.23	0.39
4	282.6	179.3	323.3	0.01	14.35	0.31	0.85	0.29	6.27	27.64	56.6	126	11534	91.42	20.12	16.96	2.56	2.73	149.2	8.79	0.39
5	188.2	98.0	345.9	0.01	13.36	0.32	0.82	0.33	6.69	29.92	61.2	135	10270	76.31	20.13	16.29	2.57	2.54	164.1	10.07	0.43
6	118.5	106.5	1031.1	0.03	14.96	2.52	4.91	1.27	34.35	110.10	169.5	263	9034	34.40	7.65	3.05	3.93	1.95	53.5	17.56	0.30
7	184.6	68.4	556.7	0.02	11.43	0.28	0.81	0.32	7.89	41.40	109.4	283	9590	33.86	35.89	14.07	1.97	2.89	348.7	24.78	0.39
8	184.3	137.4	681.1	0.02	15.41	1.62	2.99	1.16	20.15	65.43	115.3	228	10174	44.58	11.33	5.15	2.98	1.84	76.4	14.82	0.45
9	226.0	104.8	291.6	0.02	12.19	0.29	0.70	0.29	5.40	24.90	50.2	115	10931	95.22	21.26	17.50	2.54	2.36	164.8	9.42	0.46
avg	**226.8**	**131.3**	**485.8**	**1.32**	**14.09**	**0.89**	**1.61**	**1.24**	**14.97**	**50.20**	**97.4**	**877**	**9572**	**59.72**	**17.66**	**12.58**	**2.78**	**10.85**	**141.5**	**11.55**	**0.36**

Supplemental Table SP3.1. Individual analysis trace element data

Spot	*Concentrations (ppm)*													*Ratios*							
	U	*Th*	*Y*	*La*	*Ce*	*Nd*	*Sm*	*Eu*	*Gd*	*Dy*	*Er*	*Yb*	*Hf*	*Hf/Yb*	*Yb/Gd*	*Ce/Sm*	*Y/Yb*	*Sm/Nd*	*Yb/Sm*	*Yb/Ce*	*Eu**
SN08YV07																					
1	528.1	222.1	492.5	0.05	23.37	0.30	1.00	0.29	9.17	40.85	86.4	198	11300	57.20	21.55	23.31	2.49	3.33	197.0	8.45	0.29
2	480.6	216.0	348.3	0.02	25.97	0.30	0.76	0.31	7.37	31.13	62.4	145	11337	78.28	19.66	34.36	2.41	2.49	191.6	5.58	0.40
3	429.0	196.0	321.0	0.01	21.71	0.32	0.77	0.33	6.55	28.60	56.4	129	11015	85.29	19.71	28.36	2.49	2.41	168.7	5.95	0.45
4	647.6	318.1	633.0	0.02	25.47	0.84	1.88	0.70	15.74	56.70	112.1	246	10742	43.59	15.66	13.55	2.57	2.25	131.1	9.67	0.39
5	476.3	217.1	362.6	0.13	24.12	0.38	0.97	0.34	7.94	30.86	61.5	145	10642	73.26	18.29	24.89	2.50	2.53	149.9	6.02	0.37
6	533.7	190.8	424.5	0.02	20.84	0.26	0.83	0.32	7.24	34.79	76.1	183	11191	61.00	25.35	25.19	2.31	3.13	221.7	8.80	0.39
7	465.3	156.7	332.7	0.01	17.59	0.17	0.57	0.24	5.85	27.58	59.7	147	11293	76.90	25.10	31.02	2.27	3.29	258.9	8.35	0.40
8	507.6	294.7	697.6	0.02	24.08	1.17	2.37	0.82	19.03	65.95	117.8	248	10750	43.27	13.05	10.14	2.81	2.04	104.6	10.32	0.37
9	726.6	298.9	410.1	2.03	26.62	0.54	0.96	0.37	8.16	34.15	71.0	169	11550	68.16	20.78	27.68	2.42	1.80	176.2	6.37	0.40
10	334.0	146.2	621.7	0.02	18.46	0.56	1.62	0.55	14.64	58.67	106.9	217	9638	44.48	14.81	11.38	2.87	2.88	133.6	11.74	0.34
11	399.4	179.7	355.9	0.02	19.92	0.31	0.75	0.28	7.35	31.09	63.2	143	10594	74.33	19.38	26.41	2.50	2.45	189.0	7.16	0.36
12	288.2	101.4	289.0	0.02	14.88	0.16	0.44	0.17	4.80	25.09	52.2	129	11696	90.72	26.89	34.15	2.24	2.74	295.9	8.66	0.36
13	434.0	218.3	284.1	0.89	29.50	0.62	0.80	0.33	6.43	25.18	49.2	114	9172	80.43	17.72	37.09	2.49	1.28	143.4	3.87	0.45
14	804.0	389.7	718.9	0.02	29.78	0.78	1.81	0.64	14.46	59.97	126.2	296	11132	37.55	20.50	16.46	2.43	2.31	163.9	9.95	0.38
15	633.5	271.7	586.3	0.02	27.45	0.46	1.13	0.39	11.82	49.82	102.6	235	10873	46.27	19.88	24.23	2.49	2.47	207.4	8.56	0.32
16	317.7	148.9	369.9	0.02	21.16	0.31	0.84	0.30	7.38	32.96	65.8	149	11084	74.41	20.18	25.16	2.48	2.74	177.1	7.04	0.37
avg	**500.3**	**222.9**	**453.0**	**0.21**	**23.18**	**0.47**	**1.09**	**0.40**	**9.62**	**39.59**	**79.3**	**181**	**10875**	**64.70**	**19.91**	**24.59**	**2.49**	**2.51**	**181.9**	**7.91**	**0.38**

Supplemental Table SP3.2. Individual analysis trace element data

Spot	*Chondrite Normalized*									
	La	***Ce***	***Nd***	***Sm***	***Eu***	***Gd***	***Dy***	***Y***	***Er***	***Yb***
SN08AR04										
1	0.07	22.24	3.42	19.53	20.84	105.4	281.6	490.2	813.4	1740.5
10	0.07	24.57	1.52	11.54	9.80	70.5	209.0	376.5	640.3	1423.2
11	0.05	19.25	0.57	5.24	5.27	35.8	129.1	268.6	471.0	1149.8
12	0.11	35.07	2.85	17.94	18.05	99.7	326.7	620.5	1050.4	2337.6
2	0.11	21.31	0.44	4.14	4.25	29.8	107.4	209.0	365.1	848.9
3	0.11	24.05	1.92	13.29	15.56	80.3	251.9	461.5	797.4	1850.3
4	0.04	23.33	0.72	7.71	7.31	49.4	174.9	347.7	610.1	1393.4
5	0.05	27.56	0.66	6.42	5.27	43.7	141.6	272.5	473.0	1139.3
6	0.04	18.11	0.34	2.95	2.84	20.5	89.4	170.7	305.4	760.9
7	0.09	24.26	0.90	7.25	6.46	52.1	155.1	264.3	440.4	884.0
8	0.06	14.38	0.48	3.89	4.69	34.0	119.6	244.1	428.7	1091.1
9	0.07	18.14	0.94	7.94	9.79	56.7	191.2	358.1	627.7	1499.6
avg	**0.07**	**22.69**	**1.23**	**8.99**	**9.18**	**56.5**	**181.5**	**340.3**	**585.2**	**1343.2**
SN08AR06										
1	0.10	27.58	0.99	6.46	7.68	45.5	167.8	359.8	590.3	1386.7
10	0.06	20.15	0.45	4.05	5.82	32.6	112.2	216.7	367.2	876.7
11	5.77	46.03	2.71	9.52	8.50	57.7	202.4	369.1	643.7	1445.9
12	0.12	18.71	0.69	4.57	4.69	29.1	100.5	191.0	321.5	755.2
13	0.09	21.50	0.55	4.29	4.81	33.9	129.9	260.7	468.6	1200.9
14	0.10	33.79	1.10	8.52	9.09	62.3	231.7	461.5	805.6	1899.9
15	0.07	28.35	0.97	8.98	9.16	60.8	232.4	474.3	847.7	1975.3
16	0.07	34.68	1.27	10.12	10.96	64.7	258.6	477.4	837.4	1877.2
2	0.16	38.78	0.92	7.79	6.91	47.8	176.8	331.0	572.0	1312.4
3	0.08	25.21	0.87	6.94	7.69	51.4	171.4	339.8	574.7	1326.7
4	0.07	21.70	0.76	6.03	5.76	42.8	152.3	296.2	505.9	1144.8
5	0.24	18.97	0.78	5.23	5.08	32.9	113.2	218.9	380.9	912.6
6	0.05	30.25	0.96	8.05	8.33	56.1	218.6	455.0	809.6	1861.1
7	0.31	17.25	0.60	4.50	4.69	31.4	105.2	199.3	346.2	805.9
8	0.08	18.35	2.20	14.86	14.87	88.5	256.1	461.0	778.8	1666.8
9	0.05	22.15	0.36	3.91	4.59	32.3	124.5	241.2	425.6	1038.4
avg	**0.46**	**26.47**	**1.01**	**7.11**	**7.41**	**48.1**	**172.1**	**334.6**	**579.7**	**1342.9**

Supplemental Table SP3.2. Individual analysis trace element data

Spot	*Chondrite Normalized*									
	La	***Ce***	***Nd***	***Sm***	***Eu***	***Gd***	***Dy***	***Y***	***Er***	***Yb***
SN08AR11										
1	0.07	25.37	2.13	13.88	16.58	74.4	233.4	420.8	735.0	1688.0
10	0.15	18.16	4.77	21.58	33.40	99.0	259.2	464.3	751.1	1584.0
11	0.06	8.98	0.17	1.26	2.33	9.9	39.4	80.4	142.4	386.8
12	0.05	11.89	0.22	2.43	3.89	17.0	61.5	118.5	208.8	529.7
13	0.33	13.39	0.82	6.26	9.80	30.8	123.0	258.5	463.3	1165.3
14	0.09	10.01	0.28	1.30	3.47	11.9	50.1	96.6	177.4	470.8
15	0.25	41.60	10.67	52.92	92.88	239.7	543.8	892.9	1472.1	2959.2
16	0.15	17.33	3.74	16.87	25.86	77.4	198.8	351.8	593.9	1240.4
2	0.13	15.27	3.09	15.36	23.14	74.3	184.4	340.8	552.6	1169.5
3	0.07	13.01	0.22	2.17	4.19	16.6	60.7	122.9	213.2	543.5
4	0.10	16.71	2.79	15.51	21.84	72.0	186.5	328.8	538.8	1144.4
5	0.08	17.17	2.38	15.48	23.43	70.4	183.4	312.7	517.4	1100.1
6	0.07	18.75	3.44	18.02	25.50	83.7	204.6	362.7	593.3	1243.1
7	0.09	16.67	1.27	7.43	14.03	49.5	173.1	369.8	637.3	1590.6
8	0.07	15.50	1.77	11.32	19.29	61.9	166.7	300.1	495.6	1096.2
9	0.17	18.14	4.72	24.81	38.75	107.8	276.8	480.6	787.8	1607.9
avg	**0.12**	**17.37**	**2.65**	**14.16**	**22.40**	**68.5**	**184.1**	**331.4**	**555.0**	**1220.0**
06-EW35										
1	0.04	30.62	0.76	9.59	4.56	53.3	196.3	332.0	579.5	1066.5
2	0.30	27.09	8.61	42.03	27.75	189.6	531.6	815.4	1353.2	2132.8
3	0.10	24.16	5.75	33.45	22.05	161.8	445.2	665.8	1088.0	1714.6
4	0.11	26.09	0.59	5.59	3.91	43.0	154.7	264.6	456.9	867.1
5	0.08	17.10	0.63	5.16	4.17	38.2	133.8	234.6	409.2	775.3
6	0.03	25.68	0.47	5.20	3.57	36.3	148.3	254.3	454.1	862.2
7	0.09	21.35	0.52	4.55	3.58	31.7	123.3	216.5	377.9	740.3
8	0.05	25.21	0.64	6.12	4.66	44.6	161.7	274.2	473.9	869.5
9	0.06	25.72	0.52	5.76	4.07	40.4	159.3	269.8	474.0	895.0
10	0.08	22.00	3.29	22.45	16.61	129.2	361.1	550.3	897.0	1445.8
avg	**0.10**	**24.50**	**2.18**	**13.99**	**9.49**	**76.8**	**241.5**	**387.8**	**656.4**	**1136.9**

Supplemental Table SP3.2. Individual analysis trace element data

Spot	*Chondrite Normalized*									
	La	***Ce***	***Nd***	***Sm***	***Eu***	***Gd***	***Dy***	***Y***	***Er***	***Yb***
06-EW39										
1	0.08	29.34	0.41	3.32	6.27	19.0	71.8	156.3	258.7	727.3
2	0.06	23.04	0.28	2.37	5.20	15.3	50.5	114.1	189.5	538.7
3	0.05	18.33	0.28	2.53	4.80	15.6	64.5	149.7	257.5	790.5
4	0.07	33.00	0.37	2.94	6.00	17.7	74.6	172.7	293.9	851.3
5	0.11	23.24	0.39	3.27	7.37	23.2	79.9	177.6	307.5	914.2
6	0.08	30.38	0.48	3.64	7.09	23.6	72.2	144.6	244.8	658.9
7	0.09	51.82	0.51	4.08	6.99	26.3	89.0	215.7	348.7	1054.6
8	0.08	24.98	0.33	2.44	5.10	17.3	50.8	103.2	175.8	482.1
avg	**0.08**	**29.27**	**0.38**	**3.07**	**6.10**	**19.8**	**69.2**	**154.2**	**259.6**	**752.2**
SN08HH06										
1	0.07	10.43	0.24	1.02	4.26	9.6	44.8	107.5	197.9	683.4
2	0.18	9.05	1.07	5.03	13.80	30.1	101.4	179.6	325.0	807.9
3	0.14	16.56	0.82	6.26	17.48	54.6	199.0	372.6	669.8	1558.0
4	0.22	14.71	1.51	7.62	20.94	59.1	220.5	399.2	731.5	1716.8
5	0.31	12.24	1.19	6.67	17.39	50.7	166.6	297.5	545.2	1306.2
6	0.17	7.03	0.92	4.93	10.53	25.6	76.8	135.0	244.2	591.8
7	0.13	8.30	0.17	1.85	4.19	16.7	78.2	167.1	331.6	915.6
8	0.24	10.62	1.50	6.90	16.74	38.1	116.1	201.7	367.8	885.3
avg	**0.18**	**11.12**	**0.93**	**5.04**	**13.17**	**35.5**	**125.4**	**232.5**	**426.6**	**1058.1**
SN08HH07										
1	0.10	21.92	0.80	6.38	6.22	45.1	167.0	315.8	554.8	1192.4
2	0.20	15.53	5.53	35.66	28.13	218.6	636.9	952.0	1607.4	2583.1
3	0.08	20.59	2.44	21.04	15.16	142.8	411.2	636.5	1029.3	1667.7
4	0.11	19.66	0.47	4.33	3.98	31.6	119.0	238.9	429.2	1073.4
5	0.10	15.86	0.37	4.21	2.87	29.3	118.8	259.2	468.4	1197.8
6	0.09	10.21	2.98	21.69	23.02	128.8	349.2	517.7	875.0	1451.0
7	0.13	9.44	3.29	19.52	21.23	103.5	280.4	469.0	812.7	1531.1
8	0.09	24.20	0.70	5.71	4.27	38.6	150.7	297.8	511.4	1177.3
9	0.14	27.68	2.86	22.27	13.82	160.4	462.0	732.2	1206.1	1962.6
10	0.13	25.57	0.61	5.91	5.07	39.3	150.4	302.9	532.8	1268.1
11	0.09	21.85	4.71	35.71	27.24	216.0	618.3	986.3	1611.6	2626.9
12	0.15	18.00	5.71	36.86	31.21	226.6	661.0	1023.2	1716.1	2914.1
avg	**0.12**	**19.21**	**2.54**	**18.27**	**15.18**	**115.1**	**343.7**	**561.0**	**946.2**	**1720.5**

Supplemental Table SP3.2. Individual analysis trace element data

Spot	*Chondrite Normalized*									
	La	***Ce***	***Nd***	***Sm***	***Eu***	***Gd***	***Dy***	***Y***	***Er***	***Yb***
06-EW39										
1	0.08	29.34	0.41	3.32	6.27	19.0	71.8	156.3	258.7	727.3
2	0.06	23.04	0.28	2.37	5.20	15.3	50.5	114.1	189.5	538.7
3	0.05	18.33	0.28	2.53	4.80	15.6	64.5	149.7	257.5	790.5
4	0.07	33.00	0.37	2.94	6.00	17.7	74.6	172.7	293.9	851.3
5	0.11	23.24	0.39	3.27	7.37	23.2	79.9	177.6	307.5	914.2
6	0.08	30.38	0.48	3.64	7.09	23.6	72.2	144.6	244.8	658.9
7	0.09	51.82	0.51	4.08	6.99	26.3	89.0	215.7	348.7	1054.6
8	0.08	24.98	0.33	2.44	5.10	17.3	50.8	103.2	175.8	482.1
avg	**0.08**	**29.27**	**0.38**	**3.07**	**6.10**	**19.8**	**69.2**	**154.2**	**259.6**	**752.2**
SN08HH06										
1	0.07	10.43	0.24	1.02	4.26	9.6	44.8	107.5	197.9	683.4
2	0.18	9.05	1.07	5.03	13.80	30.1	101.4	179.6	325.0	807.9
3	0.14	16.56	0.82	6.26	17.48	54.6	199.0	372.6	669.8	1558.0
4	0.22	14.71	1.51	7.62	20.94	59.1	220.5	399.2	731.5	1716.8
5	0.31	12.24	1.19	6.67	17.39	50.7	166.6	297.5	545.2	1306.2
6	0.17	7.03	0.92	4.93	10.53	25.6	76.8	135.0	244.2	591.8
7	0.13	8.30	0.17	1.85	4.19	16.7	78.2	167.1	331.6	915.6
8	0.24	10.62	1.50	6.90	16.74	38.1	116.1	201.7	367.8	885.3
avg	**0.18**	**11.12**	**0.93**	**5.04**	**13.17**	**35.5**	**125.4**	**232.5**	**426.6**	**1058.1**
SN08HH07										
1	0.10	21.92	0.80	6.38	6.22	45.1	167.0	315.8	554.8	1192.4
2	0.20	15.53	5.53	35.66	28.13	218.6	636.9	952.0	1607.4	2583.1
3	0.08	20.59	2.44	21.04	15.16	142.8	411.2	636.5	1029.3	1667.7
4	0.11	19.66	0.47	4.33	3.98	31.6	119.0	238.9	429.2	1073.4
5	0.10	15.86	0.37	4.21	2.87	29.3	118.8	259.2	468.4	1197.8
6	0.09	10.21	2.98	21.69	23.02	128.8	349.2	517.7	875.0	1451.0
7	0.13	9.44	3.29	19.52	21.23	103.5	280.4	469.0	812.7	1531.1
8	0.09	24.20	0.70	5.71	4.27	38.6	150.7	297.8	511.4	1177.3
9	0.14	27.68	2.86	22.27	13.82	160.4	462.0	732.2	1206.1	1962.6
10	0.13	25.57	0.61	5.91	5.07	39.3	150.4	302.9	532.8	1268.1
11	0.09	21.85	4.71	35.71	27.24	216.0	618.3	986.3	1611.6	2626.9
12	0.15	18.00	5.71	36.86	31.21	226.6	661.0	1023.2	1716.1	2914.1
avg	**0.12**	**19.21**	**2.54**	**18.27**	**15.18**	**115.1**	**343.7**	**561.0**	**946.2**	**1720.5**

Supplemental Table SP3.2. Individual analysis trace element data

Spot	*Chondrite Normalized*									
	La	***Ce***	***Nd***	***Sm***	***Eu***	***Gd***	***Dy***	***Y***	***Er***	***Yb***
SN08MH01										
1	0.10	36.64	1.07	8.67	5.01	67.8	229.6	391.6	663.4	1206.8
2	0.13	24.29	0.63	7.00	4.69	52.5	184.8	313.2	539.2	958.4
3	0.05	32.60	0.99	7.34	4.51	60.3	208.0	347.4	600.9	1080.5
4	0.06	20.96	0.72	7.89	8.40	74.4	280.1	456.1	778.8	1306.8
5	0.09	19.92	1.20	12.13	8.83	91.0	271.3	403.3	679.9	1102.6
6	0.05	38.28	0.76	6.84	3.15	56.2	208.6	358.5	621.6	1208.5
7	0.21	28.72	2.52	19.87	13.36	132.9	365.5	557.3	917.2	1519.2
8	0.06	31.87	3.30	24.47	13.32	167.9	471.4	701.3	1141.5	1771.3
9	0.03	36.85	0.60	7.51	4.05	69.1	245.4	437.5	738.9	1405.4
10	0.13	29.71	1.31	10.16	6.47	80.0	258.4	449.6	768.0	1410.1
11	0.10	37.62	1.09	9.25	4.55	64.2	241.0	412.5	709.6	1360.9
12	0.09	25.88	1.62	14.88	8.71	92.3	291.8	451.5	776.8	1329.3
avg	**0.09**	**30.28**	**1.32**	**11.33**	**7.09**	**84.0**	**271.3**	**440.0**	**744.7**	**1305.0**
SN08MH05										
1	0.27	32.18	8.92	38.46	20.28	209.3	483.7	725.7	1116.7	1673.9
2	0.11	31.30	5.40	33.36	17.02	184.7	466.4	685.9	1058.2	1582.3
3	0.11	27.81	2.53	17.03	10.54	134.0	379.4	565.8	888.9	1418.5
4	0.07	32.86	5.75	33.96	17.70	188.2	465.2	681.0	1045.8	1564.9
5	0.13	38.58	2.93	22.87	12.36	174.5	475.6	717.0	1163.3	1787.3
6	0.05	37.78	4.22	30.32	15.88	193.5	502.6	744.5	1156.6	1752.4
7	0.07	29.17	1.99	18.79	10.35	143.5	398.4	605.9	958.1	1509.3
8	0.06	31.65	2.62	19.53	12.69	139.4	409.2	617.7	1000.1	1570.7
9	0.15	30.25	6.87	38.31	20.56	192.7	482.6	694.8	1095.3	1643.4
10	0.08	31.49	3.12	22.78	12.84	155.8	422.6	637.3	993.7	1545.0
avg	**0.11**	**32.31**	**4.43**	**27.54**	**15.02**	**171.6**	**448.6**	**667.6**	**1047.7**	**1604.8**

Supplemental Table SP3.2. Individual analysis trace element data

Spot	*Chondrite Normalized*									
	La	***Ce***	***Nd***	***Sm***	***Eu***	***Gd***	***Dy***	***Y***	***Er***	***Yb***
SN08MH11										
1	0.10	22.06	0.93	5.62	8.13	45.4	196.4	409.6	747.6	1787.8
2	2.07	24.79	2.62	7.12	9.22	34.3	139.6	279.2	511.5	1250.1
3	0.08	13.19	2.86	15.99	20.28	90.6	252.3	414.0	726.1	1422.8
4	0.11	13.17	2.91	15.31	20.47	80.9	240.3	387.0	684.3	1378.9
5	0.10	18.61	0.53	3.43	4.38	31.9	119.5	238.4	433.4	1006.7
6	0.06	12.85	1.93	12.90	18.98	75.9	213.6	354.8	610.9	1215.3
7	0.05	18.47	0.63	5.06	6.51	36.7	147.6	310.6	573.0	1399.5
8	0.20	20.00	1.17	8.16	10.39	51.6	203.9	386.3	717.0	1632.3
9	0.06	10.39	0.62	5.51	10.49	40.5	134.6	238.1	439.0	952.1
10	0.09	19.62	0.83	5.15	8.07	40.1	168.2	328.1	602.8	1474.0
11	0.10	18.24	0.81	6.65	8.40	46.3	173.8	337.6	636.9	1524.3
12	0.08	12.32	1.83	12.22	18.32	76.6	218.3	349.1	613.4	1213.9
13	0.09	12.76	1.36	11.10	15.64	65.6	194.9	330.3	567.7	1158.9
14	0.09	17.08	0.79	5.61	9.78	42.3	180.0	353.5	662.5	1577.2
15	0.50	14.95	1.46	8.43	12.41	54.9	171.0	306.4	535.3	1262.2
16	0.11	12.45	2.56	15.79	20.98	82.1	246.4	397.1	690.3	1333.7
17	0.10	21.08	0.59	5.49	5.52	37.5	145.0	269.1	493.9	1128.7
18	0.10	11.77	1.93	12.19	17.11	71.4	207.0	334.9	584.6	1176.3
19	0.06	14.12	0.38	2.73	5.03	21.7	89.0	167.0	306.5	750.3
20	0.07	19.93	0.96	5.85	7.36	44.8	174.9	347.9	653.6	1566.4
avg	**0.21**	**16.39**	**1.39**	**8.52**	**11.87**	**53.6**	**180.8**	**326.9**	**589.5**	**1310.6**
SN08RM01										
1	0.15	101.95	7.56	58.00	89.86	384.9	1395.2	2691.7	4616.8	10016.4
2	0.10	55.53	3.59	29.76	47.87	188.7	737.4	1462.5	2520.3	5796.1
3	0.04	17.37	0.71	5.73	5.05	35.0	134.2	260.2	465.0	1146.4
4	0.09	48.25	0.93	7.88	8.31	67.8	264.7	505.9	878.8	2023.1
5	0.10	2.62	0.02	0.12	0.36	1.1	13.2	39.5	100.6	453.0
6	0.09	10.13	4.44	25.42	35.27	132.4	393.7	636.4	1086.9	2149.0
7	1758.03	958.57	260.36	185.98	132.78	274.3	308.4	718.0	914.0	2164.8
8	0.10	59.63	3.69	24.64	50.92	184.8	718.6	1454.4	2524.9	5891.9
9	0.12	6.21	0.09	0.77	2.23	6.8	39.0	94.5	186.7	584.1
10	0.08	20.47	1.16	9.59	20.14	66.3	282.5	605.0	1091.9	2859.7
11	0.08	7.45	0.62	4.48	5.14	23.6	84.8	206.5	415.2	1233.7
12	0.10	16.05	2.05	16.64	20.46	117.0	412.8	716.4	1269.2	2588.9
13	0.10	127.40	9.23	66.01	105.09	423.0	1574.8	2926.8	4951.6	10250.6
avg	**135.32**	**110.13**	**22.65**	**33.46**	**40.27**	**146.6**	**489.2**	**947.5**	**1617.1**	**3627.5**

Supplemental Table SP3.2. Individual analysis trace element data

Spot	*Chondrite Normalized*									
	La	***Ce***	***Nd***	***Sm***	***Eu***	***Gd***	***Dy***	***Y***	***Er***	***Yb***
SN08RM10										
1	0.07	24.55	0.79	8.10	3.22	56.7	235.3	418.3	766.6	1543.3
2	0.05	23.14	1.04	12.93	2.98	105.7	436.7	754.1	1366.9	2486.3
3	0.42	35.13	2.93	20.50	15.26	125.7	480.4	830.0	1505.6	3102.9
4	0.05	14.05	0.33	5.77	2.56	47.4	242.2	503.2	921.8	2134.8
5	0.07	16.00	1.24	11.22	6.30	66.4	240.0	428.8	727.1	1430.8
6	0.10	26.93	0.88	9.70	4.23	72.5	308.2	551.5	1030.5	2088.5
7	-0.09	32.27	4.74	30.42	17.13	161.7	527.3	870.5	1493.8	2802.4
8	0.09	24.46	0.56	7.59	2.03	65.3	297.6	572.2	1047.7	2267.6
9	0.08	23.63	0.63	7.25	3.46	57.4	272.8	527.5	955.3	2055.8
10	5.21	39.57	15.41	29.21	17.96	85.2	285.1	601.8	1015.8	2466.2
11	0.09	26.58	0.63	7.90	3.96	60.5	300.2	580.4	1052.4	2312.4
12	0.11	48.09	2.76	25.86	9.14	186.0	661.3	1003.0	1769.4	2915.0
13	0.33	27.11	11.33	63.79	78.63	294.6	776.3	1220.1	1982.8	3835.0
14	0.07	21.31	1.27	10.37	5.23	66.4	273.7	428.1	769.1	1384.5
15	1.50	137.68	54.62	216.08	330.35	749.3	1473.4	2012.0	3002.1	5007.2
avg	**0.54**	**34.70**	**6.61**	**31.11**	**33.50**	**146.7**	**454.0**	**753.4**	**1293.8**	**2522.2**
SN08TD04										
1	7.75	45.91	12.75	33.61	12.73	94.3	285.1	545.9	934.5	2047.2
2	0.06	12.62	0.17	2.13	0.49	25.8	146.6	305.7	578.3	1344.5
3	0.08	40.10	1.86	15.49	5.93	116.1	434.3	742.6	1272.9	2299.5
4	0.13	27.83	0.63	6.72	3.96	59.6	235.5	450.9	794.0	1785.2
5	0.26	27.30	1.20	11.51	7.32	67.9	300.0	622.8	1118.7	3040.0
6	0.14	35.91	1.05	15.69	5.16	103.8	436.9	781.8	1384.6	2729.2
7	0.03	31.28	0.84	7.86	2.89	60.4	270.4	536.7	961.3	2167.8
8	0.16	21.46	0.45	5.89	2.81	46.4	262.9	565.0	1010.5	2537.1
9	0.54	49.37	18.50	105.06	104.69	506.4	1207.3	1808.2	2856.6	5023.3
10	0.12	30.68	1.64	17.60	6.09	121.4	421.9	679.4	1179.4	2037.5
11	0.12	19.10	0.33	5.39	2.02	51.4	260.6	523.1	951.8	2112.5
12	1.62	18.83	1.86	12.45	2.90	92.4	425.1	776.1	1424.0	2781.7
13	14.48	57.39	11.46	23.99	8.32	103.4	394.3	742.4	1320.2	2905.4
14	0.10	20.56	0.57	5.57	5.49	41.2	168.3	334.1	592.0	1375.2
15	0.12	24.76	0.65	6.33	3.89	48.2	207.0	400.0	707.6	1583.1
avg	**1.71**	**30.87**	**3.60**	**18.35**	**11.65**	**102.6**	**363.7**	**654.3**	**1139.1**	**2384.6**

Supplemental Table SP3.2. Individual analysis trace element data

Spot	*Chondrite Normalized*									
	La	***Ce***	***Nd***	***Sm***	***Eu***	***Gd***	***Dy***	***Y***	***Er***	***Yb***
SN08YH05										
1	0.19	54.68	5.52	32.77	12.46	134.5	286.1	476.9	718.4	1350.1
2	0.11	56.36	5.92	38.12	19.50	160.3	365.8	523.0	940.2	1834.2
3	0.12	51.45	3.32	28.12	12.64	126.7	267.0	427.2	657.6	1238.9
4	0.21	62.17	5.82	36.02	14.74	164.7	368.1	566.2	891.7	1683.2
5	0.09	54.03	3.68	27.08	11.81	128.8	275.1	438.4	662.4	1264.8
6	0.12	57.54	4.46	31.22	12.48	136.3	298.1	473.6	713.6	1352.1
7	0.11	49.83	2.50	21.64	9.26	103.2	229.5	372.9	563.2	1091.4
8	0.18	59.49	6.72	36.27	15.27	150.2	352.4	558.6	861.3	1607.7
9	0.07	53.08	2.73	22.89	10.42	116.6	265.5	421.4	641.3	1233.0
10	0.16	66.13	6.17	37.30	13.72	156.4	357.4	564.9	860.5	1664.0
11	0.08	47.98	1.02	9.62	4.35	48.3	130.9	239.7	397.4	913.5
12	0.12	59.79	4.57	31.61	14.14	150.8	320.7	504.8	769.4	1478.7
13	0.24	65.28	7.22	37.51	14.90	154.7	360.9	576.8	900.1	1734.4
avg	**0.14**	**56.76**	**4.59**	**30.01**	**12.75**	**133.2**	**298.3**	**472.7**	**736.7**	**1418.9**
SN08YH11										
1	0.12	86.36	0.66	3.21	2.64	17.8	45.4	94.7	139.5	433.7
2	0.12	72.25	0.60	3.22	2.49	14.7	38.6	81.2	119.1	372.6
3	0.13	46.19	0.32	2.58	2.20	12.5	39.8	98.5	149.8	538.8
4	0.22	96.31	3.26	16.23	11.51	62.5	125.1	257.2	368.2	1038.8
5	0.13	149.94	1.40	8.63	6.49	45.8	119.0	256.6	371.3	1069.5
6	0.08	85.00	0.66	3.94	3.29	21.2	53.3	122.7	181.7	572.9
7	0.13	110.15	0.92	5.42	4.14	24.9	59.6	121.4	182.6	552.7
8	0.12	49.48	0.33	2.76	2.17	15.0	44.4	106.2	165.9	603.8
9	0.18	123.92	1.60	8.55	5.48	32.2	65.1	119.9	176.9	501.9
10	0.12	47.16	0.45	2.40	2.30	13.5	41.7	96.4	147.4	498.1
11	0.07	113.12	0.86	5.57	4.12	27.8	65.6	137.0	207.6	622.6
avg	**0.13**	**89.08**	**1.00**	**5.68**	**4.26**	**26.2**	**63.4**	**135.6**	**200.9**	**618.7**

Supplemental Table SP3.2. Individual analysis trace element data

Spot	*Chondrite Normalized*									
	La	***Ce***	***Nd***	***Sm***	***Eu***	***Gd***	***Dy***	***Y***	***Er***	***Yb***
SN08YH13										
1	0.11	47.46	5.00	34.40	10.99	135.4	249.7	369.3	531.9	968.9
2	0.13	53.45	0.75	7.65	2.13	40.2	117.8	215.4	335.7	731.3
3	0.24	52.49	9.42	52.38	43.90	183.4	266.5	367.6	511.7	908.6
4	0.16	61.56	6.42	36.45	12.30	143.7	291.2	449.6	662.3	1228.3
5	0.08	43.34	0.49	4.42	2.29	25.2	70.4	138.6	208.7	574.6
6	0.08	49.16	0.59	5.29	3.13	31.2	75.3	143.8	214.7	577.7
7	0.10	49.77	1.07	8.14	4.04	31.2	82.0	145.6	224.4	571.1
8	0.12	39.46	1.01	8.79	4.43	40.2	95.9	175.5	265.6	652.1
9	0.12	53.11	0.56	5.44	2.15	37.4	116.7	212.5	339.6	814.0
10	0.10	68.21	0.54	4.27	2.65	23.4	60.3	115.9	180.5	505.8
11	0.06	37.20	0.36	3.64	1.90	19.1	46.3	85.9	130.1	330.2
12	0.71	275.68	36.40	166.55	128.78	511.3	792.1	1169.2	1547.4	2799.2
13	0.17	65.95	2.09	18.53	7.78	100.3	232.5	357.6	532.3	998.9
14	0.39	109.71	11.69	61.50	18.10	299.5	694.2	1095.9	1606.5	2828.3
15	0.14	52.82	0.83	6.83	2.39	33.4	100.0	175.7	272.2	618.1
16	0.15	73.28	8.11	43.96	17.19	174.9	344.9	525.3	756.5	1407.1
avg	**0.18**	**70.79**	**5.33**	**29.27**	**16.51**	**114.4**	**227.2**	**359.0**	**520.0**	**1032.1**
SN08YV03										
1	0.14	23.01	6.47	33.76	19.61	167.5	395.1	589.9	930.6	1371.7
10	0.33	36.42	1.66	10.61	9.64	67.5	226.4	419.2	724.0	1533.0
11	0.06	27.03	0.88	6.18	5.85	41.0	128.7	240.4	391.5	864.9
12	0.10	28.06	1.17	9.18	8.56	51.3	179.1	349.2	607.5	1379.2
13	0.13	19.56	1.09	6.39	6.68	41.8	130.6	234.0	381.3	768.5
14	0.07	20.75	0.61	5.10	5.06	31.5	110.6	205.7	347.8	756.7
15	31.56	1.49	10.73	10.43	55.45	189.6	355.8	591.1	1294.0	
2	0.29	26.58	1.24	7.28	7.52	45.3	147.6	275.2	470.3	1041.7
3	0.11	28.91	0.83	5.84	6.18	42.1	141.4	271.1	459.3	1016.0
4	0.05	23.40	0.68	5.71	5.20	31.5	112.4	205.9	353.6	783.6
5	0.06	21.79	0.71	5.54	5.87	33.6	121.6	220.3	382.7	835.9
6	0.11	24.40	5.51	33.17	22.55	172.6	447.6	656.7	1059.2	1631.1
7	0.09	18.65	0.62	5.49	5.76	39.7	168.3	354.6	683.5	1759.3
8	0.10	25.13	3.55	20.19	20.57	101.2	266.0	433.8	720.7	1417.6
9	0.07	19.88	0.65	4.71	5.14	27.1	101.2	185.7	313.8	713.1
avg	**2.22**	**23.00**	**2.43**	**11.31**	**12.64**	**72.2**	**202.1**	**348.9**	**608.0**	**1133.7**

Supplemental Table SP3.2. Individual analysis trace element data

Spot	*Chondrite Normalized*									
	La	***Ce***	***Nd***	***Sm***	***Eu***	***Gd***	***Dy***	***Y***	***Er***	***Yb***
SN08YV07										
1	0.23	38.13	0.66	6.78	5.16	46.1	166.1	313.7	539.7	1226.9
2	0.08	42.36	0.66	5.11	5.52	37.0	126.5	221.8	389.9	899.5
3	0.03	35.42	0.69	5.17	5.87	32.9	116.2	204.5	352.6	802.2
4	0.07	41.55	1.83	12.70	12.47	79.1	230.5	403.2	700.7	1530.6
5	0.56	39.35	0.84	6.55	5.97	39.9	125.4	231.0	384.4	902.2
6	0.08	34.00	0.58	5.59	5.62	36.4	141.4	270.4	475.4	1139.4
7	0.06	28.70	0.38	3.83	4.24	29.4	112.1	211.9	373.4	912.1
8	0.09	39.28	2.55	16.05	14.56	95.7	268.1	444.3	736.1	1543.0
9	8.55	43.43	1.17	6.50	6.51	41.0	138.8	261.2	443.7	1052.5
10	0.08	30.11	1.23	10.96	9.76	73.5	238.5	396.0	668.4	1346.0
11	0.10	32.49	0.67	5.10	5.00	36.9	126.4	226.7	395.1	885.2
12	0.10	24.27	0.35	2.94	3.00	24.1	102.0	184.1	326.4	800.7
13	3.75	48.12	1.36	5.37	5.88	32.3	102.4	181.0	307.4	708.3
14	0.09	48.58	1.71	12.22	11.42	72.7	243.8	457.9	788.6	1841.3
15	0.09	44.77	1.00	7.65	6.90	59.4	202.5	373.4	641.3	1459.5
16	0.09	34.52	0.67	5.68	5.39	37.1	134.0	235.6	411.4	925.2
avg	**0.88**	**37.82**	**1.02**	**7.39**	**7.08**	**48.3**	**160.9**	**288.5**	**495.9**	**1123.4**

Supplemental Figure SP3.3 - Rare Earth Element Plots

Supplemental Figure SP3.3 - Rare Earth Element Plots (continued)

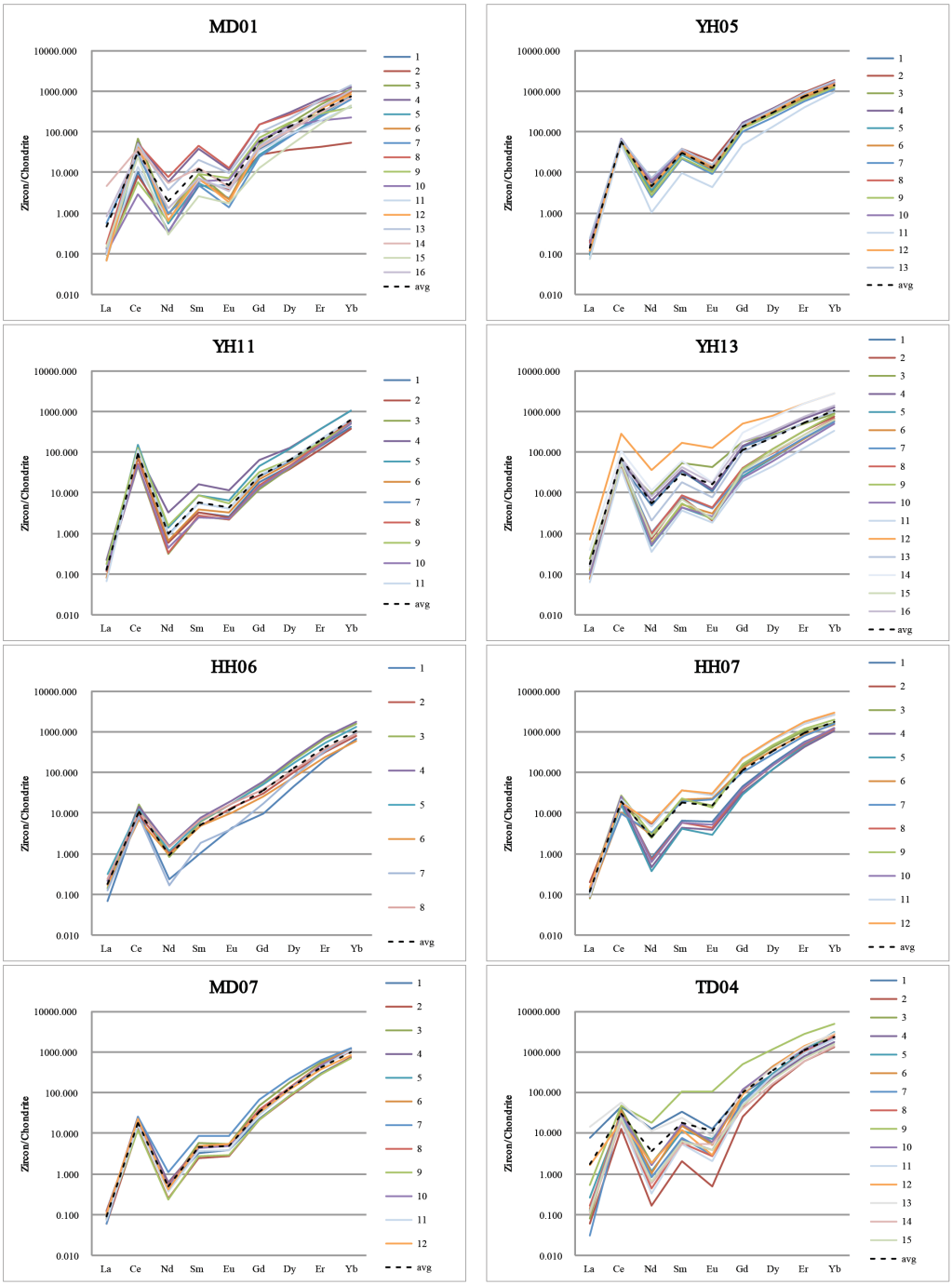

Supplemental Figure SP3.3 - Rare Earth Element Plots (continued)